Structural characterization of sulphate and chloride doped glasses for radioactive waste immobilisation

VAISHNAV, Shuchi

Sheffield Hallam University | Materials and Engineering Research Institute

Structural Characterization of Sulphate and Chloride Doped Glasses for Radioactive Waste Immobilisation

Shuchi Vaishnav

A Thesis Submitted to the
Materials & Engineering Research Institute (MERI)
Sheffield Hallam University
in partial fulfilment of its requirements for
the Degree of Doctor of Philosophy

April 2018

या कुन्देन्दुतुषारहारधवला या शुभ्रवस्त्रावृता

या वीणावरदण्डमण्डितकरा या श्वेतपद्मासना ।

या ब्रह्माच्युतशंकरप्रभृतिभिर्देवैः सदा पूजिता

सा मां पातु सरस्वति भगवती निःशेषजाड्यापहा ॥१॥

Dedicated to my pillars of strength

Renu Vaishnav

&

Ram Narayan Das Vaishnav

DECLARATION

I hereby declare, that the thesis entitled “Structural Characterization of Sulphate and Chloride Doped Glasses for Radioactive Waste Immobilisation” is result of my original work and investigation. None of the results presented in the manuscript have been lifted from any other sources and legitimate references are presented where necessary.

Name: Shuchi Vaishnav

Date: 05/06/2018

PUBLISHED WORK AND CONFERENCES

Aspects of the work described in the thesis were published in:

Modelling the sulfate capacity of simulated radioactive waste borosilicate glasses, P.A. Bingham, S. Vaishnav, S.D. Forder, A. Scrimshire, B. Jaganathan, J. Rohini, J.C. Marra, K.M. Fox, E.M. Pierce, P. Workman, J.D. Vienna, *Journal of Alloys and Compounds* 695 (2017) 656-667.

The results have been presented at various conferences:

- "Role of BaO as modifier in silicate and borosilicate glasses with high sulphate solubility", S. Vaishnav, A.C. Hannon, E.R. Barney, J.V. Hanna, P.A. Bingham, Society of Glass Technology, 2017, Cambridge, U.K.

- "Multi-spectroscopic characterisation of binary and ternary silicate glasses doped with sulphate and chloride ions", S. Vaishnav E.R. Barney, A.C. Hannon, P.A. Bingham, Society of Glass Technology, 2016, Sheffield, U.K.

- "Effects of sulfate addition on silicate glasses- a Raman, NMR and neutron diffraction study", S. Vaishnav, E.R. Barney, A.C. Hannon, P.A. Bingham, Glass & Optical Materials Division meeting, 2016, Wisconsin, U.S.

- "Incorporation of sulphate ions in silicate glasses with implications to radioactive waste immobilisation" S. Vaishnav, P.A. Bingham, International Congress of Glass- Annual Meeting, 2015, Bangkok, Thailand

- "Understanding high sulphate issue in glasses relevant to radioactive waste immobilisation" E-Poster, S. Vaishnav, P.A. Bingham, E.R. Barney, Glass Science in Art and Conservation meeting, 2014, Durham, U.K.

GLOSSARY OF TERMS

- BO: Bridging Oxygen
- BWR: Boiling Water Reactor
- CFSI: Cation Field Strength Index
- CN: Coordination Number
- CS: Centre Shift (also known as Isomer Shift in Mössbauer spectroscopy)
- DOE: Department of Energy
- DSC / DTA: Differential Scanning Calorimetry / Differential Thermal Analysis
- DWPF: Defence Waste Processing Facility
- EDX/ EDS: Electron Dispersive Spectroscopy
- EPMA: Electron Probe Micro-Analysis
- EPR: Electro-Paramagnetic Resonance spectroscopy
- EXAFS: Extended X-Ray Absorption Fine Structure spectroscopy
- FNR: Fast Neutron Reactor
- FP: Fission Product
- IAEA: International Atomic Energy Agency
- ICP: Inductively Coupled Plasma spectroscopy
- ILW: Intermediate Level Waste
- HLW: High Level Waste
- HLLW: High Level Liquid Waste
- LAW: Low Activity Waste
- LLW: Low Level Waste
- mA / MA: minor Actinides / Major Actinides
- MAS - NMR: Magic Angle Spinning - Nuclear Magnetic Resonance

- MOX: Mixed Oxide Fuel
- MO_x: Modifier Oxide (Metal Oxide)
- MW: Magnox Waste
- NBO: Non- Bridging Oxygen
- NCFSI: Normalised Cation Field Strength Index
- NEA: Nuclear Energy Association
- ND: Neutron Diffraction
- NPP: Nuclear Power Plant
- NWM: Network Modifier
- OECD: Organisation of Economic Cooperation and Development
- PF: Packing Fraction
- QS: Quadrupole Splitting
- SEM: Scanning Electron Microscopy
- SNF: Spent Nuclear Fuel
- T_c: Crystallisation temperature
- T_g: Glass Transition Temperature
- T_m: Melting temperature of crystalline phase
- TRU: Trans-Uranic elements
- VLLW: Very Low-Level Waste
- WVP: Waste Vitrification Plant
- XAFS: X-Ray Absorption Fine Structure Spectroscopy
- XANES: X-Ray Absorption Near Edge Structure Spectroscopy
- XRD: X-Ray Diffraction
- XRF: X-Ray Fluorescence

ABSTRACT

Silicate and borosilicate glasses are of great importance for both the commercial and nuclear waste glass industries. Anionic species such as chloride and, more famously, sulphate are known to play a role in melting, fining and homogenization of commercial silicate glasses. At the same time, these anions can be present in abundance in several kinds of nuclear wastes destined for confinement in a multi-oxide borosilicate glass matrix (the most widely employed glass for radioactive waste immobilisation). Beyond a certain extent, it is difficult to incorporate the anionic species in commercially used radioactive waste borosilicate glasses due to their poor solubility in the molten glass and this can limit waste loading in the final waste forms, thus increasing the waste volumes and having substantial logistical and economic impacts. Besides the technological and economic repercussions faced by the waste vitrification facilities, the undissolved sulphates that precipitate as a water-soluble salt layer, are often enriched in ^{137}Cs, ^{99}Tc and ^{90}Sr and can dissolve in the groundwater in geological waste repositories which raises environmental concerns. Similarly, the pyrochemical reprocessed chloride containing waste contains significant quantities of actinides such as ^{239}Pu and ^{241}Am which have low solubilities in the borosilicate waste glasses. Therefore, in order to formulate glass compositions with enhanced anionic capacities, a careful investigation is required to determine the anion solubility factors in such glasses. Since the structural characterisation of the industrially used borosilicate glass compositions is challenging due to the presence of multiple elements in the glass, we have designed a simpler

approach by developing binary and ternary silicate and borosilicate glasses with and without the anions added. The key focus of the thesis is to look at largely sulphate capacities of two glass systems: silicate and borosilicate glasses. Thorough spectroscopic investigation of chloride doped glasses has not been carried out due to insufficient levels of chloride retained in the two glass systems and hence makes just a side-study for the research. The undoped and sulphate doped glasses are subjected to comparative compositional and structural investigation using a range of techniques including density measurements, XRF, ICP, XRD, MAS - NMR, Raman spectroscopy, ND, and DTA, SEM - EDS, and Mössbauer spectroscopy.

This thesis mostly elucidates the influence of different essential modifier oxides that are either already present or can be added / removed in the industrial waste glass compositions to enhance sulphate solubility. Density measurements show that incorporation of sulphate slightly decreases the densities of the doped glasses. XRF, ICP, SEM-EDS analyses identify the dependence of sulphate capacity on glass composition. Raman spectroscopy and ^{29}Si MAS-NMR techniques provide measures to link sulphate capacity with structural changes in the Si/O and B/O/Si network. ^{23}Na, ^{7}Li MAS-NMR, though less informative, suggest changes in modifier environment with sulphate addition. Raman spectroscopy of sulphate doped glasses shows distinct bands corresponding to S-O stretching modes in silicate and borosilicate systems. The centre position of these modes is compared with S-O modes for corresponding crystalline sulphates to establish the cation environment around the sulphate ions. The increase in the degree of polymerisation of the glass network upon sulphate addition is consistent between silicate and borosilicate systems, with only a few exceptions. Neutron Diffraction is employed to study the change in coordination environment of the cations and anions in the glass upon sulphate addition. The results were collectively put into

different empirical models proposed to study sulphate solubility and checked for the models' versatility. Simulated sulphate doped, multi-oxide borosilicate glasses which are broadly representative of industrial U.S. HLW / LAW waste glasses, are prepared and modified as per our investigations on simpler glasses, to study changes in its sulphur solubility. Additionally, we have also considered the effect of V_2O_5 addition on sulphate incorporation in the simulated radioactive waste glasses.

Keywords: Sulphate; Silicate; Borosilicate; Raman Spectroscopy; NMR; Neutron diffraction; Chloride; Radioactive Waste.

LIST OF FIGURES

CHAPTER 1

CHAPTER 2

CHAPTER 3

CHAPTER 4

CHAPTER 5

CHAPTER 6

CHAPTER 7

CHAPTER 8

CHAPTER 9

LIST OF TABLES

CHAPTER 2

CHAPTER 3

CHAPTER 4

CHAPTER 5

CHAPTER 6

CHAPTER 7

CHAPTER 8

ACKNOWLEDGEMENTS

First and foremost, I thank my director of studies, Dr. Paul Bingham for the excellent mentoring and support he provided throughout, from the beginning of my research till the completion of this thesis. Not only has he dispensed crucial advice and direction to progress with this research at every step, but also created several opportunities for me to engage with many pioneers in glass research at various international consortiums and promote my work.

I am indebted to Dr. Alex Hannon at the ISIS neutron facility, RAL and Dr. Emma Barney at University of Nottingham for helping me extensively to process the neutron diffraction data. I extend my gratitude to Dr. David Apperley, Durham University and Dr. John Hanna, University of Warwick for conducting the NMR experiments and Dr. Kevin Fox, SRNL, US for the ICP analyses to aid this research. I greatly appreciate the MERI staff, in particular, Dr. Anthony Bell, Dr. Francis Clegg and Deeba Zahoor for patiently training me in several spectroscopic techniques and trusting me with handling those giant machines single-handed. Heartfelt appreciation goes towards Alex Scrimshire, Benjamin Allsopp and Khalid Muhammed from my research team for providing helping hand in the labs.

Shout out to my amazing girl gang: Parul and Barnali for engaging me in senseless, endless but massively entertaining conversations and activities time to time which kept this girl from becoming an ideal definition of 'NERD'. Finally, I convey my deepest, incalculable gratitude and love to my parents, Renu & Ram, brother Gurdeep for instilling strength in me, making me tough to not let the homesickness overpower my career goals, reinforcing faith when I doubted my calibre and sharing my joys and tears.

"After two laptops and a Raman spectrometer giving up on me, in the last four years, this thesis would not be possible without anyone of you."

Table of Contents

CHAPTER 1

INTRODUCTION

The abundance of anionic species such as sulphates, chlorides, molybdates and iodates in some commercial and defence high and intermediate level radioactive wastes are problematic for the nuclear waste vitrification industries due to their poor solubility in the waste host borosilicate glass matrix (Darab et al. 2001; Vienna et al. 2004; Kaushik 2014; Hrma et al. 2002; Schreiber et al. 1987; Merrill et al. 1994; Stefanovskii 1993; Fox et al. 2006; Vienna et al. 2014). In this research work, however, mostly sulphates and chlorides to a certain extent, have been considered. The excess sulphates and chlorides precipitate out of the melt during vitrification and creates a low temperature secondary, water soluble, highly acidic and corrosive salt layer on the surface upon cooling which is detrimental to vitrification process (Langowski 1996; Marra et al. 1994; Marra & Fox 2014; Kim & Hrma 1991; Hamodi & Iqbal 2009; Kruger 2013; Donald et al. 1997; Bingham et al. 2011; Sullivan et al. 1995)(Figure 1.1).

Other volatile and highly radioactive nuclides such as ^{137}Cs and ^{90}Sr may partition and mobilise to the crystalline and water soluble sulphate salt surface which in the longer run, can contaminate the groundwater present in the geological repositories where the final waste glass will be stored (Kamizono 1985; Kamizono & Nakamura 1988; Kamizono 1990; Cunnane 1994; Kersting et al. 1999; Grambow 2006). Likewise, chloride salts markedly used for pyro-chemical processing to extract weapon grade

plutonium from spent nuclear fuel, are often enriched with actinides ^{241}Am, ^{239}Pu which poorly solubilise in borosilicate glass systems (Volf 1984; Spalding 1994; Langowski 1996; Schofield et al. 2009; Schofield 2011; Vance et al. 2012). Chlorides have also been reported to increase the volatilisation of F, Cs and Cr (Langowski 1996; Donald et al. 2007)

Figure 1.1: Simulated HLW glass (left), LAW glass (middle and right) developed in the MERI lab. A white salt layer on the glass surface appears due to excess sulphate precipitation (left and right), sulphate and chloride (middle). The yellow salt layer (right) is imparted due to presence of chromium in the salt.

A sulphate concentration limit of 0.6 wt % of SO_4^{2-} (Stefanovskii 1993; Jantzen et al. 2005) has been achieved so far for industrially used glass compositions. Likewise, the solubility limit of Cl^- is also reported to be ~ 0.1 wt % in conventional borosilicate glasses (Cl^- solubility can exceed to 1-1.8 wt% in soda-lime-silicate glasses) (Volf 1984; Marra et al. 1994; Langowski 1996; Vance et al. 2012; Jena et al. 2015). It has also been recognized that the solubility limit is well dependent on glass composition besides melting environment and melt temperatures, through the work done by several researchers (Ooura & Hanada 1998a; Marples 1988; Stefanovskii 1993; Jantzen et al. 2005; Ojovan & Batyukhnova 2007; Donald et al. 1997; Hrma et al. 1994; Li-Jun et al. 2009; Cassingham et al. 2008; Sengupta et al. 2015; Kaushik et al. 2006). To increase the capacity of anionic salt retention in order to meet the waste loading and production rate requirements, it is necessary to enhance the currently used industrial glass

compositions. The glass compositions used at vitrification industries may contain up to 20-30 elements in considerable concentrations. Several of these elements can significantly induce or reduce the sulphate / chloride retention (Vienna et al. 2014). The complexity of the composition challenges the structural characterisation of such glasses and makes it difficult to determine the factors attributing to the limited capacity.

The key objectives associated with this research were:

- To improve the understanding of the effects of glass composition on sulphate solubility by developing simple binary, ternary and quaternary glasses doped with sulphate and measuring the amount of sulphate retained in the glass.
- To study the effects of sulphate addition on the structure of the glass in terms of changes in short-range bond orders, structural arrangement and coordination environment and properties such as density and molar volume.
- Develop enhanced glass compositions with higher sulphate capacity potentially suitable for industrial applications.
- To test the effect of chloride addition on the structural environment of simple silicate and borosilicate glasses in order to improve understanding of factors corresponding to its poor solubility in the glass matrix.

The objectives of the research were largely met using a range of characterisation and spectroscopic techniques. This thesis reports the experiments and analysis carried out in order to meet the objectives, and the key conclusions derived from the studies.

In Chapter 2, the literature review describes the nuclear fuel cycle through which nuclear waste is generated, the categories of nuclear waste and the different techniques

used for immobilising such wastes. We also discuss the the pros and cons of using borosilicate glass globally as an ideal waste form.

In Chapter 3, issues associated with sulphate abundance in nuclear waste are elaborated in terms of its origin in the waste, the problems associated with its poor solubility, the studies carried out over the years to understand parameters affecting sulphate solubility and the empirical models developed to predict sulphate capacity of various glass compositions. In the same chapter, we briefly discuss the route of chloride entry in the reprocessed nuclear waste, its poor solubility in industrial borosilicate waste glasses and the alternate more suitable waste forms being tested to deal with this particular waste.

Chapter 4 reports the properties of the two glass systems studied during the thesis, silicates and borosilicates. It also documents the detailed experimental methodology used for developing the glasses along with the experimental techniques employed for the spectroscopic investigation of the samples.

Chapter 5 presents the results obtained for the effect of sulphate addition on the structure and properties of simple binary and ternary alkali-alkaline earth silicate glasses measured with XRF, XRD, DTA, ND, Raman spectroscopy and MAS-NMR. The NCFSI, $CFSI_{total}$ and ratio of NBO / BO were determined from the spectroscopic investigations and verified using the sulphate solubility models proposed by (Papadopoulos 1973; Jantzen et al. 2005; Bingham & Hand 2008; Bingham et al. 2017).

In Chapter 6, the effect of BaO as a modifier on sulphate solubility in binary and ternary borosilicate glasses is discussed in detail. This study was largely inspired by the work carried out by the Waste Management Division at BARC, India where a glass SB-44

with high content of BaO and a sulphate retention capacity up to ~3 mol% SO_4^{2-} was developed and is currently being employed for vitrification purposes (Mishra et al. 2008; Kaushik et al. 2006; Kaushik 2014).

In Chapter 7, results are presented for some simulated waste glass compositions which are broadly representative of U.S. high-level radioactive waste glasses. The glasses are analysed with techniques such as XRF-ICP, Raman spectroscopy and Mössbauer spectroscopy and verified with the cation field index model (Bingham & Hand 2008) which provides clear relationships between the total cation field strength index of a glass with its sulphate retention capacity. In addition, we also assess the addition of 2.5 - 10 wt% of V_2O_5 on the change in concentration of the sulphate retained in the simulated waste glass. The study is inspired by the work of (Stefanovskii et al. 1989; Manara et al. 2007; McKeown et al. 2002; Sengupta et al. 2015) where the authors established that addition of V_2O_5 has a potential to accelerate the kinetics of sulphate incorporation in borosilicate glasses and thus increase the solubility.

In Chapter 8, we have briefly discussed the experiments those were conducted in order to determine the effect of chloride addition to the silicate and borosilicate glass compositions. Due to high volatilisation losses of chloride in the final glass compositions, and structural characterisation using Raman spectroscopy and MAS-NMR not showing any significant changes between the undoped and doped compositions, no clear conclusions could be derived.

In Chapter 9, the key conclusions from the research are summarised and the scope of future work that awaits to make progress with this research topic has been discussed.

CHAPTER 2

BACKGROUND AND LITERATURE REVIEW

2.1 Brief Overview

Production of electricity from nuclear fission resources has been used for the past few decades with thirty countries currently benefitting from the 448 nuclear power reactors under operation that hold a net generation capacity of 392 GW(e) (11 % of global electricity) (World Nuclear Association 2017; IAEA 2017). Though considered by fair means a green source of energy for avoiding approximately 2 billion tonnes of CO_2 generation per year and nil greenhouse gas emissions (Bauer et al. 2012; Qvist & Brook 2015; OECD 2010); the entire industry as per the IAEA 2017 report has produced over 270,000 tHM[1] of Spent Nuclear Fuel (SNF) accumulating at a rate of 10,000 tHM/year (IAEA 2017; World-nuclear.org 2017). It requires profound strategic management but comes with a series of technical challenges such as the composition of the reactor fleet, legal framework, economic regulations, political and public acceptance and primarily environmental protection (avoiding seepage of radionuclides into groundwater).

Up to and including the early 1970s, almost all SNF was classified as waste by many vitrification plants which resulted in huge waste inventories, but in the current age with

[1] Tonnes of Heavy Metal

the advent of Generation IV Fast Neutron Reactors (FNR) and advancements made in reprocessing technology (NEA 2012; Sherry 2014), some of it is processed for re-use and the inventory has reduced by a significant amount (IAEA 2008). At present, 28% of the SNF has been reprocessed and the remaining SNF lies in interim storage to be reprocessed and disposed. Apart from the waste produced by the Nuclear Power Plants (NPP), residues from decommissioned reactor sites, defence, and medical facilities also contribute to the total nuclear waste inventory (Murray 1981; Donald 2010). Nuclear disasters such as Fukushima (2011) have also added $> 920,000$ tonnes of contaminated waste to the inventory that needs immediate attention due to shortage of storage facilities (Tanaka 2012). On top of that, High-Level Waste (HLW) tank explosions: Kyshtym disaster (1957); Seversk (1993) and AY-106, Hanford Waste container leaks (2016) are adding urgency to improve the waste hosting technology. The financial costs of cleaning up such sites are enormous.

Thus, for future acceptance of nuclear energy, the key focus, in addition to safe nuclear power generation, is on efficient waste management through the development of highly durable material hosts ideal for long term waste disposal; which can withstand any natural or man-made disaster and are economically viable to incorporate high waste load in minimal volumes, thus reducing the costs of landfill and geological reposition.

This chapter gives an insight of the nuclear fuel cycle prompting maximum waste generation; classification of the waste, techniques used to treat the waste before final geological disposal and borosilicate glasses that are being used globally for immobilization of LAW and HLW.

2.2 Nuclear Fuel Cycle (Front End)

The front end of a nuclear fuel cycle involves a set of processes starting from the mining of unused nuclear ore to its effective utilisation in producing consumable energy. Safe management of SNF; reprocessing and disposal contribute to the back end of the cycle (Figure 2.1).

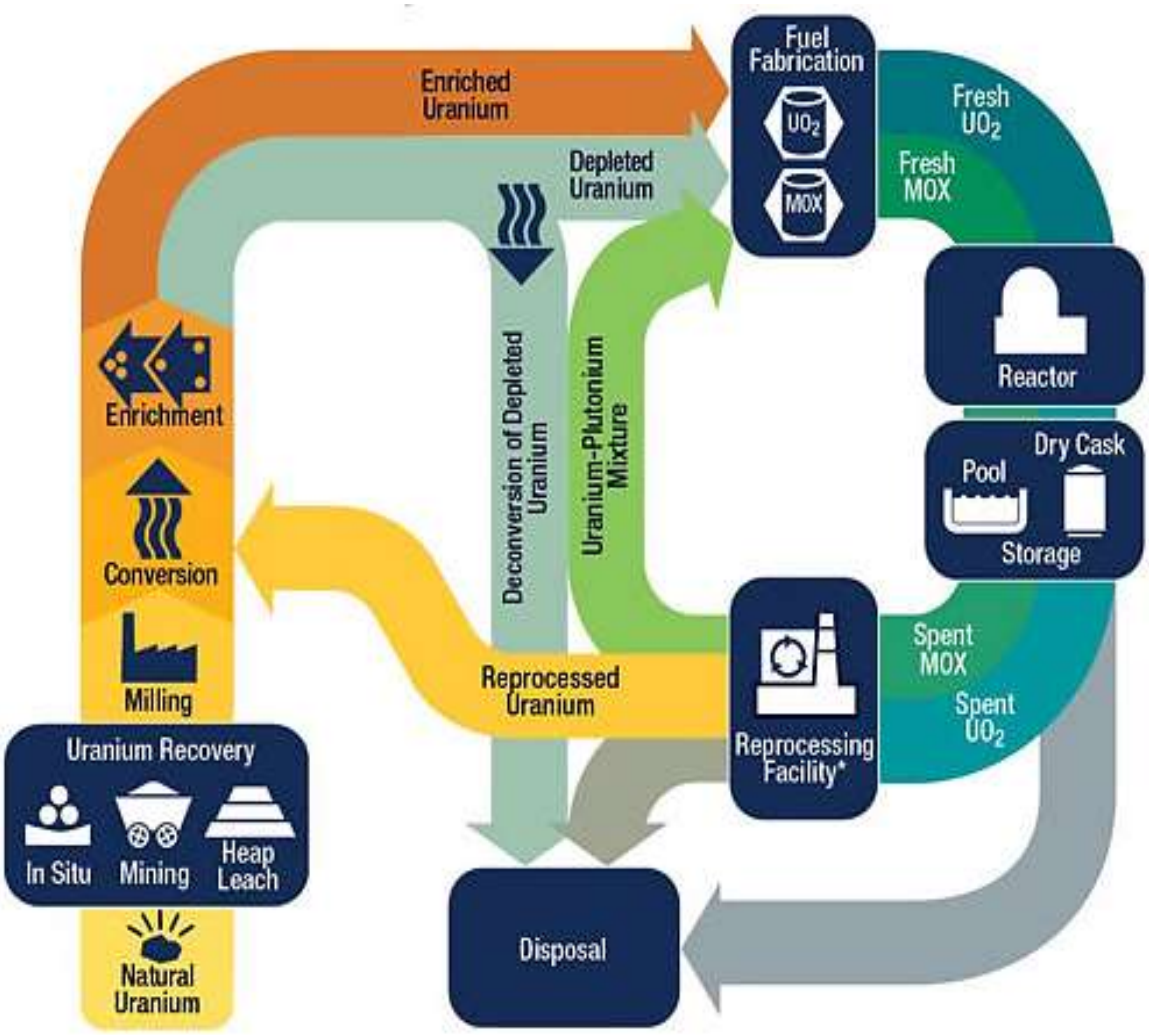

Figure 2.1: The Nuclear Fuel Cycle Flowchart
(Courtesy: U.S. Nuclear Regulatory Committee)

(i) Mining-Milling: The uranium ore in the form of uraninite / pitchblende is mined and milled to a suspension pulp of size 150-450 µm. The pulp undergoes a wet

hydrometallurgical process leading to formation of the famous "yellow cake" that contains impurities such as thorium, rare earths, iron, titania, silica, alumina, etc. besides uranium (World Nuclear Association 2011; Mudd 2014; Karpius 2017; Mudd & Diesendorf 2008).

(ii) Filtration-Fluorination: To produce nuclear grade material the yellow cake is filtered at a facility by dissolution in nitric acid. The Uranyl Nitrate (UN) solution obtained, which is thermally de-nitrated and calcined to produce UO_2 ; is further hydro fluorinated and converts to UF_6 (Merritt 1971; Fox & Koetting 1974; Wilson 1996).

(iii) Enrichment-Fuel Fabrication: The natural UF_6 contains 0.72% of fissile ^{235}U. This amount is increased up to 2-5% of enrichment and the depleted UF_6 containing 0.25% of ^{235}U is sent for interim storage. The enriched fuel is reconverted to UO_2 and fabricated into fuel pellets. In Mixed Oxide [MOX] fuelled reactors, uranium, and plutonium which are recovered from reprocessing of spent fuels are converted and refabricated into fuel (Villani 1979; Cochran et al. 1990; Wilson 1996).

(iv) Cladding-Fuel Assembly: The pellets are assembled together in a fuel rod and cladded with a thick coating of Aluminium/Zirconium (Boiling Water reactors [BWR]) (Azevedo 2011; Samskog et al. 1971); Zircalloy (Pressurised water reactors [PWR]/ Advanced graphite reactors [AGR]) (Cox 1990; Terrani et al. 2012; Azevedo 2011) or stainless steel alloys (Fast Breeder Reactors [FBR]) (Mannan et al. 2003; Lobsinger 1974). The fabricated fuel rods are arranged in a fuel assembly and sent to the NPP for burn-up inside the reactor core.

2.3 Nuclear Fuel Cycle (Back End)

2.3.1 Spent Fuel Reprocessing

The SNF from the reactor after its complete burnup reaches the storage facilities to be dealt with in three ways (Bruno & Ewing 2006; Johnson 1988; Bunn et al. 2005; Rechard 1995; Gras et al. 2007; Seong-won et al. 2010) as mentioned in the following flowchart.

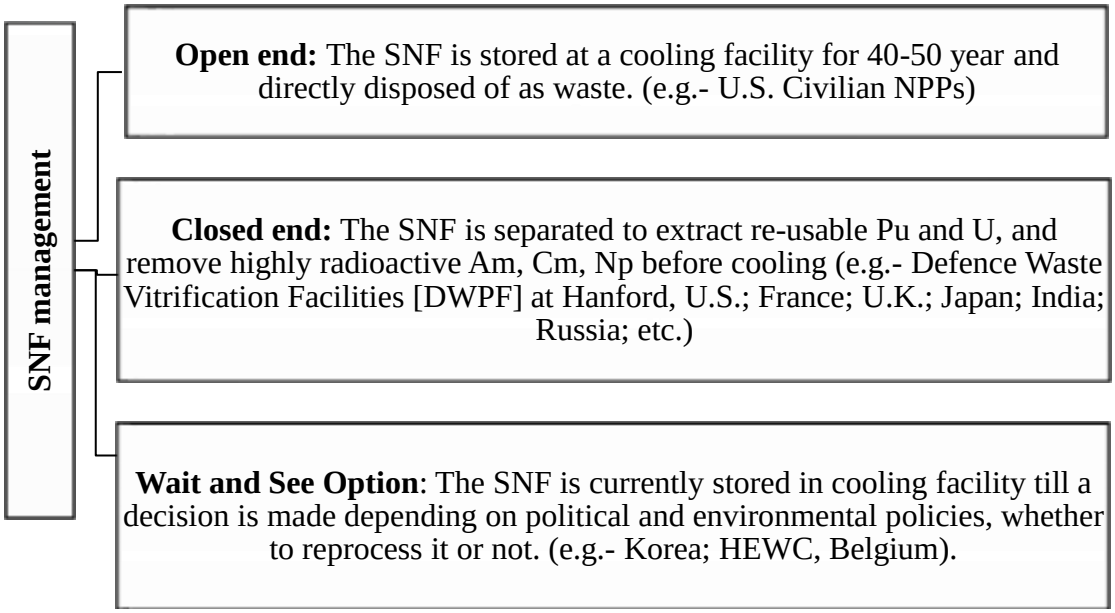

Reprocessing of SNF is undertaken for several reasons (Johnson 1988; Bunn et al. 2005; IAEA 2008):

- Recovery of the valuable fissile constituents (primarily ^{235}U and $^{239, 240}Pu$) for subsequent reuse in recycled MOX fuel or ^{238}Pu for defence weapons (controversial).
- Optimisation of waste management; reposition costs
- Minimization of final waste's environmental impact.

The SNF rods are de-cladded, chopped and dissolved in boiling nitric acid at the reprocessing facility. This is followed by chemical solvent extraction of major actinides (MA): fissionable U and Pu formed during fuel burn-up. The remainder (2 - 3% of SNF) is a High-Level Liquid Waste (HLLW) liquor which consists of impurities from cladding removal, Fission Products (FP), Transuranic elements (TRUs) from neutron capture and inactive process additives used for solvent extraction of MA, all dissolved in nitric acid (Bruno & Ewing 2006; Ewing 2006). The liquor filled in stainless steel cylinders is either stored underwater (wet storage) or in a concrete cask surrounded by inert gas (dry storage) over ground. It is further neutralized by addition of alkali (NaOH) at the waste treatment facility before immobilisation (Dey 2003).

The present approach is called the PUREX (Plutonium-Uranium Extraction) process (Mckay 1990; Mckibben et al. 1983) (Figure 2.2) which offers advantages (IAEA 2008) such as:

- 25% improved usage of fissile sources.
- Reduction in waste volumes due to increased removal of Uranium / Plutonium.
- Decrease in the radiotoxicity of the waste to be disposed.

The reprocessed U+Pu is reconverted to Mixed Oxide (MOX) which fuels the Generation IV PWRs and FBRs. Further progress is being made in upgrading techniques such as solvent extraction, ion exchange, transmutation for more efficient TRU (Am, Cm, Np) and some FP (Tc, Pd, Cs) removal from the SNF before sending to a Waste Vitrification plant (WVP). (Groska et al. 2016; Pichestapong et al. 2016; Wei et al. 2013; Gopalakrishnan et al. 1995).

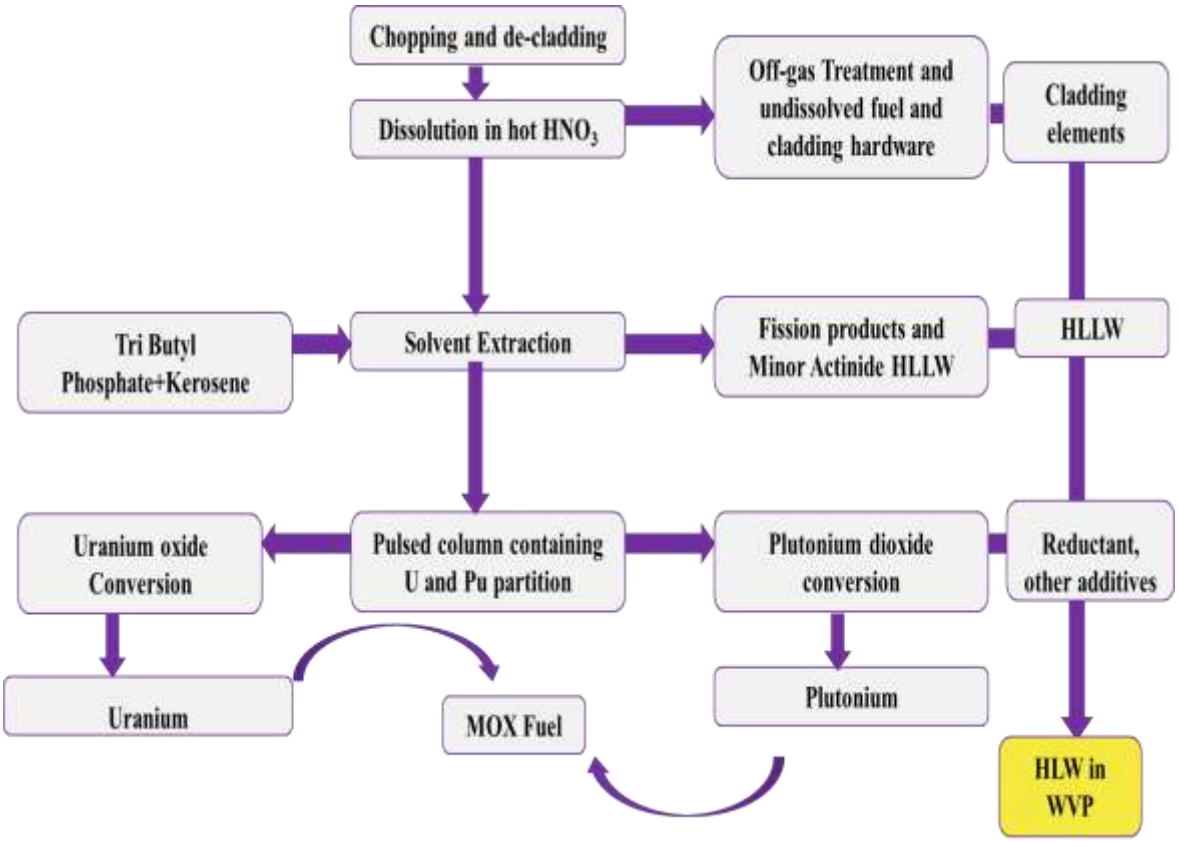

Figure 2.2: Flowsheet stating simplified steps involved in PUREX process

2.3.2 Nuclear Waste Generation

The total nuclear waste inventory varies in composition for each country based on the activity sector; the level of radioactivity and heat generation, and decay time of the radionuclides present. For most of the countries the waste is broadly classified into four categories (Ewing, 2006; Murray, 1981; Ojovan & Lee, 2005) (Table 2.1).

Type of Radioactive Waste	Radioactivity	Relative volume in total waste inventory	Shielding / Isolation requirement	Disposal Method
VLLW	1-400 Bq /g	20.10 %	None	Landfill
LLW	< $1.2x10^{10}$ Bq / t (β and γ)	70.90 %	Isolation required for ~ 100 years	10-50 m below earth's surface
ILW	>1.2×10^{10} Bq / t (β and γ) < 2 kW /m^3 (heat generation)	6.00 %	Isolation and shielding required ~ 100 years	Engineered geological repository < 500m
HLW	> 1.1×10^{18} Bq/ t (β and γ) >2 kW /m^3 (heat generation)	3.00 %	Isolation, cooling & shielding required > 100 years	Multiple barrier engineered repository > 500m

Table 2.1: Categories of nuclear waste (Bingham et al. 2011; Donald 2010; IAEA 1998)

(i) Very Low-Level Waste (VLLW): Consists mainly of demolished material (concrete, bricks, metal, soil etc.) produced during rehabilitation or dismantling operations on nuclear industrial sites. Due to very low radioactivity, it was disposed of with ordinary commercial refuse but since 2008, IAEA subdivided this category to very short-lived waste with decay time < 100 days and very long lived waste with longer half-life (Freiesleben 2013). Countries like Russia and France are now developing landfill type storage facilities for the latter e.g. The Cires facility, La Chaise.

(ii) Low Level Waste (LLW): Generated by nuclear power plants, medical institutions (Han et al. 1997), research laboratories, and defence activities

(Andrews 2006; IAEA 2011; IAEA 2013; Gershey et al. 1990). This type of waste is incinerated and mechanically compacted for volume reduction. The final packaged conditioned waste is then disposed a few meters (15-50 m) below earth's surface (Figure 2.3).

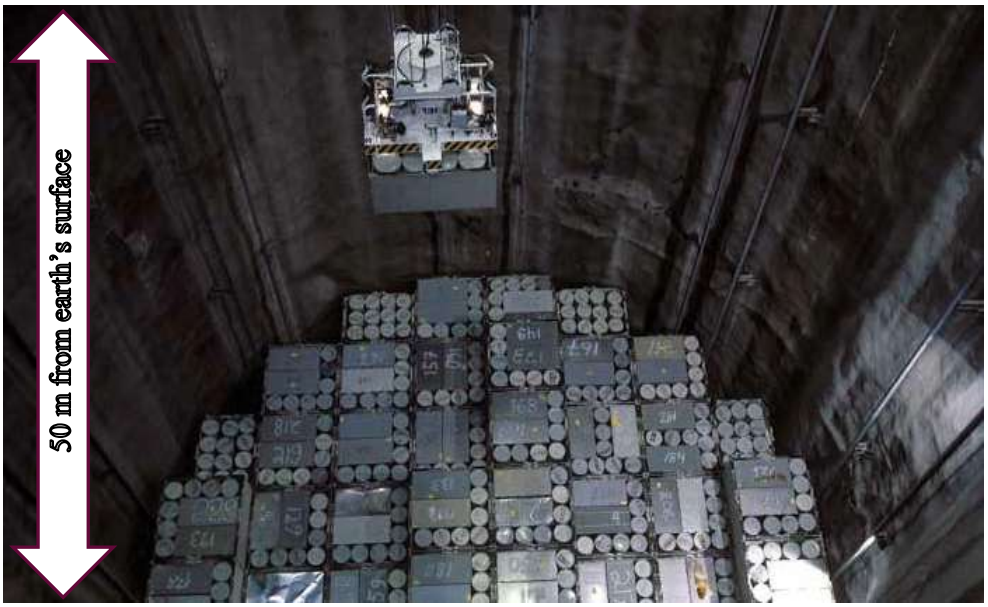

Figure 2.3: Mouth view of the geological repository at TVO, Finland for LLW (Image credit: STUK's 2014 report on the safety of spent fuel management.)

(iii) Intermediate Level Waste (ILW): ILW's high radioactivity requires shielding (Carlsson & Viitanen 1997). It consists mostly of ion exchange resins used to clean the water circulating through the reactor; chemical sludge from the PUREX process and fuel cladding. It is usually conditioned by cementation or bituminisation (Section 2.3.3.1) and disposed at ~200-500 m from the surface (Wattal 2013).

(iv) Low Activity Waste (LAW): An additional type of waste is categorised by the U.S. nuclear waste regulatory committee known as low activity waste (to be not confused with LLW). LAW is an assembly of mixed nuclear source materials from various DOE and defence facilities' activities with radiological hazard

much less than HLW and HLLW obtained after spent fuel reprocessing but the concentration of transuranic radionuclides such as uranium and plutonium with very long half- lives is substantial in this kind of waste (Kosson et al. 2008; NRC 2003; IAEA 2004). Due to the longevity of the waste, it needs deep geological disposal in a durable waste host matrix like HLW (Peeler et al. 2015).

(v) High Level Waste (HLW): HLW can be categorised in two wide groups:

- SNF no longer efficient for electricity generation.
- HLLW slurry after SNF reprocessing.

The total HLW inventory can be broadly divided into 4 groups (Table 2.2). Full elemental characterisation of the HLW is given in Appendix B. The classification is broad and individual concentration and radiotoxicity varies for each WVP depending on many factors: (Ando et al. 2000; P. K. Dey & Bansal 2006; Sengupta et al. 2013):

- Nature and content of fissile fuel used in the reactor (different burn-up rates)
- The type of reactor
- Fuel-cladding interaction
- Cladding removal process (Al cladding is difficult to be stripped off fuel pellets and hence dissolved in HNO_3 with the fuel. Such wastes have high NO_3 and Al concentration).
- The major constituents, i.e. fission products (FP), major actinides (MA) and minor actinides (mA) are generated in the reactor core. Chemical process additives are used for solvent extraction of actinides and neutralization of the reprocessed SNF slurry. Most of the HLW constituents are long-lived radionuclides (Table 2.3, Figure 2.4).

High Level Waste

Corrosion products (CP)

e.g.: oxidised Fe, Cr, Co, Mg, Al, Mo, Ni, Nb, Zr, Si

Activated radionuclides: ^{51}Cr, ^{59}Fe, $^{58,60}Co$, ^{63}Ni, ^{54}Mn, ^{94}Nb, $^{122,124}Sb$

Fission products (FP)

$^{134,135,137}Cs$, ^{90}Sr, ^{99}Tc, $^{131,129}I$, $^{141,144}Pm$, ^{151}Sm, $^{152,154}Eu$, etc.

Actinides (A)

Major actinides (MA) : $^{235, 238}U$, $^{238,239}Pu$

Minor actinides (mA) : ^{237}Np, ^{241}Am, $^{242,244}Cm$

Process additives (PA)

Na, K, Li, Ca, Mg, Fe, S, F, and Cl

organic process chemicals : kerosene and Tributyl Phosphate

Table 2.2*:* Constituents of High Level Waste (Sengupta et al. 2013; Stefanovsky et al. 2004)

Radionuclide	Half Life (years)	Source of Origin
Pu-239	$2.41 * 10^4$	Transmute decay in U-238
Np-237	$2.14 * 10^6$	Transmute decay in U-238
Am-241, 243	432.2, 7370	Transmute decay in Pu-239
Cm- 244	18.1	Transmute decay in Am-241
Cs-137	30.17	Fission Product
Sr-90	28.79	Fission Product
Tc-99	$2.11 * 10^5$	Fission Product
I-129	$1.57 * 10^7$	Fission Product
Zr-93	$1.53 * 10^6$	Fission Product
Cs-135	$2.30 * 10^6$	Fission Product

Table 2.3: Half-life of major radiotoxic nuclides present in the SNF of a standard PWR after 10 years of cooling (OECD 2006).

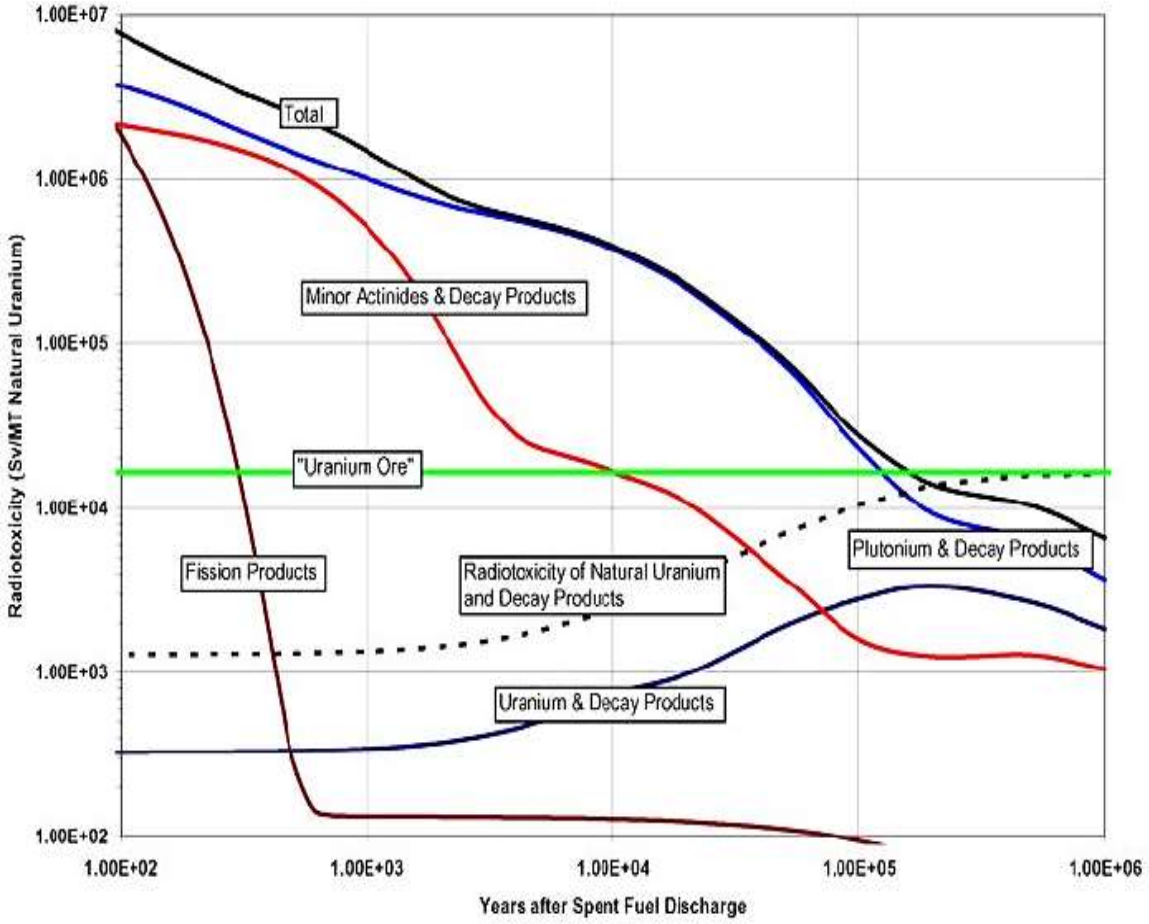

Figure 2.4: Radiotoxicity of SNF is dominated by Pu and mA. The radiotoxicity of the amount of natural uranium used to produce 1 t of nuclear fuel is used as the reference value (Image credit: Salvatores, NEA report 6090, 2006)

Thus, this type of waste should be disposed of in deep geological repositories (> 500 m from the earth's surface) (White et al. 2013; Kim et al. 2011) in a solidified glass matrix enclosed within an engineered Multiple Barrier System (MBS) (Sengupta et al. 2013; OECD 2002; Ewing et al. 2016; Marivoet et al. 1999) to avoid contact with groundwater in future.

This type of waste however requires cooling for several years and multi- level shielding prior to permanent disposal due to very high thermal heat rate and radioactivity (95% of the total radioactivity in nuclear waste). The waste is conditioned prior to temporary storage in over-ground radiation shielding facilities.

2.3.3 Nuclear Waste Immobilisation

From 1946 to 1980, ocean dumping was a primary method for discarding nuclear waste by 13 countries but after a strict prohibition act implemented by international treaties (London Convention (1972), Basel Convention, MARPOL73/78) in 1994 (IAEA 1999), the focus shifted to development of highly efficient, economical and safe ways of disposing the radioactive waste of which 'immobilisation' was widely accepted (Schreiber & Hockman 1987; Ringwood et al. 1988; Ringwood et al. 1979; Donald et al. 1997). Other processes like transmutation, and space disposal have been considered but those have not gained popularity within the decommissioning industry due to extensive costs and safety concerns.

IAEA defines immobilisation as a way of solidifying, encapsulating or embedding the waste in a durable and chemically inert matrix which minimizes the risk of dispersion of radionuclides in environment (IAEA 1997; Lee et al. 2006). Though, these methods have proven to be successful in reducing the mobility of the radioactive nuclides in the waste host, however, once repositioned in the geological storage for permanent disposal, many internal and external factors can affect the properties of the waste form resulting in release of the waste (shown in Figure 2.5).

The exact long-term behaviour of the waste forms over periods of > 100 years is difficult to assess and can only be predicted. Therefore, several essential properties are required for the longevity of the waste host (Marples 1988; Lutze 1988; Donald et al. 1997; Stefanovsky et al. 2004; Ojovan & Lee 2005c). These include:

- High waste loading capacity (capability to incorporate most elements into their structure): significant reduction in geological reposition costs.

- High chemical durability: Low leaching rates; environment protection.
- Low formation temperature: to incorporate volatile Cs-135 and Sr-90.
- High thermal stability: Resistance to radiation and heat damage.
- Cheap production technology.

Depending on the nature of waste, bitumen, cements, glasses, ceramics, and glass-ceramics are currently employed as hosts for immobilisation. In this thesis, the nuclear wastes immobilized in glasses have been considered in detail.

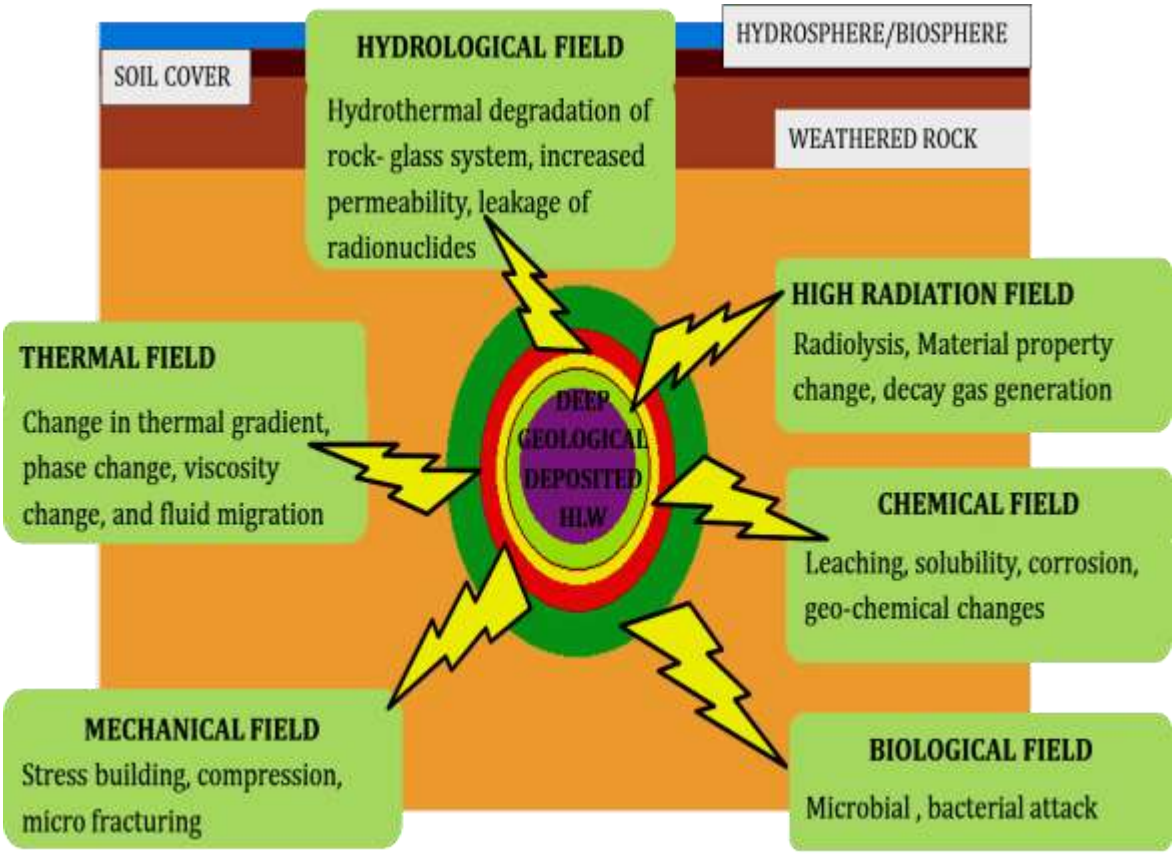

Figure 2.5: Schematic diagram showing environmental complexity associated with radioactive waste glass in a deep geological repository system.

2.3.3.1 Immobilisation of LLW and ILW in Bitumen and Cement

Bituminisation and cementation are the two main techniques used for containment of LLW and ILW (illustrated in Table 2.4).

Technique	Bituminisation	Cementation
Method of immobilisation	Embedding (IAEA 1993) (Ojovan & Lee 2013)	Encapsulation (Frizon & Cau-dit-Coumes 2006)
Material Host	Bitumen (high molecular weight hydrocarbon) (Nikiforov et al. 1986) (Ojovan & Lee 2005)	Portland Cement (Glasser & Atkins 1994) Special cements (Crawford et al. 2011)
Production cost	Low	Low
Chemical stability	Inert in water	Requires high pH environment
Radiation resistance	Low (irradiation assisted cracking)	High
Other disadvantages	Combustible Low waste loading (Guzella & Da Silva 2001)	Low waste loading Swelling (Matsuda et al. 1992)

Table 2.4: Bituminisation and Cementation key features for LLW and ILW immobilisation

These methods have been widely accepted by U.K., France, Belgium, U.S. and Finland to treat its LILW inventory. For production of cement based wasteform, ordinary Portland cement is mixed with activated alkali slag and pulverised fuel ash at a low processing temperatures which ensures retention of volatile radionuclides (Xuequan et al. 1991; Plecas et al. 1992). However, disadvantages such as swelling upon radiolysis and instability in inert environment are related to this method.

Bitumen based wasteforms primarily consist of bitumen as the waste binder. Bitumen (IAEA 1970; IAEA 1993; Ojovan & Lee 2005) is defined as a mixture of high molecular weight hydrocarbons including resins, asphalts and aromatic oils. Though, more expensive choice as a binder for the nuclear waste in comparison to cements, these provide better resistance to leaching, microbial attack and tolerance to pH variations.

2.3.3.2 Immobilisation of Nuclear Waste Through Vitrification

The process of incorporating the radionuclides in a glass matrix and melting at suitable temperatures to form a solid glassy waste form is termed vitrification (Chapman & Buelt 1978; Barrere 1978; Advocat et al. 2008). This route ensures atomistic bond formations between the species and the glass network bonds in a disordered fashion which has several advantages (Marples 1988; Lutze 1988; Vienna 2010; IAEA 1992; Ojovan & Lee 2011):

- Accommodation of a vast array of elements within the structure.
- Waste forms are durable and environmentally stable over long-time durations.
- Tolerant to impurities and can be reliably reproduced.
- Huge waste-volume reductions.
- Provide containment for up to 10 half-lives of the incorporated waste elements from biosphere.

The process of vitrification for waste immobilisation is mainly used for long lived wastes such as HLW and LAW. However, in some countries such as Russia and Korea, this route has also been used / opted to treat LLW and ILW (Lifanov et al. 2004; Sobolev et al. 2005; Sheng 2004; Sheng et al. 2000). HLLW slurry is concentrated and calcined to remove water and nitric acid and decompose nitrates to oxides using calcining agents.

The oxides react with the glass forming additives at temperatures of < 1200^{o}C resulting in a homogeneous waste containing glass melt that is poured out from the melter into stainless steel canisters and cooled to form the vitrified waste glass. The melt is filled up to 90% in the containers to keep room for decay heat generated by radionuclides and cooled for at least 24 hours before having a lid welded in place. These containers are further decontaminated in an ultrasonic bath of dilute nitric acid, rinsed with water, checked for any activity on the outer surface via swabbing, and then transferred to the interim waste storage facility to cool for several years until ready for final geological reposition (IAEA 1988; Raj et al. 2006; Bradley & Schneider 1990). The off gases produced in the calciner and melter also go through vigorous de-contamination and recycling before being discharged out through a ventilated system (Baehr 1989; Ojovan & Batyukhnova 2007). Vitrification is either one stage where the calcination and melting procedures occur in combination in a single melter (Figure 2.6) or two-stage (Figure 2.7) continuous process where calcination and melting occur separately in different vessels (Table 2.5).

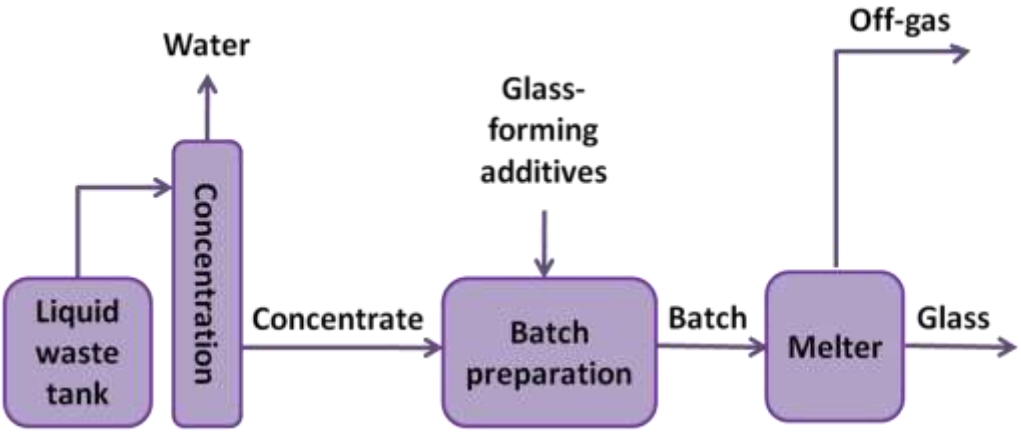

Figure 2.6: Schematic diagram of a one-step vitrification process (Ojovan & Lee 2005)

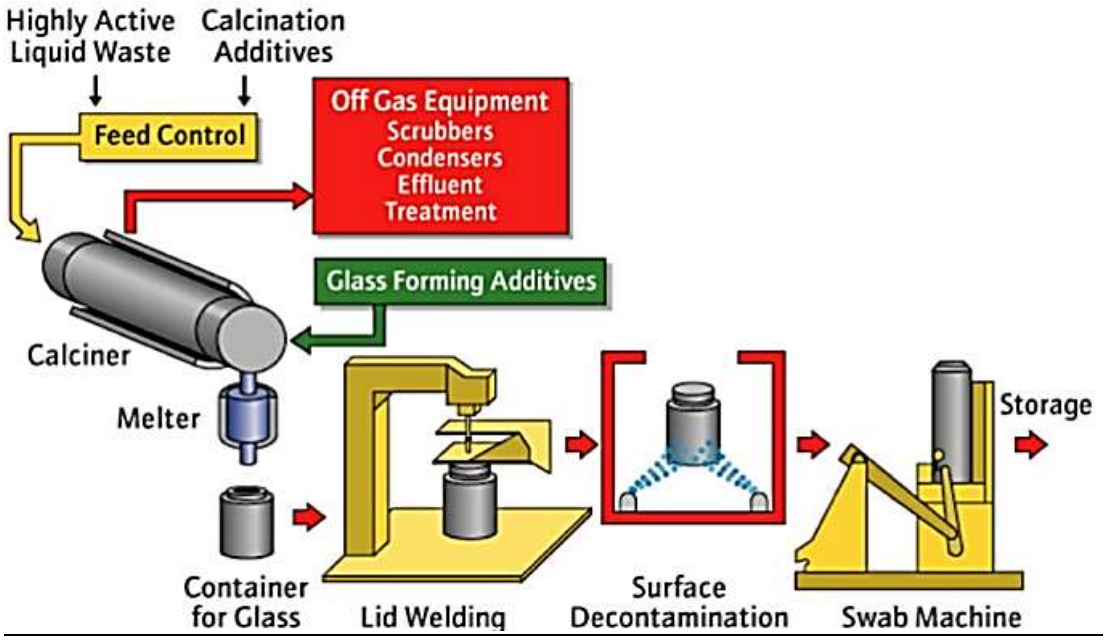

Figure 2.7: Schematic diagram of a two-step vitrification process (Riley et al. 2009)

Type of Vitrification	One Stage	Two- Stage
Process	Joule ceramic melter (Occhipinti et al. 1998) In- canister melter (Ojovan & Lee 2005) (Luckscheiter & Nesovic 1996) (Plodinec 2000)	AVM (process) – Combination of Rotary Kiln and Induction heated metal crucible (Baehr 1989) (Liberge et al. 1998)
Steps Involved	Calcination of HLW and melting with glass frit occurs simultaneously in the melter.	1. Calcination (denitration of HLW) occurs in a rotary kiln 2. Calcined waste and glass frit melted in a melter separately
Vitrification facilities	Hanford, West-valley: USA PAMELA: Belgium Tokai: Japan Trombay, Tarapur: India Mayak: Russia	La-Hague: France Sellafield: UK

Table 2.5: The two types of commercial vitrification processes.

2.4 Borosilicate Glass: The 'Preferred' Waste Host Material

The (NRC 1957) report states that the first choice of potential host to hold HLW was a pure silicate brick but the high formation temperature of 1600°C was an issue for volatile Cs and Ru present in the HLW. Around 1956, Canadian geologists synthesized an aluminosilicate glass of nephelinite syenite ($NaAlSi_3O_8$) to condition HLWs with formation temperature ~1350°C (Tait & Mandolesi 1983; Hayward, P.J.; Cecchetto 1982; Ewing et al. 1995; Bancroft 1960). Despite the high chemical durability and leaching resistance shown by aluminosilicate glasses, the research was directed towards other glass families due to the high processing temperature of aluminosilicate glasses (Harvey & Litke 1984; Melnyk et al. 1984).

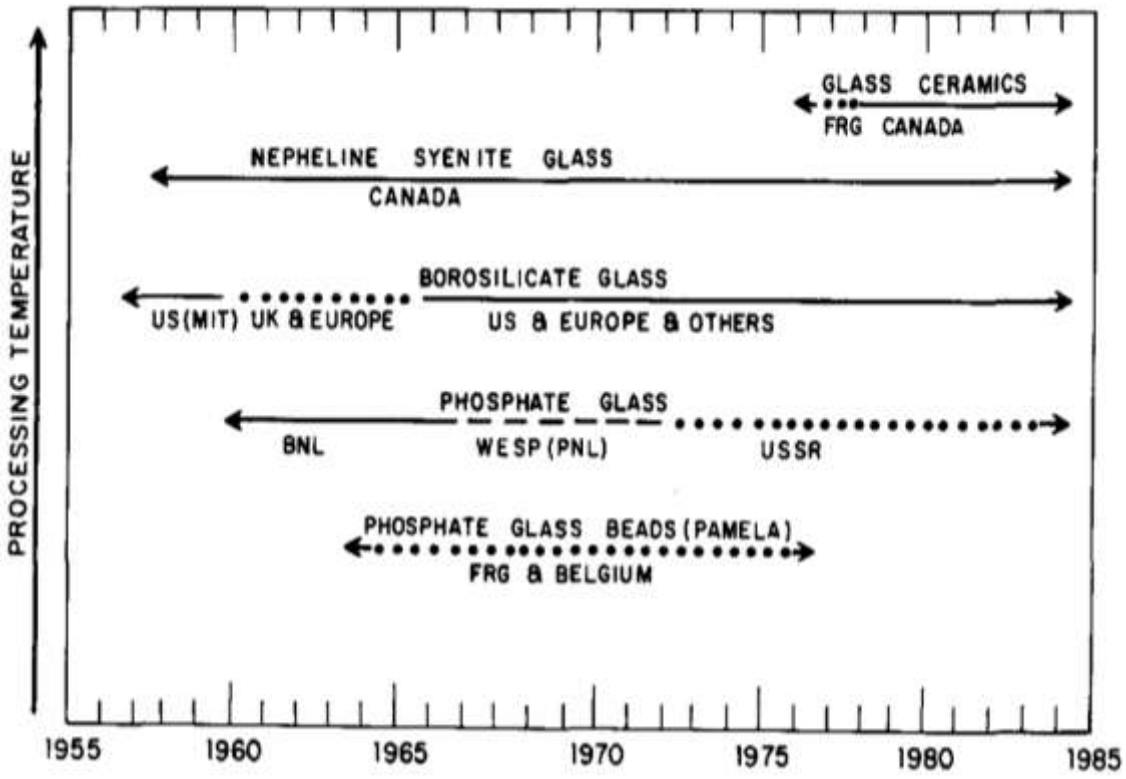

Figure 2.8: Historical development of use of glass to vitrify waste (Jantzen 1986).

Different families and compositions of glasses have been studied since before 1960 (Figure 2.8). Borosilicate and phosphate glasses both showed positive tendency towards

incorporation of a wide array of radionuclides. Though desirable for their lower fabrication temperatures and high solubility of some problematic elements in HLW (Donald et al. 2007), critical negative aspects limited the application of phosphate glasses (Donald et al. 1997; Ewing & Wang 2002):

- Highly corrosive to refractory linings
- Poor thermal stability
- Tendency to devitrify and transform to a low durability product.

Development efforts shifted to borosilicate glasses and related processing equipment (Cunnane 1994) due to the drawbacks of phosphate glasses. However, in Russia, phosphate glasses are still employed besides borosilicates for immobilization of HLW. Besides Russia, borosilicate glasses have been accepted globally as the primary waste form for HLW and some LAW (Jantzen 1986; Ojovan & Lee 2011; Bingham et al. 2009; Donald et al. 1997; Donald 2010; Marples 1988; Lutze 1988; Plodinec 2000).

The simplest borosilicate glass matrix employed for vitrification consisted of mainly Na_2O and Li_2O as modifiers. The addition of alkali oxides had a high impact on reducing the formation temperature of the waste glass which was beneficial for retention of relatively volatile radionuclides such as Cs and Ru (Roderick et al. 2000). Li_2O also reduces the electrical resistivity of the glass melt (Lutze 1988). However, the addition of the mobile alkali oxides resulted in formation of NBOs which impacted the leach rates and affected the durability of the glass (Jantzen & Plodinec 1984; Jantzen 1991; Bunker 1994). The durability was improved with small additions of Al_2O_3 to the composition. Addition of Al^{3+} ions resulted in formation of AlO_4 tetrahedra in the glass

which increases glass durability by causing the Na^+ ions to balance the charge rather than being located at the NBO sites in the matrix (McGrail et al. 2001). It also inhibited surface swelling, thereby decreasing transport rates of ions (Lyle et al. 1936; Wassick et al. 1983; McGrail et al. 1984). Small additions of ZnO and CaO to the glass frit further enhanced the corrosion resistance and chemical durability of the glass (Tait & Jensen 1982; Calestani et al. 1986; Zhang et al. 2015; Frugier et al. 2005; Smets et al. 1984). The oxides also decrease the viscosity of the glass at high temperatures (1000-1200^{o}C) (Gehlhoff & Thomas 1926).

The corrosion resistance and durability of the borosilicate glasses were subsequently improved by addition of other polyvalent elements such as Fe, Mg, Mn, etc. (Stefanovsky et al. 2004; Manaktala 1992; Ojovan & Batyukhnova 2007; Donald et al. 1997) which were tailored depending on the type of waste inventory to be vitrified. For example.- The U.S. Hanford HLW inventory has high concentrations of alumina (Kupfer et al. 1998; Joseph et al. 2009; Goel et al. 2012). Therefore, no additional Al_2O_3 is added to the base glass.

A typical industrially used borosilicate waste glass comprises 20 - 30 oxides (including glass additives and waste oxides) with significant presence of SiO_2, B_2O_3, Na_2O, CaO, Al_2O_3, Li_2O. The complex structure ensures to blocking of the diffusional pathways for radionuclides, thereby reducing the mobility of the waste elements inside the glass. Table 2.6 gives the compositions of some of the commercially used HLW glasses worldwide.

Besides the structural complexity, there are other distinguishing properties which led to the selection of borosilicate glasses over other glass families:

- More than 30 oxides, FPs, mAs and MAs constituting the calcined waste are incorporable in the glass matrix (Marples 1988; Manaktala 1992).
- Due to the presence of several modifier oxides, the processing temperatures are reasonably low (< 1200^{o}C) making it suitable to retain the semi-volatile elements such as Cs, Ru, Tc, Se etc. This also reduces the viscosity of the melts (Roderick et al. 2000).
- The corrosion resistance, mechanical strength, radiation stability and thermal stability of the glasses have been examined using various tests over several years. Borosilicate glasses showed highest resistance and sustainability when subjected to the tests (Cunnane 1994; Cunnane & Allison 1993; Plodinec 2000; Roderick et al. 2000; Marples 1988; Lutze 1988; Ramsey 1995).
- High waste loadings were achievable with borosilicate glasses ~30 wt%. This reduced the final waste volumes to be stored in the geological repositories.

Vitrification with borosilicate glasses has significant advantages over any other waste host but a major drawback lies with incorporation of elements present in the HLW such as S, Cl, Mo, I, etc. which are poorly soluble in the glass matrix and create issues during vitrification (Chapter 3) (Marples 1988; Lutze 1988; Lee et al. 2006; J.D. Vienna et al. 2004; Hrma et al. 2002; Donald 2010). This behaviour is difficult to understand as the waste and waste host, both are compositionally complex and due to the disordered nature of the host network, no single spectroscopic technique can give a clear insight into the independent effect of one element inside the whole structure. The complex composition also makes it challenging to investigate if the glass melts are entirely homogenous and whether the glass decomposition is only diffusion controlled or requires nucleation (Chick et al. 1981).

Waste Glass	Waste	Country	SiO_2	Li_2O	B_2O_3	Al_2O_3	CaO	MgO	Na_2O	Others	Waste Loading
R7/T7	**HLW**	**France**	55.0	2.4	16.9	5.9	4.9	—	11.9	18.8	< 28
DWPF	**HLW**	**USA**	49.0	3.0	8.0	4.0	1.0	2.0	12.0	27.1	< 33
Hanford	**HLW**	**USA**	59.7	—	14.2	—	3.00	—	11.2	11.9	< 25
Hanford	**LAW**	**USA**	43.2	4.1	10.0	8.6	7.3	3.1	7.9	18.7	< 30
MW	**HLW**	**UK**	47.2	—	16.9	4.8	—	5.3	8.4	17.4	< 32
K-26	**LILW**	**Russia**	43.0	—	6.6	3.0	13.7	—	23.9	9.8	< 35

Table 2.6: Compositions of selected radioactive waste glass compositions in wt % (Stefanovsky et al. 2004; Ojovan & Lee 2011; J.D. Vienna et al. 2014; Frugier et al. 2005). "Others" column includes oxides such as TiO_2, ZnO, Fe_2O_3, etc.

Of all these problematic elements, this thesis focuses mainly on understanding the sulphate solubility determining factors inside such glasses using various spectroscopic techniques and conducting comparative studies. The solubility governing factors once understood, will encourage the industry to develop modified waste glass compositions with higher sulphate solubility. The sulphur issue in a waste glass is explained in the next chapter.

Besides sulphate, the impact of chloride doping on glass compositions similar to those prepared to understand the effect of sulphate additions, was co-investigated. Due to very high volatilisation losses incurred for chloride doped glasses, this element has not been vastly discussed in this thesis.

CHAPTER 3

SULPHUR AND CHLORINE IN GLASS

3.1 Brief Overview

As stated in Chapter 2, Table 2.2, Na, K, Li, Ca, Mg, Fe, S, F, and Cl can be present in the HLW and LAW as 'process additives'. A process additive should not be mistaken for a by-product of the fission chain reactions and radiation decays occurring in the spent fuel or with the residue of fuel rod components after chopping and decladding. These get incorporated in the waste at various stages of the back end of the nuclear fuel cycle, mainly during reprocessing, but may also be present as impurities in the raw materials used for the preparation of waste glass frit. (IAEA 1992). Of these additives, S, Cl, Na, Fe, if present in substantial amounts in the spent fuel, can make the waste streams 'problematic' to be processed with the commercially available immobilisation technology in borosilicate glasses (IAEA 2007; Kent et al. 2017). Though extensive research is being undertaken to develop new waste hosts which can hold the additives effectively, any adaptations to the current routes will be expensive, in the short term.

Our research largely focusses on the study of the issues related to the presence of high sulphur concentrations in some HLW and LAW waste streams; understand the factors governing sulphur retention / non-retention in the simple and commercial waste glasses and implement the understanding to develop glass compositions that can more readily incorporate such waste streams.

The chapter also includes relevant literature for the chloride rich radioactive wastes and the issues related with its immobilisation. Since further in this thesis (Chapter 8), the author has not investigated the effects of addition of Cl^- on the chemical properties of the glass; therefore, the literature discussed in this chapter majorly focusses on the origin of chloride containing radioactive waste, the drawbacks of current waste glasses to immobilise such waste and the structural studies undertaken previously by other research groups in order to study the structural environment around chloride anions present in the glass.

3.2 Interest of Glass Industry in Sulphur

Sulphur is an element of interest to be studied by not only the waste vitrification industry but also commercial glass industry and geologists. Where the commercial glass industry uses sulphate to accelerate melting in the glass batch and produce a homogenous melt of its soda-lime glass compositions, it also acts as a refining agent to remove gas bubbles from the melt (Arkosiová et al. 2008; DiBello 1989; Hujova & Vernerova 2017). Sulphur is also used as sulphide by the coloured glass industry to provide a distinct amber colour (Beerkens & Kahl 2002) to the art glasses. Sulphur solubility in silicate magmatic systems is of interest to the geologists and the environmentalists due to atmospheric release of vast amounts of SO_2 during volcanic eruptions (Devine et al. 1984; Katsura & Nagashima 1974).

3.2.1 Sulphur in Radioactive Waste

Sulphur enters the waste streams as sulphate (SO_4^{2-}) through the reprocessing route. Sulphur based chemicals are added to high level liquid wastes (HLLW) and low activity

miscellaneous wastes (LAW) for various purposes (described in section 3.1.3). The concentration of SO_4^{2-} varies in the radioactive waste across the globe depending on the routes adopted for fuel reprocessing. Table 3.1 states the compositions of HLLW from some key vitrification facilities with significant sulphate concentration. The sulphate rich LAW produced in US DWPF is stated in Table 3.2.

Waste components	**Savannah River**	**Hanford**	**West Valley**	**Idaho Falls**	**Lanchow**	**Trombay**	**PAMELA-LEWC**
	USA	**USA**	**USA**	**USA**	**China**	**India**	**Belgium**
Waste	**HLW**	**HLW**	**HLW**	**HLW**	**MW**	**HLW**	**HLW (cemented)**
Al	7.7	1.5	3.9	4.2	4.5		44
Na	5.9	4.1	10.3	3.1	31	6.6	1.9
K	0.3	-	0.1	0.9	0.6	0.2	-
Mg	0.2	-	0.3	-	-	-	-
Fe	29.7	6.1	20.6	-	13.5	0.5	1.3
Ni	2.8	0.6	0.5	-	2.9	0.1	-
Cr	0.3	0.1	0.3	-	1.2	0.1	0.1
Mo	0.2	0.2		-	0.7		-
Zr	0.6	3.4	0.4	11.4	0.7		-
Hg	1.8	-	-	-	-	-	2.8
Cl	0.9	0.1	-	-	-	-	-
SO_4^{2-}	3.00	0.2	1.1	2.6	4.8	9.95	3.2
NO_3	4.2	2.8	20.6	12.5	-	4.1	-
FPs	< 3.0	< 2.5	< 1.5	< 1.0	2.7	1.1	0.5
TRU	< 0.2	< 0.1	< 0.2	< 0.1	17.9	8.77	0.1

Table 3.1: HLLW compositions containing SO_4^{2-}(g L^{-1}) treated at various WVP's around the world.(Courtesy: (IAEA 1992; Sengupta et al. 2013; Billings & Fox 2010))

Oxide (wt%)	**Hanford USA**
Waste	**LAW**
Al_2O_3	4.4
Cl	0.6
Cr_2O_3	0.4
K_2O	-
MoO_3	-
Na_2O	75.3
P_2O_5	7.7
SiO_2	0.5
SO_3	9.5
Other	-

Table 3.2: LAW waste concentration with SO_3 concentration > 7wt% treated at Hanford, USA (Kim & Day 2003; J.D. Vienna et al. 2004)

As understood, high level of SO_4^{2-} in nuclear waste is an issue for countries such as India (Kaushik et al. 2006; Mishra et al. 2008), China (Li-Jun et al. 2009), Belgium (legacy waste) (Hohlein et al. 1986), USA (Kim et al. 2003; J D Vienna et al. 2004; Merrill et al. 1994; Billings & Fox 2010) and Korea (Sheng 2004). Belgium and China have stopped vitrification of their sulphate loaded HLLW in glass and are looking for alternate ways to treat it. France's LLW - ILW have considerable amounts of SO_4^{2-} present, but the country has chosen the route of bituminisation and cementation for its treatment (Marion et al. 2009; Frizon & Cau-dit-Coumes 2006; Pacary et al. 2008).

3.2.2 Origin of Sulphate in Nuclear Waste

Listed below are some of the chemicals responsible for high levels of sulphate in final waste streams.

(i) **Ferrous sulphamate [Fe $(NH_2SO_3)_2$]** : most commonly used reducing agent for the conversion of Pu^{4+} to Pu^{3+} during solvent extraction (PUREX) process HLLW. (P.K. Dey & Bansal 2006; Marion et al. 2009; IAEA 2007; Tison & Bretault 2006; Gray et al. 2015; Jantzen et al. 2005).

$$\mathbf{Pu^{4+} + Fe(NH_2SO_3)_2 \rightarrow Pu^{3+} + Fe^{3+} + 2NH_2SO_3^-}$$

While Fe^{3+} ions act as reductants, sulphamate is a holding reductant and reacts with nitric acid in the acidic waste stream to produce sulphuric acid.

$$\mathbf{HNO_2 + NH_2SO_3H \rightarrow H_2SO_4 + N_2 + H_2O}$$

If NH_2SO_3H was not present, nitrate will autocatalyze Fe^{3+} oxidation and block Pu^{4+} conversion. Thus, excess of ferrous sulphamate was used to ensure complete reduction.

- La Hague, France and Sellafield, UK used Ferrous sulphamate as reductant for conditioning of HLLW till 1970. They later switched to use of uranous nitrate (UIV) with hydrazine and Hydroxyl Ammonium Nitrate (HAN) instead. Their current HLW is clear of any substantial amount of SO_4^{2-}.

- India recently (2013) modified its PUREX process by replacement of $Fe(NH_2SO_3)_2$ with a combination of UIV and hydrazine for its HLW streams (Natarajan 2017; Sengupta et al. 2013). The current HLW stored in Trombay, India has as high as 9 g L^{-1} of SO_4^{2-}.

- ❖ Since 1996, the Savannah River Site (SRS), USA HLW does not have high amount of SO_4^{2-} as majority of it is washed off from the HLW before vitrification. The Sludge Batch 3 (SB3) and Sludge Batch 4 (SB4) streams from its Defence Waste Processing Facility (DWPF) are, however, loaded with SO_4^{2-} due to the SRS Pu separations with $Fe(NH_2SO_3)_2$. (Jantzen et al. 2005; Fox et al. 2006; Lorier et al. 2005; Billings & Fox 2010).

(ii) **Amberlite IRN77, Amberlite IR120 resins**: These are cationic exchange resins with a ($-H^+ - SO_3$) sulphonic acid functional group. In US reactor facilities, resins are employed for purification of water in reactor basins / tanks where used fuel rods are stored to remove TRU's. The spent ion resin is characterised as LAW (mixed levels of low radioactivity) by SRNL, Hanford, USA and is high in sulphate. Those are vitrified by SRNL, Hanford, USA and Korean NPPs in a borosilicate glass matrix. (Sheng 2004; Hamodi & Iqbal 2009; Vienna 2010; Cicero et al. 1995; J.D. Vienna et al. 2004). The waste glass compositions for vitrifying such waste include V_2O_5 in their batch which has remarkably increased SO_4^{2-} incorporation (Aloy et al. 2006).

(iii) **$BaSO_4$**: is used for co-precipitation of strontium (^{90}Sr) to decontaminate LILW streams which cannot be concentrated by evaporation in France. Significant quantities (2 – 20 gL^{-1}) of $BaSO_4$ are used to purify streams containing the radioactive ^{90}Sr. Currently such waste is treated through bituminisation/ cementation in France (Marion et al. 2009; Pacary et al. 2008; Frizon & Caudit-Coumes 2006).

3.2.3 Sulphate Solubility in Borosilicate Waste Glass

Sulphur dissolves in the borosilicate melt as SO_4^{2-} under oxidising conditions or as sulphide (S^{2-}) under reducing conditions (Fincham & Richardson 1954; H.D. Schreiber et al. 1987; Schreiber & Stokes 2002).

$$SO_2\,(g) + ½\,O_2\,(g) + O^{2-}\,(melt) \leftrightarrow SO_4^{2-}\,(melt)\ \Delta H < 0$$

$$SO_2\,(g) + O^{2-}\,(melt) \leftrightarrow S^{2-}\,(melt)\ \Delta H > 0$$

Since the waste melter processing conditions are never intentionally reducing, our studies focus on solubility of sulphur as only SO_4^{2-} in the glasses. (Stefanovskii 1993) stated that sulphate capacity of any vitreous matrix is highly dependent on the compatibility of the chemical parameters of the participating cations in the host with sulphate anions. These chemical parameters are: cation-oxygen binding energy, cation field strength, size and polarization of the polyhedrons, and chemical bond strength. As per these considerations, a cation distribution series was generated in decreasing order of its compatibility with a sulphate tetrahedron.

S^{6+} (IV) – P^{5+} (IV) – V^{5+} (IV) – B^{3+} (III) – Si^{4+} (IV) – B^{3+} (IV) – Al^{3+} (IV) – Zn^{2+} (IV)

In accordance with the series, phosphate tetrahedral shared better compatibility with sulphate than a similar silicate. This was proven by the work of Radon Russian research group (Stefanovsky et al. 1995) through production of some alumino-phosphate glasses with very high sulphate capacities (up to 12 mol% SO_3).

Salt Phase (Yellow phase): High concentrations of SO_4^{2-} show poor solubility inside a borosilicate waste glass matrix. (< 1 wt% of SO_3 in glass) (Darab et al. 2001; Li et al. 2000; Sullivan et al. 1995; Hrma et al. 2002; J.D. Vienna et al. 2004; Billings & Fox 2010; Fox et al. 2006; Schreiber & Stokes 2002). The excess SO_4^{2-} forms an immiscible

sulphate salt layer that floats on the top of melt. The salt layer at times has a yellowish green appearance due to the presence of chromate (known as 'yellow phase') (Figure 3.1) (Marples 1988; Mishra et al. 2008; Goel et al. 2013; Greer & Kroeker 2012). The salt layer is highly undesirable as it is typically rich in alkali / alkaline earth sulphates (Kim & Day 2003) which overtime solubilise in groundwater.

Figure 3.1: "Yellow phase" salt formation in a US LAW simulant glass developed in MERI, Sheffield Hallam University

There are many potential problems associated with the yellow phase, the most important being low waste loading in the glass (maximum is approximately 25-30%.) On addition of SO_4^{2-}, the waste loading decreases to as low as 11% , thus increasing the waste volume by 30% (Aloy et al. 2006; Vienna 2010). The other issues related to salt formation are (Bickford et al. 1990; Plodinec & Wiley 1979; Jahagirdar & Wattal 1998; J.D. Vienna et al. 2014; Jantzen et al. 2005; Kim & Hrma 1991; Billings & Fox 2010):

- Corrosive to the melt linings that encounter the salt.
- Obstructs release of gas bubbles during vitrification.
- Reduces efficiency of melting due to high thermal and electrical conductivity.
- Increases waste swelling, thus volume.
- Provides pathway for Tc/ Cs/ Sr partitioning into salt, creating volatilization issues.
- Water-soluble salt can release radionuclides into the groundwater over time.

3.2.4 Possible Solutions

To avoid or remove the immiscible sulphate loaded slag there are three alternate choices:

- Decompose the sulphate segregated layer at a sufficiently high temperature to release the consequently generated sulphur-containing gases through a suitable gas-treating apparatus.

  Challenge: This solution will not only increase the complexity of the off-gas treatment technology in use but also add huge costs towards procedure upgrades.

- Develop enhanced / alternate technologies to reduce the amount of sulphate going to the vitrification facility.

  Challenge: Though countries like Russia and China are focussing on techniques such as encapsulation of SO_4^{2-} before vitrification, transmutation of SO_4^{2-}, addition of SO_4^{2-} reducing microbes in spent resin streams to tackle the issue (Sheng 2004; Sobolev et al. 2013), but those are not yet well researched and developed. Russia is currently immobilising such waste in sodium aluminophosphate glass matrices which provide higher sulphate solubility (Stefanovsky et al. 1995; Day et al. 2002; Vashman & Polyakov 1997; Bingham & Hand 2008), but development of similar phosphate waste glass plants is not economically viable at present.

- Improve the vitrification process by developing waste glass compositions with improved sulphate capacities.

  Challenge: It is highly complex to understand the solubility governing factors of sulphate anions in the commercially used glasses, as their compositions may contain >20 elements in one matrix in appreciable concentrations. Many of these

elements can have mixed influences on sulphate retention (Ooura & Hanada 1998; Papadopoulos 1973; Bingham & Hand 2008).

3.2.5 Research Approach for Sulphate Studies

Determination of sulphate capacity of a glass melt is a complex phenomenon and over the years many researchers have tried to establish relationships between sulphate solubility and compositional, physical and chemical parameters associated with the glass melt such as redox conditions, degree of polymerisation, modifier to former ratio, viscosity and optical basicity. We have divided this work in three aspects: a) compositional dependence on sulphate solubility b) structural changes on sulphate addition and c) empirical models devised to predict sulphate solubility.

3.2.5.1 Composition Dependence on Sulphate Solubility

In 1966, Holmquist (Holmquist 1966) investigated a series of Na_2O-SiO_2 binary silicate glasses with varying SiO_2 / Na_2O ratios. As per his observation, the amount of sulphate retained within the glass dropped from 4 to 0.1 wt % with an increase in the SiO_2 / Na_2O ratio from 1.5 to 2.5. Therefore, it was concluded that sulphate solubility was strongly affected by the concentration of modifier oxide in the glass.

In 1973, Papadopoulos (Papadopoulos 1973) further investigated the case of SO_3 solubility in soda-lime-silica melts as a function of composition, temperature and atmospheric conditions. His work re-affirmed that under an oxidising atmosphere, with decreasing SiO_2 content, and with increasing Na_2O replacement for CaO at a given SiO_2 level, sulphate solubility increased.

Through his experiments, he proposed the first sulphate solubility model that was based on the activities of BO, NBO and free oxide ions present in the glass melt. Under equilibrium, the BO [O^0], NBO [O^-] and free oxide ions [O^{2-}] are related with the Equation 3.1.

$$O^o + O^{2-} \overset{K_a}{\leftrightarrows} 2O^- \qquad \text{Equation 3.1}$$

Where, K_a is the equilibrium constant.

SO_4^{2-} decomposes in to free oxygen ions and SO_3 in the melt as per Equation 3.2.

$$SO_4^{2-} \overset{K_b}{\leftrightarrow} SO_3 + O^{2-} \qquad \text{Equation 3.2}$$

Therefore, on combining Equations 3.1 and 3.2, a relationship is established between [SO_4^{2-}] and [O^-] and [O^0] given by Equation 3.3

$$[SO_4^{2-}] \propto \frac{P_{SO_3} * [O^-]^2}{K_a K_b [O^o]} \qquad \text{Equation 3.3}$$

Where $\left[SO_4^{2-}\right]$ is the sulphate solubility within the glass. P_{SO3} is the partial pressure of SO_3 in the melter.

Papadopoulos (1973) suggested that a linear relationship existed between sulphate solubility and the ratio of $[NBO]^2$ / [BO] for any glass if the melt pressure is kept constant. This ratio could be readily adjusted by increasing the modifier content in the glass melt, thereby enhancing the sulphate solubility.

The relationship was validated in 1998 by Ooura and Hanada (Ooura & Hanada 1998b) through their work on R_2O-SiO_2 (where R = Li, Na, K) and Na_2O-MO-SiO_2 (where M = Ca, Ba, Mg, Sr, Pb and Zn) glasses. Not only did the sulphate solubility enhance with increase in Na_2O content but it also increased with change in the species of MO for a given Na_2O and SiO_2 level in the ternary glasses (Figure 3.2). The trend followed was:

$$BaO > SrO > PbO > CaO > MgO > ZnO$$

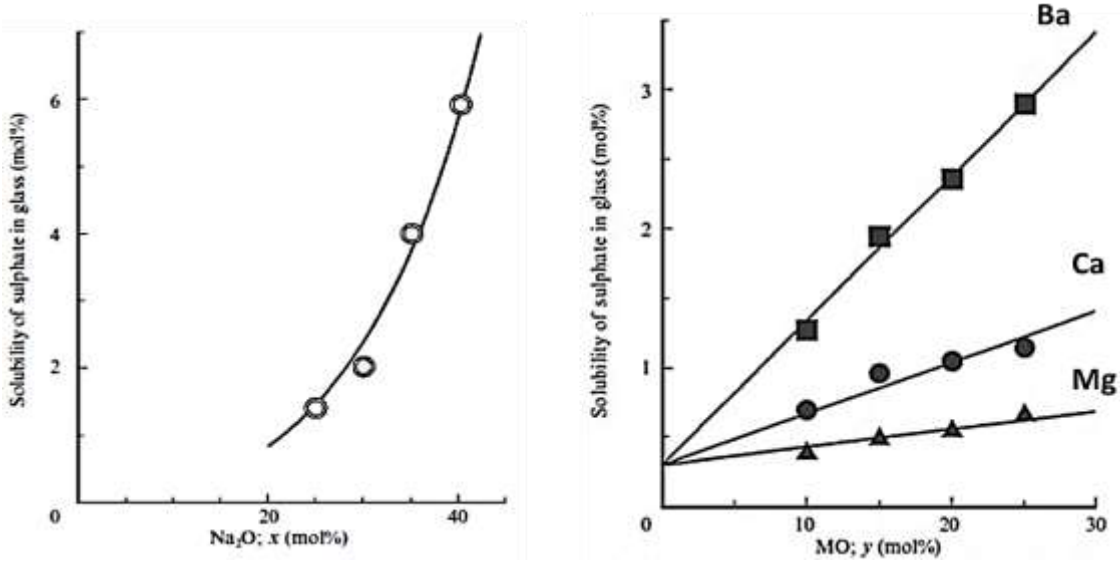

Figure 3.2: (left) Dependence of sulphate solubility (mol %) on Na_2O content in binary (100-x) SiO_2. x Na_2O glass. (right) Dependence of sulphate solubility on MO content in (85-y) SiO_2. y MO. 15 Na_2O glass (Ooura & Hanada 1998)

This might be due to the larger cations having a stronger depolymerisation effect on the glass network due to creation of higher number of NBOs. To summarise, the findings of Holmquist, Papadopoulos and Oooura and Hanada suggested that sulphate solubility not only depends on $[SiO_2]$ / $[MO_x]$ ratio but also on the nature of the participating MO_x.

In recent years, a series of sodium-barium borosilicate glasses were investigated by the Indian Waste Management Research Division, BARC, for purpose of vitrification of sulphate bearing HLW containing as high as ~10 wt% SO_3 generated at their Tarapur

nuclear plant, India (Kaushik et al. 2006; Mishra et al. 2008). The composition was chosen following the work of (Ooura and Hanada, 1998) on Na_2O-MO-SiO_2 (M= Ca, Ba, Mg, Sr, Pb and Zn) where Na_2O-BaO-SiO_2 showed the maximum sulphate retention. The choice of barium over other alkaline earth elements such as calcium or magnesium was mainly supported by the fact that larger Ba^{2+} ions lead towards higher degree of depolymerisation in glass network than Ca^{2+} or Mg^{2+} (Ramkumar et al. 2009). This implied that the waste loading could be enhanced in barium containing borosilicate glasses and higher amount of sulphate could be incorporated. Moreover, even if the sulphate is not fully incorporated in the glass network, it would form a crystalline layer of $BaSO_4$ on the surface which is the most chemically stable naturally occurring crystalline sulphate and is insoluble in water. This can provide long term reliable barrier for the radionuclides to disperse in groundwater (Mishra et al. 2008; Dera et al. 2017). Through their studies they successfully achieved SO_4^{2-} incorporation up to ~3 mol% in a sodium-barium- borosilicate glass matrix without any phase separation (Figure 3.3).

Encouraged by the lab-scale studies, a commercial plant scale sodium barium borosilicate glass (reference code: SB-44: Na_2O ~10mol%, BaO ~20 mol%, B_2O_3~ 20 mol%, SiO_2 ~30 mol %) with waste loading ~20 mol% was successfully fabricated at ~925^oC without any crystalline sulphate phase separation (Kaushik et al. 2006). The addition of Ba^{2+} also enhanced the ability of the borosilicate glass to withstand X-ray and γ-ray radiation (Kaur et al. 2013; Tuscharoen et al. 2012; Kaewjaeng et al. 2012) and the low fabrication temperature improved retention of volatile elements such as Tc and Cs in the host matrix.

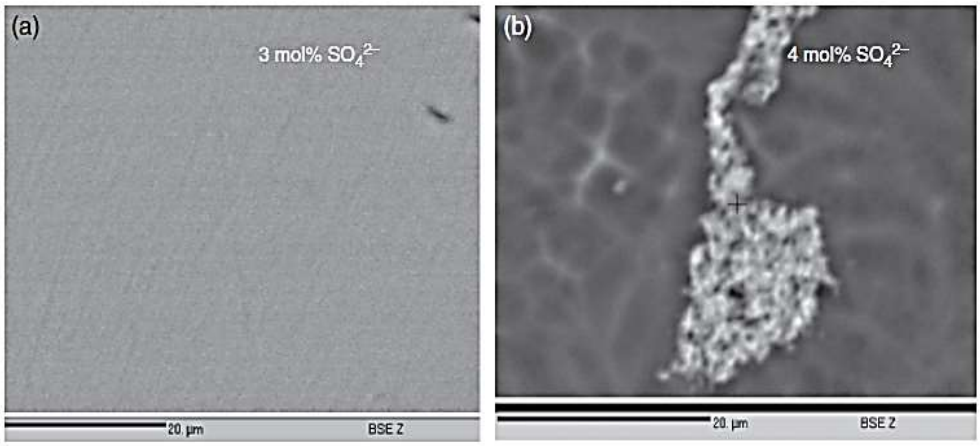

Figure 3.3: Backscattered electron images of sodium barium borosilicate glass sample with 3 (left) and 4 (right) mol% SO_4^{2-} incorporated to matrix show that beyond 3 mol% , sulphate phase separation occurs ((Mishra et al. 2008)

Besides barium, other multivalent cations were also investigated to study their effect on sulphate solubility. (Manara et al. 2007) investigated a series of borosilico-vandate glasses to investigate if addition of V^{5+} ions enhance the sulphate solubility similar to analogous pentavalent P^{5+} ions which have similar crystallo-chemical features. The authors identified that small additions of crystalline V_2O_5 enhanced sulphate incorporation upto 0.9 wt% and attributed this behaviour due to acceleration in the kinetics of sulphate dissolution with addition of the pentavalent ions. However, when (McKeown et al. 2002) conducted EXAFS and XANES studies on these sulphate doped borosilico-vandate glasses, they could not detect presence of any V-S bonds or any vanadium bonded to sulphate tetrahedron. The justification behind enhanced sulphate solubility in borosilicate glasses with V_2O_5 addition is not yet clearly understood.

3.2.5.2 Structural View Towards Sulphate Incorporation

It is crucial to understand the effect of sulphate addition on the structure of the glass in order to get an insight of the properties that are required to be regulated in order to improve sulphate capacity of the glass.

As mentioned in 3.2.3, sulphur dissolves as SO_4^{2-} in the silicate glass under normal oxidising conditions. A sulphate anion is largely symmetrical. The bonds inside the complex are strongly covalent and many times stronger than a silicon-sulphur bond (Marra 1994). Therefore, SO_4^{2-} mostly associates with the neighbouring alkali, alkaline-earth cations present in the glass as modifiers and not with the silicates. Spectroscopic investigations have been carried out over years to study the sulphur environment in conventional oxide glasses. (McKeown et al. 2001; Lenoir et al. 2009; Manara et al. 2009; Tsujimura et al. 2004) through their Raman studies on sulphate doped borosilicate and silicate glasses, concluded that the modes correlating to S-O vibrations in glass spectra had similar frequencies and relative intensities as seen for Raman spectra of corresponding crystalline sulphates. The Raman spectra of a Na-borosilicate glass and a corresponding Na_2SO_4 crystal as observed by McKeown et al. 2001 is shown in Figure 3.4. The Raman studies indicated that sulphur was present in the glasses as S^{6+} in the form of sulphate anion and associated with nearest network modifier alkali ions present in glass to form sulphate clusters.

The Raman studies were further supported by the Sulphur -K edge XAFS and XANES studies conducted by (Brendebach et al. 2009; Bingham et al. 2010) on high level nuclear waste glasses and silicate glasses respectively. The comparison between the XANES of the glasses and corresponding crystalline sulphates, revealed similar environments (Figure 3.5). (Mishra et al. 2008) studied the sulphate environment in the sodium-barium borosilicate glass and concluded that the sulphate units preferred association with the larger Ba^{2+} ions than the Na^+ ions. Their result is in contrast with the investigation of (McKeown et al. 2001; McKeown et al. 2004) who concluded that the surrounding chemical environment around sulphate anions consisted of Na^+ ions

predominantly. Therefore, whether the sulphate ions prefer to associate with alkali ions or alkaline-earth ions is still unclear.

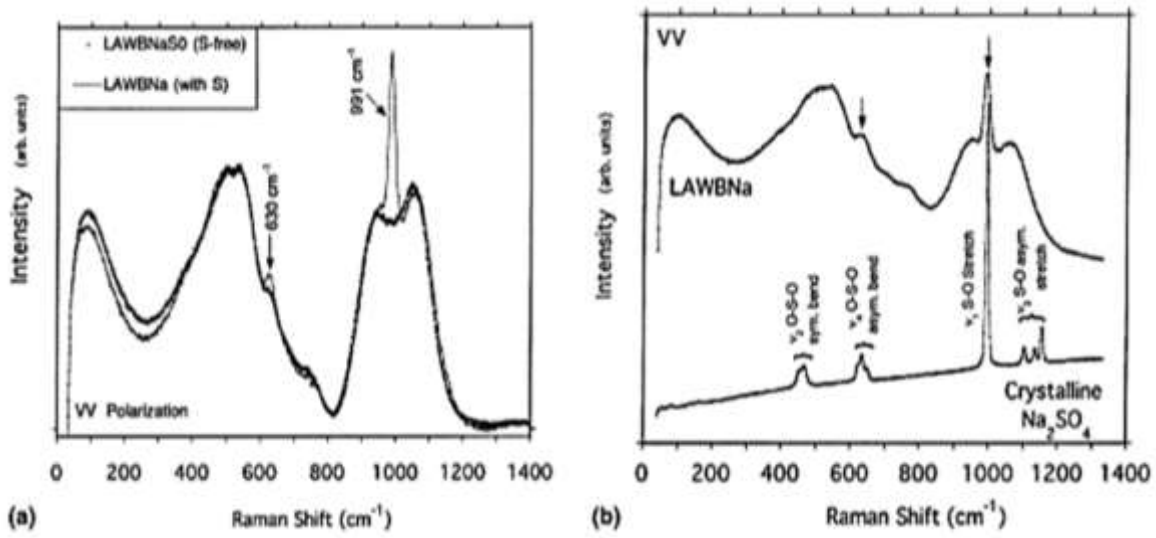

Figure 3.4: (a) Raman spectra of sulphate free and sulphate doped borosilicate waste glasses highlighting a prominent S-O stretching mode at ~990 cm^{-1} in the doped glass. (b) comparison of the sulphate doped borosilicate glass S-O band with corresponding crystalline Na_2SO_4 indicates present of sulphur as S^{6+} in the glass and association of the SO_4^{2-} ions with neighbouring Na^{2+} ions (McKeown et al. 2001).

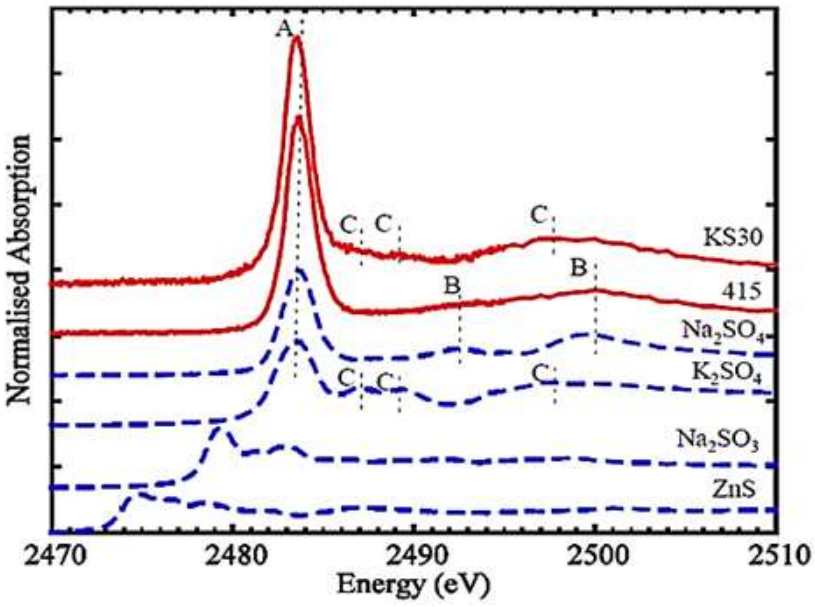

Figure 3.5: Sulphur K-edge XANES of alkali silicate glasses compared with XANES spectra of crystalline sulphates, sulphide and a sulphite compound shows similar environment within the glass and crystalline sulphate compound (Bingham et al. 2010).

3.2.5.3 Models to Study Sulphate Solubility

Several models have been suggested by various researchers to relate various chemical parameters of the glass with its sulphate capacity. The first model as stated in 3.2.5.1 was by (Papadopoulos 1973) where he proposed a linear relationship between the sulphate solubility and the $[NBO]^2/ [BO]$ ratio of the glass. The approaches by (Li et al. 2000; Jantzen et al. 2005) further illustrated linear relationships between glass composition and sulphate solubility using the concept of NBO concentrations in terms of degree of melt polymerisation and viscosity respectively.

In 2008, Bingham and Hand characterised glass compositions in terms of Normalised Cation Field Strength Index (NCFSI) to predict sulphate solubility of the glass melt. Field strength of a cation is defined as the ratio of the electronic charge on the ion over square of its interatomic distance to its anion (O^{2-} in the case of oxide melt); i.e. CFS = z/ a^2, where CFS = cation field strength of the ion; z = ionic charge and a = ion - anion (O) interatomic distance. NCFSI = $\sum(z/ a^2)$ can be therefore defined as the sum of CFS of each component present in the melt normalised to one mole cation.

The empirical model developed by (Bingham & Hand 2008) to calculate the NCFSI was used to study the normalised field strengths of phosphate and borosilicate glasses developed by the authors and also on the glasses fabricated by (McKeown et al. 2004; Manara et al. 2007; Lorier et al. 2005) to retain waste with high concentration of sulphate (Figure 3.6). A linear increase was observed in the logarithmic SO_3 solubility (mol%) with decreasing NCFSI of a glass for all the studies.

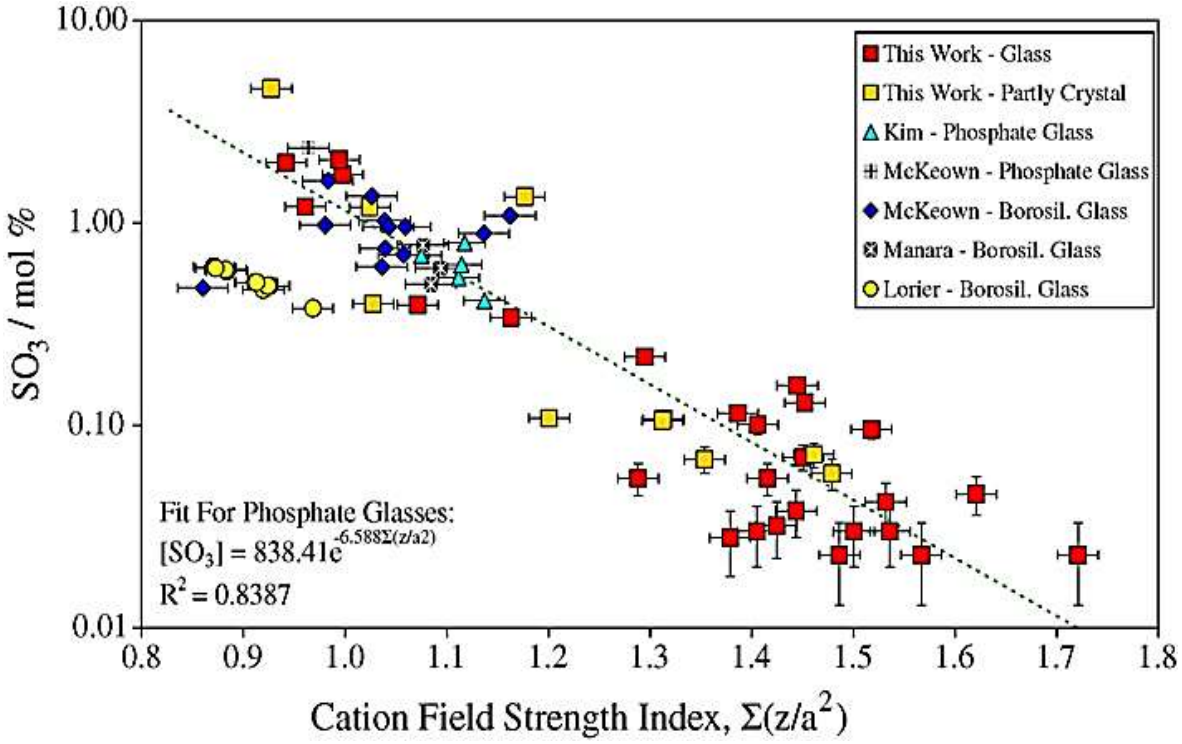

Figure 3.6: Sulphate content as a function of cation field strength index for glasses melted at 1150°C (Bingham & Hand 2008)

For our research, based on the several studies carried out so far to understand the effects of composition on sulphate solubility, we focussed on three glass families:

- Binary and ternary alkali / alkali-alkaline earth silicate glass
- Sodium / Sodium-Barium / Barium borosilicate glasses
- Multi oxide simulant borosilicate glasses with compositions similar to industrial waste glasses.

The glasses were excessively doped with SO_3 and the structural changes in the network due to the addition was carefully investigated using various spectroscopic techniques. The choice of alkali and alkaline earth modifiers to develop these glasses was inspired by pioneering work to understand SO_4^{2-} solubility as a function of various empirical

models based on glass composition dependent parameters such as fraction of Non-Bridging Oxygens (NBO) to Bridging Oxygen (BO); melt viscosity; optical basicity, cation field strength index, etc. (Table 3.3).

The referenced work in Table 3.3 has demonstrated that the amount of sulphur which solubilises within the glass is strongly dependent on glass composition. Thus, by modifying the base glass composition, sulphate incorporation can be influenced. Although this unique relationship between solubility and composition has been studied empirically, the mechanisms are not yet fully understood.

The outcomes of this research will be compared with the previous research done in order to understand the limiting factors associated with sulphate solubility and also be utilised in investigating the structural environment around the anion to aid development of modified waste glasses with enhanced sulphate capacities. Detailed compositional analysis of the modified simulant glasses will provide insight of their sulphate capacities. The information will be particularly useful to investigate their industrial applicability for vitrification operations.

Researchers	Studied glass	Approach towards understanding SO_4^{2-} solubility	Summary
Kaushik et al. (2006); Mishra et al. (2008)	Na_2O-BaO-B_2O_3-SiO_2	Partial replacement of Na_2O with BaO	Larger cations favour sulphate SO_4^{2-} solubility.
Bingham & Hand (2008)	R_xO-Fe_2O_3-P_2O_5 (R=Li, Na, K, Mg, Ca, Ba, Pb)	Cation field strength index calculations	SO_4^{2-} solubility reduced with increasing cationic field strength.
McKeown et al. (2001)	Na_2O-MO-Fe_2O_3-Al_2O_3-B_2O_3-S_iO_2 (M=Ca, Li, Ba, K, Cs) & crystalline sulphates	Comparative Raman studies of υ_1 S-O stretching peak position for glass & corresponding sulphate	SO_4^{2-} anion is closely surrounded by the alkali/ alkaline modifier and does not form bonds with the network former.
Jantzen et al. (2005)	Na_2O -Fe_2O_3-Al_2O_3-B_2O_3-S_iO_2	SO_4^{2-} solubility plotted w.r.t melt viscosity	SO_4^{2-} decreases with increasing viscosity i.e. *fn*. (NBO/BO)
Ooura & Hanada (1998)	xNa_2O-MO-SiO_2 (M=Mg, Ca, Ba) X= 10, 15, 20, 25	Composition analysis of glasses and calculation of NBO/BO	Solubility of SO_4^{2-} Mg < Ca < Ba Solubility of SO_4^{2-} increases with increasing Na_2O %
Papadopoulos (1973)	Na_2O-SiO_2	SO_3 solubility plotted w.r.t $[NBO]^2/[BO]$	Glass SO_3 capacity increases linearly with $[NBO]^2/[BO]$ of binary silicate glasses
Holmquist (1966)	Na_2O-SiO_2	Composition analysis of SO_4^{2-} w.r.t Na_2O/SiO_2 ratios	Solubility of SO_4^{2-} increases with increasing Na_2O content

Table 3.3: Summarised overview of key studies of sulphate solubility with respect to glass composition that inspired the selection of modifiers for this research (McKeown et al. 2001; Jantzen et al. 2005; Bingham & Hand 2008; Ooura & Hanada 1998b; Papadopoulos 1973; Beerkens & Kahl 2002; Mishra et al. 2008).

3.3 Chlorine in Glass

In the commercial glass industry, chloride has historically been used in the form of sodium chloride as an alternative fining agent for sodium sulphate (Volf 1984, Müller-Simon 2011, Stevenson 2012). The presence of 1.2 - 1.6 wt % Cl^- has been found in ancient Roman glasses dating back to 1st- 2nd century AD (Bingham and Jackson, 2008). In the case of commercially manufactured SiO_2-Na_2O-CaO glasses, the addition of chloride to the batch accelerates silica rich and silica deficient phase separation (Hoell *et al.* 1996, Kranold *et al.* 2001, Stevenson 2012). Typical upper limits for the chlorine content of technological (Bateson and Turner, 1939) and archaeological (Gerth *et al.*, 1998) SiO_2-Na_2O-CaO glasses are 1–1.5 wt%. In borosilicate glasses, however, the solubility of Cl^- was reported to be < 1 wt% (Marra et al. 1994; Langowski 1996).

3.3.1 Origin of Chlorine in Radioactive Waste

Chlorine is introduced as a process additive to some radioactive wastes, such as during the pyrochemical reprocessing of SNF in order to separate transuranic elements including plutonium and uranium and convert them into metallic species through electro-deposition in a molten chloride based salt medium (Coops et al. 1983; NEA 2000; Ackerman 1991; Ackerman et al. 1994; NEA 1997). Pyrochemical reprocessing is a type of electro-refinement technique in which the major actinides such as uranium and plutonium are purified by electrolytic separation from the other elements (FP, TRU, corrosion products) present in SNF (Volkovich et al. 2003; Ackerman 1991; Coops et al. 1983). During the process, SNF is chopped and loaded into an anode case. The cathode is made of solid metal, such as tungsten or cadmium. The anode/cathode are immersed in a bath of molten chloride (LiCl-KCl) salt electrolytic solution (Figure 3.7).

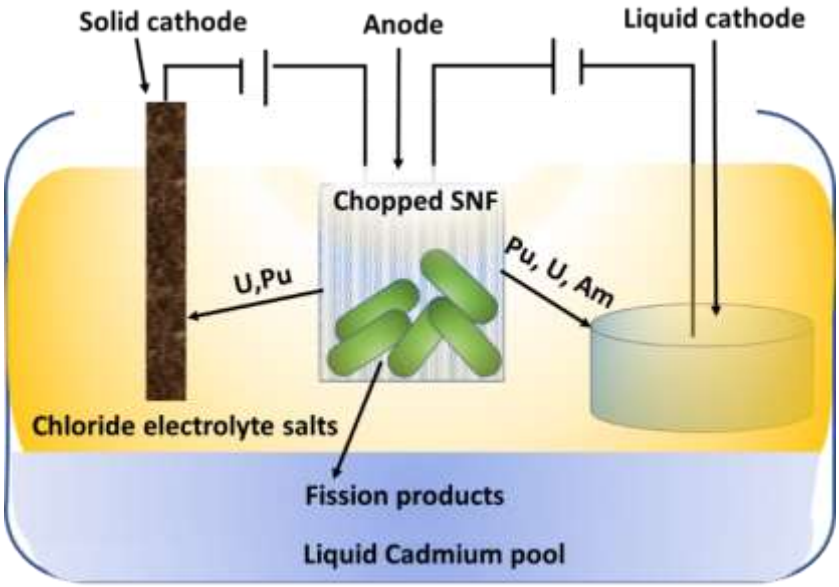

Figure 3.7: Schematic diagram of pyrochemical reprocessing of SNF to extract plutonium

Cathodes consisting of liquid cadmium in ceramic crucibles are used to harvest the balance of the actinides in the spent fuel batch (Ackerman et al. 1994). When current is passed from the anode to the cathode, electro-positive elements present in SNF are either distributed as reduced metals on the cathode, or form metal chloride in the electrolyte solution. The dense fission products transfer to the liquid metal bath at the bottom of the tank and electro-negative elements, such as noble metals, remain in the anode case. The plutonium and uranium metals can be recovered from the cathode, once the process is complete. The resultant waste stream consists of electrolytic chloride solution containing primarily molten alkali/ alkaline-earth/ rare-earth chlorides and actinides. (Schofield 2011; Langowski 1996; NEA 2000; NEA 1997).

Similarly to sulphate ions, chloride ions cannot be removed directly from the waste stream by heating the SNF as along with the metal chlorides present in the fuel, which have low boiling points and high vapour pressures, as highly volatile radionuclides such as ^{90}Sr and ^{137}Cs can evaporate (Metcalfe & Donald 2004; Vance et al. 2012; Ilyukhina et al. 2010; Schofield et al. 2009).

3.3.2 Chloride Solubility in Silicate and Borosilicate Glasses

The majority of literature related to the composition and structural investigation of halide containing glasses has been devoted to fluoride doped glasses (Kiprianov et al. 1998; Kiprianov & Karpukhina 2006; Rabinovich 1967; Carroll & Webster 1994). Reference data related to chloride ion solubility in oxide glasses is limited. Due to differences in the properties and behaviour of fluoride and chloride ions, the inferences made from the studies of fluoride-based glasses may not be applicable for chloride glass systems (Langowski 1996; Marra et al. 1994; Kiprianov et al. 2004).

The solubility of chlorine in glass primarily depends on the melt composition, besides pressure and temperature of the melt (Carroll & Webster 1994; Webster & De Vivo 2002). Researchers (Webster & De Vivo 2002) conducted an investigation of natural aluminosilicate magmatic rock glasses and suggested that chlorine incorporation in the vitreous matrix was largely affected by the type and abundance of network modifier cations (NWM) co-present with the chloride in the network. Whilst the presence of divalent cations such as Mg^{2+} and Ca^{2+} showed a strongly positive effect on Cl^- solubility; Li^+, Cs^+ were less effective in improving chloride solubility. Webster & De Vivo (2002) determined a cation association sequence with Cl^- ions in an order of improved solubility, thus:

$$Mg \approx Ca > Fe > Na > K > Al > Li \approx Rb \approx Cs$$

The order of association, as stated above, suggested that the alkaline earth elements were more influential than the alkali metals, in order to promote chloride solubility in aluminosilicate glasses. Due to the restricted compositional ranges of natural magmatic aluminosilicate rock glasses, the influence of larger alkaline earth cations such as Ba^{2+} and Sr^{2+} was not investigated.

(Kiprianov et al. 2004) developed low-alkali binary silicate glasses: (mol%) $27M_2O$-$73SiO_2$ (M= Na, K), which were doped - with 1-13 wt % of chlorine respectively. Upper limits of 3 wt% Cl^- in (M=Na) and 1.5 wt % Cl^- in (M=K) glasses were reported, with volatilisation losses ranging between 18-90%. Their results were in agreement with the NWM association series modelled by Webster and Vivo (2002), and demonstrated that the chloride capacity of silicate glasses with alkali modifiers was quite low. (Marra et al. 1994) also documented solubility of less than 1 wt% of chloride ions in alkali silicate glasses. (Kiprianov & Karpukhina 2006) suggested that poor solubility of chloride was attributable to formation of alkali chlorides with very low boiling points and high vapour pressures, which resulted in high volatilisation losses. Recently, (Chen et al. 2017) developed a series of alkali free calcium silicate bioactive glasses with high chloride solubilities (up to 27.3 mol% Cl) without noticeable phase separation. The results agreed with the suggestion of (Webster & De Vivo 2002) that Cl preferentially associates with alkaline earth metal ions over alkali metal ions in silicate glasses.

In the case of borosilicate glasses, chloride solubility of < 1wt% was achieved (Ilyukhina et al. 2010; Metcalfe & Donald 2004; Li et al. 1996; McKeown et al. 2011; Marra et al. 1994). Even though these researchers have documented minimal solubility of chloride in borosilicate glass matrices, no data, to the best of the author's knowledge, has been provided to explain this behaviour.

3.3.3 Candidate Glasses for High Chloride Retention

Clearly, borosilicate glasses did not emerge as the suitable candidate for high chloride containing wastes. Therefore new candidate wasteforms were investigated by researchers to tackle this issue. (Volkovich et al. 2003; Donald et al. 2007; Vance et al. 2012; Metcalfe & Donald 2004) suggested that replacement of the borosilicate system

with a phosphate-based network, could significantly improve the solubility of halide. Besides phosphate based glasses, aluminosilicate glasses were also studied by other researchers. (Siwadamrongpong et al. 2004) investigated chloride solubility in a range of calcium aluminosilicate glasses where the compositions were varied with change in the ratio of CaO to SiO_2 and Al_2O_3. Their glasses were developed in a reducing atmosphere and open vessels and chlorine was introduced in the melt as $CaCl_2$ (and substituted for the CaO in the glass). The resultant glasses could incorporate up to 11 mol% of $CaCl_2$ and volatilization losses incurred were minimum ranging from 0 to 10 % of the nominal value. The authors compared the fraction of NBO with the CaO content and Cl^- loading. It was concluded that Cl solubility maximised with increasing CaO content which resulted in increase in NBO fraction. In 2011, Schofield investigated a series of calcium aluminosilicate glasses doped with simulated chloride containing nuclear waste. The results were comparable to those found by Siwadamrongpong *et al.*, 2004. Both studies confirmed that over 11 mol % Cl could be incorporated in high calcium SiO_2-Al_2O_3-CaO glasses without any evident phase separation.

3.3.4 Structural View Towards Chloride Incorporation

The literature available for the research conducted on sulphate doped glass systems unanimously agrees the dependence of the anionic solubility on factors such as melting atmosphere, oxygen partial pressure, glass composition and NBO/ BO ratio. However, the research documented for chloride-based systems is diverse and contradictory. (Kiprianov & Karpukhina 2006) stated that the contradictions were justified as the melting conditions and the processes followed to introduce chlorine in the glass varied for each study. The authors predicted that a traditional glass melt where the additives are introduced as oxides, carbonates and halides had a lower halide capacity than a glass

where the metal halides substituted the oxide content in the glasses. (Takeda et al. 2003) through their work on calcium aluminosilicate glasses suggested that a dry reducing atmosphere could enhance chloride solubility. However, their suggestion of dependence of chloride solubility on melting atmosphere can be contradicted as the melting atmosphere for the calcium aluminosilicate glasses developed by (Schofield et al. 2009; Schofield 2011) was ambient and for those developed by (Siwadamrongpong et al. 2004) it was reducing. Despite the differences in the melting conditions, both research works documented similar chloride content in their glasses. This suggests that chloride solubility was unaffected by the melting atmosphere in these glasses.

Regarding the cationic bonding environment around the chloride ions incorporated in the glass matrix, several structural studies have been carried out. (Rabinovich 1967; Tsunawaki et al. 1981) detected the presence of some Si-F bonds during investigation of some fluoride doped calcium silicate glasses using Raman spectroscopy. It was suggested by the authors that Cl^- will show similar behaviour in a chloride-based glass system. (Kiprianov et al. 2004) studied a few chloride-doped low alkali silicate glasses with Electro-Paramagnetic Resonance (EPR) spectroscopy and concluded that Cl^- indeed replaced a bridging oxygen in the glass network and formed Si-Cl or Si- $(<Cl>)_2$-Si bonds in the glass. However, their proposition for chlorine bond formations with network formers has been opposed by many researchers, who suggest that chlorine associates with the network modifiers and not directly with Si or any other network former present in the glass. The relative affinity of chlorine towards the network modifier cations (where divalent alkaline earth metal ions are preferred over monovalent alkali metal ions) was first estimated empirically by (Webster & De Vivo 2002) as stated in section 3.3.2. (Sandland et al. 2004; Stebbins & Du 2002) studied silicate and aluminosilicate melts using ^{35}Cl MAS NMR and did not detect the presence

of any Si-Cl or Al-Cl bonds. They further suggested that chlorine is more likely to bond with either the alkali or alkaline earth metal ions with no strong preference.

Cl K-edge XAS, XANES and EXAFS studies were conducted (Evans et al. 2008 and McKeown et al. 2011) on calcium-magnesium silicate glasses and borosilicate waste glasses, respectively. Evans et. al. (2008) suggested that chlorine combined principally with divalent cations Ca^{2+} and Mg^{2+}. They also proposed possibility of some mixed cation-Cl species consisting of both Ca and Mg. The EXAFS data obtained for borosilicate glasses by McKeown et al. (2011) included Cl-Cl, Cl-O and Cl-Na correlations in compositions with low Ca content. As the CaO content was increased by replacement of Na_2O, the Cl-O, Cl-Na distances decreased. The Cl-Ca contributions were difficult to fit in the EXAFS data due to the narrow K-space available for analysis. Their XAS studies indicated that multiple Cl sites existed in glass with Ca^{2+} as the nearest neighbours and oxygen /sodium as the next nearest neighbours.

Recently (Chungong et. al. 2017) studied some high chloride calcium silicate bioactive glasses using ^{29}Si MAS NMR and neutron diffraction. The chemical shifts for the ^{29}Si NMR remained constant with changing chloride solubility which indicated that Si-O-Si connectively remained unaffected by $CaCl_2$ additions. In the total correlation function (T(*r*)) obtained using neutron diffraction, no structural features were observed at ~2 Å as one would expect for Si-Cl distances. Another interesting finding from the neutron diffraction work was that with increasing $CaCl_2$ content, the intensity of Ca-O bonds decreased as Ca coordinated with more Cl.

Chloride-based glasses have not been studied widely using techniques such as Raman spectroscopy and FTIR. (Schofield et al. 2009; Schofield 2011) observed limited differences in the FTIR spectra of undoped calcium aluminosilicate glasses and their

chloride doped equivalents. Unlike sulphate, where exclusive S-O bands appear in Raman and FTIR spectra with sulphur addition, with intensities varying proportionally with the amount of SO_4^{2-} incorporated, no promient bands related to Cl are visible in chloride doped glasses, despite high solubilities. However, the Si-Cl bond is Raman active, and if the chloride is indeed associated directly with the silicate network, a band corresponding to Si-Cl stretching mode should appear at ~540 cm^{-1} (Chmel and Svetlov 1996).

3.3.5 Research Approach for Chloride Studies

In this thesis, to further explore the issue of limited solubility of Cl^- in borosilicate glasses and its dependence on glass composition, the author prepared various binary and ternary silicate and borosilicate glasses doped with chloride and analysed their compositions. The glasses were further characterised using Raman spectroscopy and MAS-NMR to investigate any structural modifications that occur in the glass network with addition of chlorine. The effect of BaO addition on chloride solubility of the glass has also been studied.

CHAPTER 4

EXPERIMENTAL METHODOLOGY AND TECHNIQUES

4.1 Brief Overview

In this work, three glass families have been considered:

1. Alkali / Alkali- Alkaline Earth Silicate Glass (A/A-AE Si)
2. Alkali / Alkali-Alkaline Earth Borosilicate Glass (A/A-AE BSi)
3. Mixed Modifier Oxide Simulated Borosilicate Waste Glass (MMOS-BSi)

Each family consists of base glasses free of any anion addition and equivalent composition doped with the anions: SO_4^{2-} or Cl or both^{-}. The glasses were prepared using conventional melt -pour techniques in oxidising atmosphere. The resulting samples were investigated for the final composition using techniques such as XRF or ICP, checked for phase separation using XRD and structurally analysed using a range of techniques including Raman spectroscopy, MAS-NMR and Neutron diffraction. In the glasses comprising of Fe_2O_3, Mossbauer spectroscopy was used to determine the oxidation state of Fe in the Fe^{2+}/Fe^{3+} ratio. Besides, these techniques densities were measured, and DSC was used to determine T_g for some of them. This chapter gives an outline of the current theories regarding the structure of silicate and borosilicate glasses; details of sample preparation, and the theory of all experimental techniques used during the course of this work.

4.2 Silicate Glass

In contrast to a crystal, glass has a non-periodic structure over long range. To describe the structure of amorphous SiO_2, several theories have been put forward (Wright 1988; Greaves et al. 1981; Greaves et al. 1997), but no single theory is suitable to understand both the physical and chemical nature of a particular glass. The most widely accepted theory was originally proposed by Zachariasen (Zachariasen 1932). His continuous random network model proposed the following:

- Every silicon atom in vitreous SiO_2 is coordinated by four oxygen atoms, forming well defined SiO_4 tetrahedral units.
- In the polymerised glass network, each SiO_4 tetrahedron shares an oxygen atom with four other SiO_4 units.

Oxygen atoms shared by two SiO_4 tetrahedra are known as Bridging Oxygens (BO). The inter-tetrahedral angles in a glass network are randomly distributed accounting for the lack of long-range orders. In an alkali silicate glass, alkali oxide such as Li_2O, Na_2O etc. are added to modify the SiO_2 network; and reduce the melt viscosity and glass transition temperature. These oxides are known as Network Modifiers (NWM). Each mole of alkali oxide added to the glass leads to the breaking of a Si-O-Si bond by creating two Non-Bridging Oxygens (NBO) (Shelby 2005; Varshneya 1994). The modified cation charge balances the NBO units (Stebbins & Xu 1997). However, for larger modifier cations such as Ba^{2+}, the abundance of NBO is higher (Zhao et al. 2000). The NBO fractions in a glass are of critical importance in determining the properties of the melt such as viscosity and thermal coefficient of expansion. (Jantzen et al. 2005; Mysen et al. 1980) The SiO_4 network connectivity can be expressed in terms of tetrahedra with 'n' BO and (4-n) NBOs. In physical units, these are represented as: Q^n

(n = 0, 1, 2, 3 or 4) (Figure 4.1). Studies have shown that as the alkali concentration increases, the silicate network becomes depolymerised with Q^4 gradually replaced by Q^3 species and Q^3 by Q^2 (Dupree et al. 1986; Maekawa et al. 1991).

The mixed alkali effect occurs in glasses with varying fractions of two different alkali ions or else one alkali and another alkaline-earth ion. The replacement of an alkali ion by another, changes the mobility of both ions by orders of magnitude. The glass properties are non-linearly dependent on the mixed alkali concentration ratio and affect the modifier's mobility in the network (Isard 1969; Karlsson et al. 2005). However, measurements of diffusion coefficients have shown that the mobility of each modifier species is lower in mixed alkali compositions than equivalent single alkali / alkaline earth glasses (Kirchheim 2003).

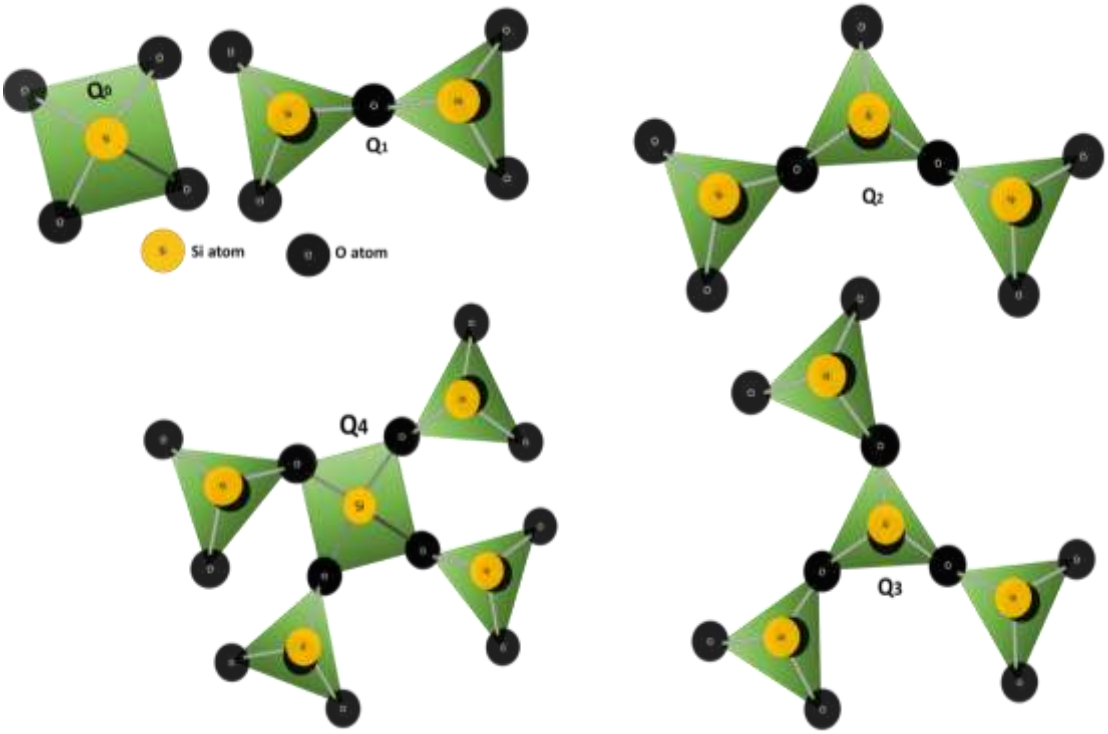

Figure 4.1: Si Q^n units in a silicate glass network

4.3 Borosilicate Glass

A borosilicate glass, as the name suggests, has two network formers: B_2O_3 and SiO_2. From a vitrification point of view, addition of Boron Oxide, not only reduces the glass melting temperature but also reduces the viscosity at very high temperatures. As a result, the glass exhibits bonds of short-range order, which is beneficial for vitrification.

Boron exhibits a variable coordination state and can exist either as 3- fold coordinated BO_3 triangles (symmetrical or asymmetrical) or 4- fold coordinated BO_4 tetrahedra. The addition of alkali atoms to vitreous B_2O_3, rather than leading to the formation of NBOs (as described for silicate glasses) initiate the conversion of symmetrical trigonal BO_3 units to charged tetrahedral BO_4. This increases the polymerisation of the boron network and minimizes the thermal expansion coefficient up to a certain concentration of alkali oxide addition (Konijnendijk & Stevels 1978; Hubert & Faber 2014; Möncke et al. 2015). Further additions of the modifier oxide push the BO_4 units back to non - symmetrical BO_3 with an NBO associated with the alkali cation (Figure 4.2). The behaviour is opposite to what is observed in an alkali silicate glass and normally referred to as the 'boron-anomaly' (Doweidar 1990).

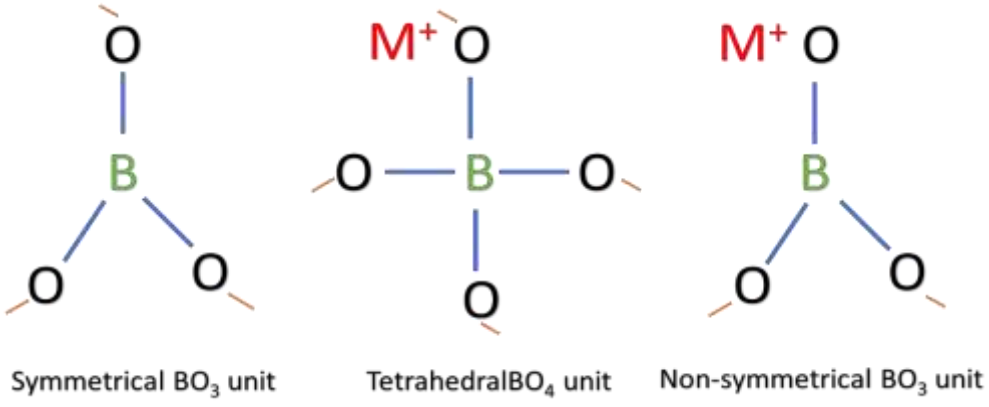

Figure 4.2: The three possible borate units that can be present in a borosilicate glass.

(Silver & Bray 1958) defined the concentration of BO_4 units in terms of N_4 fraction which is the ratio of tetrahedral BO_4 to the total concentration of borate units present in the glass. The authors observed a maximum in N_4 at around ~30 mol% alkali oxide.

In later years, (Yun & Bray 1978; Dell et al. 1983) proposed a model for estimation of N_4 based on their studies on sodium borosilicate glasses. The authors concluded that till $R<0.5$, where R is the ratio of modifier oxide to the B_2O_3 content, the network modifier preferably converted BO_3 to BO_4. The system behaved like a typical binary borate system where the silicate network remained unaffected by the alkali ions. After a critical point, the alkali oxide divided itself proportionately amongst the SiO_2 and BO_4 units to create NBOs. (Figure 4.3)

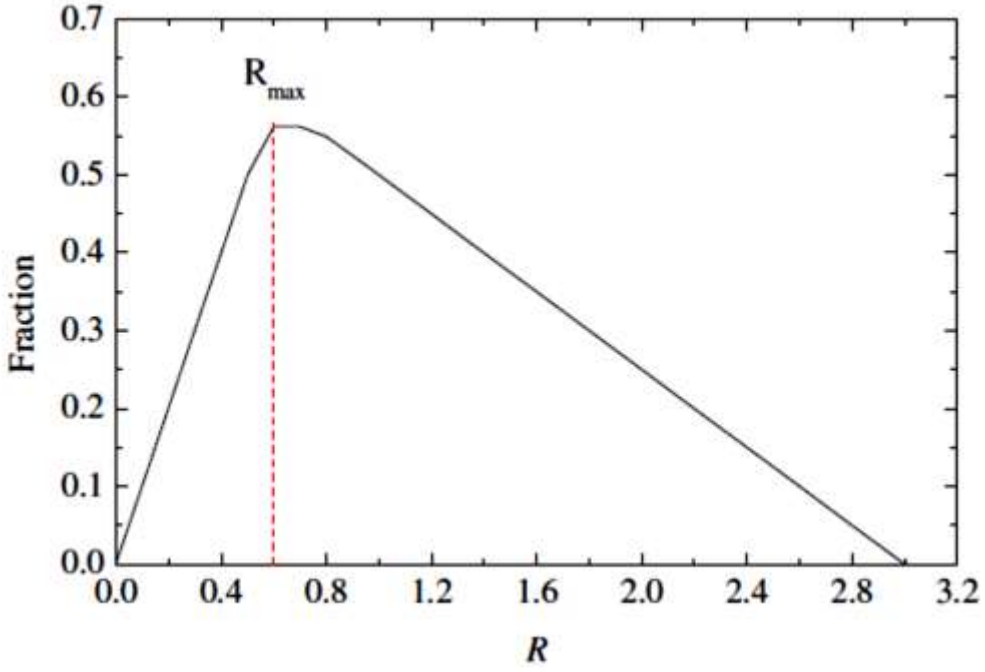

Figure 4.3: Change in the N_4 fraction plotted as a function of R (where R is the ratio of alkali oxide.B_2O3,), for a sodium borosilicate glass (Dell et al. 1983)

BO_3 is a relatively unstable component in borosilicate glass and is easily leached by acids. Thus, to increase the waste glass durability the population of BO_3 needs to be

minimized which is achieved by using alkali borosilicate glasses. The presence of more than one modifier species in the glass leads to an overall reduction in modifier mobility and hence the leachability of these species. That is why a sodium barium borosilicate glass is more durable than a sodium borosilicate glass.

4.4 Batch Preparation

High purity carbonates, oxides, sulphate and chloride salts (> 99%) were used as raw materials to prepare the glass batches (See Appendix A for the full assay of chemicals used for glass preparation). Prior to weighing, every chemical was dried in an oven at 100°C for 24 hours to remove any hydration if present, except for H_3BO_3 due to its low temperature of decomposition. The raw materials were weighed as per the batch calculations on an electronic balance with an accuracy of 0.001g. The weighed chemicals were transferred to ziplock bags and shaken vigorously to ensure a homogenous, lump free mixture. The mixture was then transferred to a suitable crucible and partially covered with a lid to avoid extensive volatilisation losses of oxides during melting. The filled crucible with lid was placed in an electric furnace and ramped at a slow rate to reach desired glass melting temperature. The size of the crucibles varied depending on the volume of the glass batch.

4.5 Melt Conditions

Table 4.1 summarises the melt conditions for the three glass families. The glasses were melted from 2-3 hours and poured in a stainless-steel mould and left to cool at room temperature with proper safety measures taken to avoid thermal stress explosions. The reason behind no annealing was to avoid any extra volatilisation losses of anions or

Na_2O as the research is focussed towards study of effect of various modifiers on anionic solubility; not the overall mechanical strength. The crucibles were covered with a lid during the melts. Only the Li_2O containing glasses were splat quenched between two iron plates as the glass phase separated under normal bulk cooling rates.

Category of Glass	**A /A-AE Si**	**A / A-AE BSi**	**MMOS-BSi**
Preparation	Melt- Pour Only, Li-Si: Melt Splat Quench	Melt- Pour (No annealing)	Melt- Pour (No annealing) Melt- Quench
Crucible Used	Pt- ZGS crucible with Lid	PT- ZGS crucible with Lid	Mullite ($3Al_2O_3.2SiO_2$) with Lid
Furnace Conditions	Electric Furnace in air (auto Ramp)	Electric Furnace in air (auto ramp)	Electric Furnace in air (ramped at 3ºC/ min)
Dwell time (Hrs)	3.5	3.5	1.5
Glass made (g)	125	35	75
Glass storage condition	Under vacuum	Under vacuum	Atmospheric pressure

Table 4.1: Melt conditions for the three families of glasses prepared for this research.

Figure 4.4: Representative photographs of stepwise production of an alkali silicate glass in the MERI lab, Sheffield Hallam University

4.6 Density Measurements

The densities of glass were calculated on a Mettler Toledo Balance-densimeter balance with an accuracy of 0.0001g. The kit is based on Archimedes' Principle and involves weighing the sample first in air and then in distilled water as fluid medium at room temperature. The volume of the sample is thus:

$$V = (m_1 - m_2) / (\rho_{water}) \qquad \text{Equation 4.1}$$

where m_1= mass of sample in air; m_2= mass of sample in water; ρ_{water}= density of distilled water at known temperature. Thus, density of the glass is: ρ_{glass}

$$\rho_{glass} = m_1 / V = m_1 * (\rho_{water}) / (m_1 - m_2) \qquad \text{Equation 4.2}$$

Five measurements were taken per sample and the density results were averaged.

4.7 Techniques Used

The glasses were subjected to compositional and phase analysis before structural characterisation. For the compositional elemental analysis, techniques such as X-Ray Fluorescence (XRF), Inductively Coupled Plasma Optical Emission Spectrometry (ICP-OES) and Energy Dispersive X-Ray spectroscopy (EDX) were used. Where XRF is useful in quantitative estimation of the concentration of heavy elements present in the glass, it stands inefficient in detection of lighter elements such as Lithium (Li) and Boron (B). ICP-OES was used to analyse the concentration of Li and B in for Lithium silicate glasses and borosilicate glass systems. EDX was performed to complement the semi-quantitative XRF results obtained for the chloride content retained in the chloride

doped silicate glasses. Powder X-Ray Diffraction (XRD) was used to detect any phase separation if present.

To comprehend the local coordination environment and the bond network formed within the glass, Neutron diffraction was performed at the GEneral Materials Diffractometer (GEM) beamline, ISIS pulsed neutron source facility, Rutherford Appleton Laboratory (RAL), Didcot, United Kingdom. The short-range bond arrangement constructed through the neutron diffraction data analysis substantiated the structural information obtained through Raman spectroscopy and Magic Angle Spinning- Nuclear Magnetic Resonance (MAS-NMR). The latter was performed at the EPSRC – Solid State NMR facility at Durham University, UK and the University of Warwick, UK.

Other techniques used to various degrees for the research were Mössbauer Spectroscopy, Differential Thermal Analysis (DTA) and Scanning Electron Microscopy (SEM). A comprehensive discourse on the experimental techniques is presented in the following subchapter.

4.7.1 Techniques for Quantitative Composition Analysis

4.7.1.1 X-Ray Fluorescence (XRF) for elemental analysis.

This non-destructive analytical tool is useful in qualitative and semi-quantitative determination of the chemical composition of inorganic materials with concentration capabilities ranging from ppm to %. XRF spectrometers are either Energy Dispersive (ED) or Wavelength Dispersive (WD). Depending on the type, the elemental detection range varies: from Sodium to Uranium for the EDXRF and from Boron to Americium for WDXRF. The precision and reproducibility of XRF analysis is limited by the quality

of sample and calibration standards. A WD Philips Magix Pro PW2440 sequential X-ray fluorescence spectrometer was used for the measurements.

a) Background: When a collimated beam of X-rays is incident upon a sample, part of it is transmitted, a portion is absorbed to produce fluorescent radiation and the rest is scattered away. Based on this interaction, the phenomenon is categorised either as Fluorescence, Compton scattering, or Rayleigh scattering. However, the interaction is affected by parameters such as composition, density, and thickness of sample along with the energy of incoming radiation (Brouwer 2010).

Production of fluorescent radiation (Bounakhla, Moussa; Tahir 2015; Brouwer 2010; Verma 2007): The classic shell model describes an atom as a nucleus made of protons and neutrons with electrons spinning around in orbital shells. The innermost K-shell can contain 2 electrons followed by L-shells (3 subshells) with 8 electrons, M-shells (5 subshells) with 18 electrons, etc. The energy of each electron depends on the occupying shell and the element itself. When an incident X-ray photon hits the atom with sufficient energy, it knocks off an electron from one of the shells creating a 'vacancy' which results in atomic instability due to the extra energy. To restore the ground state, an electron from an outer shell with higher energy moves to fill the vacancy and the remnant energy is emitted as a photon which manifests as a line in the spectrum (Figure 4.5(b)). Each element present in the sample emits characteristic fluorescent X-Ray radiation with discrete energies. Where an EDXRF detector directly measures the discreet energies, in a WDXRF spectrometer, the emitted energies from the sample are collimated and further dispersed at different angles by an analysing crystal or monochromator (Figure 4.5 (a)). This extra step leads to fewer spectral overlaps and better resolution in WDXRF but narrows down the energy detection range. (Potts & Webb 1992).

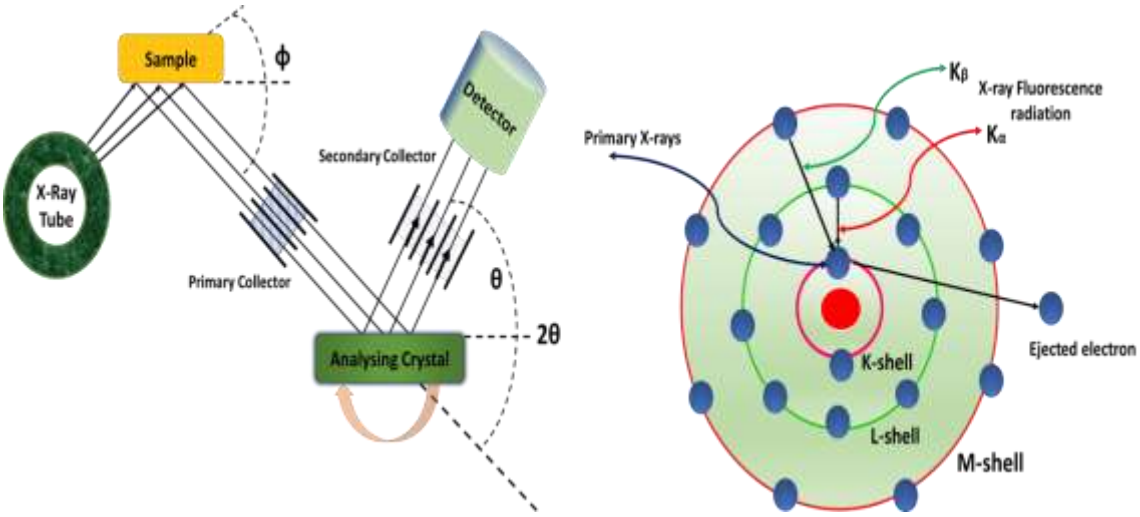

Figure 4.5: a) Schematic diagram of WDXRF. b) Production of characteristic X-rays

Only those wavelengths are reflected by the crystal which satisfy Bragg's law (Figure 4.6, Equation 4.3).

$$n\lambda=2d\sin\theta \qquad \text{Equation 4.3}$$

where n is an integer, λ is the wavelength of the radiation emanating from the sample and d is the spacing between planes of the crystal lattice.

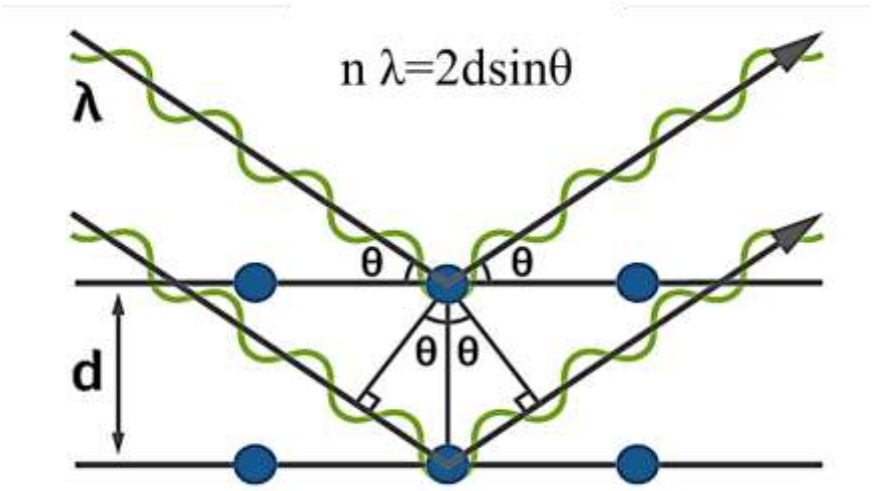

Figure 4.6 Schematic representation of the X-Ray Diffraction in crystals

The analysing crystal has a known d value. A sequential scintillation/gas proportional detector tuned for only fluorescent radiation (ejects any scattered/undesired diffracted

X-rays) measures the intensities of the emitted wavelengths which is proportional to the abundance of the element in the sample.

Ineffectiveness of XRF over lighter elements: In 1912, Moseley discovered a mathematical relationship between the element's emitted X-ray wavelength and its atomic number by calculating characteristic radiation (K_α) for each element (Stolenberg et al. 2006). As per the Moseley's law, $\lambda \propto {}^{1}/_{Z^2}$ where Z = atomic number.

Therefore, the energy of the fluorescent photons emitted by the sample correspond directly to the atomic number of the element. Light elements have lower energy levels, due to which the photons struggle to escape from the sample without being absorbed. Hence, for a lighter element, the fluorescent yield reaching the detector is negligible explaining the ineffectiveness of the technique for elements including hydrogen, lithium, and boron.

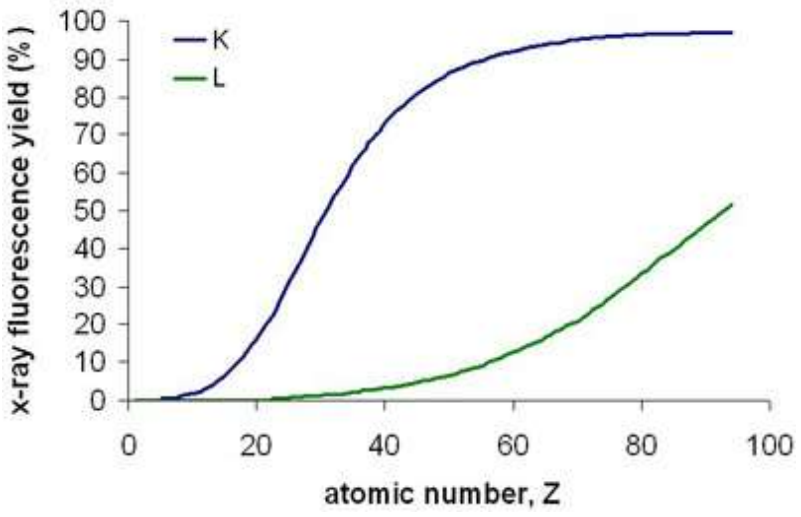

Figure 4.7: K and L Fluorescence yield as a function of atomic number, Z.
(Courtesy: www.horiba.com)

Rayleigh and Compton scattering: When a photon hits a strongly bound electron, it bounces away and scattering occurs. The electron oscillates in the shell rather than being knocked off. The oscillation leads the electron to emit radiation at the same frequency

as the incoming radiation (Singh et al. 2007). In Compton scattering, a loss of energy in the scattered radiation is observed. No such loss occurs for Rayleigh scattering. Thus, the lighter elements produce more higher Compton scattering than Rayleigh due to their more loosely bound electrons (Motz & Missoni 1961).

b) Preparation of samples: If the sample depth and thickness is high, it will lead to more absorption of incoming radiation and the characteristic radiation emitted by the sample will either have very low intensity or might not leave the sample at all. Therefore, only samples within analysis depths are analyzed with the technique. 5g of glass sample was milled in a Retsch vibration mill RS200 at 600 rpm for 1 minute in a hardened steel grinding cup and mixed with a binding additive in a ratio of 1:10. The binding additive was composed of elements immune to XRF like $Li_2B_4O_7$, $LiBO_2$, or else cellulose (Watanabe 2015) depending on sample preparation technique. Either the sample powder mixed with cellulose was pressed under very high pressure of 200kN to form a 'pressed pellet' or else 1 part of sample powder mixed with 10 parts of $Li_2B_4O_7$ and $LiBO_2$ (50:50) was melted at 1150^oC in a platinum crucible for around 15 minutes to form a 'fused bead'. A few drops of LiBr were used as releasing agent for the fused beads. Due to the re-melting involved in fuse beading, part of the sample such as CO_2, H_2O, S, Cl. evaporates and contribute towards errors but it gives more accurate results for oxides than pressed pellets (Yamada 2010). The loss on ignition can be determined by measuring the weight of the sample before and after the melt.

4.7.1.2 Inductively Coupled Plasma Optical Emission Spectroscopy (ICP-OES) for Lithium, Boron and Chlorine analysis.

ICP-OES is an effective compositional analysis tool which can determine even trace elements in a variety of samples. The elemental detection range varies from Lithium to Uranium except for halogens, low levels of phosphorus, sulphur and some other gases such as oxygen, carbon, nitrogen. The inert environment of plasma leads to low chemical interference, thus making ICP-OES more accurate than XRF.

a) Background: The principle is based on atomic emission spectroscopy where photons are ejected spontaneously from atoms and ions excited in a high-energy Argon plasma chamber (Figure 4.8). A solid sample is dissolved in an acid solution in a sealed environment (to retain the volatile elements present in the sample). The liquefied analyte is nebulised to form an aerosol by a high-pressure stream of argon gas introduced in the nebulizer. The finest drops of aerosol are drawn into an inductively coupled plasma chamber where it attains temperatures of approximately 10,000K (Hou & Jones 2000). At such high temperatures, the nebulized solution evaporates and the elements to be analyzed are released as free atoms in the gaseous state rather than forming polyatomic species. The liberated free atoms undergo several collisions with the charged argon ions in the plasma leading to ionization of the atoms with high thermal excitation. The extra energy is liberated as a photon of characteristic wavelength. The emitted radiation reaches the optical emission spectrometer where a diffraction grating separates the component wavelengths; an array of CCD detectors assesses the intensity of the separated wavelengths which are discrete and element specific. The measurement of intensity is converted into relative abundance by comparison with calibration standards.

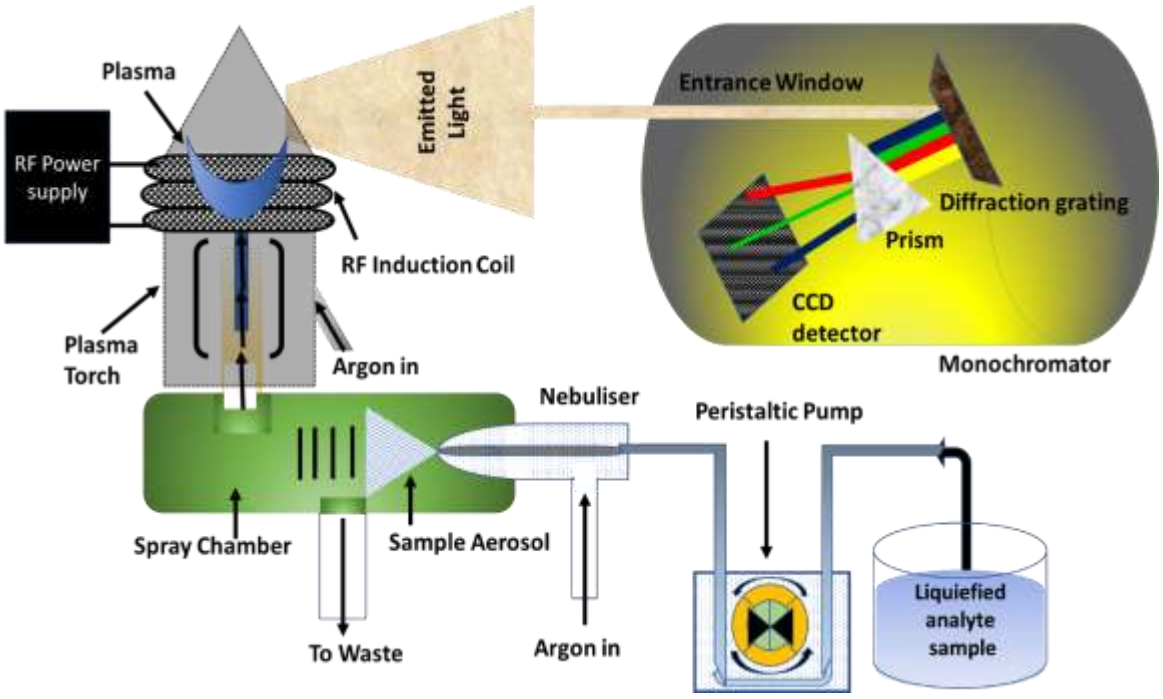

Figure 4.8: Schematic diagram of the ICP-OES technique.

b) Preparation of samples: There are two methods of sample preparation: Acid Digestion and Alkaline Fusion. The latter was used for the research. During alkaline fusion, the sample is fused with either lithium metaborate/tetraborate or sodium peroxide. The fused pearl is later dissolved in concentrated HNO_3 acid solution and the volume is increased by mixing it with deionized water. HNO_3 is preferred as the solubility of the nitrates is quite high and it is relatively free of any chemical or spectral interferences (Gaines 2011). The solution is further nebulised and introduced into a high-temperature plasma chamber.

4.7.1.3 Scanning Electron Microscopy- Energy Dispersive X-Ray Spectroscopy (SEM - EDX)

A scanning electron microscope provides high magnification imaging of almost all materials. EDX used in conjunction with the scanning electron microscope is chemical

microanalysis where a detector characterizes the elemental composition of a sample by detecting the X-rays emitted by it due to bombardment by an electron beam. The electron excited characteristic X-rays provide identification of all elements with H, He and Li as an exception (Newbury & Ritchie 2013). With SEM in combination with EDX, it is also possible to find out the topographical distribution of each element in the overall sample surface. A FEI NOVA 200 Nano SEM was used for analysis.

a) Background: The fundamental principle behind SEM-EDX is same as for EDXRF. An electron beam with electrons accelerating through a voltage of 1-30 KeV is focused on the area of interest in vacuumed environment of around 10^{-4} Pa and is scanned sequentially across the specimen. The bombarding electrons collide with the atoms in the sample; some knocking off electrons from the atoms and other being scattered away. The collision produces characteristic X-rays which are recorded by detectors surrounding the sample (Figure 4.9). A Secondary Electron Detector (SED) and Back-Scattered Electron Detector (BSED), as name suggests, measure the secondary and back scattered electrons from the sample respectively. In the EDX detector, the emanated fluorescent radiation is directed into photo-sensitive semi-conductors. The resulting voltage pulse is proportional to the energy of emitted photons. A semi-quantitative analysis is possible if the intensities of each element in the sample are measured and compared with the measurement of same element in a calibration standard of known composition.

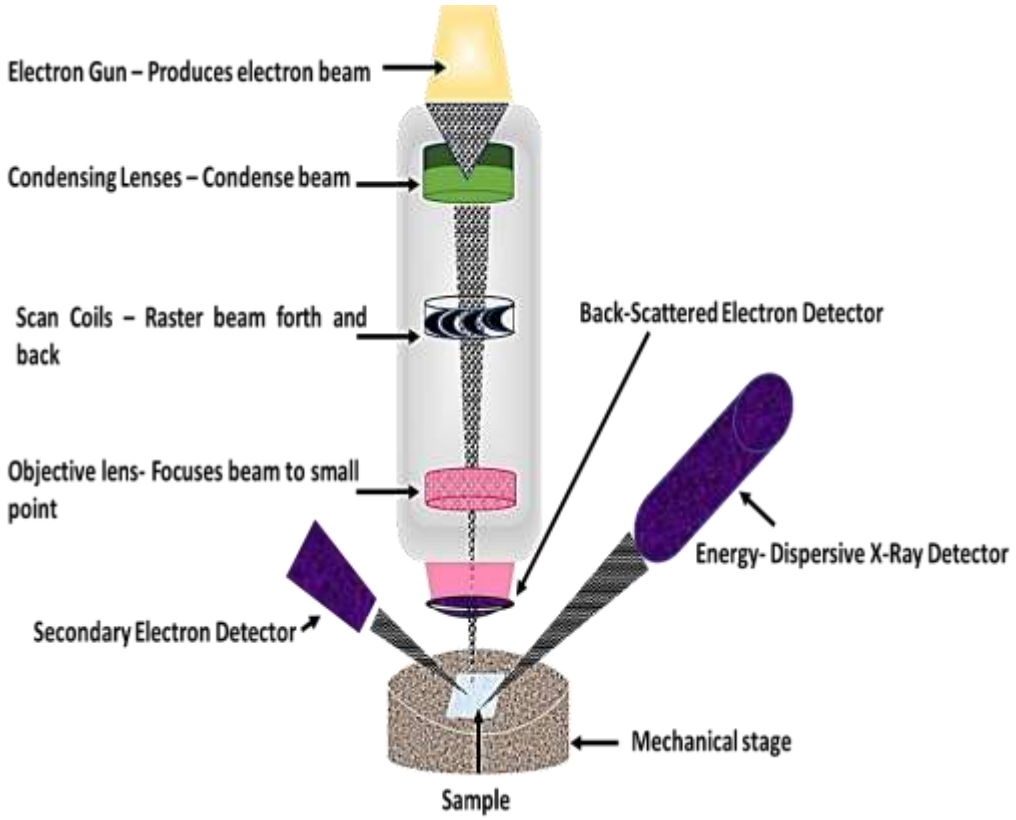

Figure 4.9: Schematic diagram of the SEM and its detectors

b) Preparation of the samples: A low viscosity resin blend formed by mixing 100 parts of resin to 36 parts of hardener was poured over the glass samples in a ring form rubber cup greased with mold release wax and cured at room temperature for 24 hours. The resin bound glass samples were then subjected to series of grinding (silicon carbide grinding paper P240 to P1200) until the glass surface was exposed and then polished with two grades of diamond polishing suspensions (9 _m and then 3 _m). The polished samples were mounted on an aluminum stub and sputter coated with an ultra- thin film of conductive carbon (around 10 nm) to avoid electrostatic charge deposition on the poor conductive sample surface as charging causes uncalibrated deflection of the incoming electron beam. For all investigations, the beam energy was kept 15 kV to obtain the excitation of all the elements. EDX analysis of the elements was carried out using the OXFORD INCA system software.

4.7.2 Techniques for Phase Analysis

X-Ray Diffraction is very commonly used technique to obtain structural information and identify phases as each phase in a crystalline material produces a characteristic diffraction pattern. The composition can be estimated through identification of positions and intensities of diffraction peaks which are unique to a given chemical compound (Chauhan & Chauhan 2014). In case of glasses, it is a challenge to elucidate structure using XRD, but it is useful as it confirms if the sample is entirely or partially X- ray amorphous.

4.7.2.1 X-Ray Diffraction (XRD)

Amorphous materials do not have long range order like crystalline materials and therefore the resulting XRD diffraction pattern does not show the typical series of peaks associated with crystalline materials (Figure 4.10).

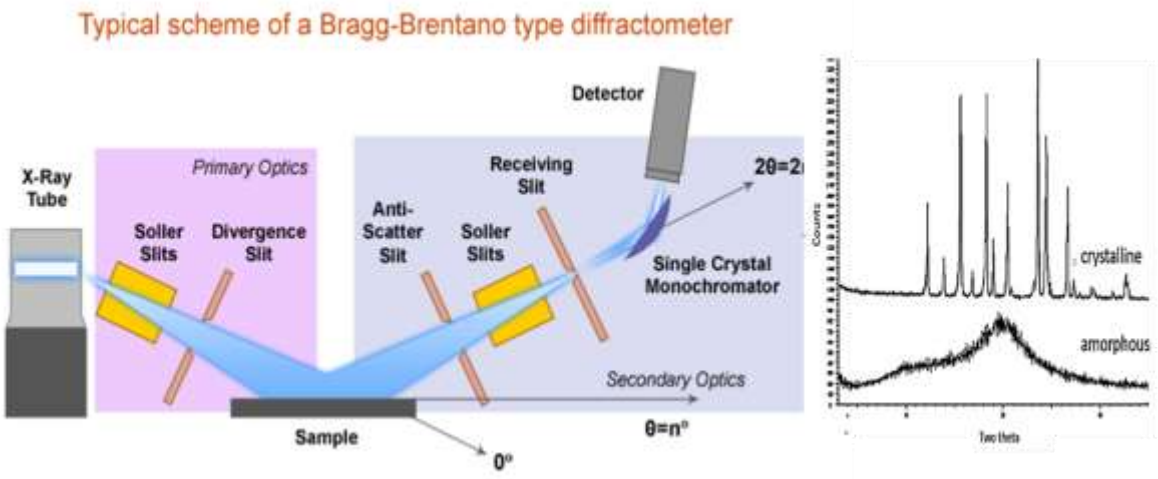

Figure 4.10: Left - Schematic diagram of Bragg Brentano type diffractometer. Right - Typical XRD pattern for a purely crystalline material (top) and an amorphous material (bottom) (Courtesy: (Young 2012)

The pattern instead shows a broad "hump" with few or single maxima (Saw et al. 2006; Fultz & Howe 2013; Klug & Alexander 1954). Although this "hump" pattern does not

uniquely identify the material being studied it provides critical knowledge needed for characterization. The Empyrean PANalytical X-Ray diffractometer based on Bragg-Brentano θ- θ geometry equipped with a 40kV and 40mA (λ = 1.54 Å) Cu X-ray tube was used for the measurements.

a) Background: When an X-Ray beam of a known wavelength is directed towards the sample at the desired angle, the oscillating electric field of the incident ray moves the atomic electrons and their accelerations generate an outgoing wave which scatters away from the sample and is captured by the detector. The interaction of the rays with the lattice planes of the crystalline sample produces constructive interference only if the conditions satisfy Bragg's Law (Equation 4.3). Per the law, diffraction in general only occurs when the wavelength of the electromagnetic wave hitting the sample is of the same order of magnitude as the distance between two lattice planes (Skoog et al. 2007). Clearly, diffraction is a scattering phenomenon in which only periodically arranged atoms participate in constructive interference. Hence, XRD is not very useful to study the molecular arrangement inside glasses, but it helps to identify crystallinity in glasses which hydrate over a period producing crystalline structures or the glasses that have been heat treated. The position or d-spacing of the amorphous hump can be useful in providing information on average interatomic distances as well.

b) Preparation of samples: Solid samples were powdered in a vibration mill inside a grinding cup with hardened steel rings at 600 rpm for 1 minute. The powders were pressed in the powder specimen holders and mounted on a reflection-transmission spinner stage. The diffracted X-rays passed through a Ni filter that reduced the intensity

of K_β lines reaching the PIXcel 3D detector. Each sample was analyzed in a range of 5°- 80° (two theta), step size 0.013° and scan speed of 0.0037° (two theta) /minute.

4.7.3 Techniques for Structural Analysis

To understand the properties of glass, its structure must be studied, for which XRD is clearly not powerful. A 'glass lattice' can be assimilated as a disordered network that introduces distribution of range of bonds and bond angles. A drawback encountered in the study of glass structure is that one experimental technique reveals only a part of structural characteristics. The structural concepts of glass must emerge from the joint interpretation of spectroscopic techniques such as NMR, Raman scattering, and neutron diffraction that can primarily provide local information about the first few coordination spheres. (Short-range order ~1.5 – 3 Å).

4.7.3.1 Raman Spectroscopy

Raman spectroscopy is one of the main spectroscopic techniques employed to study the chemical bond formations in glass by studying the vibration modes of molecules. Thorough literature research aided identification of the bonding. The change in structure due to sulphate doping is identifiable. A Thermo Scientific DXR™ 2 Raman spectrometer installed with a laser of wavelength 532 nm and 10mW power was used for analysis. The grating was set to 900 lines/mm, estimated resolution between 5.5 – 8.3 cm^{-1} and estimated spot size was 2.1 µm. The glass samples were exposed under the laser for 60 seconds per scan. The scans were repeated 30 times within the range of 100-2000 cm^{-1} and co-added to generate the final spectrum. A 50X microscope objective was used for all Raman experiments.

a) Background: The molecular groups forming bonds in glass are characterized by several vibrational modes determined by the masses of the constituent atoms, the interatomic forces, and the geometry of their arrangement. A Raman spectrometer irradiates the glass sample with monochromatic laser beam and the scattered radiation from the molecule is detected in units of Raman Shift (expressed as a shift in energy from that of the incident radiation and referred to as cm^{-1}). The light scattered from each molecular vibration is uncorrelated to that from any other molecule (Long 2002).

In Raman scattering, the photons interact with the molecule and distort (polarize) the cloud of electrons around the nuclei to form a short-lived unstable virtual state and are quickly re-radiated (Figure 4.11). If the transition starts at the ground state energy level and ends at a higher level it is called 'Stokes Raman scattering' resulting in energy gain by the molecule and loss of energy in the scattered beam (Figure 4.12b) whereas 'Anti-Stokes Raman scattering' occurs when the transition occurs from higher to lower energy level resulting in loss of energy by the molecule (Figure 4.12c). At ordinary temperatures since most of the molecules are at ground state, Stokes scattering is more prominent than Anti-Stokes.

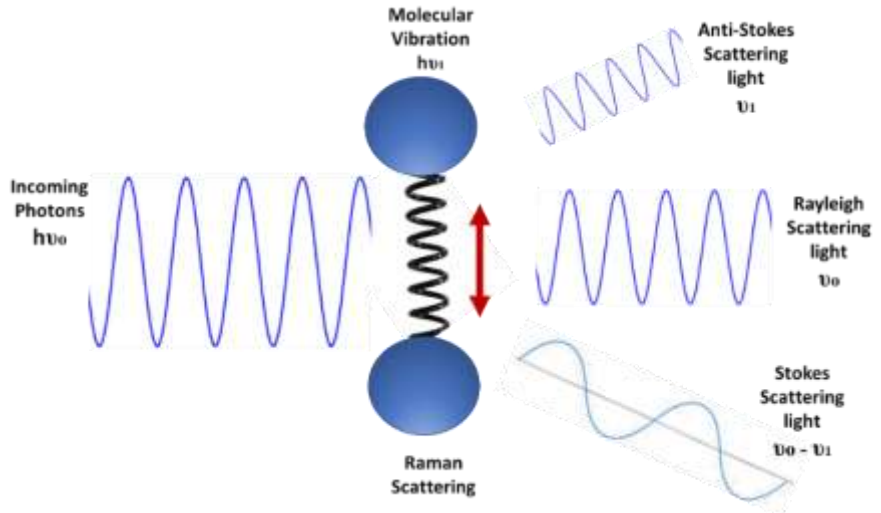

Figure 4.11: Schematic diagram of scattering that occurs due to molecular vibration

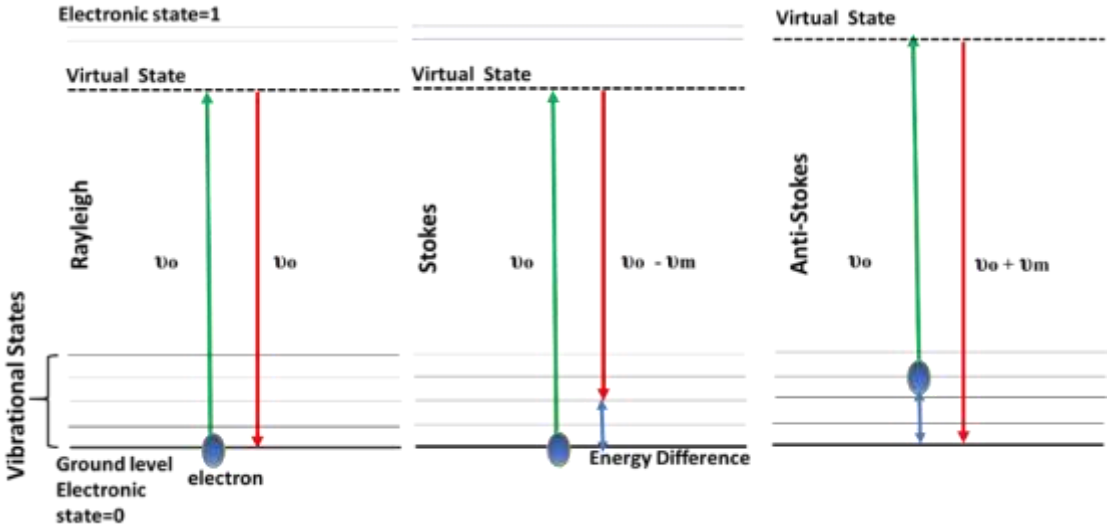

Figure 4.12: Types of energy transitions with Rayleigh, Stokes, and Anti-Stokes Scattering

The scattered photons are observed by collecting light at an angle to the incident light beam and provided there is no absorption from any other electronic transitions, the efficiency increases as the fourth power of the frequency of the incident light (Smith & Dent 2005).

b) Preparation of samples: The low durability glasses (alkali silicates and borosilicates) and those with undissolved sulphate salt deposited on surface were polished with SiC grade P240 to P1200 to remove any hydration/ salt if present to avoid. The system was calibrated with a polystyrene film scan before every measurement. All the data was corrected for fluorescence and photo-bleaching if occurring. Auto background removal out using OMNIC software.

c) Peak-fitting of Raman data: The Raman data obtained from the software is composed on true data alongwith extra counts generated due to fluorescence from the glass sample. The raw data was first corrected by defining a polynomial baseline for each spectrum and then subtracting it from the actual data. The remainder was a linear spectrum devoid of any fluorescence effect. The corrected data was further normalised between values

of 0 to 1. A free licensed peak fitting tool: Fityk 0.9.1 (Wojdyr 2010) was used to deconvolute the normalised Raman spectrum. A Gaussian response function with a Fourier filtering algorithm was used for the deconvolution. The auto-placement feature of the software identified local maximas in the normalised data and placed initial peaks. During the entire peak fitting regime, the fitting parameters such as height, area and the full width half maxima (FWHM) for all peaks were kept unconstrained. After placing the identifiable initial peaks, the residual procedure revealed the hidden peaks which were then added to largely match the fitted Raman spectrum with the normalised original spectrum. Literature mostly aided the identification of each fitted peak with individual atomic interactions.

4.7.3.2 Magic Angle Spinning- Nuclear Magnetic Resonance (MAS-NMR) Spectroscopy

NMR spectroscopy complements Raman spectroscopy and Neutron Diffraction and provides a versatile method for the structural characterization of samples consisting of atoms with nuclei that have spin (e.g. ^{29}Si, ^{23}Na, ^{6,7} Li, ^{11}B etc.) by probing the local environment of the nucleus. In the mid-80's the power of magic angle spinning (MAS) was recognized to have drastically increased the resolution of solid state NMR and allowed identification of distinctly different local environments (Todd & Janelle 2012). A typical NMR spectrum is depicted in terms of chemical shift, which is correlated to the structure; peak positions indicate parameters as coordination number and the nature of the bonded atoms and peak intensities lead to quantitative determination of short-range order. All the NMR experiments presented here were carried out at the EPSRC UK National Solid-state NMR Service at Durham University and at the University of Warwick.

a) Background: Atomic nuclei that possess spin, have an angular momentum (**L**) and a magnetic moment (**μ**). When inserted in a magnetic field, the interaction between the nuclear magnetic moment of the atom and the magnetic field cause the atomic beam to split, producing quantized energy levels separated by energy ΔE (Equation 4.4), with different spin orientations. It is called the 'Zeeman effect' (Figure 4.13 a).

$$\Delta E = \pm(\mu/L)\, B \qquad \text{Equation 4.4}$$

where B is the static magnetic field.

However, in case of a molecule, the net field which the nuclei are subjected to, is affected due to the local magnetic fields generated by the electron motion surrounding the bonds (Figure 4.13 b). The phenomenon known as 'magnetic shielding' produces resonance shifts which are characteristic of local electron environment and the orientation of electrons with respect to external magnetic field.

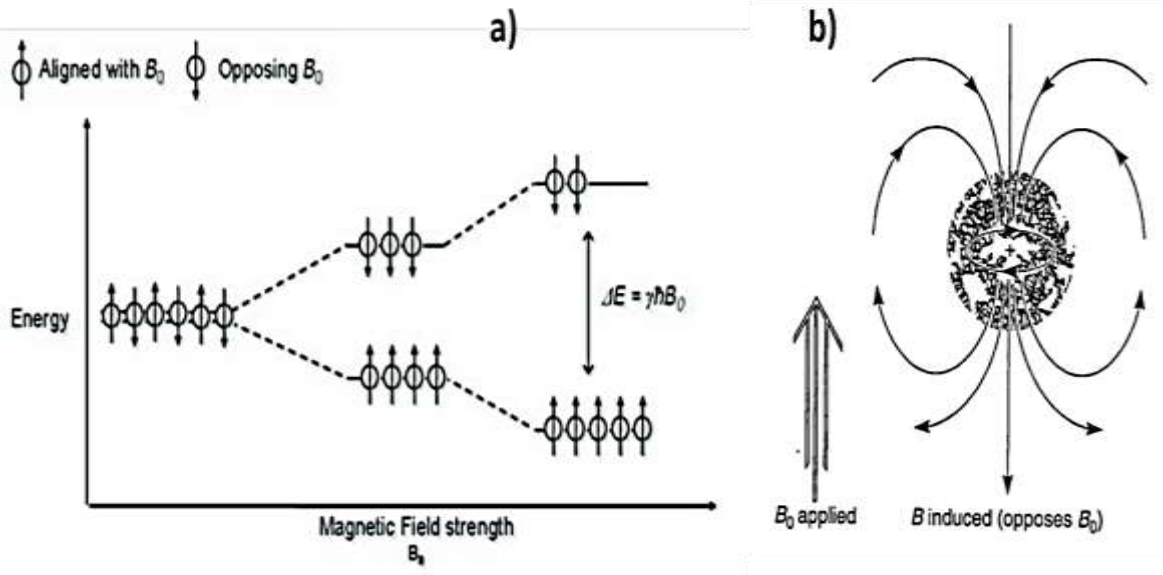

Figure 4.13: a) The Zeeman Effect energy level splitting diagram. b) The shielding effect of local electron density around nucleus against applied magnetic field.

The shielding factor (σ) is thus denoted as:

$$\sigma(ppm) = \left(\frac{\nu_n - \nu_s}{\nu_n} \right) 10^6 \qquad \text{Equation 4.5}$$

where υ_n is resonant frequency of bare nucleus and υ_s is the frequency of the same nucleus in local electron environment in the sample.

Fundamentally υ_n is not measurable, so a new term was introduced known as 'chemical shift (δ)' which is relative chemical shielding by the sample with respect to shielding by a reference standard (Equation 4.6).

$$\delta(ppm) = \left(\sigma_{ref} - \sigma_{sample} \right) 10^6 \qquad \text{Equation 4.6}$$

Thus, by measuring the chemical shift it is possible to study the local electron environment around the nuclei. A wide study of molecules observed that chemical shifts are more shielded (i.e., lower frequency) as the coordination number increases (Mason 2012; Webb 1995; Wojcik & Kamienska-Trela 2013). Other than the Zeeman effect and magnetic electron shielding a variety of anisotropic interactions (Mitchell & Costisella 2004) take place which result in broad and featureless peaks in the NMR spectra difficult to be analysed (Affatigato 2015). In a MAS-NMR experiment, the sample rotates about an axis oriented at 54.74° with respect to the external magnetic field, averaging out most of the anisotropic broadening, thus enhancing the resolution. The faster the spinning, the better is the resolution of data. A typical MAS NMR probe schematic is presented in Figure 4.14.

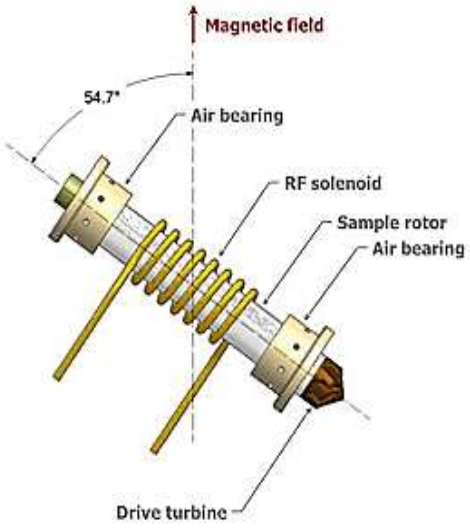

Figure 4.14: Schematic diagram of a MAS-NMR sample probe.

b) Preparation of samples: Milled glass samples were sent to the NMR facility which were then filled in 6mm and 4mm ZrO_2 sample rotors at Durham University and University of Warwick respectively. A Varian VNMRS spectrometer with a 9.4 T magnet was used at the Durham facility. The standard reference material used were silicon and a neat tetramethylsilane. Only ^{11}B NMR measurements were taken at the Warwick Facility. A Multiple Quantum Magic Angle Spinning (MQMAS) NMR was performed to obtain better resolution. The 500 Mhz Bruker Avance III spectrometer with a 11.75 T magnet was used for the analysis.

4.7.3.3 Neutron Diffraction (ND)

Neutron diffraction is a highly powerful technique for determining structure of glasses in combination with NMR, Raman spectroscopy, and XANES A ND experiment can accurately measure the distribution of interatomic distances of short-range order by characterizing the coordination number and bond lengths. This helps in determination of the coordination polyhedral that forms the base of the glass structure. The intermediate range order distances in which the polyhedral units are connected can also

be determined but with aid of modelling (empirical modelling in our case) to the ND, results obtained. The GEneral Materials diffractometer (GEM) at the ISIS Facility pulsed neutron source facility, Didcot, United Kingdom was used for the experiments.

a) Background: The critical advantage of scattering through neutrons is that being neutral charged, it interacts with the atomic nuclei than the electron cloud. Thus, the scattering power of atom is independent of its atomic number and it is easier to detect the local environment of lighter elements.

Single wavelength ND: Monochromatic ND obeys the same Bragg's Law of diffraction as X-rays. The nuclear force with which the neutrons interact with nuclei is much weak, unlike the electromagnetic forces with which X-rays hit the atoms in XRD, making ND intensity limited technique. For this reason, large sample sizes (~1-2 cm^3) and long collection times are chosen for each measurement and data collection is time consuming.

Time-Of-Flight (TOF) ND: Modern spallation neutron sources create neutrons by sending pulses of accelerated proton beam (comes from a synchrotron) at a heavy element target, which when hit by the proton beam, emits neutrons of multiple wavelengths. A neutron spectrometer has a beam guide to channel the neutrons from the source to the sample, collimating the beam and eliminating very fast and very slow neutrons at the same time. The pulse mechanism is ideal for TOF ND which is faster and efficient as diffraction patterns are obtained at a single scattering angle and incident neutron flux is high as monochromator is unnecessary. TOF is the time taken from creation of the neutron by proton spallation until the detection of neutron after

diffraction. The total flight path distance is denoted as L. Thus, in TOF- ND the Bragg's law is modified where TOF (t) is calculated (Equation 4.7). A schematic diagram of a TOF-ND is shown in Figure 4.15.

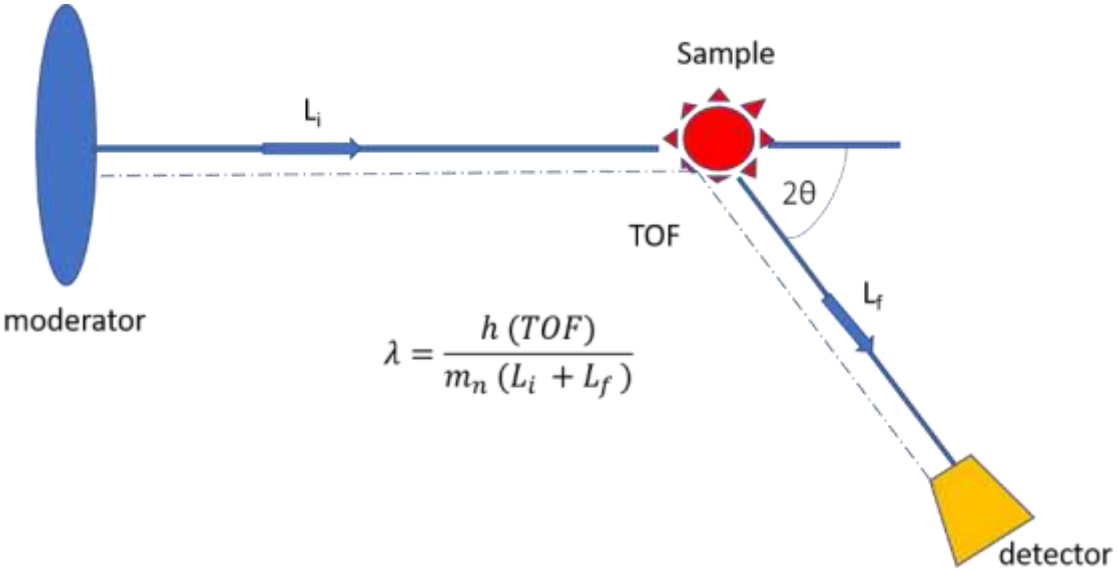

Figure 4.15: Schematic diagram of time-of-flight ND with pulsed neutron source

λ is not fixed due to multiple wavelengths of neutron. θ is fixed for all measurements. As per the De-Broglie relationship:

$\lambda = \frac{h}{mv}$ where m and ν are mass and velocity of neutron respectively.

$v = \frac{L}{t}$ where L is total flight path of neutron ; t is time taken to traverse L.

Therefore, $t = \frac{2mL\,sin\,\theta}{h}\; d = 258.82\,L\lambda\;\; (\mu s\; m\; Å)$ Equation 4.7

b) Diffraction from Glass: For randomly ordered structures like glass, the diffraction pattern consists of broad peaks and troughs. There can also be local structures within, different from the overall average structure of glass for which refinement of the diffraction pattern is important. In a disordered material, we measure 'Total Diffraction'

(all neutrons are detected regardless of any energy exchange if or if not occurred) in terms of differential cross section: $\frac{d\sigma}{d\Omega}$ where,

$$\left(\frac{d\sigma}{d\Omega}\right)_{total} = \frac{R_{total}}{N\Phi d\Omega}$$

R_{total} = rate at which neutrons of wavelength λ are scattered into solid angle dΩ in direction (2θ,φ); N = Number of atoms in the sample

Φ = The total flux of neutrons incident on sample.

dσ/dΩ, in general, depends only on the magnitude of momentum transfer for elastic scattering in glasses and is denoted as, scattering vector **Q**;

where $Q = K_0 - K_f$ (K_0 and K_f are the neutron wavevectors before and after scattering.)

Thus, $$\left(\frac{d\sigma}{d\Omega}\right)_{total} = i(Q) + \langle\overline{b^2}\rangle_{avg}$$

Here, *i(Q)* is distinct scattering due to interference between two different atoms and $\langle\overline{b^2}\rangle_{avg}$ is self- scattering due to correlations between atom and itself.

For diffraction, the second term is featureless. The distinct scattering provides information about interatomic distances and hence, the structure of short and mid-range bonds made by the glass.

The neutron spectrum is obtained in terms of total correlation function, *T(r)* w.r.t bond distance r (Figure 4.16), where *T(r)* is obtained by Fourier transforming the distinct scattering *i(Q)*

$$T(r) = T^o(r) + \frac{2}{\pi}\int_0^\infty Qi(Q)M(Q)\sin(RQ)dQ \qquad \text{Equation 4.9}$$

Where,

$T^o(r)$ = average density contribution to the correlation function;

$M(Q)$ = modification function such as Lorch or step function used to modify the data up to finite value of maximum momentum transfer Q_{max}, from infinity as suggested in equation 4.9

$$T^o(r) = 4\pi r\rho^o \left(\sum_{l=1}^{N} C_l\, \bar{b}_l\right)^2 \qquad \text{Equation 4.10}$$

Where,

r = atomic separation between atoms

ρ^0 = average atomic number density

N = number of elements per sample

C_l = atomic fraction for element l

$\bar{b}_l$ = coherent scattering for element l

The Total correlation function $T(r)$ can be thus written as a weighted summation of all possible partial correlation functions $t_{l\,l'(r)}$ and is given by equation 4.11

$$T(r) = \sum c_l\ \bar{b}_l\ \bar{b}_{\acute{l}}\, t_{l\acute{l}}\,(r) \qquad \text{Equation 4.11}$$

At short range r < 3-4 Å, $T(r)$ arises from one particular set of elements l and l' with a peak area $A_{ll'}$ and interatomic distance $r_{ll'}$. The coordination number for the pair can be calculated as:

$$n_{ll'} = \frac{r_{ll'}\, A_{ll'}}{(2 - \delta_{ll'})c_l \bar{b}_l \bar{b}_{l'}} \qquad \text{Equation 4.12}$$

where δ is Kronecker delta for the pair ll'.

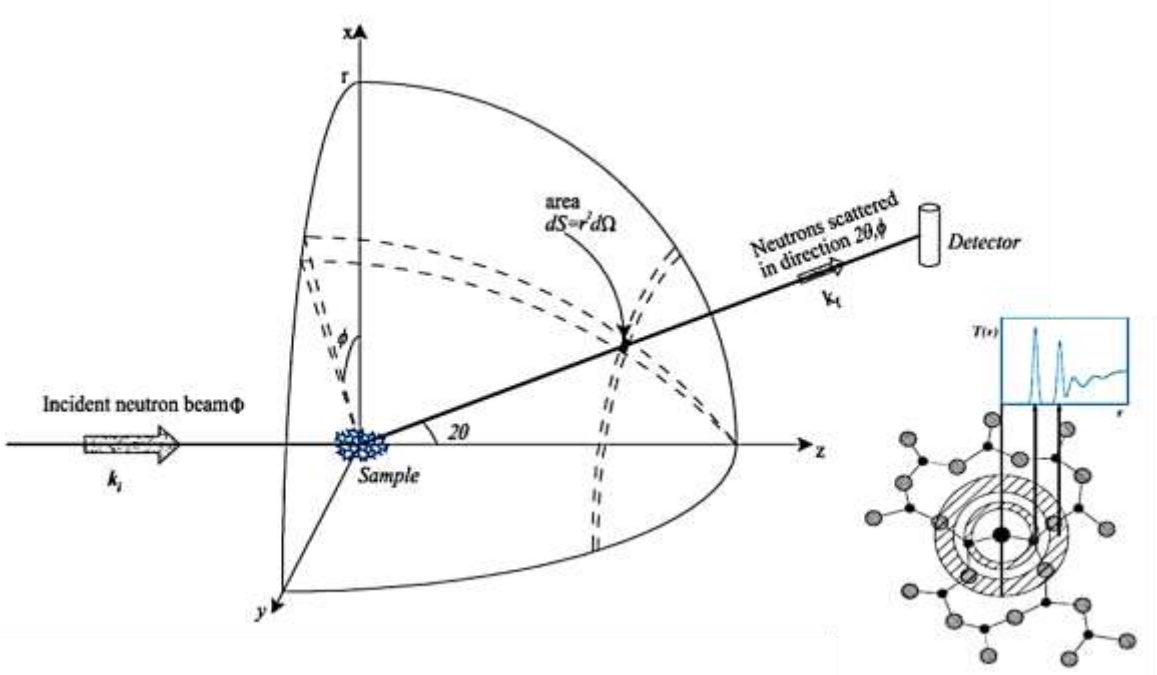

Figure 4.16: Schematic representation of the scattering geometry of a neutron diffraction experiment for glass (ISIS Neutron training school 2016 booklet).

b) GEneral Materials (GEM) Diffractometer: The GEneral Materials diffractometer, GEM, at the ISIS Facility pulsed neutron source is the world's most advanced materials neutron diffractometer (Figure 4.17) (Hannon 2005; Affatigato 2015). The vacuum vessel made of 304 grade stainless steel embodies a wide loop of the detector array, which covers a very large area and a wide range in scattering angles and gives data with a high stability and high resolution. GEM receives neutrons from a normal view of a liquid methane moderator at a temperature between 100 and 110 K. The length of the incident flightpath, *Li*, is 17.0 m which is why resulting data has high resolution. The diffractometer is surrounded by eight banks of ZnS scintillator detector arrays at different scattering angles which allows time resolved stroboscopic measurements to be performed. A major consideration in the design of the diffractometer is the ability to use these detector banks simultaneously, which leads to very substantial effective count rate gains. Additional choppers are used at

several distances from the moderator to chop off the beam at $t = 0$ and restrict the wavelength range of incident beam. This prevents very fast neutrons and prompt gamma rays from reaching the sample and ensures low background and avoid frame overlap that occurs when slower neutrons from a pulse of the source are overtaken by faster neutrons from the subsequent pulse. The scattered flight path, L_f ranges from 1 to 2.9 meters.

c) Preparation of samples: The glass samples were crushed to fine powder using a mortar and pestle in open environment. These were then filled in 80mm long, 0.004 cm thick cylindrical vanadium foil cans. Vanadium cans were ideal for measurements as the scattering from vanadium is almost incoherent. Therefore, the Bragg peaks due to the can itself are very small. The height and weight of the sample were calculated to obtain the packing fraction prior to the experiment. A vanadium rod was used as glass standard. An empty vanadium can was measured prior to experiments to subtract any signals due to background effect. This helps in inter-normalization of the results obtained from different detectors. OpenGenie is a user-friendly interface developed at the neutron facility to view preliminary raw data during collection. The raw data was reduced, corrected and analysed using GudRunN, a computer program equipped with a graphic interface for full correction of the ND data (McLain et al. 2006; Soper 2012). The correlation functions were obtained by Fourier transforming the experimental data using the Lorch modification function (see equation 4.10) and a maximum momentum transfer of $Q_{max} = 45$ in all cases except for lithium silicate glass where the data was cut off at $Q_{max}= 40$. The correlation functions were fitted in the *T(r)* spectra using a neutron correlation function fitting software 'pnfit'.

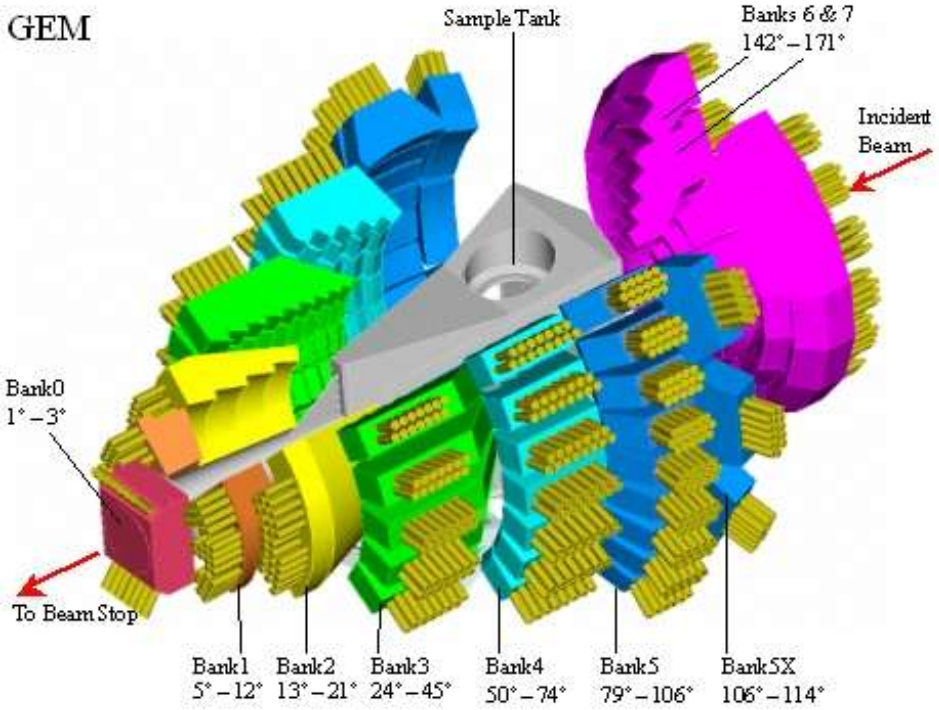

Figure 4.17: The GEneral Materials Diffractometer at the ISIS pulsed neutron source facility. (courtesy: ISIS, neutron source facility)

4.7.4 Other Techniques

4.7.4.1 ^{57}Fe Mössbauer Spectroscopy

The technique was primarily used to determine the oxidation state of iron and the type of coordination polyhedron occupied by the Fe atoms present in the complex borosilicate glasses. Determination of the iron redox ratio (Fe^{2+}/Fe^{3+}) aids the modeling of the cation field index model and optical basicity (Bingham et al. 2017). A room temperature ^{57}Fe Mössbauer spectrometer with a 25 mCi source of ^{57}Co in Rh. was used for the measurements.

a) Background: The method utilizes a solid source of radiation such as a radioactive isotope, where energy transition occurs from an excited nuclear state to the ground state with emission of a gamma ray.

In the Mössbauer spectrometer, a beam of gamma radiation passes through the sample, and a detector on the other end measures the intensity of the beam transmitted through the sample (Figure 4.18). The atom in the source emitting the gamma rays must be of the same isotope as the atoms in the sample absorbing them. ^{57}Co is the parent source used for ^{57}Fe spectroscopy. An atom of ^{57}Co decays to excited state of ^{57}Fe by electron capture giving off a γ-ray, which further decays to ground state ^{57}Fe releasing a γ-ray of 14.4keV energy. The γ-ray may be absorbed without recoil by a nearby ^{57}Fe, which have just the right splitting between the energy levels in its nucleus to absorb it (Figure 4.19).

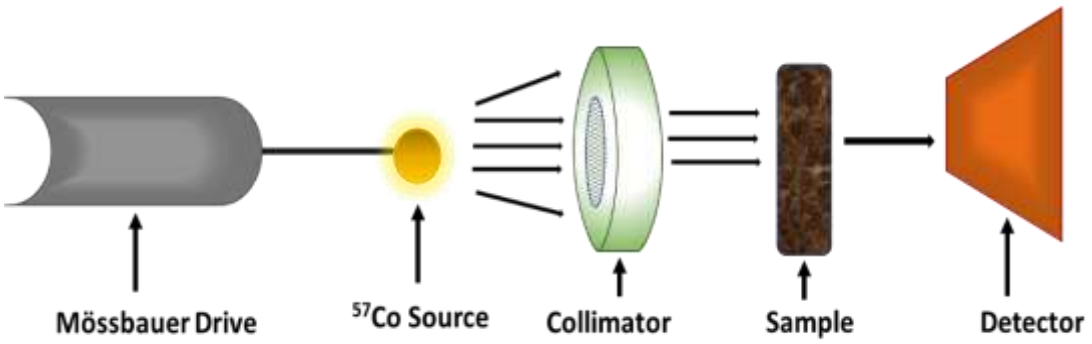

Figure 4.18: Schematic diagram of a Mössbauer spectrometer.

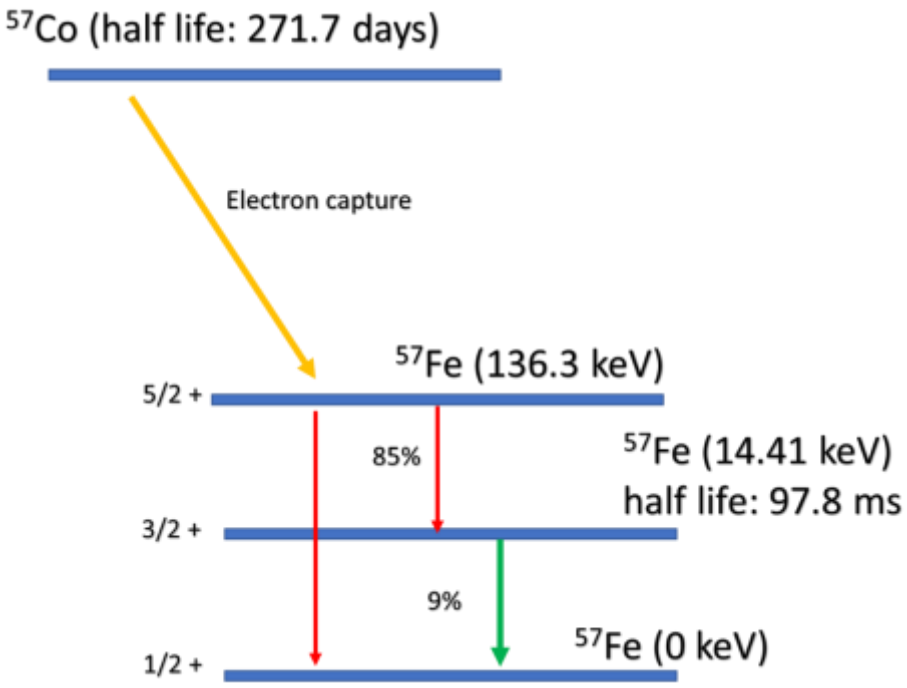

Figure 4.19: Schematic diagram of the ^{57}Co decay process

Mössbauer spectra are described using three parameters (Figure 4.20) (Muller-Warmuth & Eckert 1982; Dyar et al. 2006)

- Centre shift (δ) (also known as Isomer Shift) due to difference in *s*-electron density between source and absorber.
- Quadrupole splitting (Δ) due to shift in nuclear energy levels induced by an electric field gradient caused by nearby electrons.
- Hyperfine splitting that occurs only for magnetic materials.

Iron atoms in different local environments (affected by the coordinating anions with Fe and symmetry of the site) and different oxidation states are absorb at separate energies (Darby Dyar 1985; Bingham et al. 1999; Jayasuriya et al. 2004; Williams et al. 1998). Combination of isomer shift and quadrupole splitting is used to identify the valence state and site occupancy of Fe in the glass.

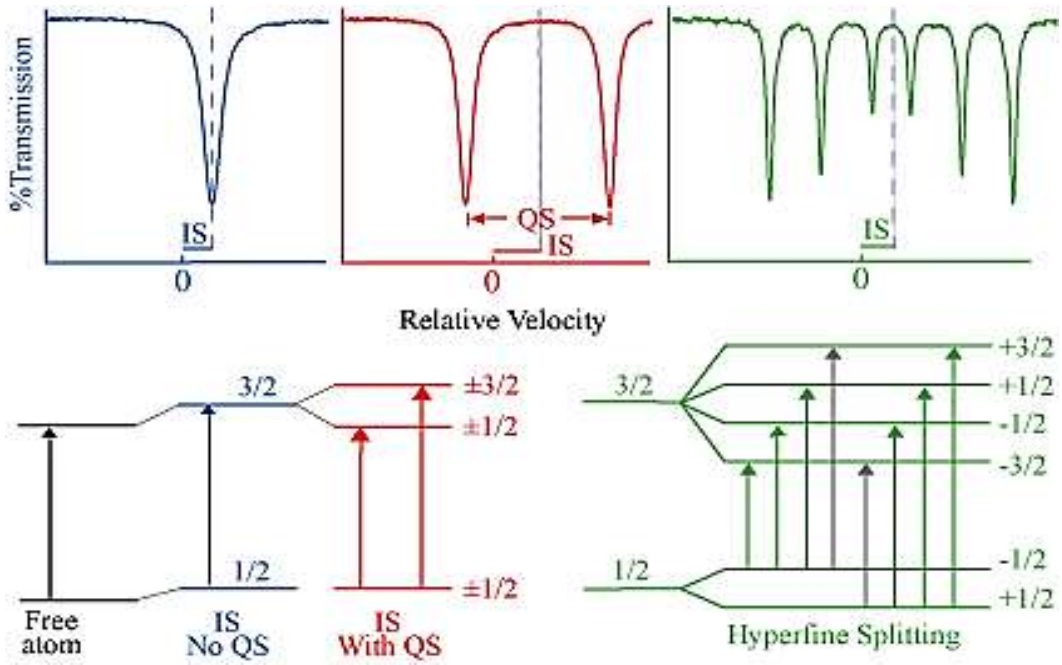

Figure 4.20: The three Mössbauer parameters: Isomer shift (IS)-shift from zero to midpoint of a doublet; Quadrupole split (QS)- split between two peaks of a doublet; Hyperfine splitting-sextet set due to six possible nuclear transitions.

d) Preparation of samples: The glass samples were powdered in the vibration mill at 600 rpm for 1 minute in a hardened steel milling set. The powdered sample was mixed with graphite powder that is inert to the gamma rays and spread evenly in the sample holder. The obtained data was fit using a Recoil analysis software package.

4.7.4.2 Differential Scanning Calorimetery (DSC)

The DSC technique was useful in determination of thermal behaviour of A/A-AE Si family over a wide temperature range and find the crystallisation temperatures (T_x) of each sample. At known T_x, a glass ceramic was formed. XRD on the glass ceramic revealed crystal structure formations by glass which aided the ND studies done on the glass. A NETZSCH STA (Simultaneous Thermal Analysis) 409PG Luxx®, coupled to

an Aëolos mass spectrometer was used for all the measurements. The furnace can operate up to 1500 °C with heating rates from 0.1 to 50 °C/min

a) Background: When the glass undergoes transition, crystallization, melting, or sublimation, the latent heat produced is either absorbed by the sample (endothermic) or lost to the atmosphere (exothermic). This gradual thermal transition is recorded in a DSC curve (Figure 4.21) with respect to temperature relative to an inert material that undergoes no phase transitions in the temperature range of interest used as a reference. The sample and reference both pass through identical thermal cycles. The DSC equipment is coupled with mass spectrometers to provide a Thermogravimetric Analysis (TGA) which provides both mass and temperature loss against temperature.

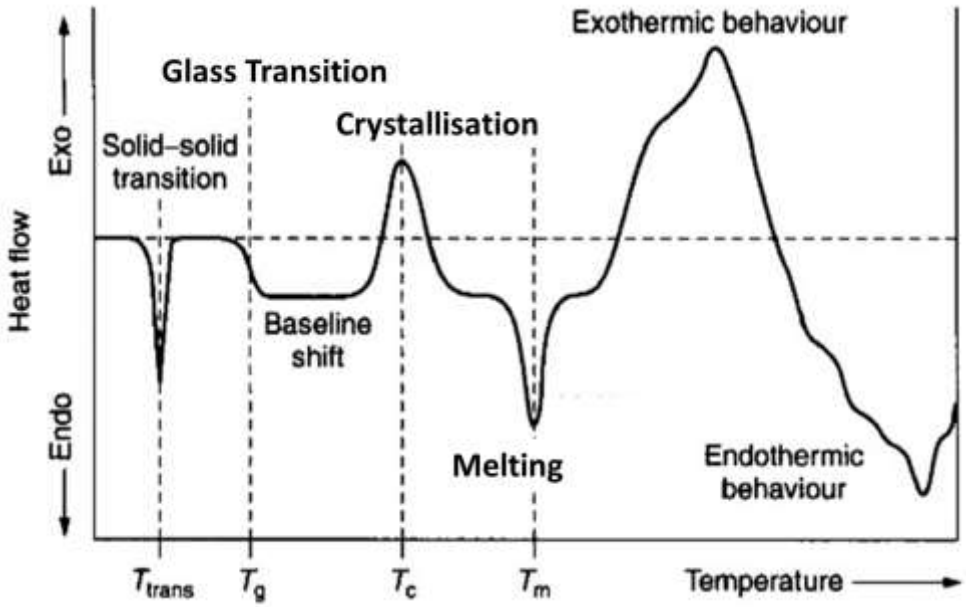

Figure 4.21: The glass transition DSC temperature profile

b) Preparation of samples: 40 mg of powdered glass samples were filled in alumina crucible and inserted with an empty alumina crucible used as the inert reference. The

sample along with an empty crucible were together put in the spectrometer and the furnace was ramped up to 1300 ºC from room temperature at rate of 5ºC/minute.

CHAPTER 5

SULPHUR INCORPORATION IN SILICATE GLASSES

This chapter describes the effects of sulphate incorporation on the structure and properties of simple binary and ternary alkali / alkali-alkaline earth silicate glasses. The compositional and structural changes on moving from a SO_3 free silicate glass to the SO_3 containing (i.e. pro rata additions of SO_3) equivalent, were analysed using density measurements; XRF (ICP for Li content); XRD; Raman Spectroscopy; ^{29}Si,^{23}Na, ^{7}Li MAS NMR; and Neutron Diffraction. DTA revealed the transition temperature T_g and crystallisation temperature T_x for Na_2O containing binary and ternary glasses which was followed by heat treatment at the onset of T_x. The crystalline phases developed in the amorphous structure were further investigated with XRD and the commercial Crystal Maker software package.

5.1 Glass Preparation

Four sets of glasses were prepared for the silicate glass series. Each set contained one SO_3 free 'undoped' base glass and a corresponding SO_3 'doped' equivalent. The targeted doping was ~ 5 mol% SO_3. The base glasses comprised two binary systems: R_2O-SiO_2 (R = Li, Na) and two ternary systems: Na_2O-MO-SiO_2 (M = Ca, Ba). The ternary compositions were achieved by substituting half of the molar concentration of

Na_2O with MO in Na_2O-SiO_2. Analytical grade carbonates Na_2CO_3, Li_2CO_3, $BaCO_3$, $CaCO_3$ ~ purity > 99.9%) and high purity sand (99.99% purity) were used for glass batch preparation. Sulphur was added as Na_2SO_4 in the Na_2O containing doped glasses and Li_2SO_4 in the Li_2O-SiO_2-SO_3 glass. Batch compositions were prepared for 125g of glass on a calibrated balance with precision of ± 0.001 g; mixed thoroughly, and melted in a Pt-ZGS (ZrO_2 Grain Stabilised) crucible loosely covered with a Pt-ZGS lid to reduce volatilisation losses and contamination. The melts were attained within a temperature range of 1300-1350°C with a dwell time of 3 hours per melt and poured on a clean steel plate to cool gradually to room temperature. The Li_2O-SiO_2 and Li_2O-SiO_2-SO_3 glasses were splat quenched between two uniform stainless-steel bars to maximise the cooling rate and avoid crystallisation. The glasses, however, partially crystallised in the lapse of time (2-3 seconds) between pouring and splat quenching. The glassy parts were visually identified and separated from the cooled melt for the analysis. The cooled binary melts were immediately transferred into a vacuum desiccator to avoid any hydration in consideration of its poor chemical durability (Douglas & El-shamy 1967; Day 1976; Paul 1977). Details of the eight glasses produced in the silicate glass series are tabulated in Table 5.1. A few key points should be noted before scrutinizing the nominal compositions:

Note 1: No binary alkaline-earth silicate base glasses or doped equivalents were produced as the maximum temperature attainable by the electric furnaces available for the experiments had an upper limit of ~1450 °C. To fabricate the desired alkaline earth binaries, melt temperature beyond 1550 °C are required.

Note 2: Only 2 mol% of SO_3 was added to Na_2O-CaO-SiO_2 glass as this glass reached its sulphate saturation limit beyond this point.

Note 3: The amount of sulphate added to Na_2O-SiO_2-SO_3 batch was higher than the targeted load for other glasses (~ 6.5 mol% SO_3).

It is important to note that the focus of this set of experiment was to investigate the inherent sulphate capacity as dissolved species in the glasses within their atomic structure under imposed near-sulphate-saturation conditions. It is acknowledged that in real world industrial vitrification, conditions such as melting temperature, redox, pressure. are different than studied in laboratories (Bingham *et al.* , 2017). Any of these factors can influence sulphate solubility and capacity in glass but the inherent capacity of any glass to incorporate sulphate is a function of glass composition and structure. The glasses were milled to form a glass powder in the vibration mill at 700 rpm for 1 minute for purpose of XRF, XRD, ICP-AES, NMR, ND and DTA.

5.2 Dependence of Sulphate Capacity on Glass Composition

5.2.1 XRF-ICP-EDS Analyses: Results and Discussion

The milled glass powder was mixed with $Li_2B_4O_7$ in 1:8 ratio and melted in platinum crucibles in an electric furnace set at 1100^{o}C, with 30 minutes dwell time per sample and removal to room temperature to produce fused beads. Figure 5.1 shows the analysed SO_3 content retained within the doped glasses as a function of glass composition, all of which retained > 85% of batched SO_3 (within an error limit of ± 0.1 - 0.3 mol%). No salt phase separation was observed on surface of the pristine melts, which would indicate that the sulphate capacity of the glass melt had been exceeded. Therefore, the sulphate capacity in the glass can be shown to be same or greater than the molar content of SO_3 measured for the glass with XRF and ICP. Table 5.1 shows the nominal and

analysed compositions in brackets for the eight silicate glasses. The ratio of SiO_2 to the total amount of modifier oxide (MO_x) is also shown. The error bars were generated by the IQ+ software used for XRF data analysis by calculating the standard deviation of the multiple measurements made per sample.

Sample	SiO_2 (mol%)	Li_2O (mol%)	Na_2O (mol%)	CaO (mol%)	BaO (mol%)	SO_3 (mol%)	$\frac{[SiO_2]}{[MOx]}$	Melt Temp (°C)
LiSi	57.50 (62.50)	42.50 (37.50)	0	0	0	0	(1.66)	1320
LiSiS	54.63 (60.32)	40.37 (35.45)	0	0	0	5.00 (4.23)	(1.70)	1320
NaSi	57.50 (60.35)	0	42.50 (39.65)	0	0	0	(1.52)	1300
NaSiS	53.76 (56.32)	0	39.74 (37.23)	0	0	6.50 (6.45)	(1.51)	1300
NaCaSi	57.50 (57.92)	0	21.25 (20.77)	21.25 (21.31)	0	0	(1.38)	1350
NaCaSiS	56.35 (57.44)	0	20.83 (19.99)	20.83 (20.53)	0	2.00 (2.04)	(1.36)	1330
NaBaSi	57.50 (59.62)	0	21.25 (23.40)	0	21.25 (16.98)	0	(1.48)	1350
NaBaSiS	54.63 (56.63)	0	20.19 (22.51)	0	20.19 (16.40)	5.00 (4.46)	(1.46)	1330

Table 5.1: Nominal vs analysed (in brackets, normalised to 100%) compositions in mol% for the eight silicate glasses.

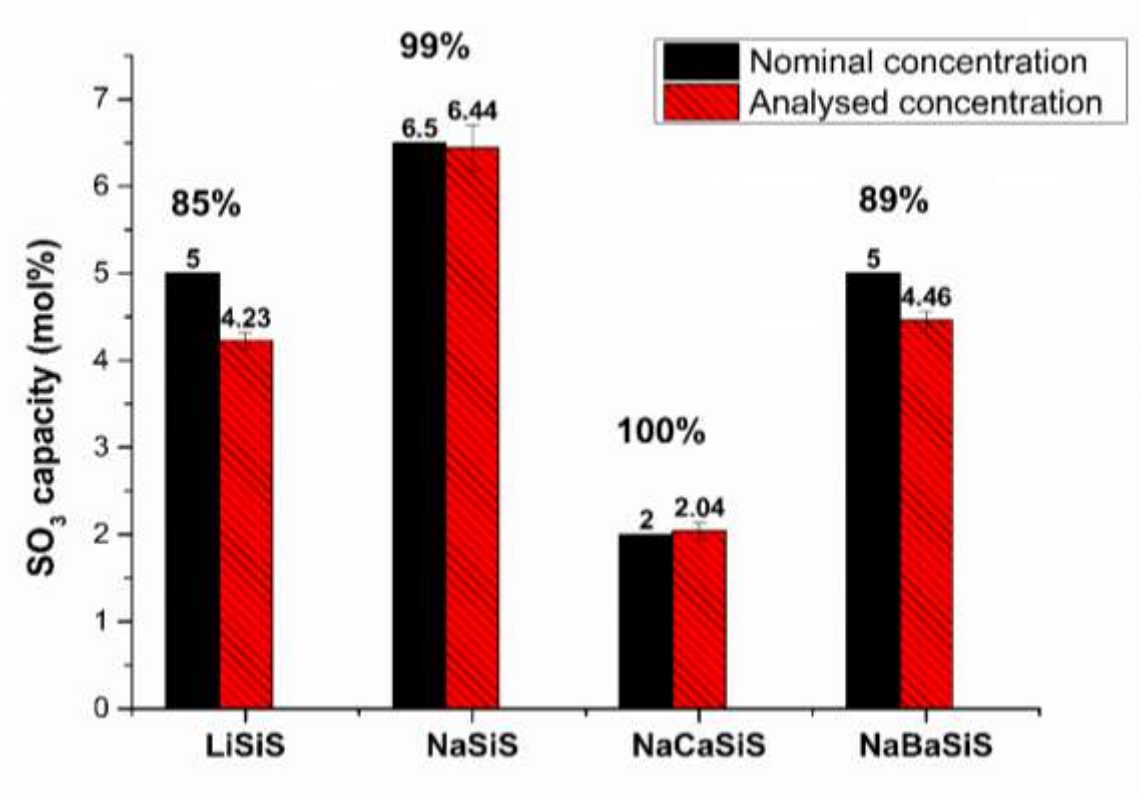

Figure 5.1: SO_3 capacity as a function of. changing glass composition

The discrepancy between the nominal and analysed values of Na_2O and SO_3 may be due to volatilisation losses. The lower concentration of Li_2O measured for samples LiSi and LiSiS could be attributable to the phase separation that occurred in the lapse of time between pouring and splat quenching which may have resulted in crystalline phase with higher Li_2O content and a glassy phase with lower concentration of Li_2O. The difference between nominal and measured values for BaO is either due to the reference standard used for XRF BaO measurement or else impurities present in the raw materials used for glass preparation. The latter rationale was ruled out after the purity of $BaCO_3$ and SiO_2 used for batch preparation was investigated using XRD which implies inaccuracies associated with either the XRF spectrometer itself or the calibration programme used, to determine exact BaO content. Other potential sources of error include those associated with XRF and ICP analyses and the fused bead sample preparation. The

concentrations of BaO retained within samples NaBaSi and NaBaSiS were counterchecked with SEM-EDS and the results are tabulated in Table 5.2. Figure 5.2.1 and 5.2.2 show the EDS spectra for the two glasses. The semi-quantitative concentrations measured with SEM-EDS show that no significant BaO loss is incurred for NaBaSi and NaBaSiS as was suggested by the XRF results.

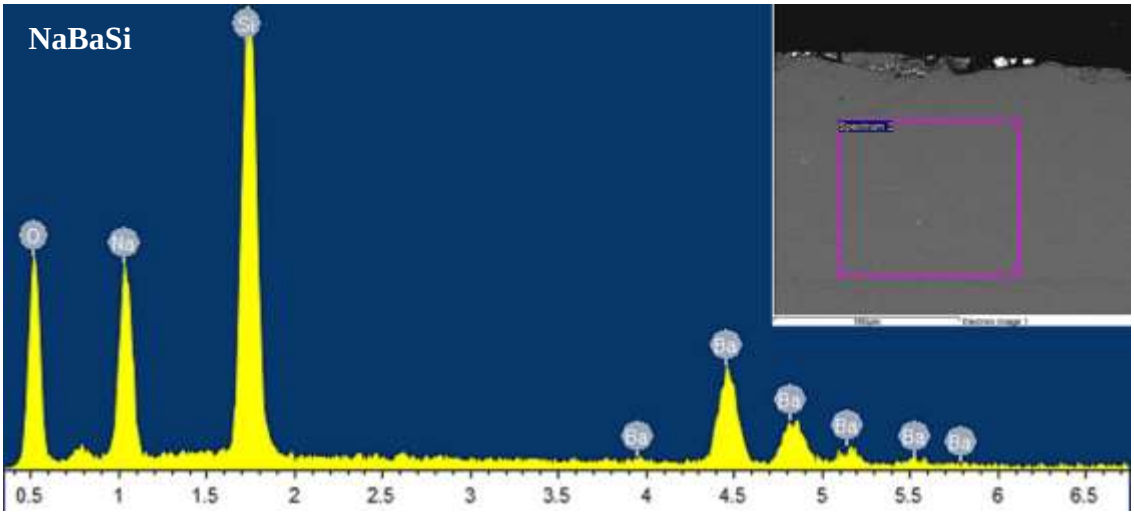

Figure 5.2.1: EDS spectrum obtained for glass NaBaSi showing the presence of Na, Si, O - K lines and Ba- L lines

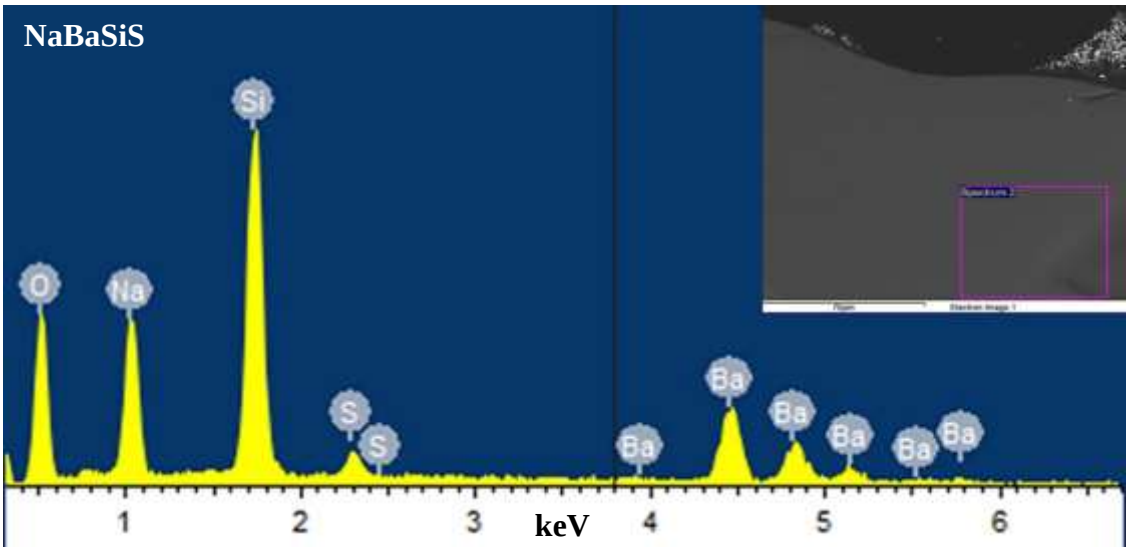

Figure 5.2.2: EDS spectrum obtained for glass NaBaSiS showing the presence of Na, Si, O- K lines and Ba- L lines

	Na_2O (mol%)	BaO (mol%)	SiO_2 (mol%)	SO_3 (mol%)	$\frac{[SiO_2]}{[MOx]}$
NaBaSi	20.57	21.62	57.81	-	1.37
NaBaSiS	19.10	20.70	55.70	4.50	1.39

Table 5.2: Concentration of oxides present in samples NaBaSi and NaBaSiS obtained from SEM-EDS

Nevertheless, the $[SiO_2]$ / $[MO_x]$ ratio for all four sets of glasses between the SO_3 free and SO_3 doped systems are consistent within experimental uncertainties. Therefore, direct comparisons between the base and doped glasses are valid and any structural changes observed between the two systems can be safely concluded to be related to SO_3 incorporation.

The SO_3 capacity of the binary NaSiS glass is higher than in its corresponding ternary compositions. The trend followed is: NaSiS >NaBaSiS >NaCaSiS. Clearly, the reduced concentration of modifier alkali cation in the ternary system has influenced the sulphate limit.

The SO_3 incorporation capacity of the NaBaSiS sample is almost double than the NaCaSiS glass, which suggests that besides the concentration of the alkali ion in the ternary glass, sulphate capacity is also dependent on the nature of the co-participating alkaline earth cation. This is consistent with the studies of Na_2O-MO-SiO_2 (M=Mg, Ca, Ba) glasses by Ooura & Hanada (1998), where they realised change in sulphate solubility with type of MO in the order BaO > CaO > MgO.

The SO_3 content of the LiSiS glass was lower than the NaSiS glass. This may be due to the preference for Na^+ ions with lower cation field strength than Li^+ by the sulphate ions present in the glass it may be due to the lower concentration of Li_2O retained in the glass. This case is further investigated in the next section.

5.2.2 Cation Field Strength Index (CFSI): Results and discussion

The cation field strength, CFS of a cation is related to the valence and the interatomic distance between the cation and its neighbouring oxygen with the relationship stated in equation 5.1

$$F = \frac{z}{a^2} \qquad \text{Equation 5.1}$$

where *z* is the cationic charge and *a* is the cation-oxygen atomic bond distance (Å).

'*a'* depends on the coordination of cations present in the glasses with respect to their neighbouring oxygen ions. The coordination numbers and respective cation-oxygen bond distances were determined through the Neutron diffraction studies (see later in section 5.3.3.2 and 5.3.3.3) and are as follows:

Si (4), Na (6), Li (4), Ca (6), Ba (8).

Based on the work of (Hawthorne 1994; Mountjoy 2007; Hoppe et al. 2007) and the average oxygen coordination number calculated using an empirical model (based on bond valence parameters; see section 5.3.3.3) for the glasses studied in this case, oxygen is assumed to be 4 coordinated with an ionic radius of 1.38 Å (Shannon 1976). The individual CFS of the modifier cations were calculated using equation 5.1.

The CFS of the cations present in the glasses studied in this case, are tabulated in Table 5.3. However, in the actual glass melt a distribution of bond lengths and coordination environment exists around the cations and neighbouring oxygens. This has been taken into consideration while calculating uncertainties associated with CFS.

Cation	Valence	Coordination	CFS
Si	+4	4	1.487± 0.010
Na	+1	6	0.174 ± 0.011
Li	+1	4	0.258 ± 0.010
Ca	+2	6	0.353 ±0.010
Ba	+2	8	0.255 ± 0.015

Table 5.3: The cation field strength calculated for the cations present in the glass compositions from (Shannon 1976)

The cation field strength of the cations decreases in the following order:

$$Si^{4+} > Ca^{2+} > Li^{+} > Ba^{2+} > Na^{+}$$

Previous work by various researchers (Ooura & Hanada 1998; McGann et al. 2012; Bingham et al. 2017; Kaushik et al. 2006; Jantzen et al. 2005) suggests that addition of a larger cation (lower field strength) can enhance sulphate solubility. This can be due to the fact that a cation with lower CFS contribute to higher oxygen anion activity in the melt which improves the dissolution of sulphate (Harding 1972). Taking into consideration, the CFS listed in Table 5.3, it is therefore expected that sulphate solubility should enhance with addition of ions such as Na^{+} for Li^{+} and Ba^{2+} for Ca^{2+}. The SO_3 content analysed for the glasses, are consistent with this predicted behaviour.

5.2.2.1 Normalised Cation Field Strength Index (NCFSI)

Besides calculating the CFS of individual cations, the author has calculated the NCFSI: Normalised Cation Field Strength Index ($\sum(z/a^2)$) i.e. the summation of CFS of each oxide normalised to one mole cation. The calculations were based on the empirical model developed by Bingham & Hand (2008) to study the effect of NCFSI on sulphate capacity of a combination of phosphate and borosilicate glasses. The authors observed a linear decrease in the SO_3 capacity of glasses with increasing NCFSI. Figure 5.3 shows the sulphate capacity of the glasses plotted against the NCFSI and a linear relationship is observed between the two parameters with R^2 value close to unity. The horizontal error bars reflect the upper and lower limit of NCFSI for each sample due to multiple cation-oxygen bond distances that can be present within the glass.

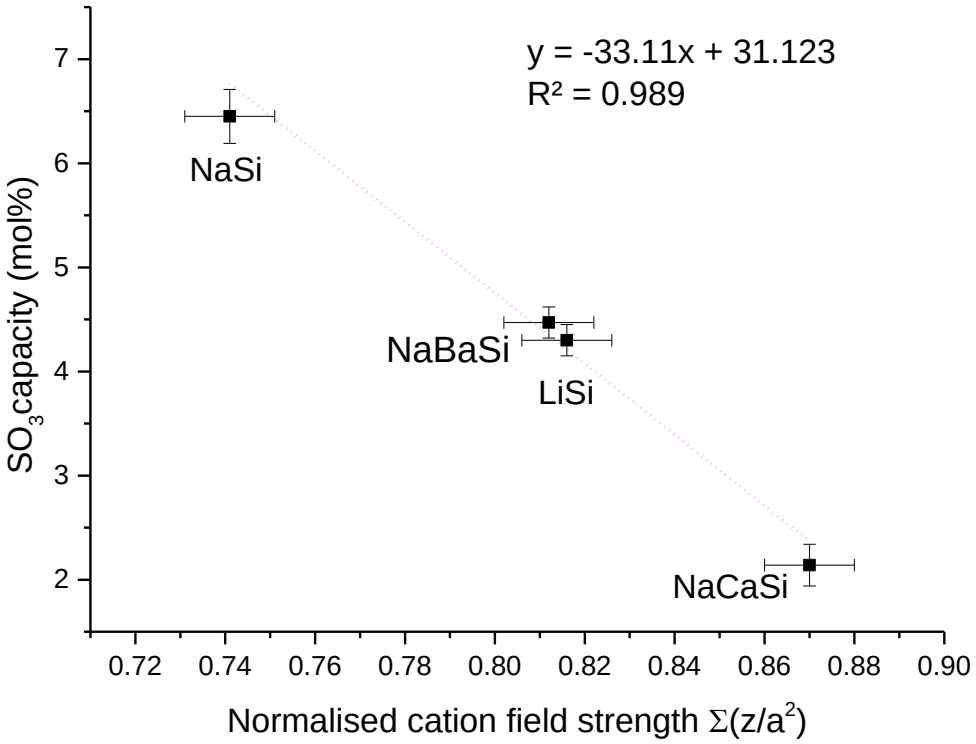

Figure 5.3: Sulphate capacity plotted as a function of normalised cation field strength index calculated for silicate glasses

5.2.2.2 Total Cation Field Strength Index ($CFSI_{total}$)

The total cation field strength index ($CFSI_{total}$) is also calculated for the SO_3 doped glasses with the empirical cation field index model developed by Bingham and colleagues (2017) for multiple-oxide containing borosilicate waste simulant glasses, based on equations 5.1 and 5.2. The $CFSI_{total}$ model calculations include an extra factor due to the normalised molar concentration of oxides present in the glass. The computations were carried out including and excluding sulphate concentrations in the formula (Table 5.4), as the authors suggested that sulphate capacity and $CFSI_{total}$ are inversely proportional when sulphate concentrations are excluded in the model. The XRF analysed glass compositions were used for input values for modelling. The horizontal error bars in Figure 5.4 are representative of upper and lower limit of TCFSI for each sample due to change in CFS of the oxides present in the glass with changing cation-oxygen bond distances.

$$CFSI_{total} = \sum_{i=1}^{n} n_i c_i \left(\frac{z}{a^2}\right)_i \qquad \text{Equation 5.2}$$

Where, n_i = molar fraction of the i^{th} oxide in the glass;

c_i= number of cations in one formula unit of i^{th} oxide;

$\left(\frac{z}{a^2}\right)_i$ =CFS of the i^{th} oxide

Sample	$CFSI_{total}$ (without sulphate)	$CFSI_{total}$ (with sulphate)
LiSiS	1.093 ± 0.020	1.174 ± 0.020
NaSiS	0.963± 0.020	1.086 ± 0.030
NaCaSiS	1.010± 0.020	1.042 ± 0.020
NaBaSiS	0.948 ± 0.020	1.046 ± 0.030

Table 5.4: $CFSI_{total}$ of the doped glasses calculated including and excluding sulphate.

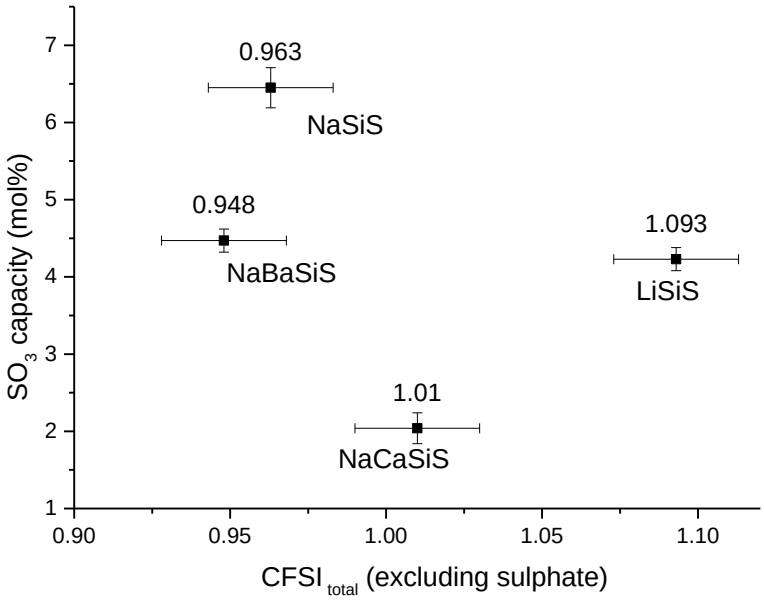

Figure 5.4: Sulphate capacity as a function of the total cation field strength index calculated for silicate glasses

In Figure 5.3, the NCFSI model shows a linear correlation between sulphate capacity and ionic field strength of the glasses studied. These results are consistent with the work of (Bingham & Hand 2008) where the authors investigated the applicability of the NCFSI model over a range of phosphate and borosilicate glass compositions and obtained linear trends between sulphate capacities and the normalised cation field strength index of the glasses. However, in Figure 5.4, the $CFSI_{total}$ model shows a less clear pattern against the sulphate capacities of the glasses. The rationale for this behaviour might be due to the high concentration of participating modifier oxides in these glasses. Inaccuracies are related with XRF measurements of oxide contents in the glasses, as already been discussed in section 5.2.1. Even a slight shift from the actual values of modifier concentration and/or coordination numbers, can impact the calculations significantly (see equation 5.2). The model is well applicable for the multiple oxide borosilicate compositions as investigated by the authors (Bingham et al. 2017), where the individual concentration of each modifier was less < 10 mol%.

Therefore, slight inaccuracies in the concentration and/or coordination numbers averaged out in the final value. To understand the limitations, it is suggested to develop a range of other binary and ternary silicate compositions and analyse them with the most robust and accurate analytical techniques such as ICP-OES or EPMA. This is a suggestion for future work.

5.2.3 Density Measurements: Results and Discussion

Density of a glass is a strong function of its composition and is affected by the atomic weights of the atoms, the packing arrangement, and the volume they occupy. The densities obtained for the glasses as shown in Figure 5.5 are in good agreement with previous studies of similar glasses (Megahed 1999; Shartsis et al. 1952; Doweidar et al. 1999; A.Paul 1982; Kitamura et al. 1998; Neuville 2006). The error bars are the standard deviation of the 5 measurements carried out per sample. The error values are less than 0.001 g cm^{-3} and comparable to symbol size. Figure 5.5 shows that addition of SO_3 to the silicate glasses lead to a slight decrease in their respective densities.

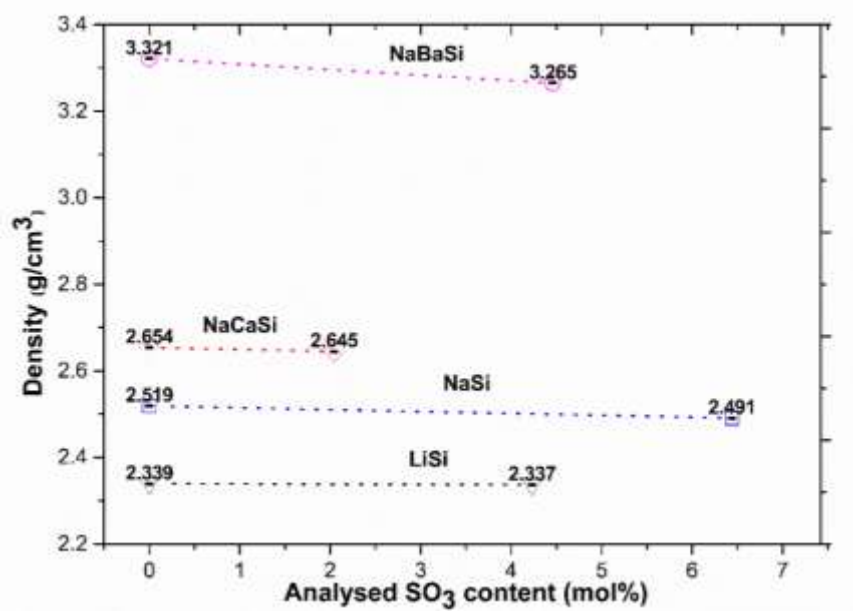

Figure 5.5: Densities of the four sets of silicate glasses as a function of analysed sulphate content using XRF (mol%)

The decrease in density of the glasses is in the following order:

LiSi < NaSi < NaCaSi < NaBaSi

LiSiS < NaSiS <NaCaSiS < NaBaSiS

Density of a material is related to its molar mass and molar volume as stated in equation 5.3.

$$\rho = \frac{\sum_i n_i * m_i}{V_m} \qquad \text{Equation 5.3}$$

Where, n_i = molar fraction of i^{th} oxide in the glass;

m_i = molar mass of the i^{th} oxide in the glass;

and V_m = molar volume of the glass

Where molar mass is a quantity only affected by the concentration and mass of oxides present in the matrix, molar volume besides the glass composition is strongly affected by the spatial structure of the oxygen network in the glass; the interstices (free volume) in the overall matrix; and the arrangement of modifier cations in the glass (ratio of BO / NBO, coordination numbers of the modifying cations).(Doweidar 1998; Jen & Kalinowski 1980).

The molar mass and molar volumes were calculated for the glasses along with the packing fraction using equation 5.4 and are tabulated in Table 5.5. For the calculations, analysed molar concentrations of the oxides were used. Literature was not identified for packing fractions in ternary silicate glasses, but for binary silicate glasses, the fractions obtained with the calculations are consistent with the work of (Giri et al. 2004; Feller 2008).

$$pf = \frac{\frac{4}{3}\pi \sum_i {r_i}^3 * c_i * n_i * A}{V_m}$$ Equation 5.4

Where, r_i = ionic radius of the i^{th} atom in the glass (Shannon 1976)

c_i = number of the corresponding i^{th} atom in the structural formula

n_i = molar fraction of i^{th} oxide in the glass,

V_m = molar volume of the glass, and

A= Avogadro's number ($6.022 * 10^{23}$)

Sample	Density (g cm^{-3})	Molar mass (g mol^{-1})	Molar volume (cm^3 mol^{-1})	Packing fraction (%)	Volume of ions (cm^3 mol^{-1})
LiSi	2.339	48.761	20.847 ± 0.005	41.504	8.652
LiSiS	2.337	50.226	21.491 ± 0.008	41.506	8.913
NaSi	2.519	60.839	24.151 ± 0.020	45.163	10.931
NaSiS	2.491	62.082	24.823 ± 0.120	45.298	11.164
NaCaSi	2.654	59.628	22.474 ± 0.002	45.047	10.121
NaCaSiS	2.645	60.052	22.720 ± 0.001	45.194	10.204
NaBaSi	3.321	82.301	24.830 ± 0.019	47.046	11.376
NaBaSiS	3.265	82.388	25.260 ± 0.010	47.174	11.523

Table 5.5: Molar mass, molar volume and packing fractions calculated for the glasses.

The calculated packing fractions in the LiSi and LiSiS glasses are lower than in the corresponding Na_2O containing glasses. This is intuitive as the ionic radius of Li^+ ions is much smaller than Na^+, Ca^{2+} and Ba^{2+}. This suggests that in in LiSi glass many

interstitial sites in the silicate network might be unoccupied due to lower concentration of Li^+ ions in the glassy phase of LiSi glass after splat quenching, resulting in lower packing fraction. In the LiSi, NaSi and NaBaSi glasses, the increase in density is directly influenced by the increasing molar mass of the sample upon complete substitution of lighter Li_2O (29.88 g mol^{-1}) with Na_2O (61.98 g mol^{-1}) in the binary system, and partial substitution with BaO (153.33 g mol^{-1}) for Na_2O in sample NaBaSi.

For sample NaCaSi, the molar mass reduces on partial substitution of CaO (56.08 g mol^{-1}) for Na_2O but the measured density is higher than that of NaSi glass. This suggests that the influence of molar mass on density is counteracted by the decrease in the molar volume of NaCaSi glass. Since the ionic radii of Na^+ and Ca^{2+} are similar ~1Å (assuming the average CN of Na and Ca to be 6) and the packing fraction of the NaSi and NaCaSi glasses are also similar, it is difficult to deduce the factors contributing towards the difference in molar volumes of the two compositions as the property is influenced by several factors.

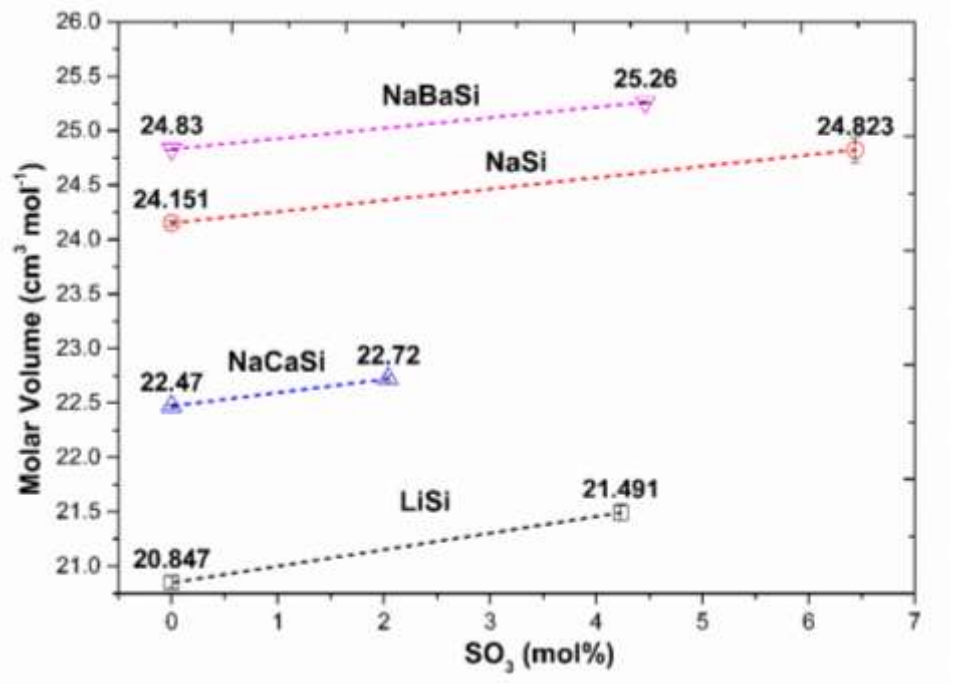

Figure 5.6: Molar volume of the four sets of silicate glasses plotted as a function of sulphate content (mol%)

Doweidar suggested an empirical approach to relate molar volume of glass with its structure (Doweidar 1999). As per his model, molar volume can be also formulated as:

$$V_m = \sum N_u * V_u \qquad \text{Equation 5.5}$$

Where N_u = Number of structural units 'u' per mole of glass

V_u = volume of the 'u' structural units (Q^n units)

Using the equation 5.5, the author calculated the volume of the Q^n structural units for various binary and ternary silicate glass compositions and found that V_u increases in the following fashion:

$$V(Q^4) = 0.453 Å^3 < V(Q^3) \approx 0.604\ Å^3 < V(Q^2) \approx 0.709\ Å^3 < V(Q^1) \approx 0.992\ Å^3$$

Key conclusions derived from Doweidar's model were:

1. The volume of Q^4 units remains constant for all glasses due to the structural unit being independent of the effect of modifier.
2. The volume of Q^n units decreases with n, where n = number of BOs.
3. The volume of the Q^n units (n = 0, 1,2,3) decreases with increasing cation field strength of the cations bonding with the Q^n units

Based on the Doweidar's model, average volume of the structural units in NaCaSi glass should be lower than NaSi glass as the CFS of Na^+ is less than Ca^{2+}.

Both, the calculated molar volume (V_m) and the volume of Si-Q^n units (V_u) are low in glass NaCaSi than NaSi. To determine the concentration of the structural units (N_u), characterisation of the two glasses using Raman spectroscopy and ^{29}Si-MAS NMR is necessary.

On addition of modifier cations to vitreous silica, these might occupy the interstitial spaces, break the Si-O-Si bonds and associate with the oxygen ions for charge neutralization in the SiO_4 network. If the modifier cation has a large ionic radius, it can create interstices larger than those already present. So, in order to accommodate these larger ions, the network expands, and the overall glass volume increases. For this reason, Ba^{2+} (ionic radius =1.42 Å) when substituted for Ca^{2+}, show increase in the molar volume by ~1.7 $cm^3\ mol^{-1}$ in both SO_3 free NaBaSi and doped NaBaSiS. This could also explain the increase in molar volume between SO_3 free and SO_3 doped compositions. With higher concentration of SO_3 incorporated in the glass matrix, more interstices are occupied which leads to increase in the overall molar volume and packing fraction.

5.2.4 Thermal Analysis

The DSC spectra obtained for Na_2O bearing binary and ternary silicate glasses are shown in Figure 5.7, 5.8 and 5.9. Samples LiSi and LiSiS were not measured due to insufficient sample remaining after crystallisation due to splat quenching. Samples were heated at a rate of 10°C/min. A negative deviation indicates endothermic phase transitions such as T_g (glass transition temperature) and T_m (melting point of crystalline phase). A positive deviation indicates exothermic transition such as T_c (crystallisation temperature). T_g and T_c were determined from the onset of first endothermic and exothermic peak. The thermal processing window (T_w) i.e. the temperature difference between the T_g and onset of crystallisation T_c ($T_w = T_c - T_g$) is also calculated.

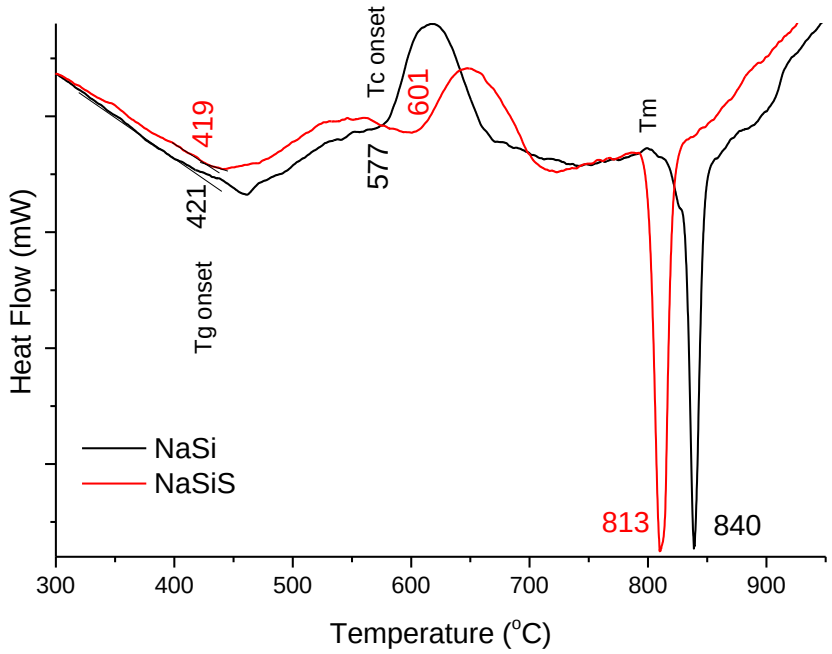

Figure 5.7: DSC curves for NaSi and NaSiS glasses shows the Tg (onset), Tc (onset) and Tm (crystallisation).

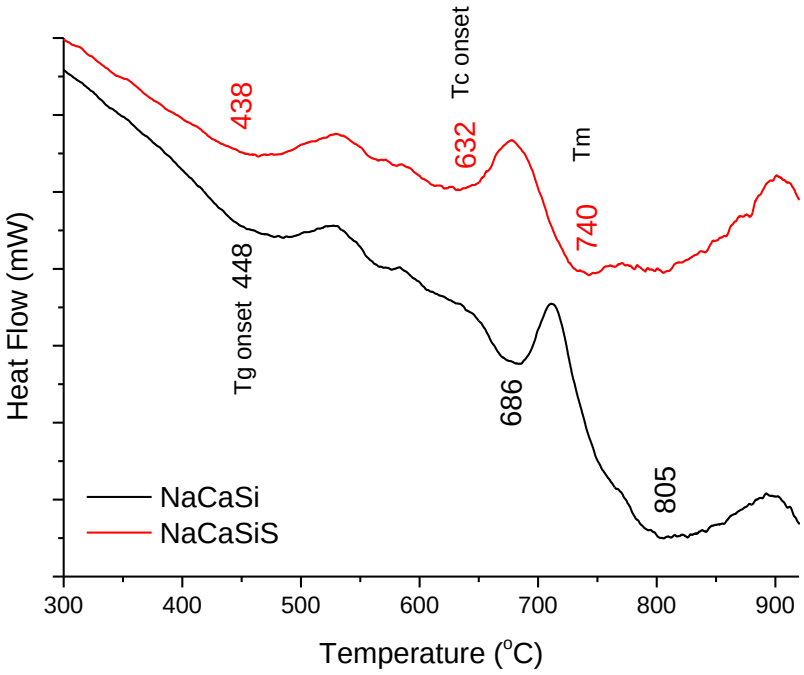

Figure 5.8: DSC curves for NaCaSi and NaCaSiS glasses

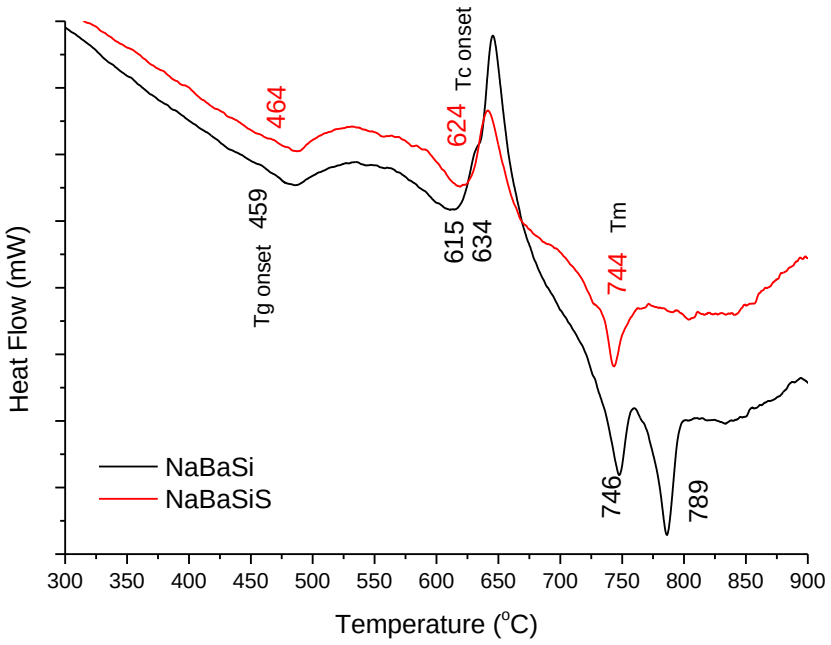

Figure 5.9: DSC curves for NaBaSi and NaBaSiS glasses. Presence of two Tm peaks for NaBaSi glass suggests present of two crystallisation phases.

Sample	T_g (onset) °C (±3)	T_c (onset) °C (±3)	T_m (centre) °C (±2)	$T_w = T_c - T_g$ (°C)	Hruby's Parameter $T_w / T_m - T_c$
NaSi	421	577	840	156	0.593
NaSiS	419	601	813	182	0.858
NaCaSi	448	686	805	238	2.000
NaCaSiS	438	632	740	194	1.796
NaBaSi	459	615, 634	746, 789	156, 175	1.191
NaBaSiS	464	624	744	160	1.333

Table 5.6: Tg, Tc and Tm obtained from the DSC curves of silicate glasses

The thermal transitions for glass NaCaSi set are broad, and weakly defined. Therefore, uncertainties associated with the determined temperatures are slightly greater than for the other two glass sets. Two Tc and Tm are obtained for NaBaSi, suggesting development of two different crystalline phases potentially enriched with Na^+ and Ba^{2+}, respectively. The DSC curves show an increase in T_g from NaSi to NaCaSi to NaBaSi glass. Within sulphate doped glass, the glass transition temperature is slightly affected by sulphate incorporation. Limited explanations (contradictory to an extent) are available in literature to link structure and composition of a glass with T_g. As per (Avramov et al. 2003; Avramov et al. 2005), T_g increases with increase in concentration of modifiers with larger ionic radius as a larger ion creates elevated hindrance in structural rearrangement of the SiO_4 network. Our results for the un-doped base glasses, agree with their observation. (Vassilev et al. 2016) suggested two reasons for decreases in T_g through their work on borate glasses:

a) Increase in depolymerisation (higher number of NBO) and decreased connectivity of the network forming cations. The same rationale was presented by (Manara et al. 2007) for the low T_g in their low sulphate doped borosilicate compositions.

However, in this study, it has been observed that the degree of polymerisation is enhanced with sulphate addition due to reduced availability of the modifier cations to interact with SiO_4 tetrahedra (see section 5.3.1 and 5.3.2 for the Raman spectroscopy and ^{29}Si-MAS NMR results), but except for NaBaSi-NaBaSiS glasses, a decrease in T_g is observed for glass sets NaSi-NaSiS and NaCaSi-NaCaSiS.

Moreover, amongst the three undoped glasses, polymerisation improves in the following trend: NaSi< NaBaSi< NaCaSi. But the highest T_g was recorded for NaBaSi glass. Therefore, the effect depolymerisation on T_g does not entirely explain the DSC results.

b) Replacement of high CFS cations with cations of low CFS as the bonds between the cations and neighbouring oxygen anions become weaker thus reducing the energy barrier for transition. The effect of CFS can be strong enough to overcompensate the effect of depolymerisation.

These studies imply that influence of both, depolymerisation effect and cation field strength of modifier cations can simultaneously co-exist and influence the T_g in the glasses being studied.

In sulphate doped glasses, T_g decreases for NaSiS and NaCaSiS glass. This may be caused due to interaction of sulphate ions with the modifier cations in the glass which results in reduction of the energy barrier required for silicate network relaxation as the concentration of cations interacting with the SiO_4 network reduces. On the other hand, the effect of polymerisation compensates the sulphate modifier interaction in case of glass NaBaSiS. Hence, T_g increases.

The T_w and Hruby's parameter are measured to determine thermal stability (delay in nucleation and growth of crystals) and vitrification ability of an amorphous system. (Hrubý 1972; Cabral et al. 2003; Cabral et al. 1997). The higher the value of these parameters, the higher is the stability. The results for our glasses suggest that addition of cations with high ionic field strength enhance the stability of glass. NaCaSi are the most stable compositions of the three cases studied with DTA. The stability of glass improves with sulphate addition for NaSiS and NaBaSiS glasses.

5.2.5 XRD Analysis: Results and Discussion

XRD patterns obtained for SO_3 free and SO_3 doped glasses are shown in Figure 5.10 and 5.11. The average inter-atomic distance for the four sets of glasses is calculated based on Bragg's law and plotted in Figure 5.12. The broad hump at 2θ = 20-40^o and no visible signs of any crystalline peaks suggests the glasses to be perfectly amorphous. Presence of a secondary amorphous hump at around 2θ= 35-45^o is noticeable but has not been investigated in this thesis.

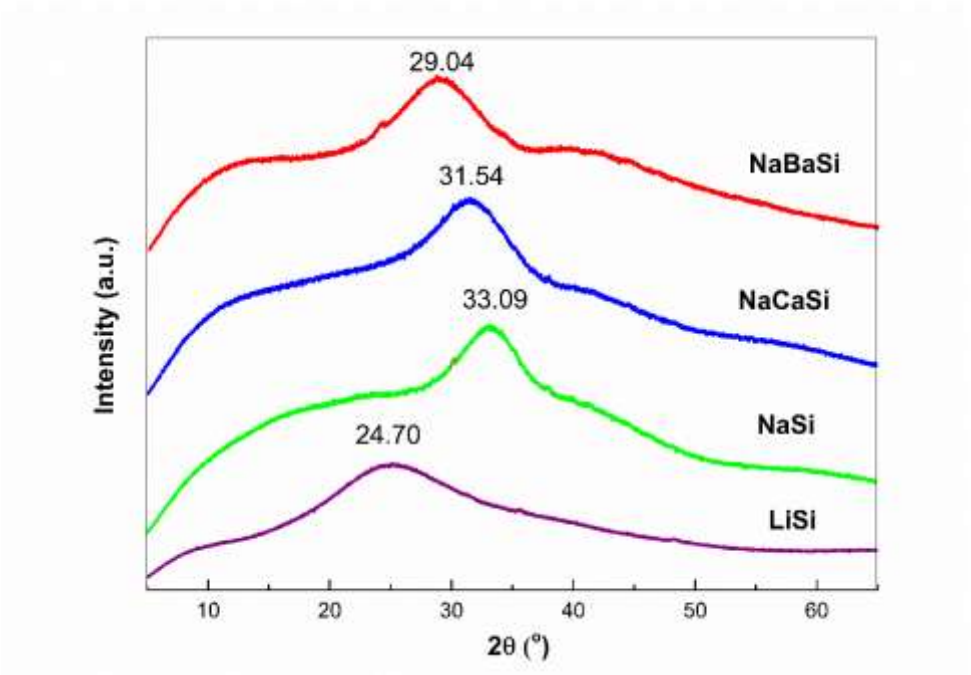

Figure 5.10: XRD patterns obtained for SO_3 free silicate glasses

The position of the amorphous hump shifts to lower diffraction angles as we move from NaSi to NaCaSi to NaBaSi glass sets. Such behaviour is predictable as to incorporate larger Ba^{2+} ions, there is an overall network expansion, resulting in dilation stresses and shift of the amorphous hump towards lower diffraction angles. Between NaSi and NaCaSi, the size of both ions is comparable. However, in NaCaSi glass the hump is an averaged convolution of Si-O, Ca-O and Na-O distances in the first coordination shell. Therefore, the diffraction angle shifts to a lower value, according to Bragg's law.

Of interest is the binary glass systems, where a significant shift of the broad hump towards lower diffraction angles (from 33.18^{o} to 24.70^{o}) is observed between NaSi to LiSi glass. The ionic radius of Li^{+} ion: 0.59Å is lower than the Na^{+} ionic radius: 1.02 Å and so is the molar mass. Therefore, it is expected for the amorphous hump to shift towards higher angles due to lower d-spacings. The contradictory behaviour is interesting. It may be caused as Li^{+} is a light element and poor scatterer of X-Rays. X-Ray scattering is proportional to the square of atomic number of the element. This suggests that less scattering centres are available in glasses LiSi and LiSiS. Therefore, the diffraction contributions are primarily due to Si-O, Si-Si distances in first and second coordination shells respectively. However, in NaSi glass the diffraction hump would be the averaged convolution of the Na-O, and Si-O distances in their first coordination shells.

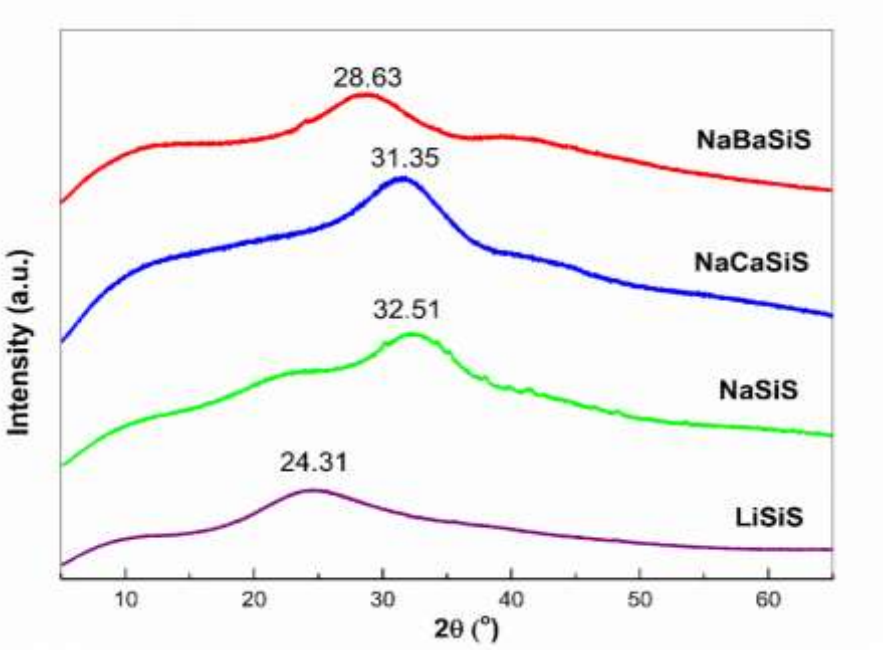

Figure 5.11: XRD patterns obtained for SO_3 doped silicate glasses

A comparison of the peak position of amorphous humps between the SO_3 free and SO_3 doped equivalents shows a shift towards lower 2θ in doped glass which is attributable to increase in the average atomic spacing. Magnitude of this shift ($\nabla 2\theta = 2\theta_{undoped}$ -

$2\theta_{doped}$) is plotted against the concentration of SO_3 retained within the glass. (Figure 5.13) and found to be linearly proportional with the SO_3 capacity of the three glass compositions.

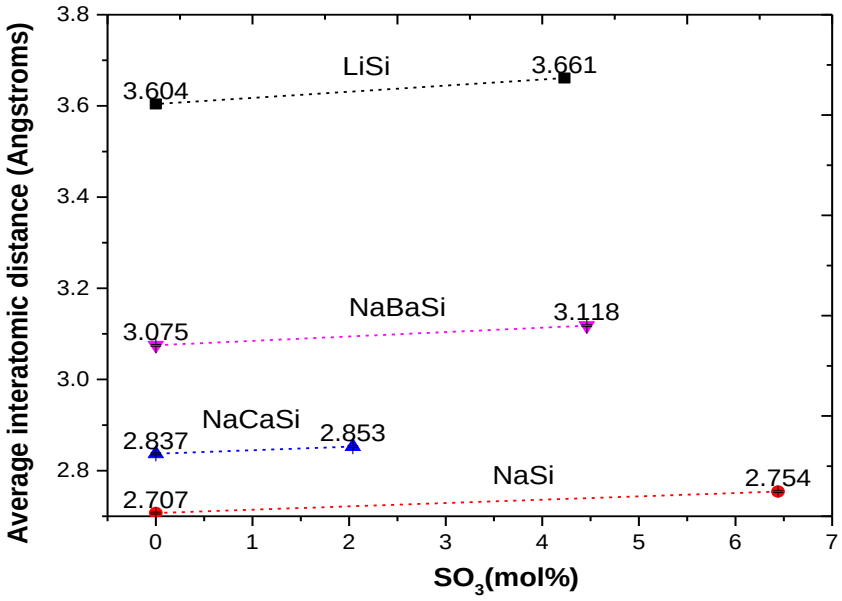

Figure 5.12: Change in average interatomic distance of the SO_3 free and SO_3 doped glasses plotted as a function of sulphate capacity of glasses.

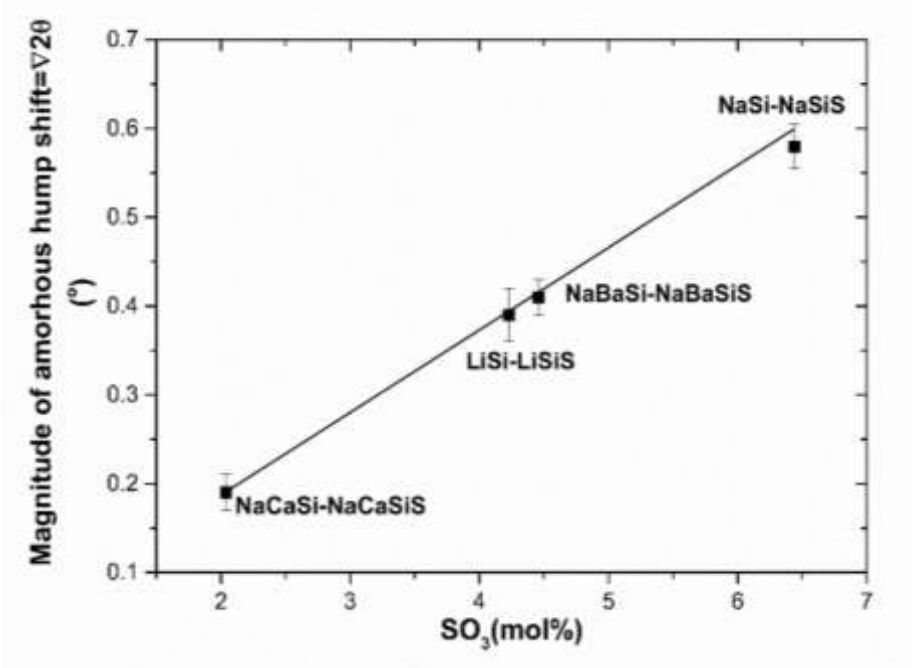

Figure 5.13: Shift in the amorphous hump position between the SO_3 free and SO_3 doped glass plotted as a function of sulphate capacity of the glasses

The shift in the amorphous hump diffraction angle and d-spacing as a function of concentration of dopant in amorphous materials has not been studied in the past. However, the linear correlation obtained between the sulphate capacity of glasses and the magnitude of the amorphous hump shift is interesting.

Note: Tiny perturbations were visible in the XRD scan of NaSi and NaSiS glasses, but the relative intensity was too low for the software's peak identification ability. Over a period of 60 days, the sample set was re-analysed. The perturbations had developed into identifiable crystalline peaks corresponding to Na_2CO_3 (ref code : 00-019-1130) (Figure 5.14).

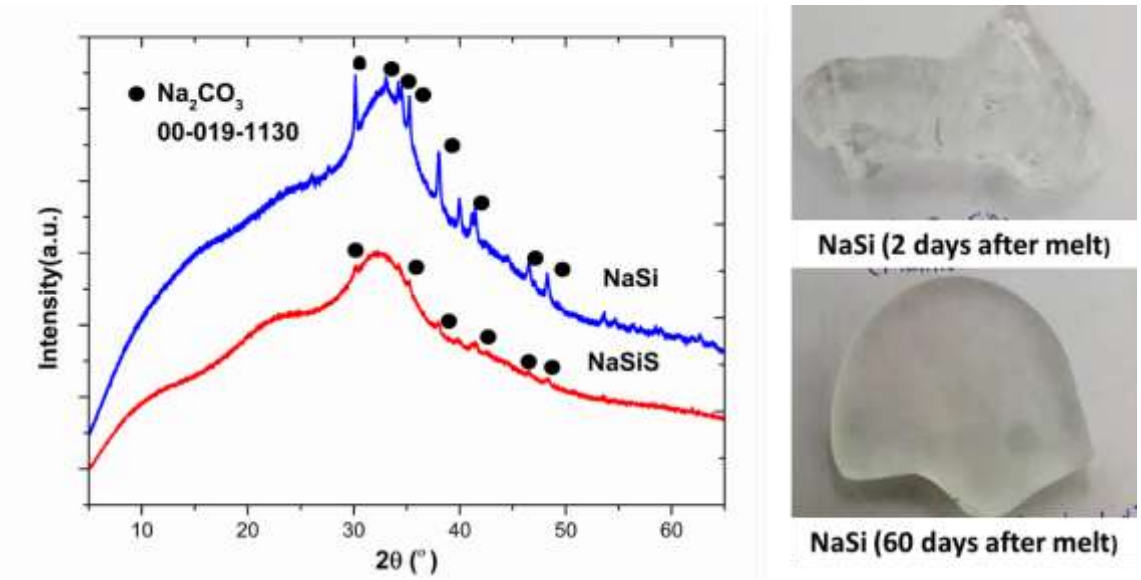

Figure 5.14: XRD patterns obtained for NaSi and NaSiS glasses after 60 days. The right side shows image of NaSi glass taken 2 and 60 days since the melt. The glass becomes opaque in 60 days due to deposition of a thin layer of Na_2CO_3 on the surface.

The carbonate growth was also consistent with visual changes as the surface of the glass had a thin layer of white deposition. The chemical durability of alkali silicate glasses containing high concentration of modifier alkali cation is known to be low (Paul 1977). The outward diffusion of Na^+ ions towards the surface is influenced directly by its

concentration present in the glass. The Na^+ ions in the Na_2O rich NaSi are highly mobile and diffuse towards the surface (Schaeffer et al. 1979), interact with environmental CO_2 to form Na_2CO_3. The hygroscopicity of these glasses is also high. However, the intensity of these peaks is greater for glass NaSi than glass NaSiS as the SO_4^{2-} introduced in the glass bonds with the alkali ions and reduces the free volume in the glass matrix. Due to the S^{6+} ---O —R^+ bond formations, less alkali ions are available to diffuse towards the surface and consequently the incorporation of sulphate improves the durability of such glasses (Persson 1962; Williams & Weyl 1945; Paul 1977).

5.3 The Effects of Sulphate on the Structure and Properties of Silicate Glasses

5.3.1 Raman Spectroscopy

All Raman spectra presented here were normalized and corrected to remove effects of fluorescence and photobleaching using the OMNIC™ Spectra software. A linear baseline was defined for each sample and subtracted from the measured data. Deconvolutions of the spectra were carried out using the Fityk 0.9.8. peak fitting software (Wojdyr 2010). Figure 5.15 and 5.18 show the corrected, normalised Raman spectra obtained at room temperature for the SO_3 free and SO_3 doped silicate glasses respectively.

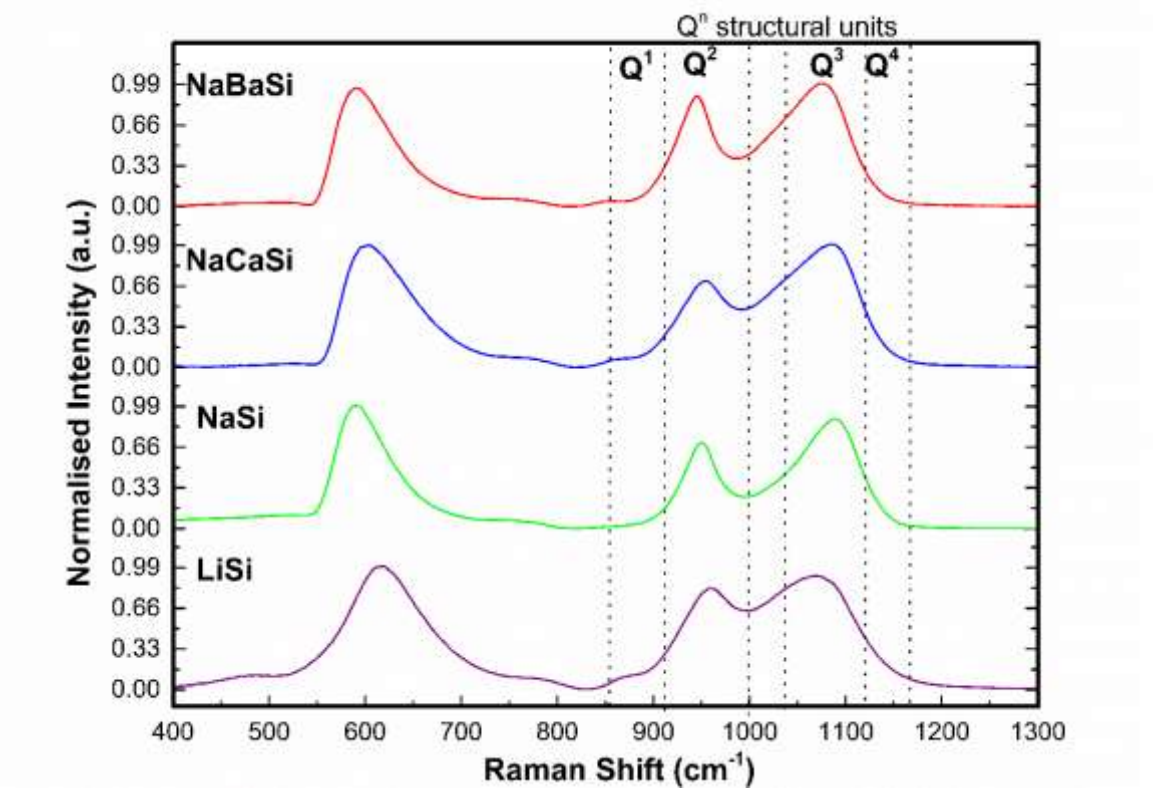

Figure 5.15: Raman spectra of the SO_3 free silicate glasses, dotted lines show silicate Q^n units

The Raman spectra for silicate glasses can be broadly divided into three regions: the low frequency region between 400-700cm^{-1}, the mid frequency region between 700-850 cm^{-1} and the high frequency region between 850-1250 cm^{-1}. The asymmetric band at low frequency (~600 cm^{-1}) is assigned to mixed (inter- and intra- tetrahedral) vibrations of BOs in the SiO_4 network and bending motions of Si-O-Si in the depolymerised SiO_4 tetrahedral units. Both of these vibrations are highly sensitive to the Si-O-Si bond angles (Matson et al. 1983; Konijnendijk & Buster 1977). The mid frequency band is attributed to Si-O-Si symmetric stretching. The bands at high frequency, stem from Si-O stretching modes in the Q^n structural units where Q represents the SiO_4 tetrahedron and n is the number of BOs in the unit (Brawer & White 1975; Yadav & Singh 2015; McMillan & Piriou 1983; Mysen et al. 1982). The Q^n structural units in the glasses studied here, mainly comprise of the Q^2 and Q^3 species as

visible in the Raman spectra. The relative abundance of the different Q^n units is determined by de-convoluting the high frequency region in the Raman spectrum and obtaining the area under each band. De-convolution enables estimation of the concentration of NBOs per tetrahedral unit. The mean number of NBOs per silicate tetrahedron are important for estimation of the averaged depolymerisation in the network.

Note: For silicate glasses, whether the bands in the Raman spectrum appear asymmetric due to individual peaks being asymmetric or whether this is due to the superimposition of more than one symmetric peak with different line parameters, or whether a combination of both, has not been established clearly. In accordance with the literature available (Mysen et al. 1982; Frantz & Mysen 1995; Mysen 1990; Mysen & Frantz 1992; Neuville 2006; Seuthe et al. 2013) , we assumed the peaks to be symmetric and deconvoluted the high frequency region by fitting 6-7 Gaussian curves to obtain fitted curves with low χ^2. All parameters associated with curve fitting, i.e. frequency, line width, area and intensity, were kept independent and unconstrained. The relative intensity was calculated for each peak (Figure 5.16).

It is important to note that the relative intensity calculation of the curves in the high frequency region of the Raman spectrum gives a qualitative estimation of the distribution of Q^n units in the bulk glass matrix and are not representatives of the exact structural arrangement of the units within the glass. As per (Frantz & Mysen 1995), the band area (A^n) and the concentration of the $X(Q^n)$ unit follow the relation: $X(Q^n) = r^n * A^n$, where r is the Raman scattering coefficient. Determination of the value of the coefficient is difficult. Hence, for our studies, we have considered the relative areas to be representatives of the concentration of the Q^n units and validated it further with ^{29}Si-MAS NMR spectral deconvolutions in the following section.

The small peak between 820-850 cm^{-1} is associated with Q^0 units where one Si unit bonds with 4 NBOs (McMillan 1984). Peaks between 850- 920 cm^{-1}, 920-1000cm^{-1}, 1050- 1100cm^{-1} and 1150-1250 cm^{-1} correspond to Q^1, Q^2, Q^3 and Q^4 units (Furukawa et al. 1981; Frantz & Mysen 1995; B. O. Mysen et al. 1982; Lenoir et al. 2008; Mysen & Frantz 1994; Brawer & White 1975; Fukumi et al. 1990; Mysen et al. 1982; Mysen & Frantz 1992; McMillan & Piriou 1983; McMillan 1984).

The presence of the large band between 1000-1050 cm^{-1} has not been investigated in detail for alkali silicate glasses in detail in the past. However, the limited literature available is debated. While researchers (Mysen & Frantz 1994) assigned the peak to the asymmetric Si-O^0 bridging oxygen stretching mode, Fukumi *et al.* (1990) and Neuville (2006) construed it as Si structural units associated with modifier metal cations. As per the authors' work on binary alkali silicate glasses, the intensity of this band was found to be independent of the choice of modifier cation but varied according to the concentration of the modifier cations present in the glass (Fukumi et al. 1990).

The deconvolutions carried out on the four undoped samples (Figure 5.16) show the presence of mainly Q^2 and Q^3 units. A relatively low intensity band is present at ~900 cm^{-1} corresponding to Q^1 units and at ~1160 cm^{-1} corresponding to the Q^4 units (only in LiSi and NaCaSi glasses). The widths of the Q^2 and Q^3 bands increase in the order NaSi< NaBaSi< NaCaSi< LiSi (in the order of CFS of contributing cations). The relative areas calculations are all within ±3 % error limits and tabulated in Table 5.7.

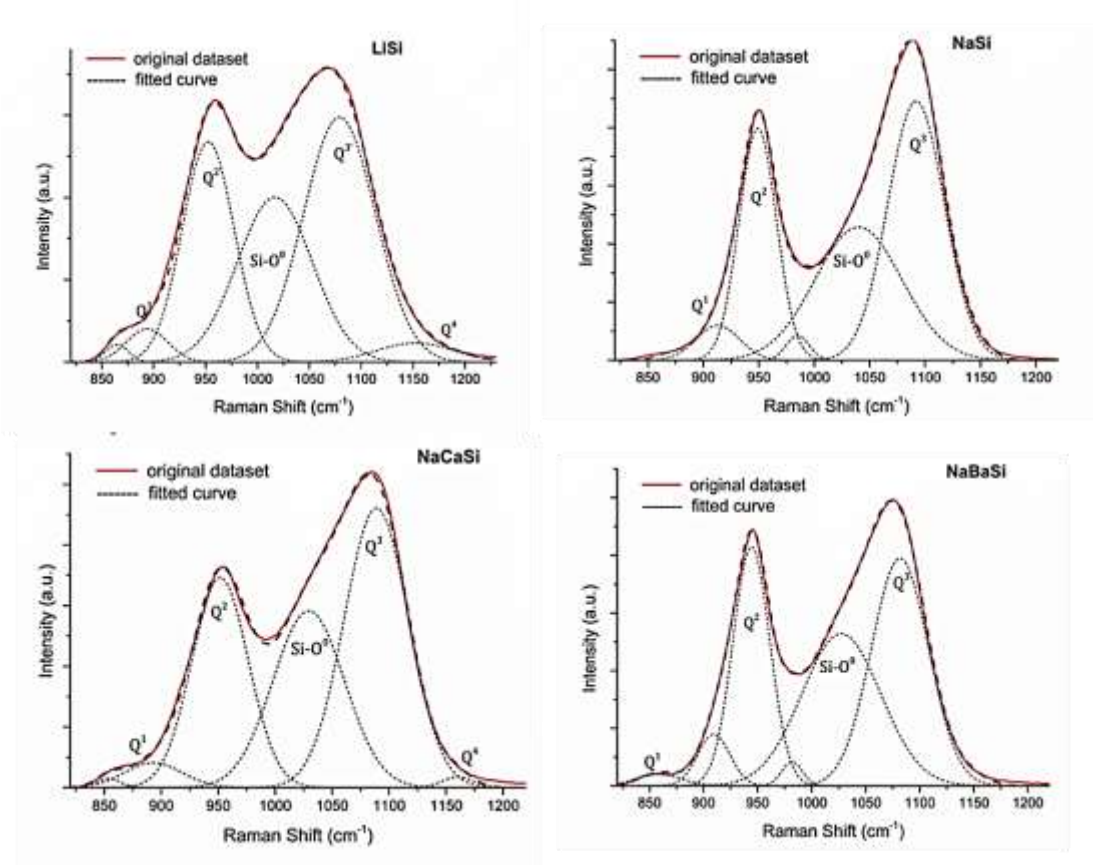

Figure 5.16: Deconvoluted Raman spectra in the high frequency region between 850-1200 cm^{-1} for SO_3 free silicate glasses (red line shows the original spectrum and – is the fit for each dataset).

Sample	Q^1 %	Q^2 %	Q^3 %	Q^4 %	$Si\text{-}O^0$ %	NBO/Si	BO/Si	NBO /BO	Q^3/Q^2	$(Q^3+Q^4)/(Q^2+Q^1)$
LiSi	4.27	25.57	39.82	2.63	27.70	1.04	1.86	0.56	1.56	1.42
NaSi	4.38	25.10	39.28	0.00	31.24	1.02	1.72	0.59	1.56	1.33
NaCaSi	3.50	22.39	43.43	0.89	29.79	0.99	1.82	0.54	1.94	1.71
NaBaSi	1.30	29.35	39.94	0.00	29.42	1.03	1.80	0.57	1.36	1.30

Table 5.7: Concentration of Si Q^n units based on the deconvolution of the Raman spectra obtained for SO_3 free glasses (two d.p.)

Where, the Na_2O containing binary and ternary glasses show either minimal or no existence of Q^4 units, a low intensity Q^4 peak (~2 % relative area) is present in the LiSi glass, possibly due to lower concentration of modifier content (Li_2O) in this glass compared to others. The same reason can be attributed to low intensity of its Si-O^0 peak, as the concentration of metal cations interacting with the Si-O structural units is slightly lower in comparison to the other three glasses. Considering the deconvoluted Raman spectrum for NaBaSi glass, larger Ba^{2+} ions appear to deconstruct the silicate network through formation of depolymerisingQ^2 units.

Finally, the $(Q^3 + Q^4)/ (Q^2+Q^1)$ ratio shows that the NaCaSi glass is the least depolymerised of the four compositions.

The centroid position of the Raman bands is plotted as a function of the total CFSI in Figure 5.17. The low frequency region consists an asymmetric band centred at 589- 603 cm^{-1} for the Na_2O containing NaSi, NaCaSi, and NaBaSi glass spectra which shifts to 616 cm^{-1} for the LiSi. glass spectrum. Similarly, the centre position of the mid frequency band increases to higher frequencies with increasing total CFSI of the glass. This shift towards higher frequencies with increasing total CFSI of the glass indicates the influence of the field strength of the modifier cations on the Si-O-Si bending and symmetric stretching modes.

Deconvolution studies of the low frequency region in Raman spectra of silicate glasses have not been identified in literature and nor have they been investigated in detail in this thesis, as most of the modes contributing towards the asymmetric band (400-600cm^{-1}) and its shoulder at higher Raman shifts (600-650 cm^{-1}) are strongly affected by the O-Si-O and Si-O-Si bond angles. Since glass has a wide range of bond angle formations

in the bulk matrix, it is difficult to assign a deconvoluted peak in this region towards one particular vibration mode and further work in this area is suggested.

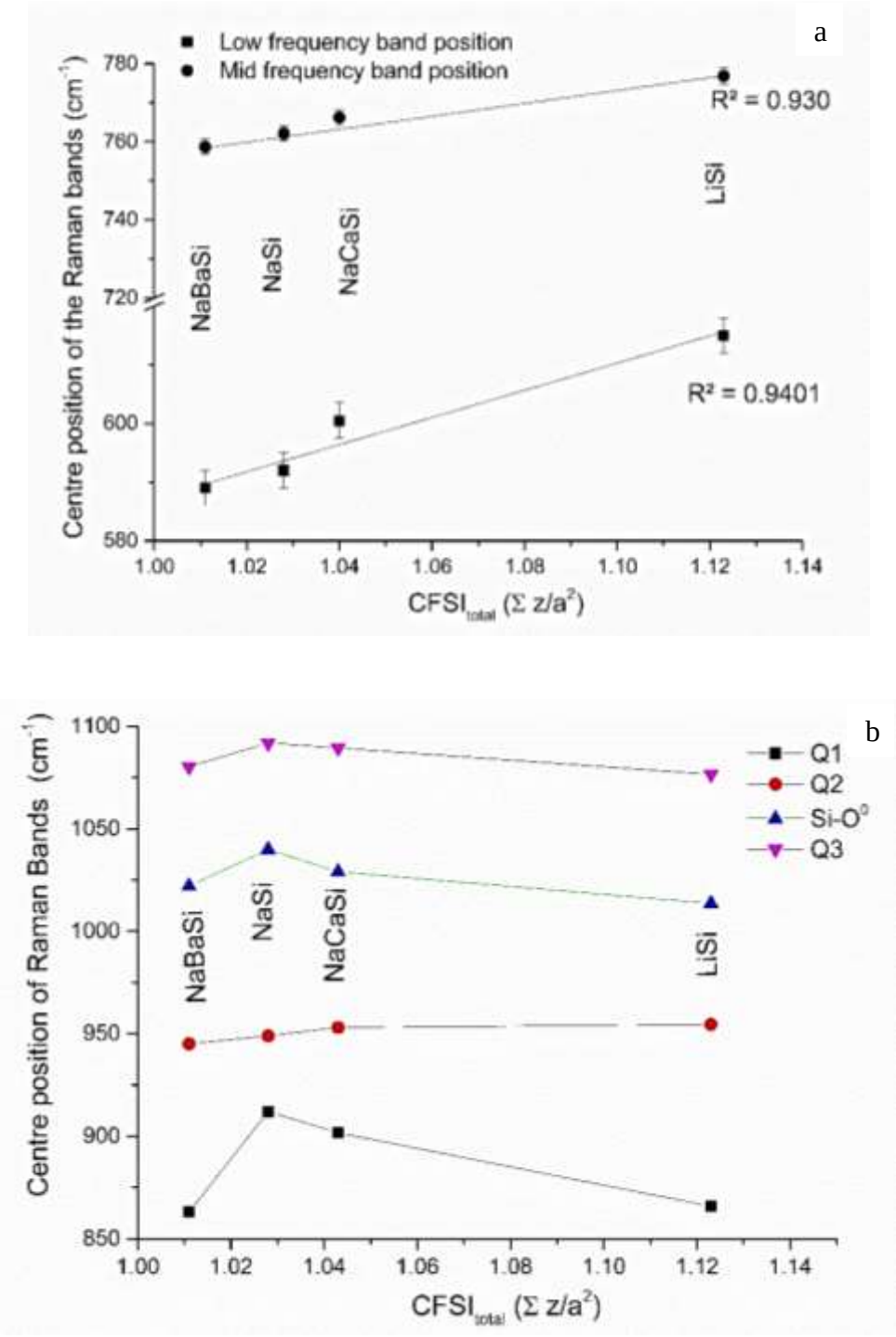

Figure 5.17: Centre position of Raman bands in a) low and mid frequency region b) high frequency region as a function of the total cation field strength index.

The Raman spectra for the sulphate doped silicate glasses (Figure 5.18) shows the presence of four additional bands with two in the low frequency region and two at higher frequencies (McMillan 1984; Tsujimura et al. 2004; Lenoir et al. 2009; Lenoir et al. 2008; Konijnendijk & Buster 1977; Wilke et al. 2011).

- 460 cm^{-1}: υ_2 symmetric O-S-O bending mode
- 630 cm^{-1}: υ_3 asymmetric O-S-O bending mode
- 990 cm^{-1}: υ_1 symmetric S-O stretching mode
- 1100 $cm^{-1:}$ υ_4 asymmetric S-O stretching mode

The position of these bands coincides with the Raman band positions of corresponding crystalline alkaline sulphates (Figure 5.19) and is consistent with the Raman studies of (McKeown et al. 2001; Lenoir et al. 2009; Manara et al. 2007) on silicate and borosilicate glasses. The results strongly suggest that sulphur is present in the form of SO_4^{2-} anion within the glasses and associating itself with the nearest network modifying cation.

Where the υ_1 mode at around ~990cm^{-1} is intense and distinct without any strong influence from the overlaps due to the neighbouring Si-O stretching modes; the intensities of the other three bands are low. The relative intensity of the peak under the υ_1 symmetric S-O stretching mode can give a rough estimation of the sulphate retained within the glass. as seen by (Lenoir et al. 2009; Morizet et al. 2017) υ_2 and υ_3 are prominent only in the glasses with> 1mol% SO_4^{2-} solubility. υ_3 and υ_4 are mostly superimposed by the vibrational modes due to the Si-O-Si network. The peak width of υ_1 S-O (990-1000cm^{-1}) stretching mode increases in the following order

LiSiS > NaCaSiS > NaBaSiS > NaSiS

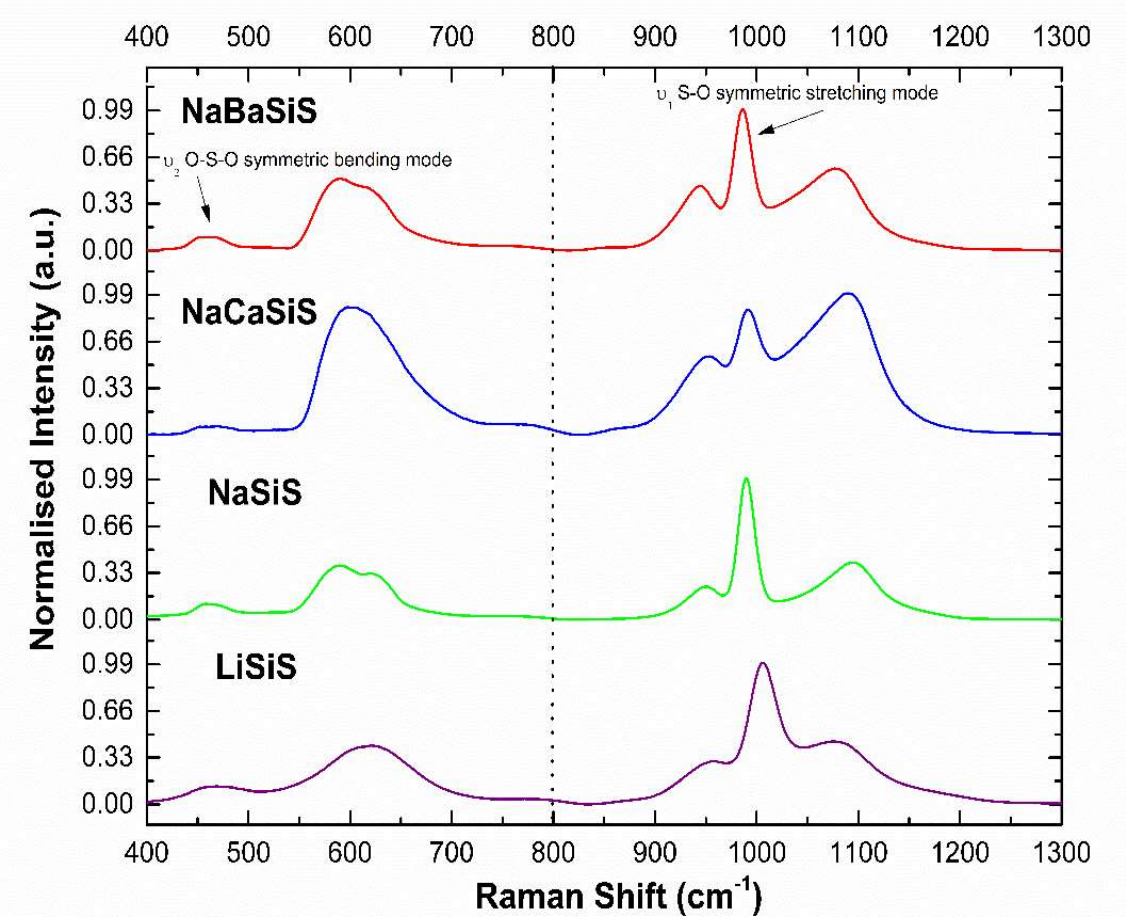

Figure 5.18: Raman spectra of the SO_3 doped silicate glasses

The de-convoluted high frequency region shows decrease in the intensities of the Q^3, Q^2 and Q^1 bands with simultaneous increase in the intensity of Q^4 upon sulphate addition for the simple NaSiS and LiSiS glasses but for the quaternary glasses, NaBaSiS and NaCaSiS, the intensity of the Q^3 band is largely unaffected. The intensity of the Si-O^0 band for the SO_3 doped glasses is logical as with doping, SO_4^{2-} is predicted to bond with the nearby modifier cations, resulting in reduced concentration of modifier cations associating with the structural units to depolymerise the silicate network. For sulphate doped glasses, the higher intensity of the band at around 1150-1220 cm^{-1} with respect to the corresponding base glasses is due to the superimposition of the υ_4 asymmetric S-O stretching mode within this region.

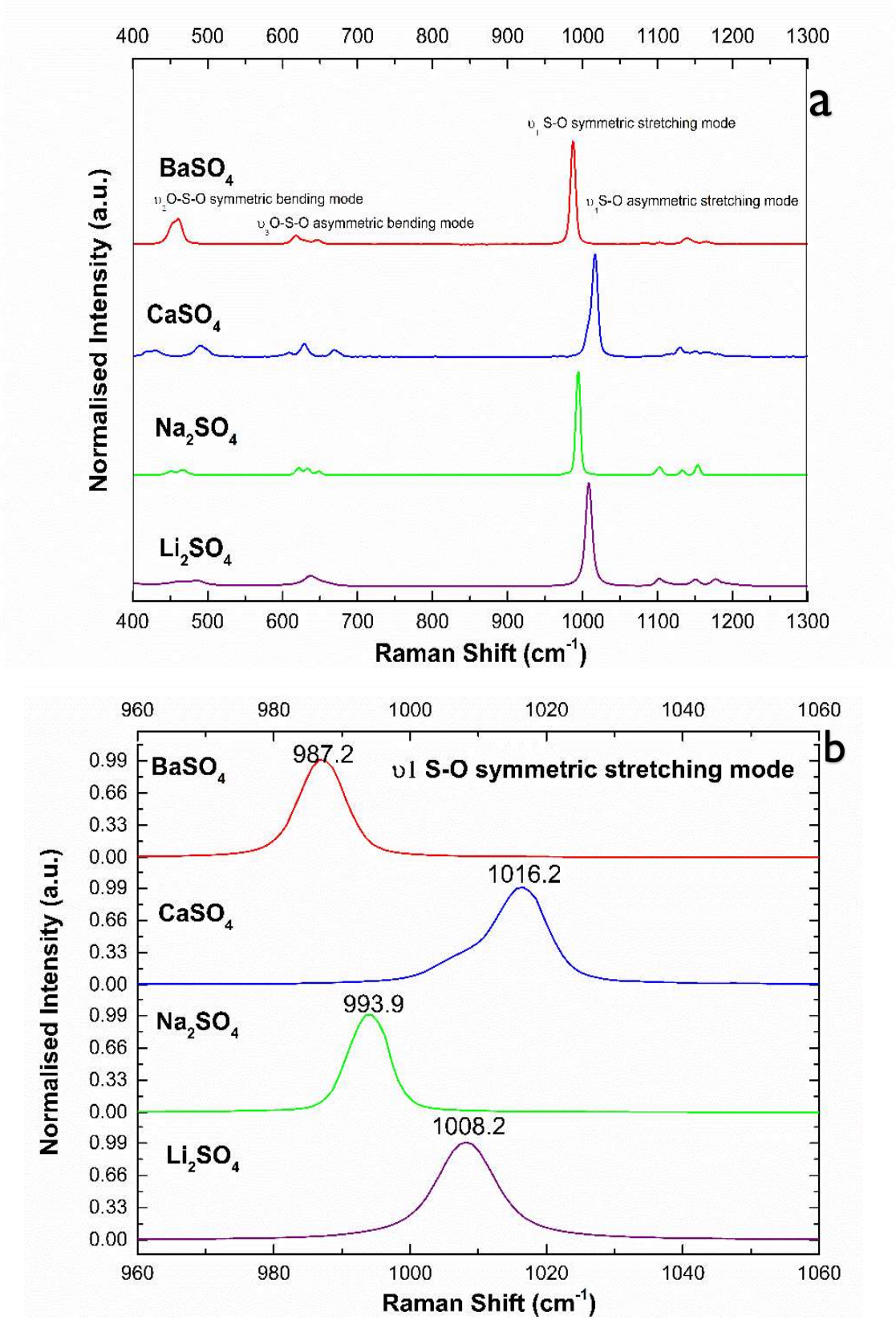

Figure 5.19: a) Raman spectra obtained for crystalline alkali/alkaline earth sulphate compounds. b) Position of the υ_1 S-O symmetric stretching mode for the crystalline sulphates.

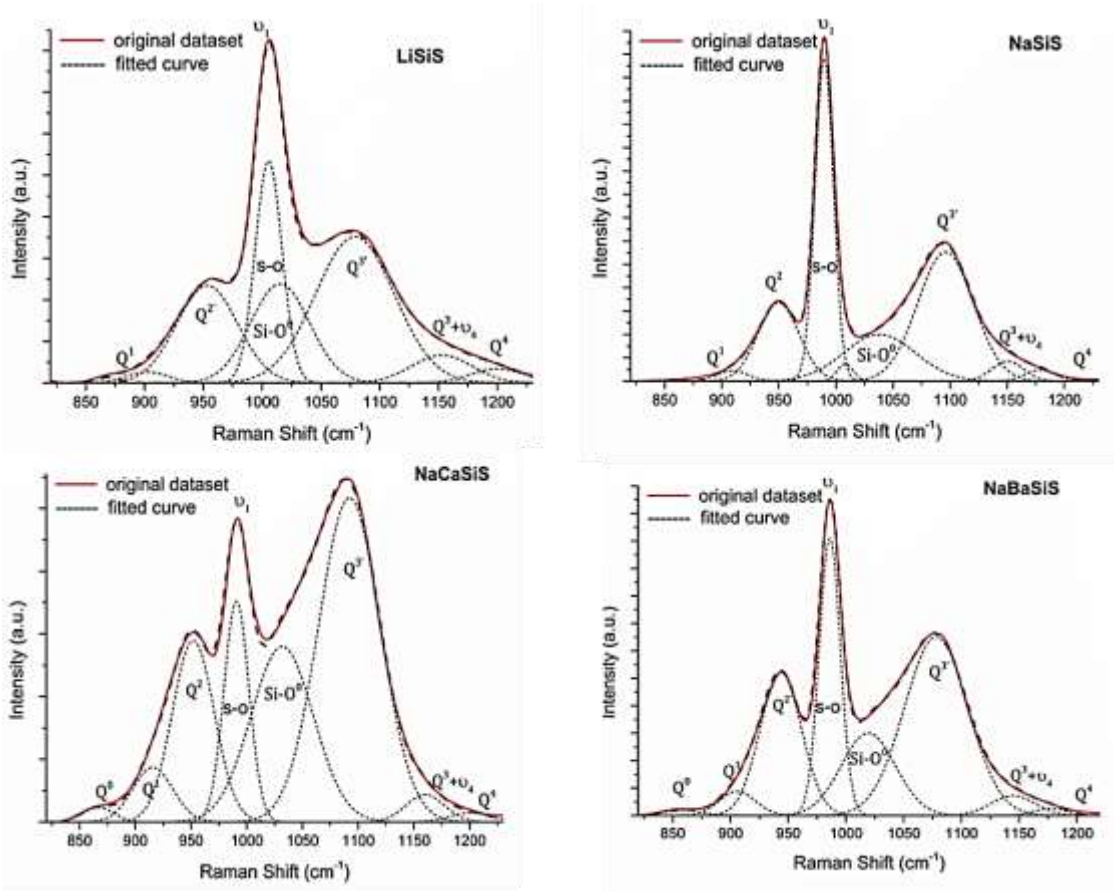

Figure 5.20: Deconvoluted Raman spectra in the high frequency region (850-1200 cm^{-1}) for SO_3 doped silicate glasses.

The individual concentrations of Si Q^n units obtained from deconvolution are tabulated in Table 5.8. Relative intensity of the υ_1 mode is calculated with the following formula:

$$\text{Relative Intensity (R.I.) of } \upsilon_1 = \frac{\text{Area under the S-O peak}}{\text{Total area of the Si-O between 850-1200 cm}^{-1}}$$

When plotted against the XRF analysis for molar concentration of sulphate retained by the glass, the relative intensity of the υ_1 mode follows a linear increase with sulphate content in the glasses except for the NaSiS glass which slightly deviates from the trend. (Figure 5.21) This shows that Raman spectroscopy can provide a qualitative estimation of the concentration of sulphate present in the glass and is consistent with the work of (Lenoir *et al.* 2008; Morizet *et al.* 2017)

Sample	Q^1 %	Q^2 %	Q^3 %	Si-O^0	Q^4 %	R.I. of υ_1	Q^3/Q^2	Q^3+Q^4/Q^2+Q^1
LiSiS	1.43	18.44	40.90	18.06	2.33	18.46	2.22	2.18
NaSiS	1.51	15.13	36.70	15.71	1.60	27.98	2.43	2.30
NaCaSiS	4.52	15.81	43.77	22.69	0.77	11.49	2.77	2.19
NaBaSiS	2.97	19.92	40.95	15.01	0.78	19.67	2.06	1.82

Table 5.8: Concentration of Si Q^n units based on the deconvolution of the Raman spectra obtained for sulphate doped glasses

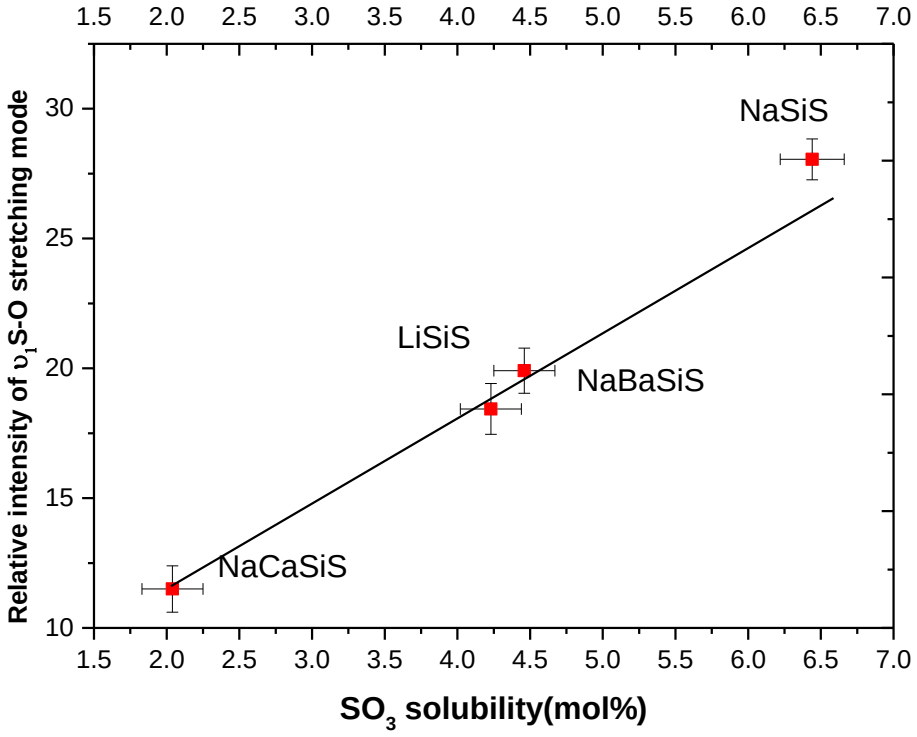

Figure 5.21: Relative intensity of the Raman υ_1 S-O stretching mode obtained by calculating the ratio of the area under S-O stretching mode to the overall area under the Si-O Q^n region between 850-1200 cm^{-1}, plotted as a function of analysed SO_3 content (mol%). The vertical error bars were generated by calculating the change in the area under the S-O peak by fixing one peak parameter (FWHM, centre, height) per scan.

It is evident that the change in the abundance of the Si Q^n units between the undoped and SO_3 doped glasses for each glass composition (Table 5.7 and 5.8) are independent of the amount of sulphate incorporated in the glass matrix.

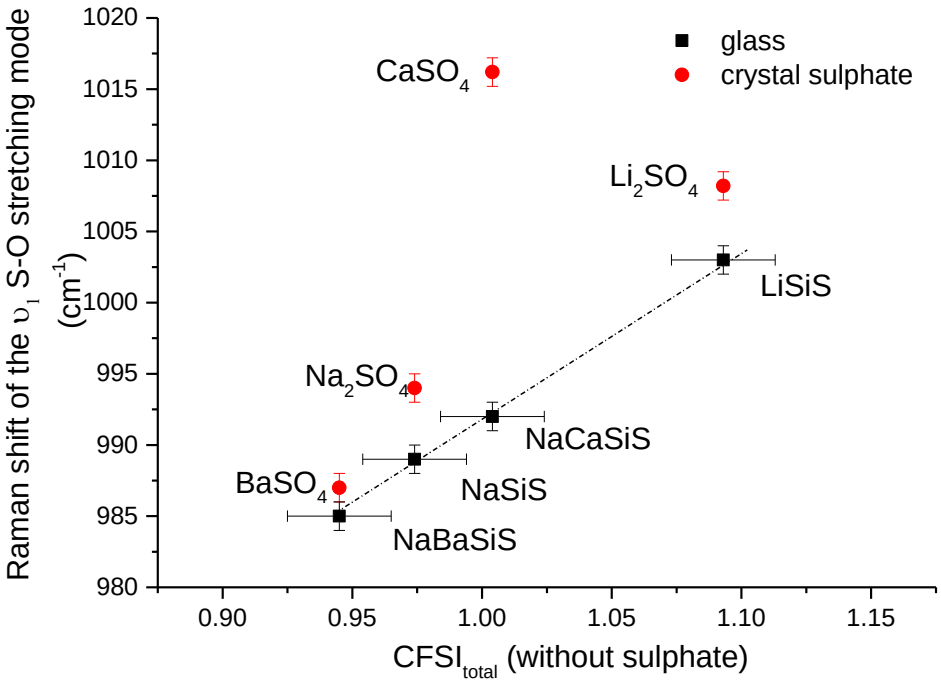

Figure 5.22: Centre position of the Raman υ_1S-O stretching mode for the SO_3 doped glasses and corresponding crystalline sulphates as a function of total cation field strength index.

The centre peak position of the Raman shift for the υ_1 S-O stretching mode in the doped glasses and corresponding crystalline alkali/alkaline-earth sulphates are plotted as a function of field strength of the glass (Figure 5.22). The lower υ_1 S-O frequency in the glass compared to the corresponding crystalline sulphate indicates that bonding around the SO_4 tetrahedra is weaker in glass than in the corresponding crystal. Based on the frequencies, sulphate anions appear more closely associated with Na^+ ions than Ca^{2+} in NaCaSiS glass, as seen on comparing the υ_1 positions for NaCaSiS glass with Na_2SO_4 and $CaSO_4$, Contrastingly, in NaBaSiS glass, indication is that sulphate anions are atleast partially charge compensated by the Ba^{2+} ions.

5.3.2 ^{29}Si, ^{23} Na and ^{7}Li MAS NMR Results

5.3.2.1 ^{29}Si-MAS NMR

^{29}Si MAS NMR spectra were obtained at 79.438 MHz and a pulse duration of 4.5 µs. The acquisition time per scan was 20 ms and 500-600 scans were acquired for each sample. Gaussian line shapes were used to fit the contribution due to the Q^n units. At a spinning speed of 6 kHz, the sidebands were removed if the intensity was only up to 4-5% of the total. Therefore, Q^1 and Q^4 units were not visible in the spectra. Figure 5.23 shows the ^{29}Si MAS NMR spectra for the SO_3 free and SO_3 doped glasses. The individual concentrations of the Q^n units were obtained by 2-3 component peak fitting. However, for the NaBaSi, NaCaSi and LiSi glass spectra, strong overlaps occur between Q^n units. The uncertainties related to the fitting are estimated to be ±5%. Table 5.9 shows the chemical shift positions and the concentrations of the Q^3 and Q^2 units.The data obtained from MAS-NMR is useful in providing information about coordination environment, short-range order in simple glasses, and the nature of the nearest modifier cations.

In Figure 5.23(a), slight decrease towards negative ppm is observed in the centroid positions of the chemical shifts for Q^3 and Q^2 units, from spectra for NaSi to NaCaSi to NaBaSi glasses. In sulphate doped glasses, the centroid positions of the Q^3 and Q^2 chemical shifts shifted to a lower value with respect to their sulphate free base glass equivalents (Figure 5.23b).

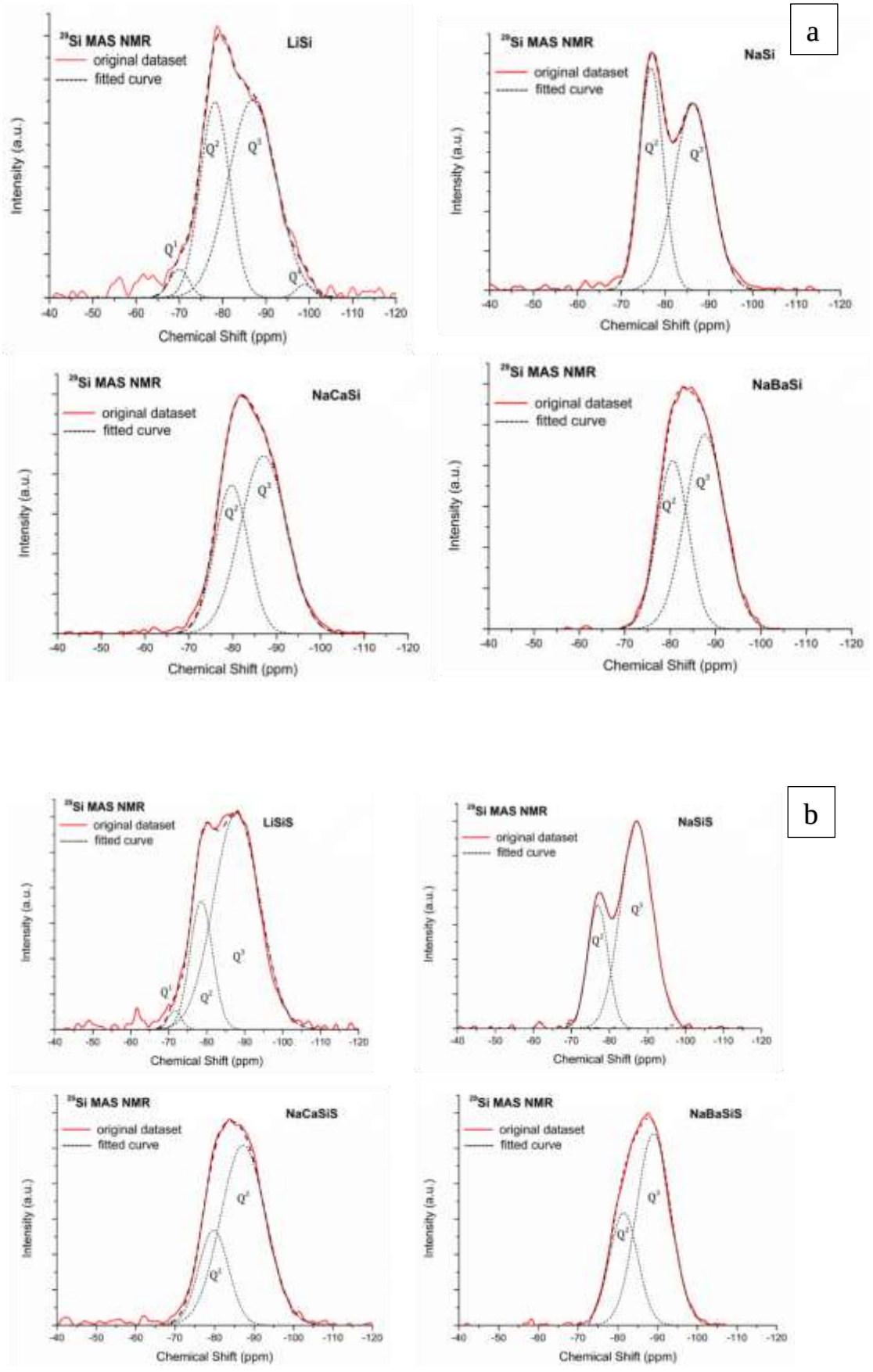

Figure 5.23: Deconvoluted ^{29}Si MAS NMR obtained for (a) sulphate free (b) sulphate doped silicate glasses

Sample	Q^3 % (δppm)	Q^2 % (δppm)	Q^1 % (δppm)	Q^4 % (δppm)	NBO/ Si	BO/ Si	NBO/ BO	Q^3/ Q^2
LiSi	59.17 (-86.86)	33.56 (-78.22)	4.47 (-69.96)	2.80 (-98.89)	1.39	2.60	0.54	1.76
LiSiS	68.65 (-88.41)	29.73 (-78.71)	1.617 (-70.01)	-	1.34	2.66	0.50	2.31
NaSi	56.5 (-86.33)	43.5 (-76.83)	-	-	1.43	2.57	0.56	1.30
NaSiS	72.52 (-87.13)	26.48 (-76.96)	-	-	1.27	2.73	0.47	2.64
NaBaSi	59.50 (-87.69)	40.50 (-80.57)	-	-	1.40	2.60	0.54	1.47
NaBaSiS	64.70 (-88.96)	35.30 (-81.71)	-	-	1.35	2.65	0.51	1.83
NaCaSi	63.80 (-87.02)	36.20 (-79.74)	-	-	1.36	2.64	0.51	1.66
NaCaSiS	73.97 (-87.23)	26.03 (-79.74)	-	-	1.26	2.74	0.46	2.84

Table 5.9: Concentration of Si Q^n units and corresponding chemical shifts obtained using ^{29}Si-MAS NMR (rounded off to 2 d.p.)

The chemical shift of the four coordinated ^{29}Si nucleus is well studied in literature and lies in the range of -70 to -100 ppm (Dupree et al. 1984; Dupree et al. 1986; Maekawa et al. 1991; Murdoch & Stebbins 1985). Usually, the centroid position of chemical shifts vary with changes in coordination number and bond lengths (Maekawa et al. 1991; Dupree et al. 1984; Charpentier 2012). The decrease in the chemical shifts for sulphate doped glasses is possibly due to the polymerisation of the Si-O network as observed with change in the ratio of Q^3 and Q^2 units.

The concentrations obtained for LiSi and NaSi glasses are in close agreement with previous work by (Maekawa et al. 1991; Larson et al. 2006) on alkali silicate glasses. The calculated Q^3/Q^2 ratios obtained for the glasses are in close agreement with the results obtained from deconvoluted Raman spectra. It is confirmed that the addition of sulphate leads to polymerisation of the silicate glass networks as the concentration of Q^3 units increases and Q^2 decreases. The empirical models suggested by (Papadopoulos 1973; Jantzen et al. 2005; Ooura & Hanada 1998) predicts that sulphate solubility increases linearly with increasing $[O^-]^2/ [O^0]$ where $[O^-]$ is the ratio of NBO/T and $[O^0]$ is the ratio of BO/T. The ratio $[O^-]^2/ [O^0]$ has been calculated using the values obtained from Raman spectroscopy and ^{29}Si MAS NMR and plotted against the sulphate capacity of the glasses in Figure 5.24.

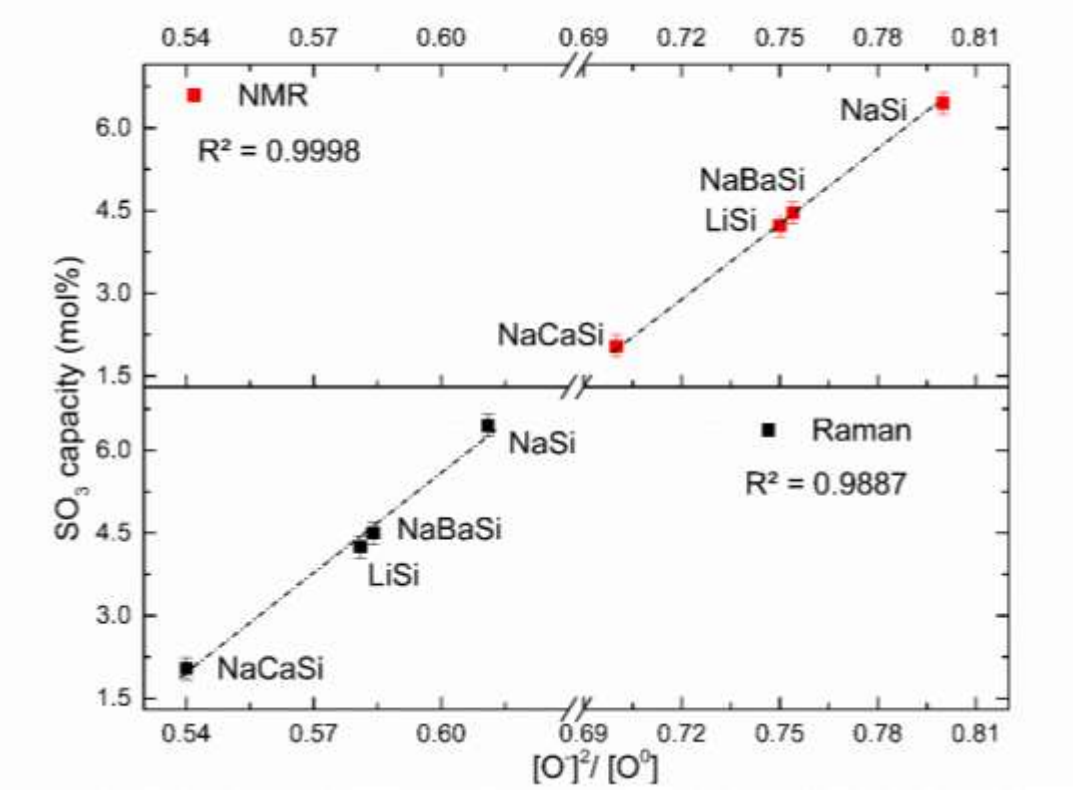

Figure 5.24: Sulphate capacity of the glasses plotted against the $[O^-]^2/ [O^0]$ ratio as obtained with Raman spectroscopy and ^{29}Si MAS NMR

Although the ratios obtained for the samples with both techniques do not overlap (as calculation of $[O^-]^2/ [O^0]$ using Raman spectroscopy deconvolution results takes into account the Raman coefficient for every Q^n unit), a linear increase in sulphate capacity with $[O^-]^2/ [O^0]$ is observed from both techniques which indicates that the model can be used to predict the sulphate capacity of simple silicate glasses such as those studied here.

5.3.2.2 ^{23}Na-MAS NMR

^{23}Na, a quadrupolar nucleus with a spin quantum number of 3/2 has a very narrow chemical shift range and large quadrupolar broadening. The NMR spectrum is at times featureless when the sample studied has structural disorders. Spectra were acquired using a single pulse sequence at Larmor frequency of 105.78MHz (9.4 T) and pulse duration of 1.0 µs. The acquisition time per scan was around 10.0 ms and repetitions close to 950 per sample. A 4mm probe was used for the measurements. Figure 5.25 shows the ^{23}Na NMR spectra acquired for the six Na_2O containing glasses studied in this chapter. Limited literature is available to interpret the ^{23}Na-MAS NMR analysis for our glasses. The interpretation of the peak positions has been carried out by comparisons with literature available on similar crystalline structures studied using this technique.

The spectra exhibited a single, broad, asymmetric peak tailing towards lower frequencies due to quadrupolar broadening. The low magnetic field used for the measurements is partially responsible for the broadening, as it has been observed by (Lee & Stebbins 2003; Angeli et al. 2000) that using a high field (~14 T) can

significantly narrow the broadening by reducing the secondary quadrupolar interactions.

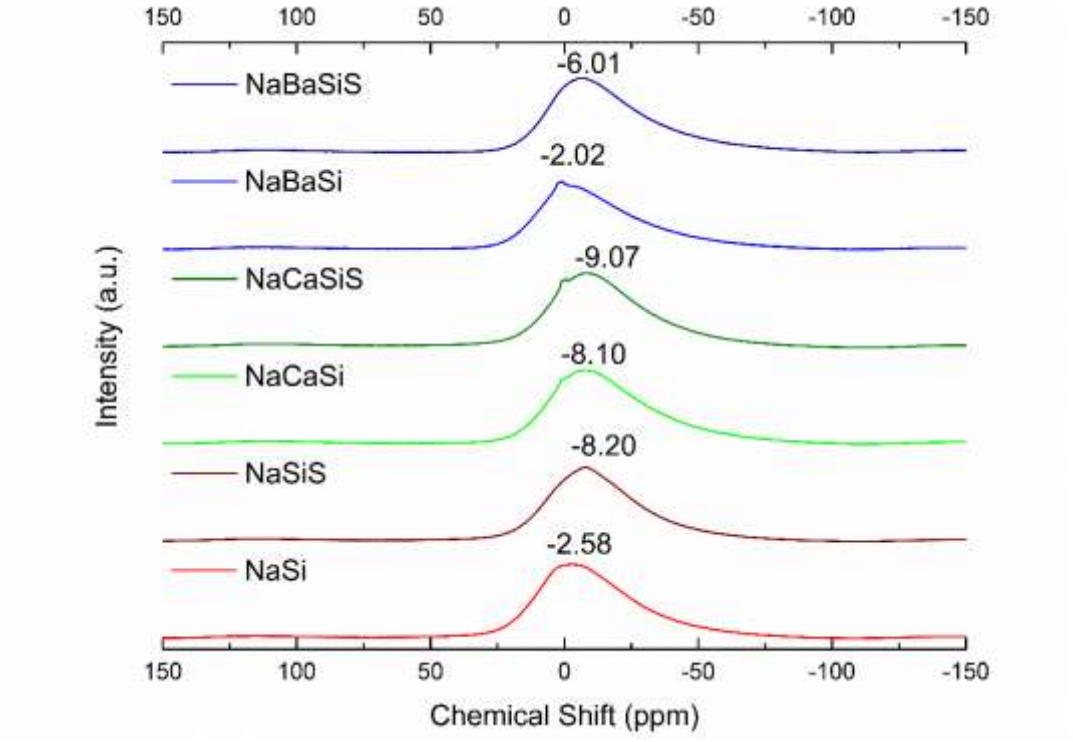

Figure 5.25: ^{23}Na-MAS NMR signal obtained for the SO_3 free and SO_3 doped silicate glasses

The peak maximum moves towards more negative values in spectra for sulphate doped compositions with respect to their corresponding undoped base glass but the overall area under the peaks does not change. The tiny perturbations in the spectra of NaCaSiS and NaBaSi glasses at around ~ -0.9 ppm need further investigation. The possibility of nano-phase separation around Na^+ ions is possible, but no evidence of any crystallinity could be found in the XRD patterns and neutron diffraction total correlation functions of these glasses (see section 5.3.3) as ND technique is particularly sensitive to any crystallinity. ^{23}Na triple quantum filtering (3Q) -MAS NMR on the samples is suggested to further investigate the source of the perturbations in future. Triple quantum

filtering as the name suggests, filters the quadrupolar interactions which cause the broadening of the ^{23}Na MAS NMR peak (Angeli et. al. 2007; Lee & Stebbins 2003)

Several researchers (Charpentier et al. 2004; Angeli et al. 2011; Angeli et al. 2007; Lee & Stebbins 2003; Angeli et al. 2000; Gambuzzi et al. 2014; Gaudio et al. 2015; Maekawa et al. 1997) suggested that the chemical shifts are mainly governed by average Na-O bond distances. Decreasing chemical shifts are characteristic of longer Na-O bond lengths, increasing Na^+ coordination number and decreasing number of NBOs coordinating with Na^+ ions. (Xue & Stebbins 1993) studied anhydrous silicate and aluminosilicate melts using ^{23}Na MAS NMR and concluded that the isotropic chemical shifts correlate well with changes in the Na coordination number and the degree of melt polymerisation (reducing number of NBO). They also observed that in ternary aluminosilicate glass systems, presence of a dissimilar modifier cation besides Na^+ had a strong influence on the chemical shift due to variations in the average Na coordination environment and the ratio of NBO/BO bonding with the Na^+ ions.

In this study, through the neutron diffraction results (see section 5.3.3.3), the authors have confirmed that upon sulphate addition, a change in the distribution of average Na-O bond lengths occurs with a higher concentration of longer Na-O bonds in sulphate doped glasses compared with their respective base glasses. Since ND provides only average CN, comparison between chemical shifts and CN are not likely to yield useful results and further work is suggested.

The shift in the ^{23}Na MAS NMR peak maximum in ppm between undoped and sulphate doped samples has been plotted against the sulphate content of the glass series (Figure 5.26). The trend between the two parameters, i.e. the sulphate content and the magnitude of chemical shift in the peak maximum is linear to an extent. This stongly suggests that

upon addition of SO_3, a fraction of sodium ions acting as network modifiers in the base glass appear to switch the role to charge compensators for the sulphate anions, which results in a decrease of Na-NBO concentration.

To investigate further, the authors plotted the peak maximum of the chemical shifts for the un-doped and doped systems as a function of their total cation field strength index (Figure 5.27). The peak shifts are found to be inversely related to the $CFSI_{total}$ of the glasses. The inverse relationship between the two parameters is in agreement with the work of (Kanehashi 2017; Wu & Stebbins 2009) on aluminosilicate and borosilicate glasses.

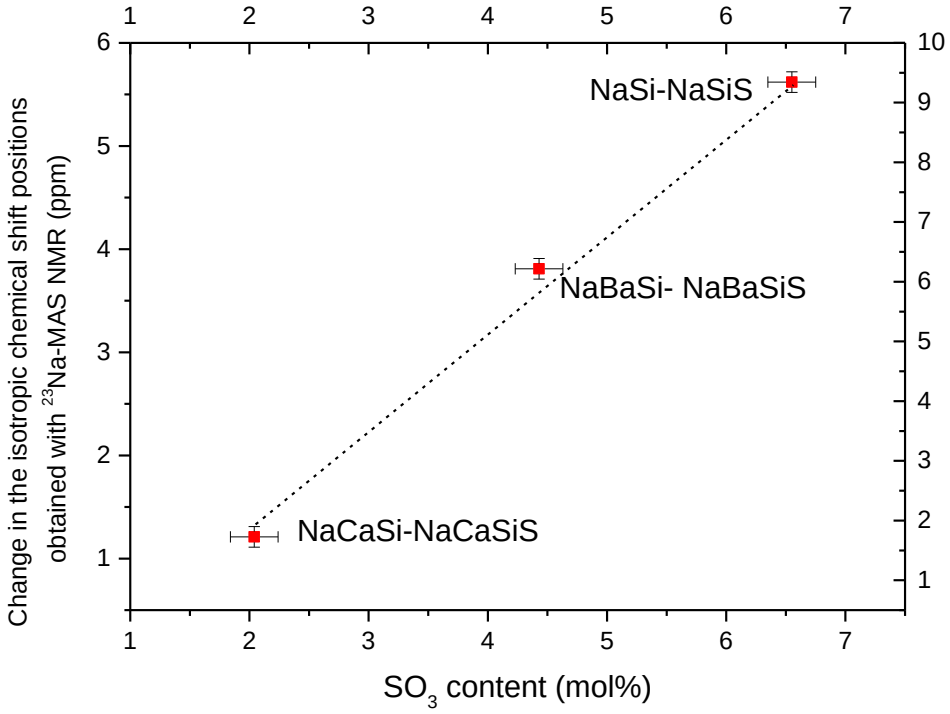

Figure 5.26: ^{23}Na MAS NMR peak maximum shift between sulphate free and sulphate doped glasses as a function of the SO_4^{2-} capacity. Dotted line is a line of best fit as a guide to the eye.

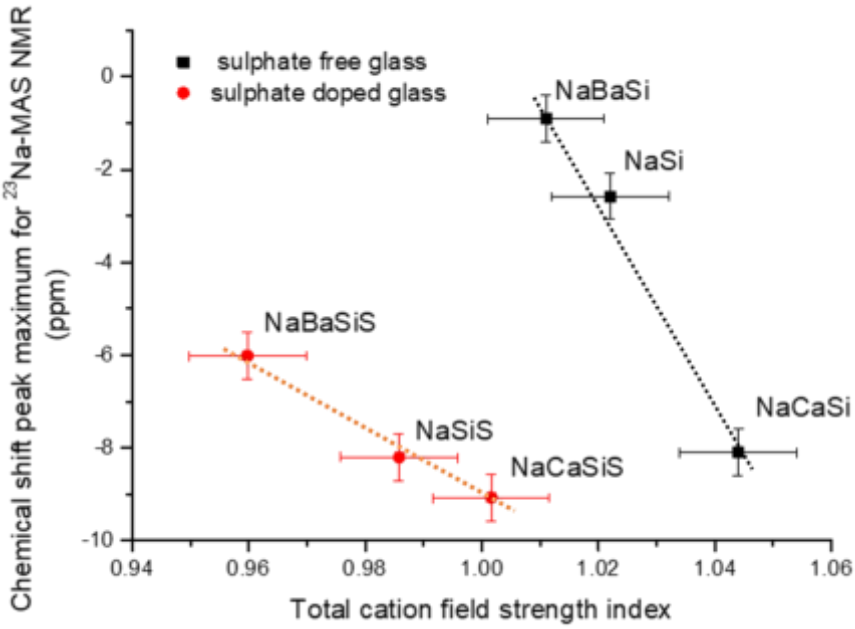

Figure 5.27:^{23}Na MAS NMR chemical shift peak maximum of sulphate free and sulphate doped glasses as a function of total cation field strength index

Several key observations can be made from this study:

- The increase in the Na-O average bond lengths on addition of sulphate is seen in all three glass sets . This is attributed to change in degree of polymerisation of silicate network.
- The ^{23}Na chemical shift peak position increase slightly on partial substitution of Na_2O with BaO in NaBaSiS and to lower frequency in NaCaSiS. Based on the work of (Angeli *et. al.* 2000; Angeli *et. al.* 2007; Inglis *et. al.* 2016; Kanehashi 2017; Xue & Stebbins 1993; Charpentier *et. al.* 2013; Gambuzzi *et. al.* 2014), higher chemical shifts occur when the cation acts as a modifier than charge compensator and participates in the formation of NBOs. By this rule, in NaCaSiS the Na^+ ions act as charge compensators for the sulphate anions while Ca^{2+} modifies the silicate network. Whereas, in NaBaSi glass, the larger Ba^{2+} ions act either entirely or partially as charge compensators while Na^+ ions modify the network.

Thus, upon sulphate addition, Na^+ ions compensate the negative charge on the sulphate ions in both NaSiS and NaCaSiS glasses, while Ba^{2+} ions perform this role in NaBaSiS glass.

5.3.2.3 ^{7}Li-MAS NMR

^{7}Li has a spin quantum number 3/2 and a quadrupole moment of 0.04 $\times 10^{-28}$ m^{-2}. Relatively small quadrupolar coupling constants are found in lithium compounds. ^{7}Li-MAS NMR was performed at a Larmor frequency of 155.41 MHz and pulse duration of 1.0 µs. The acquisition time was 100 ms per scan and around 80 repetitions were made for each sample.

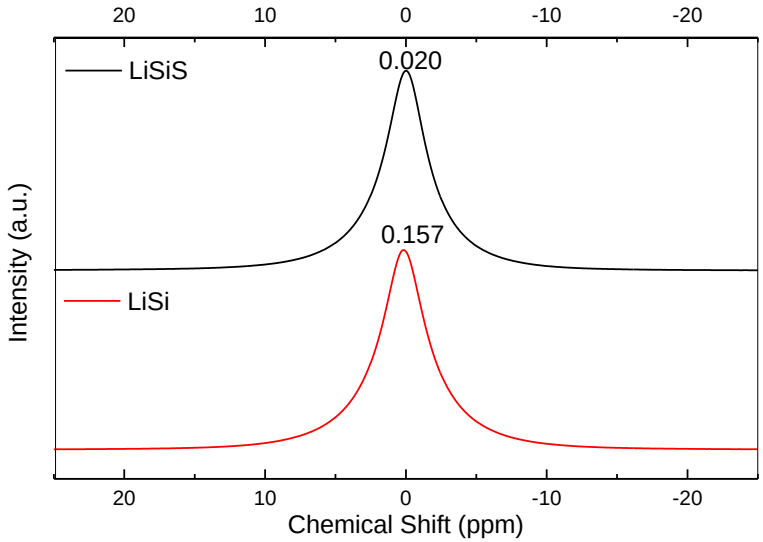

Figure 5.28: ^{7}Li MAS NMR obtained for LiSi and LiSiS glasses

Figure 5.28 shows the ^{7}Li NMR spectra for LiSi and LiSiS glasses. The sulphate doped LiSiS shows a slight decrease in the chemical shift with respect to LiSi glass. The same interpretation as suggested for ^{23}Na NMR shifts is made here, that Li^+ ions distribute their role as charge compensators for sulphate anions and modifiers for the Si-O network in LiSiS which results in decrease of Li-NBO upon incorporation of sulphate.

5.3.3 Neutron Diffraction studies

The neutron diffraction data obtained at the GEM diffractometer, ISIS, UK were corrected for background scattering, inelastic and self-scattering using the GudrunN program. Figure 5.29 presents the real space total correlation functions (T(*r*)) plotted as a function of bond distance.

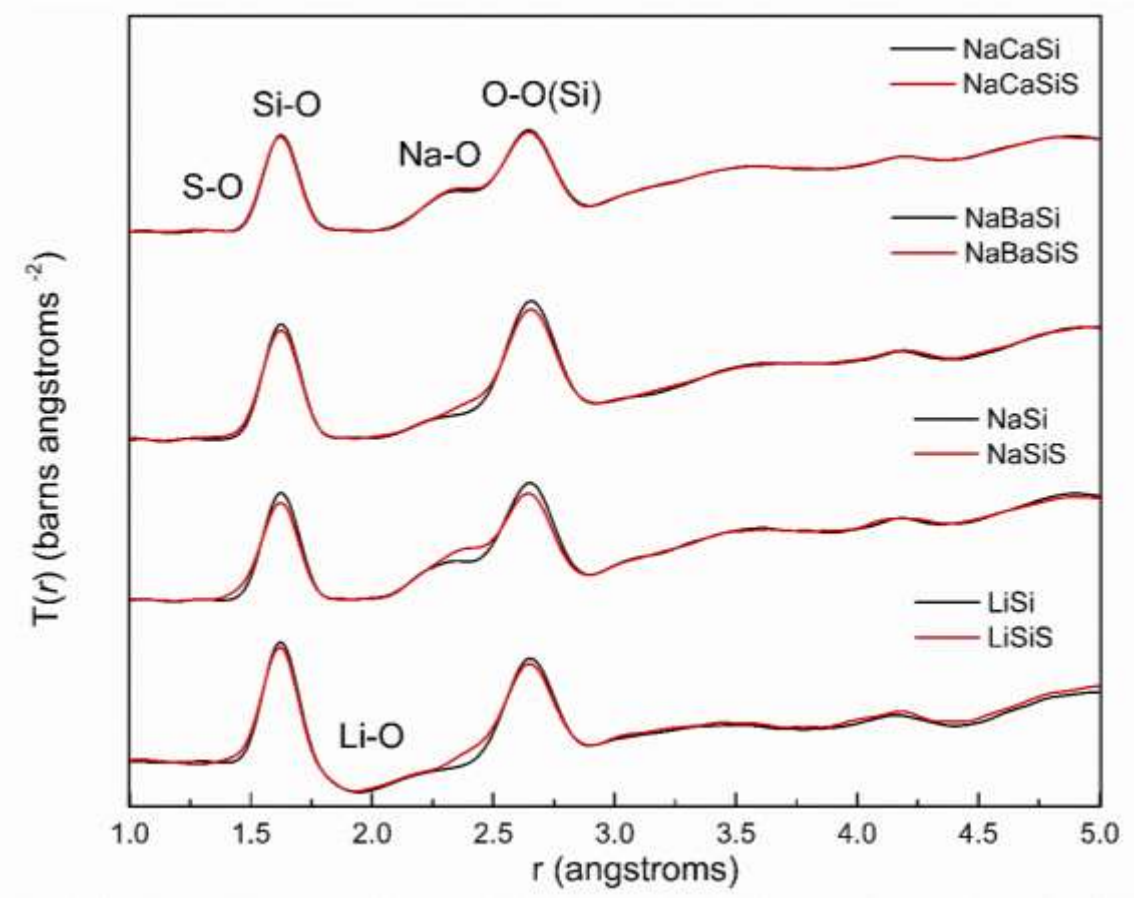

Figure 5.29: Total neutron correlation function (T(*r*)) plotted as a function of bond length for the SO_3 free and SO_3 doped silicate glasses

The correlation functions for all samples show two prominent peaks at ~1.62Å and ~2.65 Å corresponding to Si-O and O-O (Si) correlations of the first coordination shell respectively. This is in agreement with previous studies (Vessal et al.1996; Wright 1994; Wright et al. 2001) done on alkali silicate glasses where similar correlations were obtained for Si-O and O-O bonds.

5.3.3.1 S-O environment

In the SO_3 doped glasses, sulphur environment is of particular interest. The S-O bond length (r_{SO}) for hexavalent S^{6+} in a SO_4^{2-} unit with four equal S-O bonds should be ~ 1.474Å (Brese & O'Keeffe 1991). In an ideal SO_4^{2-} tetrahedron, the distance between two O'-O' (O' notates the oxygens in sulphate units), in the tetrahedron: $r_{O'O'}$ can be calculated as:

$$r_{O'O'} = \sqrt{\frac{8}{3}} * r_{SO} = 1.633 * 1.474 = 2.407 \text{ Å}$$

The O'-S-O' bond angle $\theta = \cos^{-1}(-1/3) = 109.47^{o}$ can be calculated using equation 5.3:

$$\text{Sin}(\theta/2) = \frac{r_{O'O'}}{2 * r_{SO}} \qquad \text{Equation 5.3}$$

The S-O and O'-O' (S) bond lengths in crystalline alkali/alkaline earth sulphate vary slightly around these values, depending on the ionic field strengths of the cations bonding with the tetrahedral units. To obtain the correlations due to S-O and O'-O'(S), a simple difference of the neutron correlation functions, T(r) is evaluated:

$$\Delta T(r) = T_{doped}(r) - (100 - SO_3\ capacity\ \%) * T_{undoped}(r) \qquad \text{Equation 5.4}$$

This approach was followed as the SO_3 concentrations are low in comparison to other modifier oxides and SiO_2 present in the doped glasses. Therefore, the correlation from the S-O is often superimposed by the much larger and broader Si-O correlation at ~1.61 Å. The use of this 'difference approach' as stated in Equation 5.4 also highlights the structural changes, besides decoupling the correlation due to S-O and O-O (S) from Si-O and O-O (Si) in the doped glass. The differences between the correlation function for undoped and sulphate doped glass samples is shown in Figure 5.30.

Peaks were fitted in the range of 1.3-1.6 Å and 2.3- 2.65Å without any parameter constraints to obtain the average S-O and O'-O'(S) bond distances, respectively. The average coordination number was calculated (Table 5.10) using equation 4.12 (Chapter 4) and the average bond angles are obtained using equation 5.3.

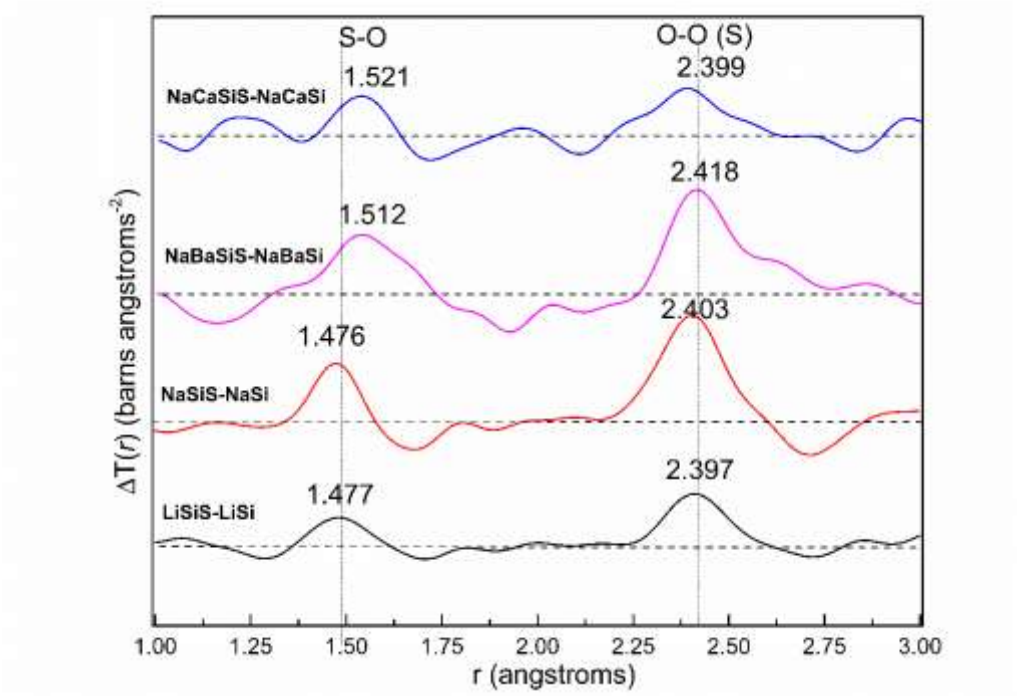

Figure 5.30: Difference between total neutron correlation functions (Δ T(r)) for SO_3 free and SO_3 doped glass

Sample	<S-O> bond length (Å)	<S-O> CN	<O-O> bond length (Å)	<O-O> CN	Average Bond Angle S-O'-S
LiSiS	1.477 ± 0.003	3.875 ± 0.012	2.387 ± 0.013	0.364± 0.019	109.25 ± 0.001
NaSiS	1.476 ± 0.0004	3.986 ± 0.006	2.403 ± 0.007	0.501 ± 0.002	107.95 ± 0.0005
NaBaSiS	1.512 ± 0.012	3.866 ± 0.071	2.418 ± 0.007	0.365 ± 0.001	106.18 ± 0.008
NaCaSiS	1.521 ± 0.003	3.782 ± 0.081	2.399± 0.014	0.150± 0.002	104.14 ± 0.021

Table 5.10: Average S-O, O'-O'(S) coordination numbers obtained for doped silicate glasses

The coordination number for O'-O' in the isolated sulphate tetrahedron is 3. However, in the case of neutron diffraction, the O'-O' CN measured from $\Delta T(r)$ is a smaller value. The reason behind this is that ND measures only average coordination number (by measuring the area under the peak in *T(r)*at a particular distance) and the doped glass contains both 'sulphate oxygens' (oxygens in the SO_4 units) and network oxygens (oxygens in the Si-O-Si / Si-O-MO_x units). Therefore, the sulphate O'-O'(S) coordination number ($n_{O'O'}$) can be calculated to be:

$$n_{O'O'} = 3 * \frac{\text{number of sulphate oxygens}}{\text{total number of oxygens}} \qquad \text{Equation 5.5}$$

The number of sulphate oxygens, assuming no S-O'-S bridges are formed, is equal to four times the SO_3 concentration measured. ($No_{sulphate}$= 4* SO_3 concentration/100). The average S-O and O-O(S) bond distances obtained for the binary alkali silicate glasses LiSiS and NaSiS confirm the presence of sulphur environments broadly similar to those in crystalline Li_2SO_4 and Na_2SO_4 in the glasses. The S-O and O'-O' bond distances measured in the two binary glasses (LiSiS and NaSiS) are closely similar to the S-O', O'-O'(S) bond lengths measured for crystalline Li_2SO_4 and Na_2SO_4(V) (anhydrous thenardite).

The higher average S-O' bond distance at ~1.51 Å obtained for the NaBaSiS glass should not be confused for the presence of sulphite (S^{2-}) ions with S-O bond lengths ~ 1.602 Å in this glass. It was validated with Raman spectroscopy results that sulphur is only present in the form of S^{6+} in all SO_3 doped glasses (Section 5.3.1). The presence of sulphur as S^{2-} units should have resulted in an intense Raman band at low frequencies in the range of 250-450 cm^{-1} (Wilke et al. 2011; Evans & Bernstein 1954; Degen & Newman 1993).Since no corresponding bands were observed, therefore it was confirmed that no sulphite units were present.

The increase in the average S-O' and O'-O'(S) bond distance for NaBaSiS glass is most likely due to the association of SO_4^{2-} units with divalent Ba^{2+} ions. The structure of crystalline $BaSO_4$ studied by Miyake et al. (1978) and Jacobsen et al. (1998) verified the presence of longer S-O bonds in barite structures. The three types of S-O bonds formed in crystalline $BaSO_4$ were 1.472 ± 0.006 Å; 1.449 ± 0.006 Å and 1.519 ± 0.004 Å. The presence of S-O-Ba bonding was also verified with Raman spectroscopy by comparing the position of the υ_1 S-O stretching modes in NaBaSiS glass with crystalline Na_2SO_4 and $BaSO_4$. (see section 5.3.1). Therefore, both techniques strongly suggest association of sulphate with Ba^{2+} partially or entirely in the ternary NaBaSiS glass.

In NaCaSiS glass, the average S-O distance is found to be ~1.52Å. The results from the Raman spectrum for NaCaSiS glass indicate that the sulphate units are stabilised by Na^+ ions and not Ca^{2+} ions. The only two crystalline sulphates to compare the S-O correlations in NaCaSiS glass with, are thus Na_2SO_4 or $Na_2Ca(SO_4)_2$ (glauberite). Structural studies related to glauberite phase is limited (López et al. 2013) due to the low abundance of the geological mineral analogues. However, Raman studies carried out on a glauberite mineral by Lopez et. al, 2014 shows the presence of an intense band at 1002 cm^{-1} and many other antisymmetric bending and stretching bands, as the sulphate ion loses its symmetry in the mineral. Therefore, the stabilisation of sulphate ions by a combination of Na^+ and Ca^{2+} is unlikely. The most likely explanation is the stabilisation of sulphate by Na^+ in this glass as Na_2SO_4 like units. The average S-O' bond length (~1.52 Å) in NaCaSiS glass is, however, larger than the average S-O' bond length (~ 1.47 Å) corresponding to Na_2SO_4 (V) [thenardite] obtained for the NaSiS glass. This suggests the presence of more than one Na_2SO_4 like environment in the NaCaSiS glass .

Therefore, multiple spectroscopies suggest that the arrangement of sulphates in the glasses is very similar to their local environment (S-O bond lengths and its next nearest neighbouring cations) in corresponding crystalline alkaline/ alkaline earth sulphates as was suggested previously for alkalis in alkali iron phosphate glass on the basis of S-K edge XANES by (Bingham et al. 2010).

5.3.3.2 Si-O environment

Broad ND peaks observed at ~1.62 Å and 2.65 Å correspond to the average Si-O and O-O (Si) bond distances. Peak widths and area are obtained for Si-O correlations and the average <Si-O> CN is ~4 in all the glasses (Table 5.11). The width of the peaks is close to 0.05Å. The slightly lower Si-O CN obtained for SO_3 doped glasses compared to the corresponding undoped base glasses are due to the overlapping S-O peak at ~ 1.47- 1.5 Å in the low r region (see Figure 5.31).

Sample	<Si-O> bond length (Å)	<Si-O> CN	Sample	<Si-O> bond length (Å)	<Si-O> CN
LiSi	1.620 ± 0.005	4.021 ± 0.001	**LiSiS**	1.621 ± 0.006	3.895 ± 0.071
NaSi	1.623 ± 0.003	4.011 ± 0.004	**NaSiS**	1.623 ± 0.006	3.955 ± 0.012
NaBaSi	1.625 ± 0.002	3.910 ± 0.005	**NaBaSiS**	1.625 ± 0.003	3.957 ± 0.012
NaCaSi	1.623 ± 0.012	3.945 ± 0.011	**NaCaSiS**	1.624± 0.014	3.986± 0.005

Table 5.11: Average <Si-O> coordination numbers and bond lengths obtained for the silicate glasses

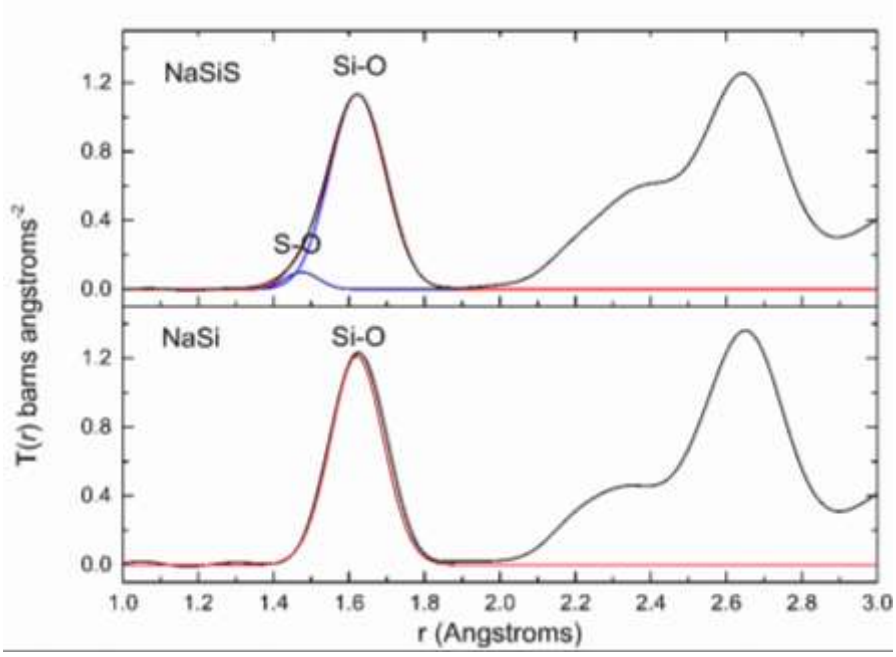

Figure 5.31: Si-O and S-O fits obtained for NaSi and NaSiS glass total neutron correlation functions

Resolving the O-O(Si) correlations for Na_2O containing glasses is challenging. The first Na-O correlation appears as a shoulder on the lower r side (~2 to 2.6 Å) of the intra-tetrahedral O-O (Si) peak. In the case of ternary glasses, additional overlap occurs at lower r values (2.4- 2.7 Å)due to Ca-O in glass NaCaSi and at higher r values (2.7 to 3.1 Å) due to Ba-O short range bond distributions in glass NaBaSi. To resolve the correlations an empirical approach is undertaken, as follows.

Empirical approach: If x Na_2O. (1-x) SiO_2 is the original composition of the binary glass, upon addition of SO_3 the composition changes to:

$$ySO_3.\ (1\text{-}y)\ ((x\ Na_2O.\ (1\text{-}x)\ SiO_2))$$

It has been demonstrated that sulphur is present as only sulphate units in the doped glasses. So, one can write the composition of doped glass as:

$$J\ (SO_3.Na_2O)\ *\ R\ (Na_2O.SiO_2)$$

Where $$J = \frac{y}{(1-y)(1-x)} = \frac{SO_3}{SiO_2}$$

$$R+J = x / (1-x) = Na_2O/SiO_2$$

$$x = R+J / R+J+1 \; ; \quad y = J / R+2J+1$$

Using these equations, the composition of a glass can be expressed in terms of J and R.

In a SiO_4 tetrahedron, the average O-O distance r*oo* is given as:

$$r_{oo} = \sqrt{\frac{8}{3}} * r_{sio} = 1.633 * 1.625 \approx 2.653 \text{ Å}$$

In J ($SO_3.Na_2O$). R ($Na_2O.SiO_2$), oxygens due to sulphate are in J($SO_3.Na_2O$) and oxygens due to silicate are in R ($Na_2O.SiO_2$). Therefore, the no. of oxygens in the silicate network are: $(NO_{Si}) = 2+R$

In pure silica, R=0, $(NO_{Si}) = 2 * N_{Si}$ and oxygens are present only as BO.

If R>0, one unit of Na_2O converts one BO into two NBOs.

Thus, $$N_{NBO} = 2 * R * N_{Si}$$

$$N_{BO} = (2 - R) * N_{Si}$$

The fraction of NBO and BO can be given by the formula:

$$f_{NBO} = N_{NBO} / NO_{Si} = 2R / (2+R)$$

$$f_{BO} = N_{BO} / NO_{Si} = (2-R) / (2+R)$$

A BO has 6 oxygen neighbours whereas a NBO has only 3. Therefore, the average coordination number for O-O (Si) is = $6 f_{BO} + 3 f_{NBO} = 12 / (2+R)$. The J and R ratios can be obtained from the XRF analyses of the samples. The f_{BO} and f_{NBO} can also be

calculated from ^{29}Si MAS NMR results. The average CN for O-O (Si) is calculated and presented in Table 5.12. The average CN for the first O-O peak in the silicate network calculated using the empirical approach is ~ 4.4 – 4.5 which is slightly higher than the expected value of 4. However, it should be noted that R was calculated using the analysed concentrations of MOx and SiO_2 which may not be perfectly accurate.

Sample	<O-O> bond length (Å)	<O-O> CN	Sample	<Si-O> bond length (Å)	<O-O> CN
LiSi	2.653 ± 0.005	4.515 ± 0.210	**LiSiS**	2.653 ± 0.006	4.562 ± 0.312
NaSi	2.652 ± 0.003	4.516 ± 0.610	**NaSiS**	2.653 ± 0.006	4.682 ± 0.450
NaBaSi	2.655 ± 0.002	4.482 ± 0.310	**NaBaSiS**	2.656 ± 0.003	4.560 ± 0.301
NaCaSi	2.654 ± 0.012	4.401 ± 0.120	**NaCaSiS**	2.645 ± 0.014	4.495 ± 0.210

Table 5.12: Average <O-O> bond distance and coordination number calculated for silicate glasses.

5.3.3.3 Modifier-oxygen environment (O-O (Si) modelling)

The parameters from the empirical calculations for the O-O (Si) i.e. CN = 4.40; bond distance = 2.65 Å and an arbitrary width of 0.09 Å were used to obtain an O-O(Si) fit. While the area (a factor of CN) and distance were fixed for the fitting model, the width of the peak was unconstrained. The O-O modelled peak was then subtracted from *T(r)* to reveal the modifier-oxygen pair distributions. The subtracted *T(r)* was fitted to obtain Na-O, Ba-O and Ca-O correlations in the un-doped samples. In the SO_3 doped samples, the O'-O'(S) fit from the difference method and the O-O(Si) fit from the empirical calculations, both were subtracted from *T(r)* to obtain the modifier-oxygen correlations. The fitted correlations between modifier-oxygen are shown in Figure 5.32. A negative

broad peak corresponding to Li-O correlation is visible at ~1.85Å for LiSi and LiSiS. The negative value is due to the negative neutron scattering lengths for lithium (-2.2 $*10^{-6}$ nm for ^{7}Li)(Uhlig et al. 1996). In Na_2O containing glasses, the first Na-O contribution appears as a shoulder on the lower r side of the intra-tetrahedral O-O (Si) peak. Based on the modifier-oxygen bond distances, average M-O coordination numbers have been calculated and are summarised in (Table 5.13).

Sample	<Modifier-O> bond length (Å)	<M-O> CN	Sample	<Modifier-O> bond length (Å)	<M-O> CN
LiSi	Li-O 1: 1.947 Li-O 2: 2.236	3.719±0.080 0.125±0.012	**LiSiS**	Li-O 1: 1.936 Li-O 2: 2.175	3.815±0.090 0.101 ±0.011
NaSi	Na-O 1: 2.306 Na-O 2: 2.509	2.260±0.500 3.212±0.610	**NaSiS**	Na-O 1: 2.270 Na-O 2: 2.484	2.894±0.300 3.264 ±0.411
NaBaSi	Ba-O: 2.924	7.268±0.310	**NaBaSiS**	Ba-O: 2.898	7.805±0.512
NaCaSi	Ca-O 1: 2.258 Ca-O 2: 2.396	2.929±0.490 3.324±0.121	**NaCaSiS**	Ca-O 1: 2.313 Ca-O 2: 2.450	2.276±0.910 3.939±0.451

Table 5.13: The average Modifier-oxygen bond lengths and coordination number obtained for silicate glasses

The average M-O CN obtained for the modifier -oxygen in its first coordination shell is ~ Li-O (4); Na-O (5-6); Ca-O (6) and Ba-O (7-8). The CN for Ba-O could possibly be higher as the Ba-O correlation in its first coordination shell at higher r values > 3Å (mid-range) could not be fitted due to the technique constraints as at higher r (mid frequency region) multiple secondary correlations due to Na-Na, Si-Si, Na-Ba bonds overlap. Therefore, resolving the second Ba-O correlation is difficult. Ba EXAFS is suggested for future work to study the local environment around the ions and aid this work.

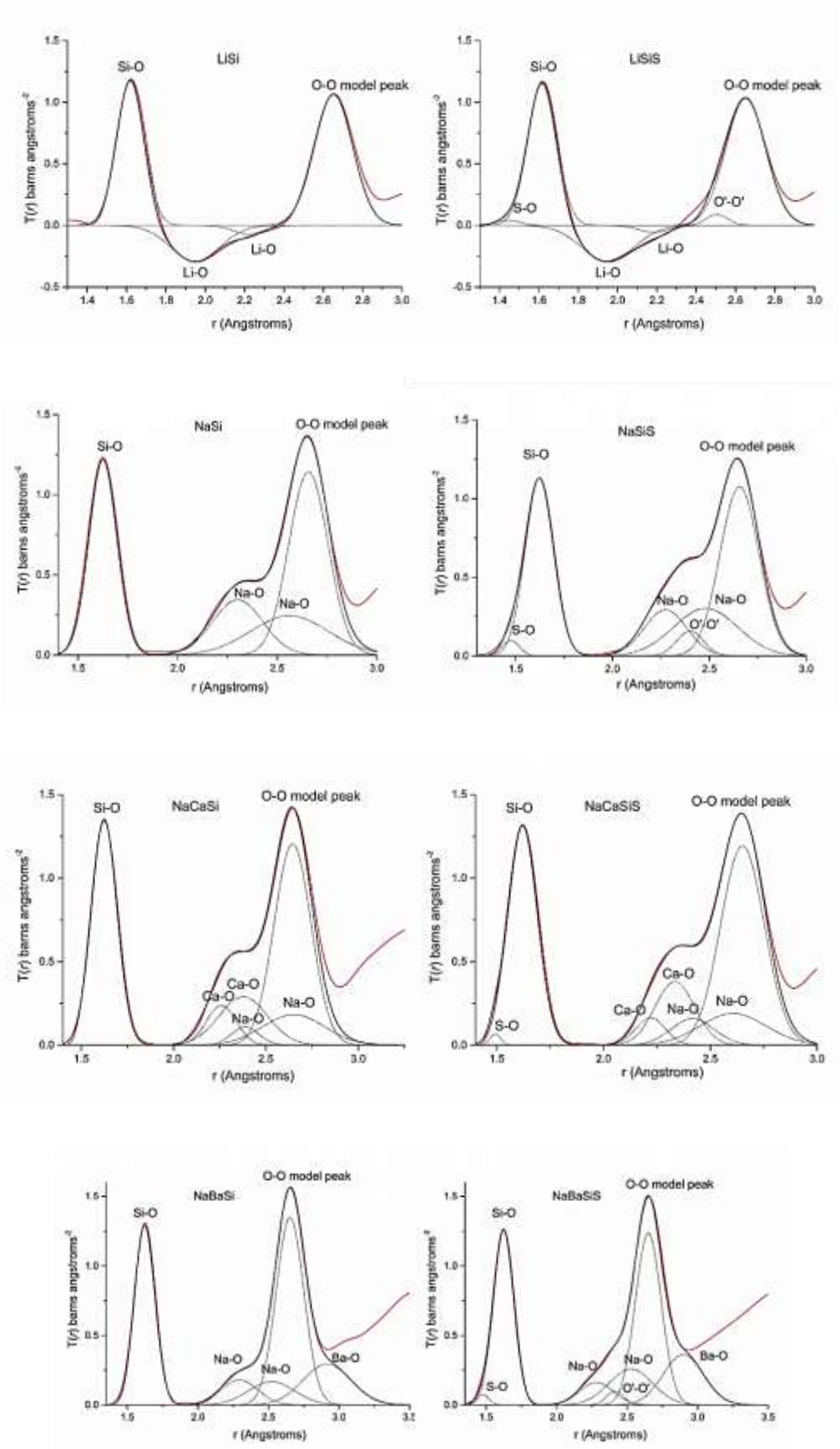

Figure 5.32: Modifier-oxygen correlations obtained for silicate glasses

5.4 Conclusions

Study of the effects of sulphate doping on the properties of R_2O-SiO_2 (R= Li, Na) and ternary glasses Na_2O-MO-SiO_2 (M=Ca, Ba) has generated the following conclusions:

- Glass NaSi provides the highest sulphate capacity of up to ~6.45 mol% while in glass NaCaSi, the saturation is attained beyond ~2 mol% SO_3. NaBaSi and LiSi show appreciable sulphate retention of up to ~4 mol%
- The density of sulphate doped glass samples in higher and molar volume lower in comparison to their undoped equivalents.
- The sulphate capacity increases linearly with reducing normalised cation field strength index of the glasses.
- The glass transition temperature (T_g) increases upon replacement of Ca with Na in glass NaCaSi and Ba with Ca in glass NaBaSi. T_g decreases to lower temperatures in sulphate doped samples except for glass NaBaSiS glass
- The XRD amorphous hump shifts to lower diffraction angles and higher average interatomic distance in sulphate doped silicate glasses compared to their undoped equivalents. The magnitude of the shift increases linearly with the sulphate capacity of the glass.
- ^{29}Si MAS NMR and Raman spectroscopies show that addition of sulphate has a polymerising effect on the glasses. However, the degree of polymerisation does not change significantly between glasses NaBaSi and NaBaSiS. The comparison of the S-O stretching mode Raman band with corresponding crystalline sulphates shows that while in glass NaCaSiS, sodium compensates for the negative charge on the sulphate anions, Barium takes on this role in glass NaBaSiS while sodium modifies the silicate glass network. This view was

further supported by comparing the ^{23}Na-MAS NMR peak maxima of the chemical shifts and the S-O bond distances in the doped glasses obtained from neutron diffraction.

This study suggests that addition of BaO and Li_2O has a positive effect on the sulphate retention capacity of silicate glasses. In real world practice, though, borosilicate glasses are employed to vitrify the nuclear waste. Hence, we will next study the role of BaO in sulphate retention capacity of simple binary and ternary borosilicate glasses in Chapter 6.

CHAPTER 6

ROLE OF BARIUM IN SULPHATE INCORPORATION IN BOROSILICATE GLASSES

The high sulphate capacity of some Na_2O-SiO_2 and Na_2O-BaO-SiO_2 silicate glasses was established in Chapter 5. In this chapter, the author investigated the sulphate capacity of Na_2O-B_2O_3-SiO_2, Na_2O-BaO-B_2O_3-SiO_2, and BaO-B_2O_3-SiO_2 borosilicate glasses. The glasses were spectroscopically analysed for changes in the structure and chemical properties between a SO_3 free base glass and a SO_3 doped equivalent achieved by pro-rata addition of SO_4^{2-}. The range of techniques used for this study are XRF, ICP analysis, XRD, Raman spectroscopy, ^{29}Si, ^{23}Na, ^{11}B MAS-NMR, Neutron Diffraction and Density measurements.

6.1 Glass Preparation

Three sets of glasses were prepared for the borosilicate series, each set containing one SO_3 free 'undoped' base glass and a corresponding SO_3 'doped' equivalent. The targeted doping was ~ 5 mol% SO_3. The base glasses comprise two binary systems: Na_2O-B_2O_3-SiO_2; BaO- B_2O_3-SiO_2 and one ternary system: Na_2O-BaO- B_2O_3-SiO_2.The ternary composition were achieved by substituting half molar concentration of Na_2O with BaO in Na_2O- B_2O_3-SiO_2. Analytical grade carbonates from Better Equipped (Na_2CO_3, $BaCO_3$ ~purity >99.9%); high purity sand (99.99% purity) and isotopically enriched H_3BO_3 (99.27% ^{11}B) and B_2O_3 (99.78% ^{11}B) from Eagle Picher were used for batch preparation. Sulphur was incorporated as Na_2SO_4 in the Na_2O containing SO_3 doped glasses and $BaSO_4$ in the BaO-B_2O_3-SiO_2-SO_3. The raw materials were dried at 100°C (50°C for H_3BO_3) for 24 hours to remove any physical water. Batch compositions were prepared for 35g of glass on a well calibrated balance with precision of 0.001 g; mixed thoroughly, and melted in a Pt-ZGS (ZrO_2 Grain Stabilised) crucible loosely covered with a Pt-ZGS lid to reduce volatilisation losses of oxides and contamination. The melts were attained within temperature range of 1100-1200°C with a dwell time of 3 hours per melt. The melts were poured onto a steel plate to cool gradually to room temperature. The cooled melts were immediately transferred in a vacuum desiccator.

6.2 Sulphate Capacity as A Function of Glass Composition

6.2.1 XRF-ICP Analysis

Fused beads were prepared in same way as done for silicate glasses (see section 5.2.1). ICP analysis was carried out to measure the B_2O_3 content of each glass. The nominal and analysed oxide concentrations are tabulated in Table 6.1.

Sample	SiO_2 mol%	B_2O_3 mol%	Na_2O mol%	BaO mol%	SO_3 mol%	$\frac{[SiO_2 + B_2O_3]}{[MOx]}$	Melt Temp (°C)
NaBSi	40.00 (42.35)	20.00 (18.41)	40.00 (39.24)	0	0	(1.55)	1100
NaBSiS	38.00 (40.00)	19.00 (17.68)	38.00 (37.43)	0	5.00 (4.89)	(1.54)	1100
NaBaBSi	40.00 (41.01)	20.00 (18.48)	20.00 (19.53)	20.00 (20.98)	0	(1.46)	1130
NaBaBSiS	38.00 (39.44)	19.00 (17.53)	19.00 (18.88)	19.00 (19.78)	5.00 (4.37)	(1.47)	1130
BaBSi	40.00 (41.34)	20.00 (17.48)	0	40.00 (41.18)	0	(1.42)	1200
BaBSiS	38.00 (40.72)	19.00 (16.50)	0	38.00 (40.51)	5.00 (2.27)	(1.41)	1200

Table 6.1: Nominal vs analysed (in brackets, normalised to 100%) compositions in mol% for the borosilicate glasses.

The analysed glass compositions are close to their targeted nominal compositions within acceptable error limit of ± 3%. Analysed Na_2O and B_2O_3 are slightly lower than nominal, and this is attributable to volatilisation losses. Where NaBSiS glass retained > 90% of the sulphate added to the batch, BaBSi shows sulphate retention < 50%. The sulphate capacity trend for NaBSiS and NaBaBSiS glasses is similar to that obtained for the silicate glasses NaSiS and NaBaSiS, but due to unavailability of data for a binary BaSiS glass (barium silicate doped with sulphate), sulphate capacity of BaBSiS cannot be directly compared to a silicate glass. However, it is interesting to note that where BaO improves sulphate retention in the presence of a alkali oxide (in this case Na_2O),

the individual capability of glass modified by only Ba^{2+} ions to incorporate sulphate, in the absence of any other modifier, is lower than the corresponding alkali silicate glass.

6.2.2 Density Measurements

The densities of the SO_3 free borosilicate glasses are slightly higher than their SO_3 doped equivalents as seen in Figure 30 The values obtained for the glasses are consistent with literature (Krzhizhanovskaya et al. 2015; Konijnendijk 1975; Roderick et al. 2001). The density of the glass increases upon moving from NaBSi to BaBSi system. The increase is directly affected by increasing molar mass upon substitution of Na_2O with heavier BaO. The standard deviation errors associated with the measurements are low (< 0.001 cm^{-3}) and thus comparable to symbol size. The overall trend is as follows:

BaBSi > BaBSiS > NaBaBSi > NaBaBSiS > NaBSi > NaBSiS

The molar masses and molar volumes of the glasses were calculated for the six glass compositions based on the analysed concentration of oxides and are tabulated in Table 6.2. It is evident that molar volume increases upon sulphate addition.

Sample	Density (g/cm^3)	Molar Mass ($g\ mol^{-1}$)	Molar Volume ($cm^3\ mol^{-1}$)
NaBSi	2.501	62.679	25.072 ± 0.013
NaBSiS	2.471	63.648	25.368 ± 0.014
NaBaBSi	3.252	81.874	25.139 ± 0.012
NaBaBSiS	3.233	81.199	25.192 ± 0.013
BaBSi	3.891	99.305	25.528 ± 0.009
BaBSiS	3.862	98.967	25.639 ± 0.008

Table 6.2: Density, Molar mass and molar volume calculated for the SO_3 free and SO_3 containing borosilicate glasses

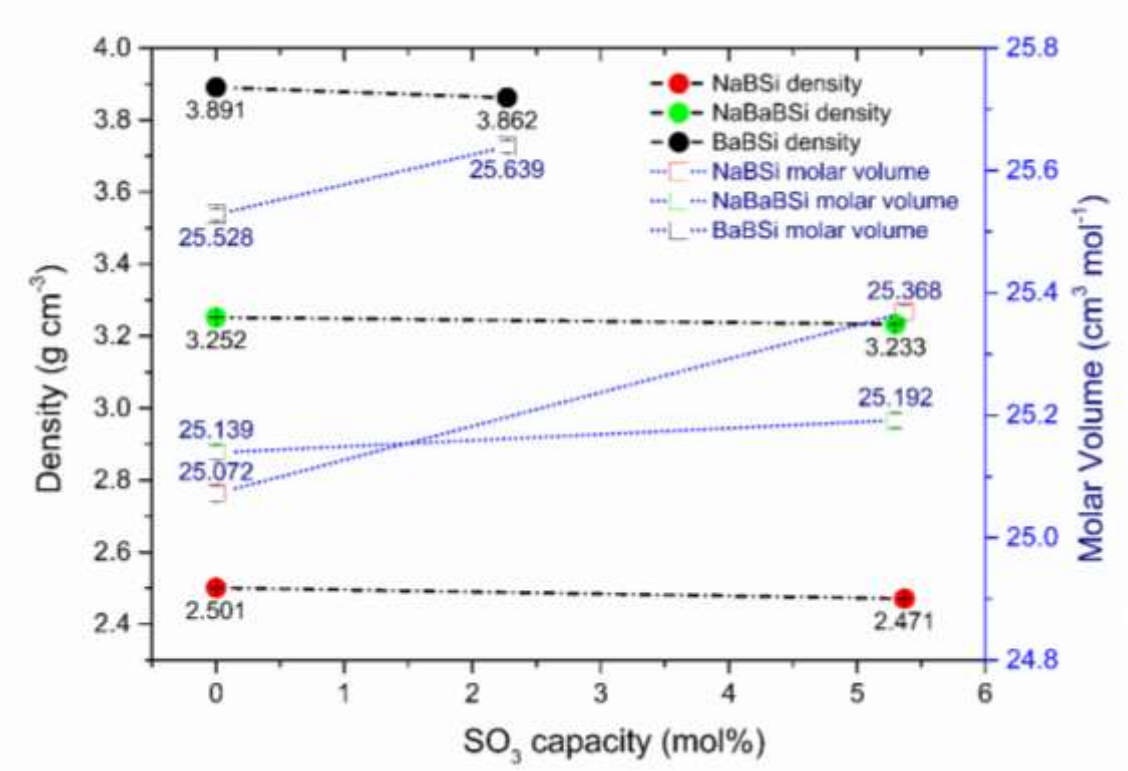

Figure 6.1: Densities and molar volume of the SO_3 free and SO_3 containing borosilicate glasses as a function of their sulphate capacity

6.2.3 XRD Analysis

XRD patterns of the SO_3 free and SO_3 doped borosilicate glasses are shown in Figure 6.2. A broad amorphous hump is present at 2θ = 20-35^o and there are no visible signs of any crystalline peaks, which indicates that the glasses are X-Ray amorphous. Tiny peaks corresponding to Na_2CO_3 (ref code: 00-037-0451) are identified in the NaBSi glass XRD pattern. The presence of a second amorphous phase at around 37-47^o is observed in XRD patterns of BaO containing glasses but its origin has not been investigated here. The average interatomic distance for each glass were calculated using the Bragg's law and the centre position of the amorphous humps. These are plotted as a function of sulphate content retained within the glass (Figure 6.3).

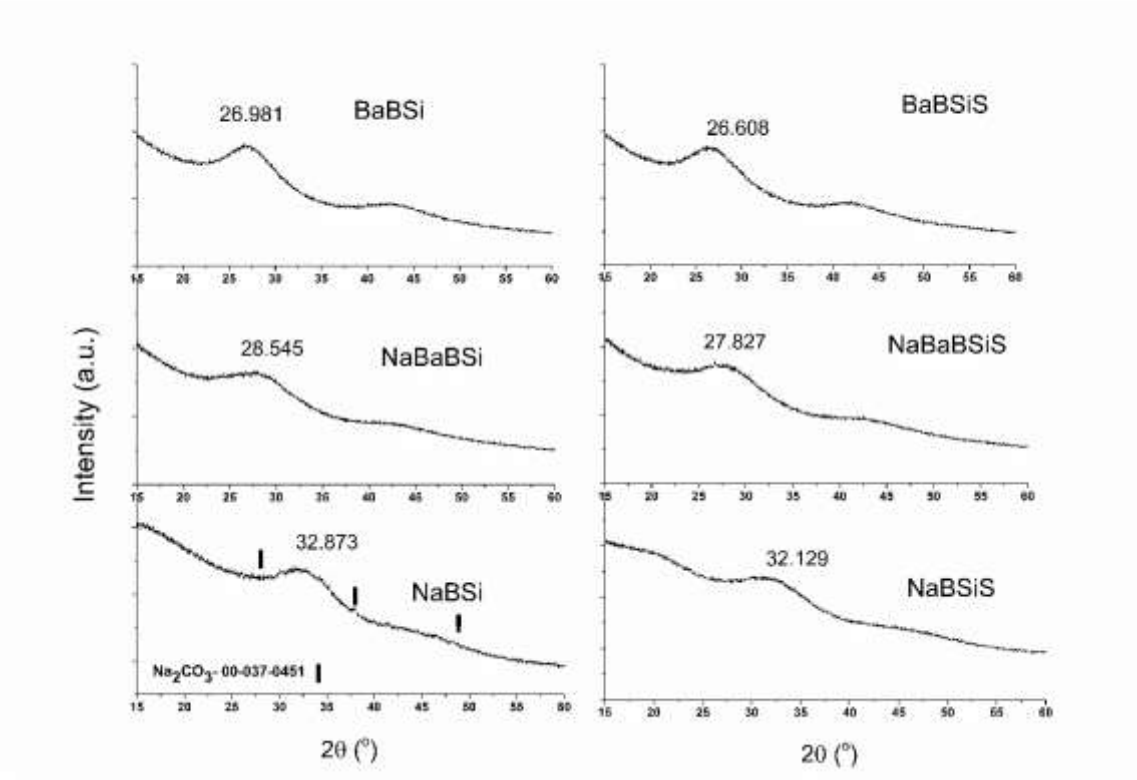

Figure 6.2: XRD patterns obtained for SO_3 free and SO_3 containing borosilicate glasses.

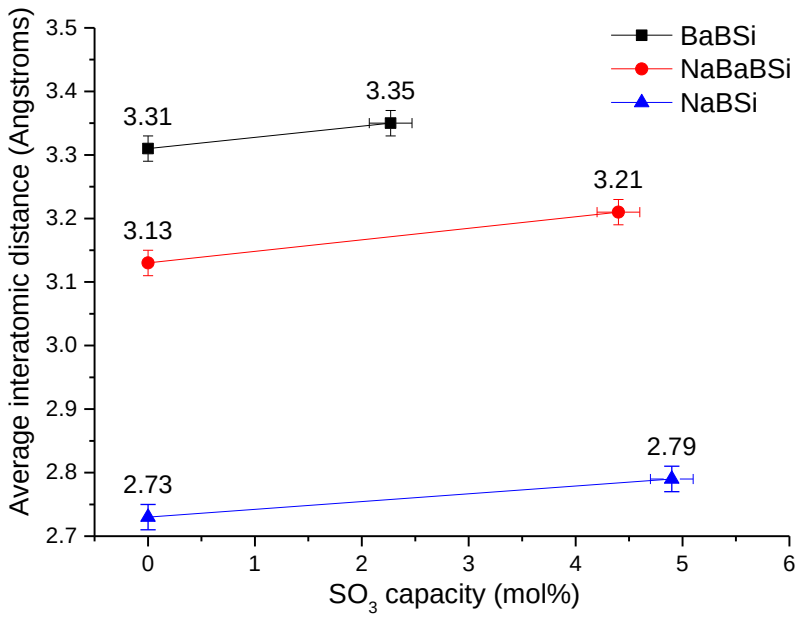

Figure 6.3: Change in average interatomic distance for the borosilicate glasses, obtained from amorphous hump position and plotted as a function of sulphate capacity.

Figure 6.2 shows that the position of the amorphous humps in the XRD patterns shift to lower diffraction angles as we move from NaBaSi to NaBaBSi to BaBSi glasses. To incorporate larger Ba^{2+} ions, there is an overall network expansion, resulting in dilation stresses, increased average interatomic distance and a shift of the amorphous hump towards lower diffraction angles. With addition of sulphate to the glass, the centroid of the hump shifts further to lower diffraction angles. This behaviour is attributable to increase in average atomic spacing due to incorporation of large S^{6+} ions within the glass network. The average atomic spacing determined for BaO containing glasses are long > 3Å. This is sensible as the large Ba^{2+} ions in these glasses generate longer Ba-O, Ba-Ba correlations (as also seen from the ND results for NaBaSi glass in section 5.3.3.3).

6.3 Structural Effects of Sulphate Addition

6.3.1 Effects on Si Q^n Speciation – Raman Spectroscopy Results

Room temperature Raman spectra presented in Figure 6.4 and 6.5 were normalized and corrected to remove the background, fluorescence effect and photobleaching. A linear baseline was defined for each glass and subtracted from each spectrum. The limitation of using Raman spectroscopy for analysing these borosilicate glasses is that it cannot identify whether the Si units are connected to a meta/tetraborate unit or other Si-O units in the Q^n region. For this reason, to assign the bands to different vibrational modes, the spectra are compared to literature available for similar silicate and borate glasses /crystals analysed using Raman spectroscopy (Meera et al. 1990; Maniu et al. 1995; Osipov & Osipova 2013; Meera & Ramakrishna 1993; Konijnendijk 1975; Winterstein-Beckmann et al. 2014; Tokuda et al. 2015; Osipov & Osipova 2009; Osipov et al. 2013;

Konijnendijk & Stevels 1975; Hubert & Faber 2014; Manara et al. 2009; Yadav & Singh 2015).

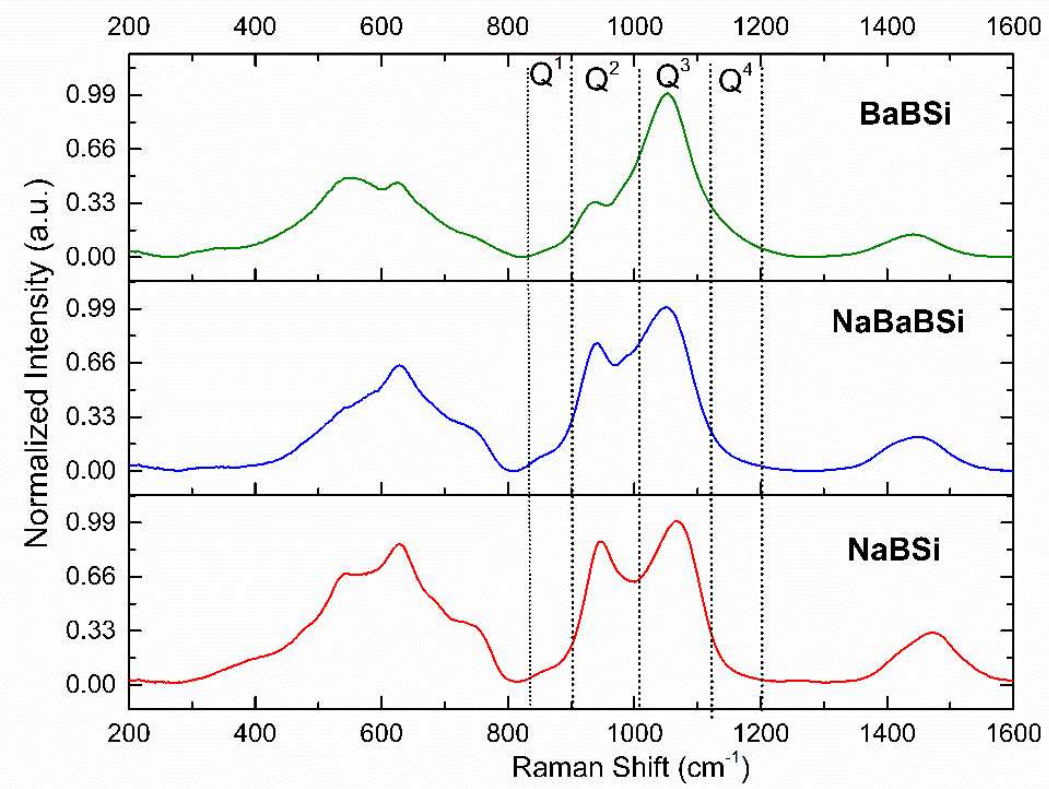

Figure 6.4: Raman spectra of the SO_3 free borosilicate glasses

The spectra can be divided into three regions: (i) a low frequency region between 300-800 cm^{-1} (ii) a high frequency region subdivided between 800-1250 cm^{-1} corresponding to Q^n structural units and (iii) very high frequency region between 1250-1600 cm^{-1} assigned to $B\text{-}O^-$ stretching modes in metaborate groups. In the low frequency region, peaks in the 300 to 500 cm^{-1} frequency range correspond to bending modes due to Si-O-Si motion. The peaks in 550- 800 cm^{-1} frequency range are a characteristic of ring breathing modes due to metaborate, diborate and borosilicate ring units (Meera & Ramakrishna 1993; Manara et al. 2009; Parkinson et al. 2008; Maniua et al. 2003). Manara et al. (2009) deconvoluted this region with four Gaussian bands and concluded the following:

a) The vibrational modes at ~780- 800cm^{-1} and ~750-780 cm^{-1} correspond to three and four coordinated boron in diborate and boroxol rings, respectively.
b) The band at ~630-650 cm^{-1} corresponds to breathing modes of danburite $(B_2Si_2O_8)^{2-}$ like rings including two SiO_4 and two BO_4 tetrahedra with Na_2O compensating the charge of B_{IV} atoms.
c) The band at ~580 cm^{-1} most likely corresponds to breathing modes of reedmergenite $(BSi_3O_8)^-$ like rings including one BO_4 and 3 SiO_4 tetrahedral.

In this case of study, as one can see in Figure 6.4, the intensity of the band at ~770cm^{-1} increases with increasing Na_2O content. This suggests that Na^+ present in the glass are compensating the charge on BO_4^- units at the expense of BO_3 units. The band at 795 cm^{-1} corresponding to three coordinated boron is almost non-existent in NaBSi and NaBaBSi suggesting the presence of boron as mostly four coordinated BO_4^- units in these glasses. The position of the band at 630 cm^{-1} corresponding to tetrahedral borosilicate ring units shifts to higher wavenumbers from NaBSi to NaBaBSi to BaBSi indicating its dependence on the modifier cations associated with these units (Osipov & Osipova 2009; Konijnendijk 1975; Winterstein-Beckmann et al. 2014; Manara et al. 2009; Meera & Ramakrishna 1993) . Its intensity increases with increasing Na_2O concentration in the glass. This observation possibly suggests an increase in the borosilicate units bonded with the modifier cations.

The high frequency region at 850-1200 cm^{-1} was deconvoluted using 5-6 Gaussian bands to obtain a fit with low χ^2 (Figure 6.5). The bands were assigned to different Q^n units according to the deconvolution studies of (Manara et al. 2009; Fukumi et al. 1992) on borosilicate and borate glasses respectively. The band between 850-920 cm^{-1} correspond to Q^1 units, 930-980 cm^{-1} to Q^2 units, 1050-1100 cm^{-1} to Q^3 and 1150-1200

cm^{-1} to fully polymerised Q^4 units. The relative area of the band at 990-1050 cm^{-1} associated with structural units interacting with modifier cations, is small in comparison to similar alkali silicate glasses studied in Chapter 5. This can be attributed to lower concentration of SiO_2 present in these glasses and/or stronger interactions between the Na-B than Na-Si to form tetrahedral borate units.

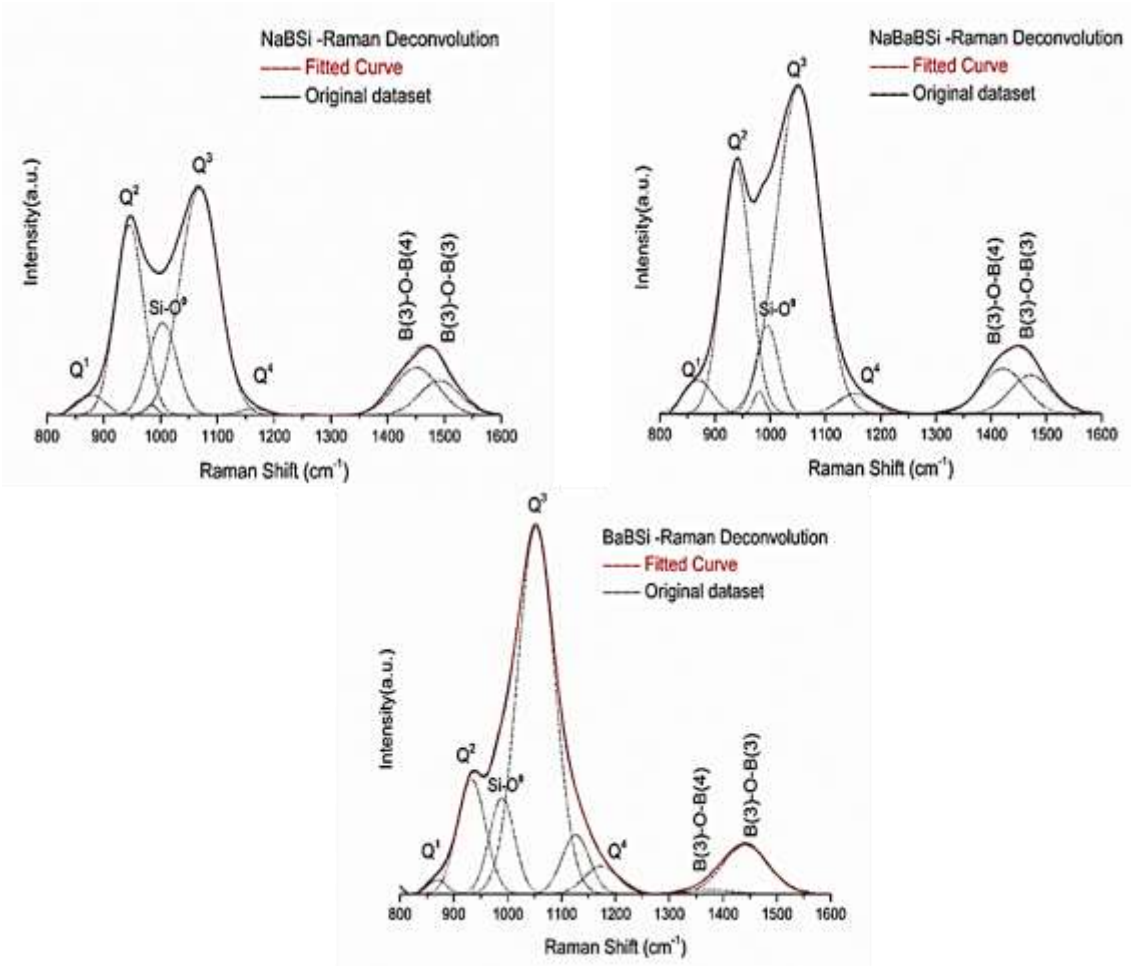

Figure 6.5: Deconvoluted Raman spectra of the SO_3 free borosilicate glasses in the high frequency region.

(Note: The assignment of the bands in high frequency region are not in accordance with the work of (Parkinson et al. 2008) on quantitative analysis of Raman spectra of waste simulant borosilicate glasses. Parkinson and colleagues (2008) suggested that the broad peak between the frequency range 1000- 1200 cm^{-1} corresponds to Q^3 units due

to mixed contributions from Q^3 associating with another Si cation Q^3(Si), Q^3 associating with a Boron cation Q^3(B) and Q^3 units associating with a modifier cation Q^3(M) **)**

The broad asymmetric band visible in the very high frequency region between 1300-1600 cm^{-1} was deconvoluted into two components. The first component at ~1410 cm^{-1} is assigned to BO_3 units interacting with BO_4 units, while the second component at ~1480 cm^{-1} corresponds to BO_3 units bonding BO_3 units (Meera et al. 1990; Maniu et al. 1995; Manara et al. 2009). The frequency of the two components shifts to lower values upon moving from glasses NaBSi to NaBaBSi to BaBSi glass.

Sample	**Q^1 %**	**Q^2 %**	**Q^3 %**	**Q^4 %**	**Si-O^- %**	**NBO/Si**	**BO/Si**	**NBO /BO**	**Q^3/ Q^2**	**Q^3+Q^4/ Q^2+Q^1**
NaBSi	2.57	26.13	42.80	0.67	11.64	1.42	2.58	0.55	1.64	1.51
NaBaBSi	3.34	25.57	49.17	2.44	6.93	1.17	2.63	0.44	1.92	1.79
BaBSi	1.42	13.19	66.54	2.79	6.22	1.16	2.84	0.41	5.04	4.75

Table 6.3: Relative areas of the Q^n structural units in SO_3 free borosilicate glasses obtained with deconvolution

The ratio $(Q^3+Q^4)/ (Q^2+Q^1)$ has been calculated to investigate the degree of network polymerisation (Table 6.3). The $(Q^3+Q^4)/ (Q^2+Q^1)$ ratio shows that the BaBSi glass has the most polymerised silicate subnetwork of the three glasses and favours the formation of less depolymerised Q^3 units. It is interesting to note this behaviour because in silicate glasses, the addition of heavier BaO favoured the formation of Q^2 to Q^3 units and

resulted in overall network depolymerisation. In the frequency range of 1200-1600 cm^{-1}, the relative area of the peak at 1410 cm^{-1} corresponding to BO_4 units in metaborate groups, disappears. This suggests that with addition of large Ba^{2+} ions, the BO_3 units appear only as chain-type metaborate groups and this is consistent with the Raman spectroscopy results of (Konijnendijk & Stevels 1975; Osipov & Osipova 2013) on barium borate glasses.

As sulphate is introduced in the glass, the Raman spectra in addition to change in the intensity of the existing bands, also show four new bands corresponding to S-O symmetric and antisymmetric stretching and bending modes (Figure 6.6). The peak positions for these modes are allocated in the same frequency ranges as seen in corresponding sulphate doped alkali silicate glasses and crystalline sulphates (section 5.3.1). The deconvoluted spectra in the high frequency region are shown in Figure 6.7.

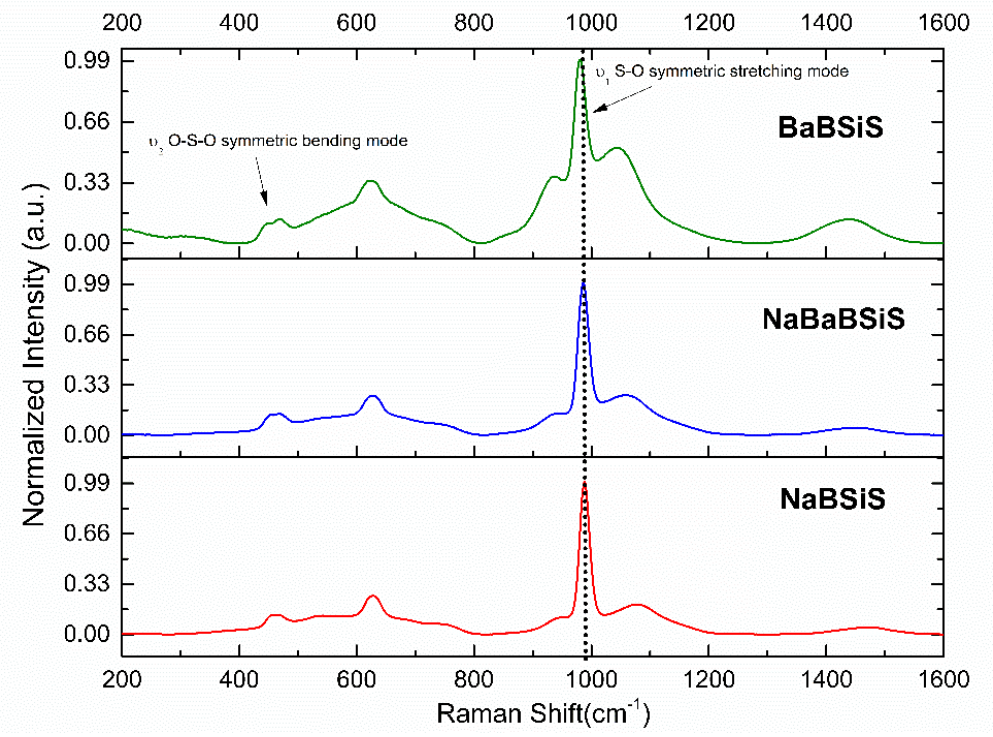

Figure 6.6: Raman spectra of the SO_3 containing borosilicate glasses

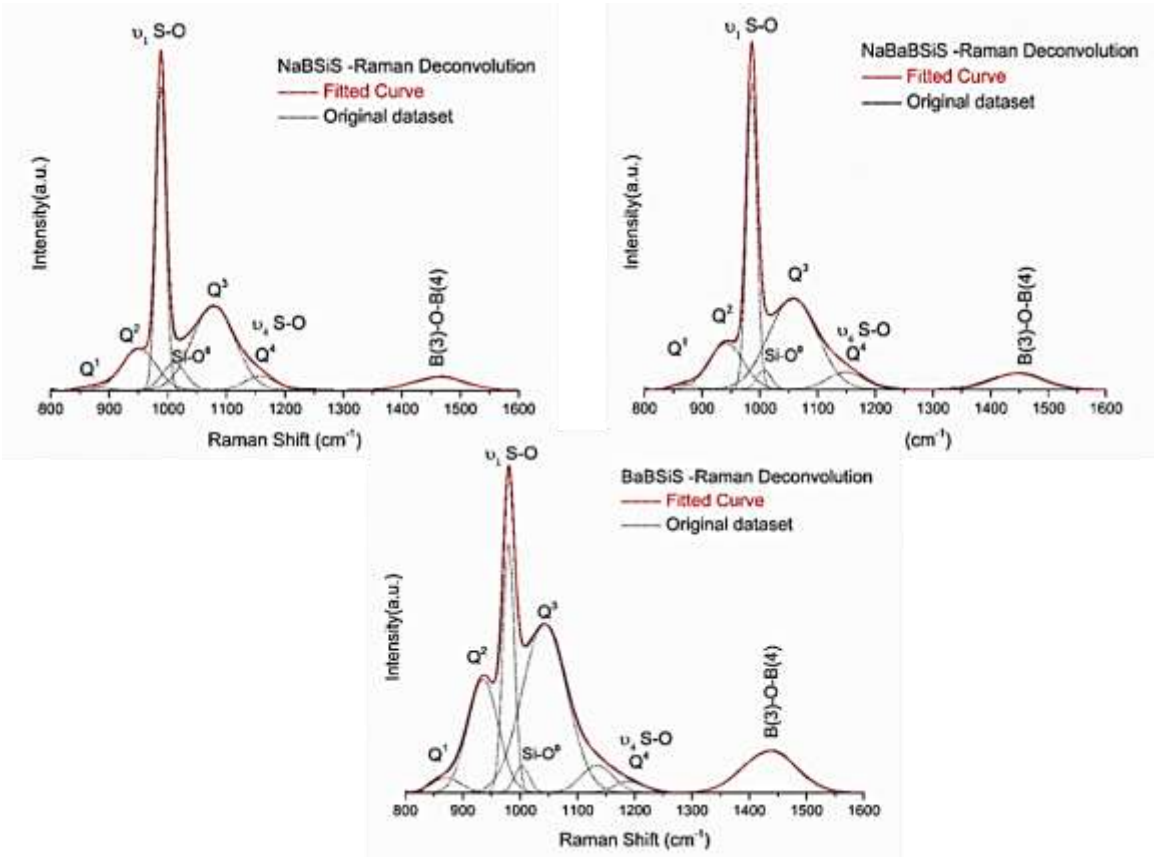

Figure 6.7: Deconvoluted Raman spectra of the SO_3 doped borosilicate glasses in the high frequency region.

Sample	Q^1 %	Q^2 %	Q^3 %	Q^4 %	$Si-O^0$	R.I. of υ_1	Q^3/Q^2	Q^3+Q^4/Q^2+Q^1
NaBSiS	0.93	14.39	36.56	4.42	6.44	30.26	2.54	2.67
NaBaBSiS	0.95	14.45	40.06	5.79	2.52	28.89	2.77	2.98
BaBSiS	2.41	19.10	46.24	1.86	2.17	15.80	2.42	2.24

Table 6.4: Relative areas of the Q^n units and S-O symmetric stretching mode of the SO_3 doped borosilicate glasses.

The relative areas of the S-O symmetric stretching mode at ~980-990 cm^{-1} and the Q^n units tabulated in Table 6.4 show that the NaBSiS and NaBaBSiS glass networks polymerise with sulphate addition. In contradiction, the network depolymerises for the BaBSiS glass. If Ba^{2+} ions act as charge compensators for the SO_4^{2-} added to the glass, the network can be expected to polymerise. The opposite behaviour observed for the BaBSiS sample suggests that besides the modifier, the depolymerisation of borate and silicate networks foster the sulphate retention in the BaBSiS glass, although the specific structural evolution leading to this effect is unclear and needs further investigation. The relative area of the S-O symmetric stretching mode has been plotted as a function of the sulphate retained within the doped glasses (Figure 6.8). The linear correlation between the two parameters (also observed for sulphate doped silicate glasses) strongly supports the conclusion made previously in section 5.3.1 and by (Lenoir et al. 2009; Morizet et al. 2017; Manara et al. 2007) that the area under this peak is a qualitative indicator of the sulphate incorporated within the glass.

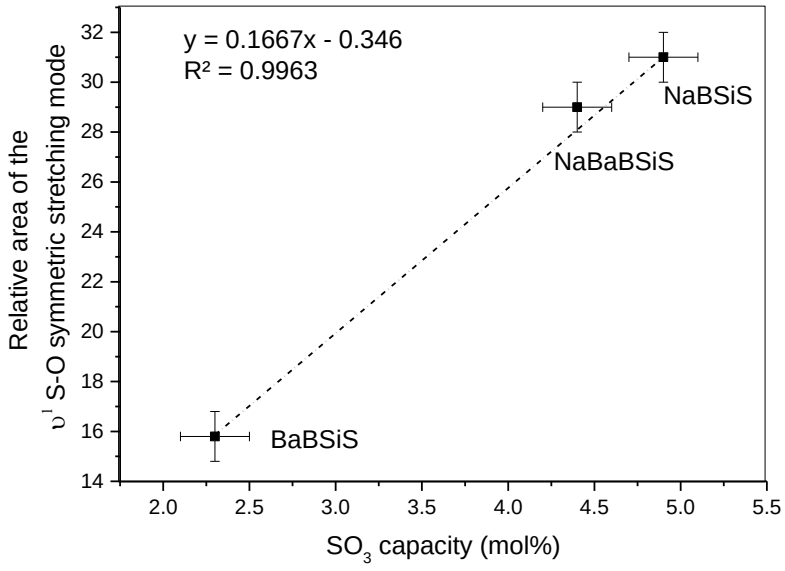

Figure 6.8: Relative area of the S-O symmetric stretching mode plotted as a function of sulphate retained within the borosilicate glass. The vertical error bars were generated by calculating the change in the area under the S-O peak by fixing one peak parameter (FWHM, centre, height) per scan.

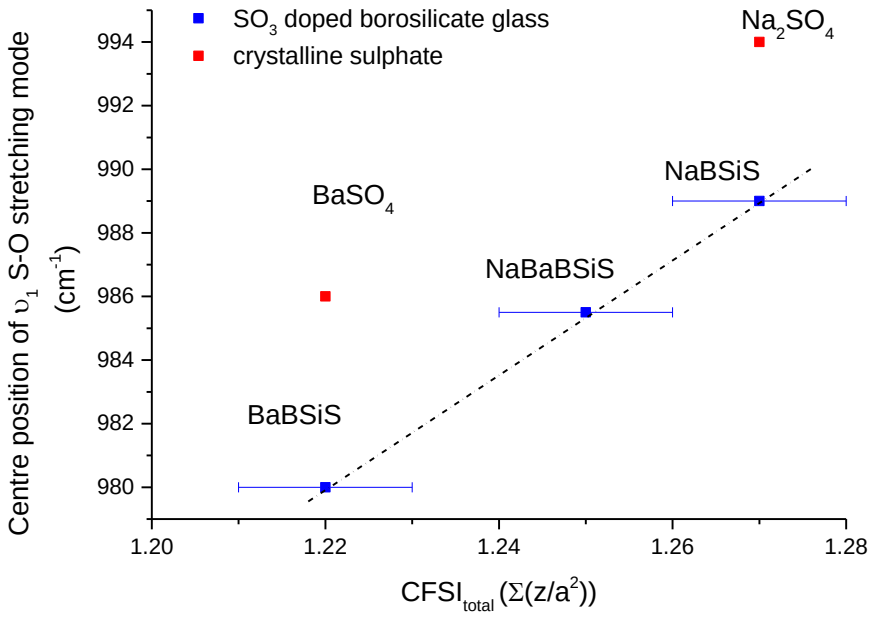

Figure 6.9: Centre position of υ_1 S-O symmetric stretching mode in sulphate doped borosilicate glasses and corresponding crystalline sulphate plotted as a function of total cation field strength index.

The centroid of the υ_1 S-O symmetric stretching mode in the SO_3 containing borosilicate glasses is compared with the centroids for corresponding crystalline Na_2SO_4 and $BaSO_4$ standards and plotted as a function of $CFSI_{total}$ (calculated in section 6.4) (Figure 6.9). The graph suggests that sulphate is either partially or entirely stabilised by Ba^{2+} ions in glass NaBaBSiS.

6.3.2 ^{29}Si, ^{23}Na, ^{11}B MAS NMR Results

^{29}Si MAS NMR spectra were obtained at 79.435 MHz and pulse duration of 4.5 µs. The acquisition time per scan was 20 ms and 500-600 scans were acquired for each sample (Figure 6.10). Gaussian line shapes were used to fit the contribution due to the silicate Q^n units. At a spinning speed of 6 kHz, the sidebands were removed if the intensity was only up to 4-5%. The chemical shift for the silicate network lies in the range of -70 to -

100 ppm with two major contributions due to Q^2 units (-70 to -80 ppm) and Q^3 units (-80 to -90 ppm). A small contribution due to Q^4 units (-90 to -100 ppm) is also visible. The chemical shift centre position for the silicate Q^n units (n= 2, 3, 4) decreases with composition (NaBSi > NaBaBSi > BaBSi) indicating changes in average Si-O bond lengths through the series. Relative Q^n unit concentrations obtained through spectral deconvolution are shown in Table 6.5.

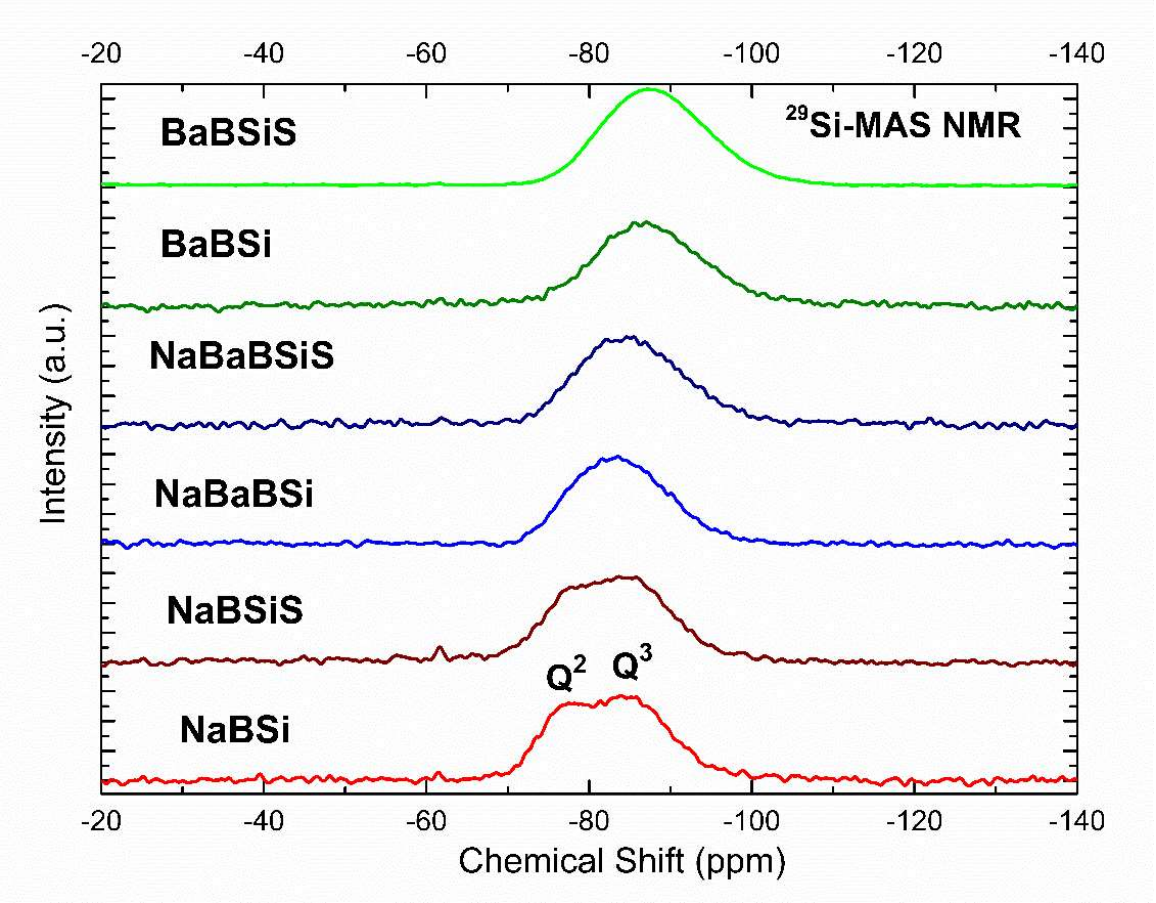

Figure 6.10: ^{29}Si-MAS NMR obtained for borosilicate glasses

Sample	Q^1 %	Q^2 %	Q^3 %	Q^4 %	NBO/Si	BO/Si	NBO /BO	Q^3/Q^2	Q^3+Q^4/Q^2+Q^1
NaBSi	0	26.02	70.22	3.76	1.22	2.78	0.44	2.70	2.84
NaBaBSi	0	22.19	73.49	4.32	1.18	2.82	0.42	3.31	3.51
BaBSi	0	12.88	83.60	3.52	1.09	2.91	0.37	6.49	6.76
NaBSiS	0	20.79	74.63	4.58	1.16	2.84	0.41	3.59	3.81
NaBaBSiS	0	16.46	75.90	7.64	1.09	2.91	0.38	4.61	5.08
BaBSiS	0	15.83	77.87	6.31	1.10	2.91	0.38	4.92	5.32

Table 6.5: Relative areas of the Q^n units obtained with deconvolution of ^{29}Si- MAS NMR of borosilicate glasses

The ^{29}Si MAS NMR Q^n speciation results are in clear agreement with the Raman spectroscopy results that with sulphate incorporation, the silicate network polymerises for glasses NaBSiS and NaBaBSi glasses but for glass BaBSiS it depolymerises.

^{11}B MAS NMR results obtained at a Larmor frequency of 192.4 MHz (14.1 T) are shown in Figure 6.11. A single hard 0.3 µs long pulse of RF frequency 200kHz was used to obtain each spectrum. Due to the high magnetic field, signals arising due to 3-fold coordinated boron in BO_3 units and 4-fold coordinated boron in BO_4 units are well resolved and separated at 10 and 0 ppm respectively. The relative intensities of the BO_3 and BO_4 units are obtained using Topspin 3.5pl software and presented in Table 6.6. The uncertainties associated with the calculations were ±1%.

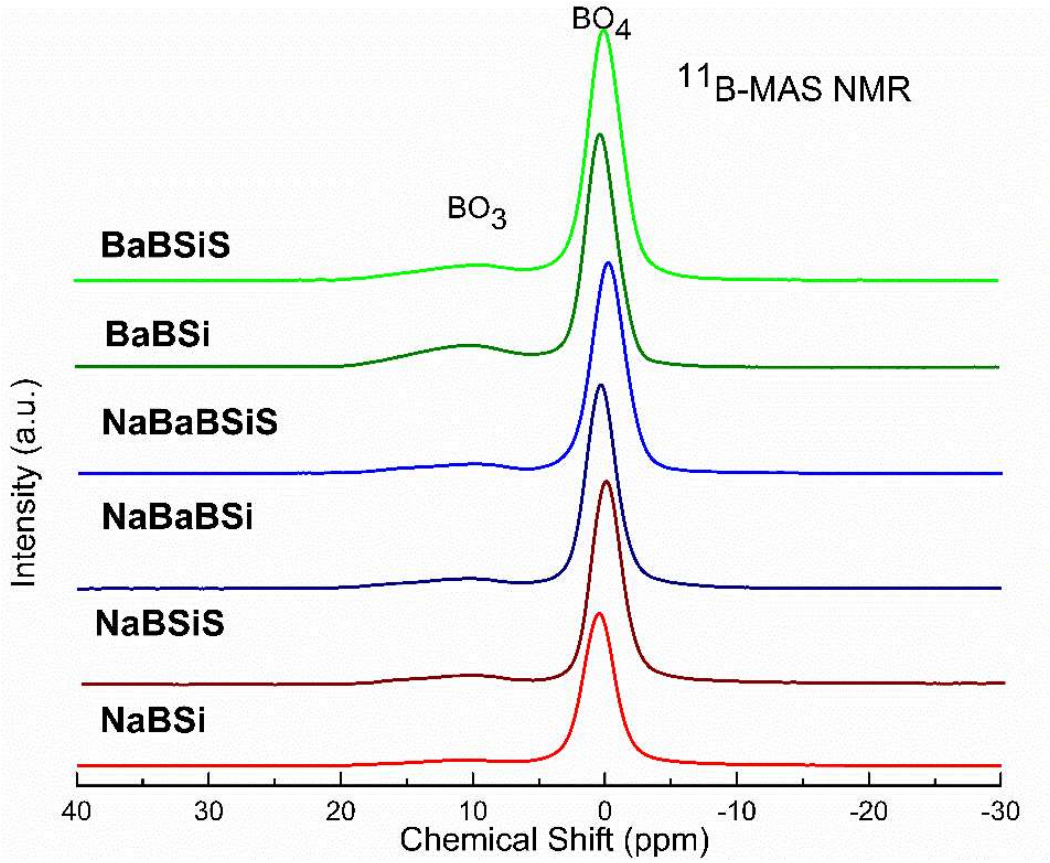

Figure 6.11: ^{11}B-MAS NMR spectra obtained for borosilicate glasses

Sample	% R.I.(B_{III})	% R.I.(B_{IV})	δ(B_{IV})/ppm
BaBSiS	8	92	0.17
BaBSi	16	84	0.2
NaBaBSiS	3	97	-0.17
NaBaBSi	5	95	0.28
NaBSiS	2	98	0.19
NaBSi	3	97	0.38

Table 6.6: Relative intensities of the B_{III} and B_{IV} units present in borosilicate glasses obtained with ^{11}B MAS NMR.

The relative intensity calculations reveal that on partial and complete replacement of Na_2O with BaO in NaBaBSi and BaBSi glasses, the concentration of 3-fold coordinated

Boron units increases. These calculations suggest that between Na^+ and Ba^{2+} ions, the monovalent sodium ions are preferred by the borate units for charge compensation. Therefore, with decrease in concentration of Na_2O from NaBSi to NaBaBSi, the relative concentration of 4-fold coordinated BO_4^- reduces. With addition of sulphate to the glass the relative concentration of BO_4 to BO_3 units increases which suggests that the borate network polymerises with sulphate incorporation. This behaviour is contradictory to the author's expectations as with introduction of sulphate anions, the BO_3 units and the SO_4^{2-} both will compete for charge balance with the modifier cation. As the sulphate ions are incorporated, the availability of Na^+ cations available for charge compensation of trigonal borate units should reduce. Further investigation is required to study this behaviour. As the sulphate anions are introduced in the borosilicate glasses, the isotropic chemical shift for 4-fold coordinated boron units decreases for sulphate doped borosilicate glasses suggesting an increase in average B-O bond lengths (L. Du & Stebbins 2003; Bouty et al. 2014; Dell et al. 1983).

^{23}Na-MAS NMR spectra presented in Figure 6.12, were acquired using single pulse sequence at Larmor frequency of 105.78MHz (9.4 T) and pulse duration of 1.0 µs. The acquisition time per scan was around 10.0 ms and repetitions close to 600 per sample. As observed for ^{23}Na-MAS NMR done on Na_2O containing binary and ternary silicate glasses (section 5.3.2), the peak is asymmetric tailing towards lower chemical range due to quadrupolar interactions. The peak maximum of the symmetric part in the chemical shift range of -50 to 25 ppm decreases in sulphate doped borosilicate glasses suggesting longer Na-O bond lengths. The peak maximum for NaBaBSi glass is higher than for NaBSi glass. The movement of the chemical shift for ^{23}Na-MAS NMR to positive values was attributed to an increase in the fraction of Na-NBO to Na-BO by Xue and Stebbins (1993) through their studies of silicate crystals and melts using this technique.

As per their rationale, partial replacement of Na^+ ions with large Ba^{2+} ions in NaBaSi glass, may result in an increased concentration of NBOs in the borosilicate network which may lead to an increase in fraction of Na-NBO bonds. However, it is difficult to assign the role of Na_2O as a modifier or compensator as in a borosilicate glass as the Na^+ can either compensate the charge for the 4-coordinated borate units , modify the silicate network or do both. The chemical shift centroid position displaces to slightly lower ppm in the SO_3 doped glasses compared to their SO_3 free base glass equivalents which suggests a change in the Na-O coordination environment with sulphate incorporation.

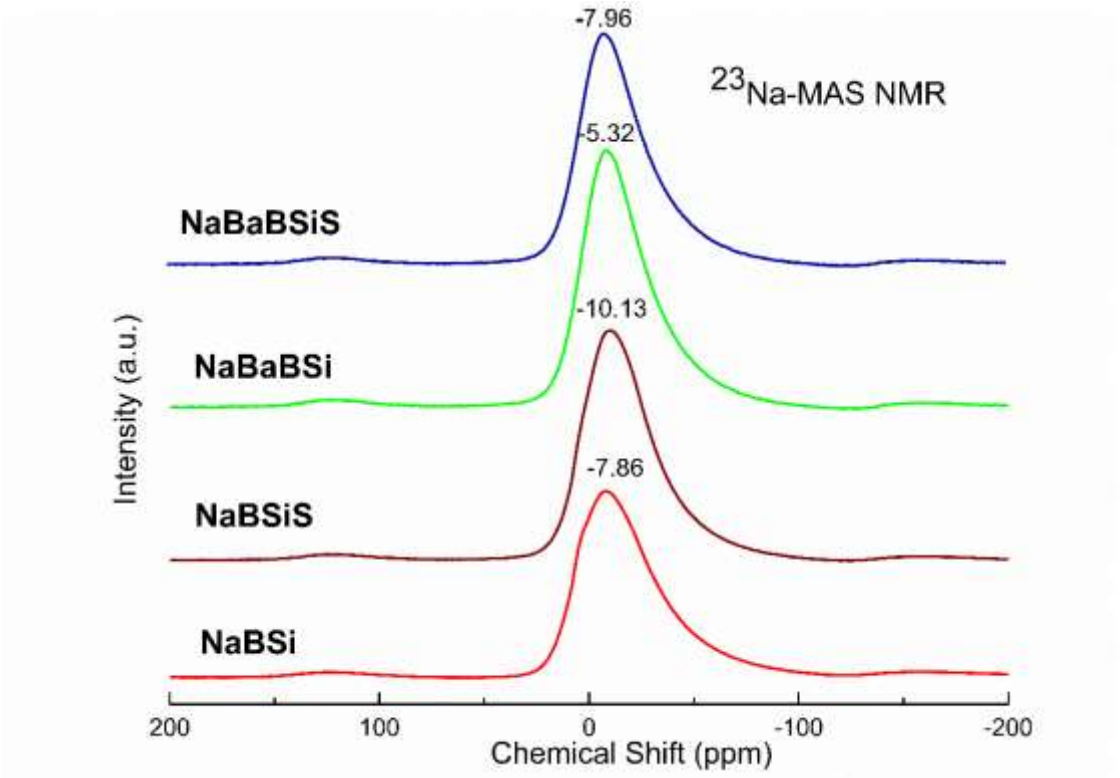

Figure 6.12: ^{23}Na MAS NMR obtained for borosilicate glasses

6.3.3 Neutron Diffraction results

The neutron diffraction results are presented as total correlation functions (T(*r*)) plotted as a function of the bond distance (Figure 6.13). The difference plot between the correlation functions of SO_3 free and SO_3 containing borosilicate glasses reveals the S-O environment. The difference approach was used as the S-O and O-O(S) peaks are strongly overlapped by the $B_{(IV)}$-O and O-O(B) bonds in the first coordination shell at ~1.37-1.39 Å and at 2.49-2.51 Å respectively.

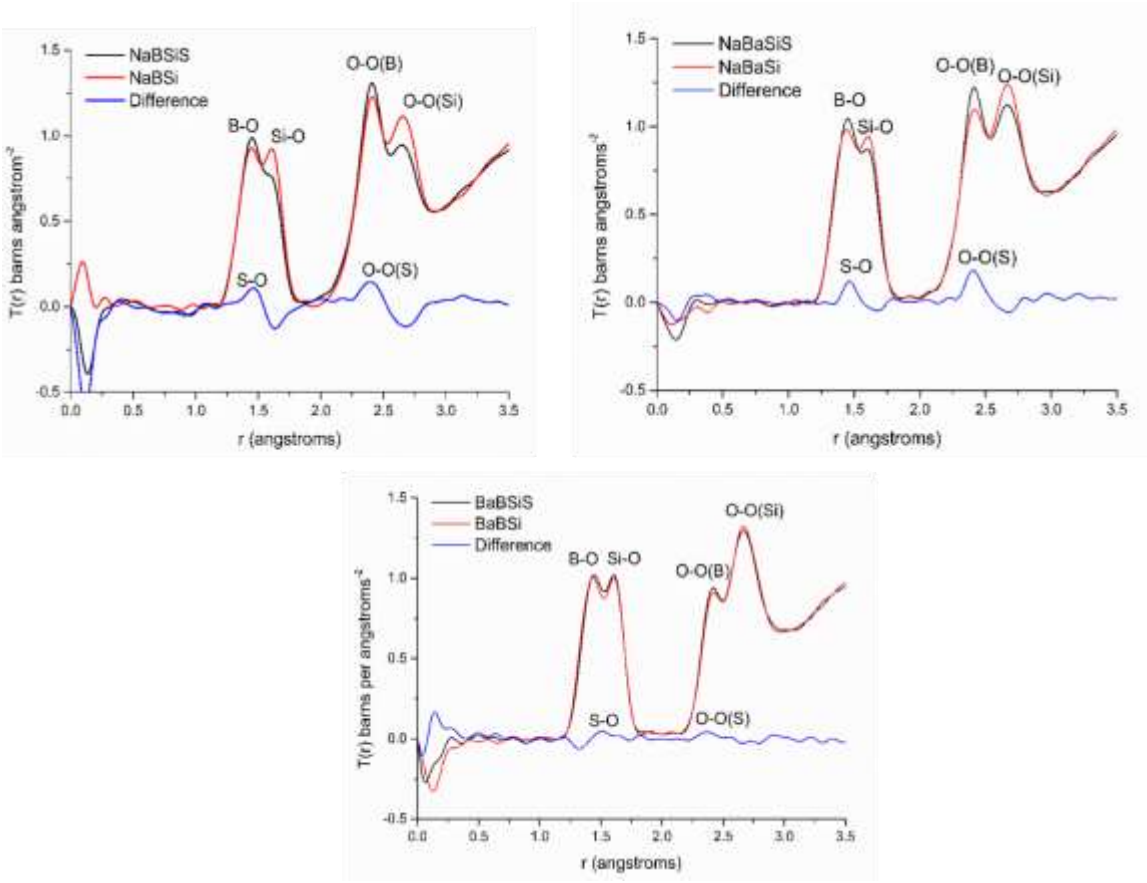

Figure 6.13: Total correlation functions obtained for SO_3 free and SO_3 containing borosilicate glasses are plotted as a function of bond distance

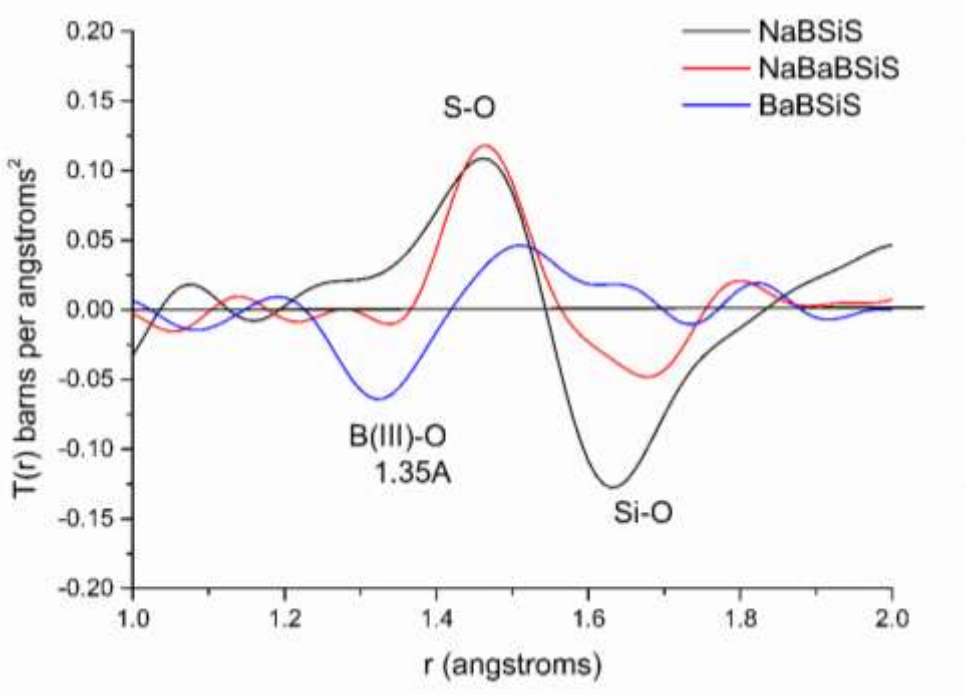

Figure 6.14: S-O correlation function obtained with difference method for borosilicate glasses plotted as a function of bond distance.

Figure 6.14 shows that the S-O correlation function shifts to higher r (1.51Å) from (1.47 Å) on moving from NaBSiS to BaBSiS glass. The r value obtained for S-O in NaBSiS and BaBSiS glasses is comparable to bond distances between S and neighbouring oxygens in crystalline Na_2SO_4 and $BaSO_4$ structure (see Appendix C). Though the peak maxima for the S-O correlation function in NaBaBSiS glass is present at 1.49 Å, a tail towards higher r (~1.50 Å) suggests that sulphate units might be charge balanced by both, Na^+ and Ba^{2+} ions in this glass.

Keeping the fitting parameters unconstrained, two peaks attributed to $B_{(IV)}$-O (1.39 Å) and Si-O (1.61 Å) were fitted in the range of 1.2 – 1.8 Å. The average CN obtained for B-O and Si-O was close to 4 for all three glass sets. The average B-O CN in BaBSi glass was slightly lower ~3.92 Å due to presence of considerable amount of $B_{(III)}$ units (as also confirmed with ^{11}B-NMR). Resolving the Na-O and Ba-O correlation functions

in the range 2.2 – 3Å was challenging due to multiple contributions from O-O (B), O-O(Si), O-O(S) and Na-O. Similarly, to the empirical approach used to fit an O-O (Si) peak in ND spectra for silicate glasses, and its subtraction from the total correlation function to obtain individual modifier- oxygen correlation function, an empirical model is being developed at present to fit a O-O(B) and O-O (Si) in the T*(r)* and reveal the Na-O correlation functions. This will be a part of the future work.

6.4 SO_3 capacity as a function of NBO/BO and CFSI

Sulphate capacity of the three glasses has been plotted as a function of $[O^-]^2/[O^0]$ based on the NBO/BO model suggested by (Papadopoulos 1973; Ooura & Hanada 1998a; Jantzen et al. 2005) and the cation field strength index models suggested by (Bingham & Hand 2008; Bingham et al. 2017). Total cation field strength index was calculated for the three sulphate doped glasses including and excluding sulphate concentration. The analysed concentrations were used for the calculations. The NBO/BO ratios were obtained from the deconvoluted Si-O Q^n speciation results using Raman spectroscopy and ^{29}Si MAS-NMR. The average CN for Boron was based on the ratio of $B(_{III})$ /$B(_{IV})$ obtained from ^{11}B-MAS NMR and neutron diffraction. Na^+ and Ba^{2+} were assumed to be 6- fold and 8-fold coordinated, respectively for all glasses. Oxygen was assumed to be 4 coordinated based on the work of (Fábián et al. 2008; Mountjoy 2007; Hoppe et al. 2007; L. S. Du & Stebbins 2003). The horizontal error bars in Figure 6.15 and 6.16 reflect the upper and lower limit of NCFSI and TCFSI for each sample due to multiple cation-oxygen bond distances that can be present within the glass, respectively.

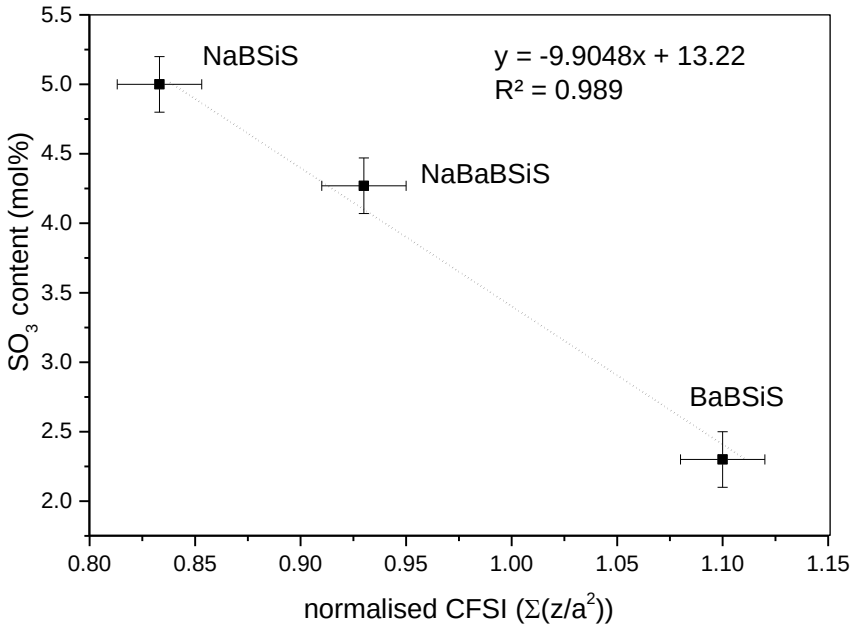

Figure 6.15: SO_3 capacity plotted as a function of normalised cation field strength index for borosilicate glasses

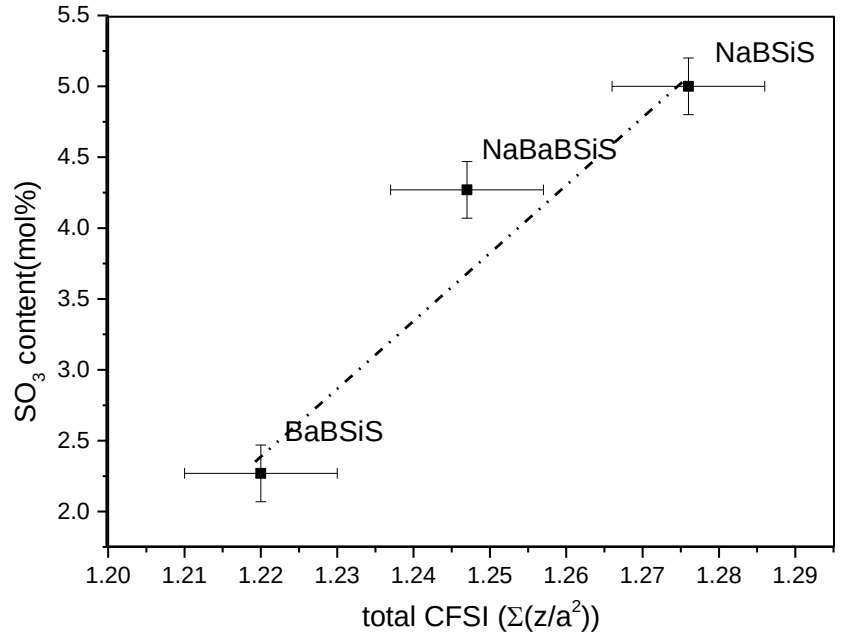

Figure 6.16: SO_3 capacity plotted as a function of total cation field strength index (excluding sulphate) for borosilicate glasses

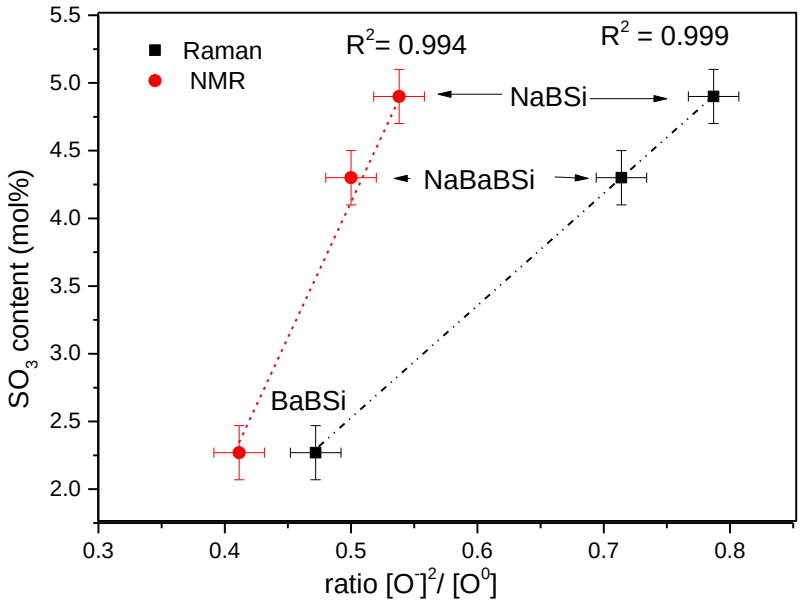

Figure 6.17: SO_3 capacity plotted as a function of ratio of NBO/BO in borosilicate glasses obtained using Raman spectroscopy and NMR

Figure 6.15 to 6.17 show that while the NCFSI model and the NBO/BO sulphate solubility models are consistent for the borosilicate glasses studied here, the $CFSI_{total}$ has limitations. The inverse linear correlation obtained between NCFSI and SO_3 capacity suggests that partial and full replacement of low ionic field strength Na^+ ions with Ba^{2+} with a higher CFS, leads to increased sulphate retention due to higher oxygen activity. Similarly, sulphate capacity is induced in glasses with higher NBO/ BO ratios.

6.5 Conclusions

- The compositional analysis shows that ~ 4.3 mol % of sulphate can be retained within the borosilicate glass with equimolar concentrations of Na_2O and BaO. However, if the entire Na_2O content is replaced by BaO, the sulphate retained within the glass reduces significantly. This indicates, that the high sulphate solubility in

BaO containing borosilicate glasses arises due to cumulative effect of BaO and Na_2O, and not only BaO.

- The density of sulphate doped borosilicate glasses is slightly lower than the corresponding undoped compositions due to the presence of the large sulphate anions. The molar volumes of the borosilicate glasses increase with sulphate addition.
- The XRD amorphous hump shifts to lower diffraction angles due to increase in the average interatomic distance for the borosilicate glasses doped with SO_3
- Raman spectroscopy and the ^{29}Si MAS NMR results reveal that with addition of sulphate the silicate network polymerises for NaBSiS and NaBaBSiS glasses. Depolymerisation of the SO_3 doped BaBSi glass is observed but the behaviour cannot be yet explained.
- ^{11}B-MAS NMR shows an increase in the ratio of $B_{(IV)}/B_{(III)}$ upon sulphate addition in the three borosilicate glasses studied.
- A decrease in the chemical shift for the ^{23}Na MAS NMR peak maximum in the spectra for sulphate doped borosilicate glasses, suggests formation of longer Na-O bonds.
- The r values obtained for S-O correlation functions from ND suggest that sulphate anions are partially stabilised by both Na^+ and Ba^{2+} ions in NaBaBSiS glass.
- When plotted as a function of NCFSI and NBO/BO ratio, sulphate capacity shows a linear relationship with the two parameters. Decrease in sulphate capacity with increasing normalised cation field strength index and decreasing NBO/ BO confirms that these sulphate solubility models suggested by (Papadopoulos 1973; Jantzen et al. 2005; Bingham & Hand 2008) are consistent for simple ternary and quaternary borosilicate glasses.

CHAPTER 7

SULPHATE DOPED MULTI-OXIDE COMPLEX BOROSILICATE GLASSES

In this chapter, we have investigated sulphate doped multi-oxide complex borosilicate glass compositions which are broadly representative of industrially used U.S. HLW and LAW glasses at the Savannah River Waste site. Sulphate capacity of these simulated waste glasses was studied as a function of glass composition. The concentrations of the components and the sulphate retained within the matrix was analysed using ICP and XRF. The analysed compositions were used in the total cation field index model to examine the effect of the CFS of the glass on sulphate retention and to investigate the versatility of the empirical model in different glass systems. Structural analysis was carried out using Raman spectroscopy. NMR on these glasses was not possible due to the high concentration of Fe_2O_3 present in the composition. Mössbauer spectroscopy was performed on some of the glasses to investigate the oxidation state and coordination of iron.

7.1 Composition change by varying SiO_2/ Modifier oxide

7.1.1 Experimental details

Eleven borosilicate glass samples were prepared in two inter-connected series, notated as Series A and Series B. The glass compositions were broadly representative of the HLW waste glasses used industrially at the Savannah River Waste Vitrification Facility U.S. (Billings & Fox 2010; Fox et al. 2006;) In Series A, the concentration of all modifier oxides in the glass were raised with reducing SiO_2 content. Whereas, in Series B, except for CaO and Na_2O the concentration of all other modifier oxides was kept constant. The nominal compositions are shown in Table 7.1. Sulphate was introduced in the form of Na_2SO_4. As the maximum sulphate retained by the U.S. waste glasses is ~ 1 wt% of SO_4^{2-}, we doped the compositions to a modest excess of 2wt% of SO_4^{2-} to enable sulphate saturation on the surface. Analytical grades chemicals and sand of purity > 99.90% were used for batch preparation. The raw materials were dried at 100^oC for 24 hours prior to batching except for H_3BO_3 which was not dried due to its low decomposition temperature, weighed for 150g glass on an electronic balance of precision 0.01g and thoroughly mixed in the sample bags to ensure homogeneity. Those were then transferred into a Pt-ZGS crucible and melted in an electric furnace at 1150^oC for 1 hour. The crucible was covered loosely with a Pt-ZGS lid to reduce volatilisation losses. The melt was poured on a stainless- steel mould and allowed to cool naturally to room temperature. A sulphate layer was formed on the surface of every melt which indicates that the sulphate capacity limit was exceeded in all melts (Figure 7.1).

Figure 7.1: Left HLW simulant glass with high SiO_2 shows presence of undissolved sulphate on the surface. Right: Glass with low SiO_2 content shows negligible sulphate flaking on the surface.

wt%	B6	B5	B4	B2	B1	A6	A5	A4	A3= B3	A2	A1
Al_2O_3	5.94	5.94	5.94	5.94	5.94	7.59	7.04	6.49	5.94	5.39	4.84
B_2O_3	5.94	5.94	5.94	5.94	5.94	7.59	7.04	6.49	5.94	5.39	4.84
CaO	12.13	10.39	8.66	5.20	3.46	8.85	8.21	7.57	6.93	6.29	5.65
Fe_2O_3	15.84	15.84	15.84	15.84	15.84	20.24	18.77	17.30	15.84	14.37	12.91
Li_2O	4.95	4.95	4.95	4.95	4.95	6.32	5.87	5.41	4.95	4.49	4.03
Na_2O	22.52	19.30	16.09	9.65	6.43	16.44	15.25	14.06	12.87	11.68	10.49
SO_3	2.00	2.00	2.00	2.00	2.00	2.00	2.00	2.00	2.00	2.00	2.00
SiO_2	29.70	34.65	39.60	49.49	54.44	29.70	34.65	39.60	44.55	49.49	54.44
ZrO_2	0.99	0.99	0.99	0.99	0.99	1.26	1.17	1.08	0.99	0.90	0.81
Sum	100.0	100.0	100.0	100.0	100.0	100.0	100.0	100.0	100.0	100.0	100.0

Table7.1: Nominal compositions of the U.S.- simulant HLW glasses studied in wt%

7.1.2 ICP-XRF Composition Analysis

The cooled melts were washed under hot water for 5 minutes to remove most of the excess sulphate on the surface, and dried overnight, prior to compositional analysis. The washed, dried glasses were powdered and further washed in dilute nitric acid to ensure complete removal of excess sulphate salts. The samples were prepared for ICP analysis using sodium peroxide and lithium tetraborate fusion separately and subjected to ICP-OES. The results from both methods were averaged to obtain a single value for each component. Errors associated with the ICP analysis are estimated to be ± 1 % of the measured concentrations. Glasses were further analysed using XRF for which samples were prepared using the fused bead method. Errors related to XRF analysis are ± 2 %. Analysed compositions are tabulated in Table 7.2. Analysed concentrations of sulphate retained in each glass is plotted vs. SiO_2 content in the glass (Figure 7.2)

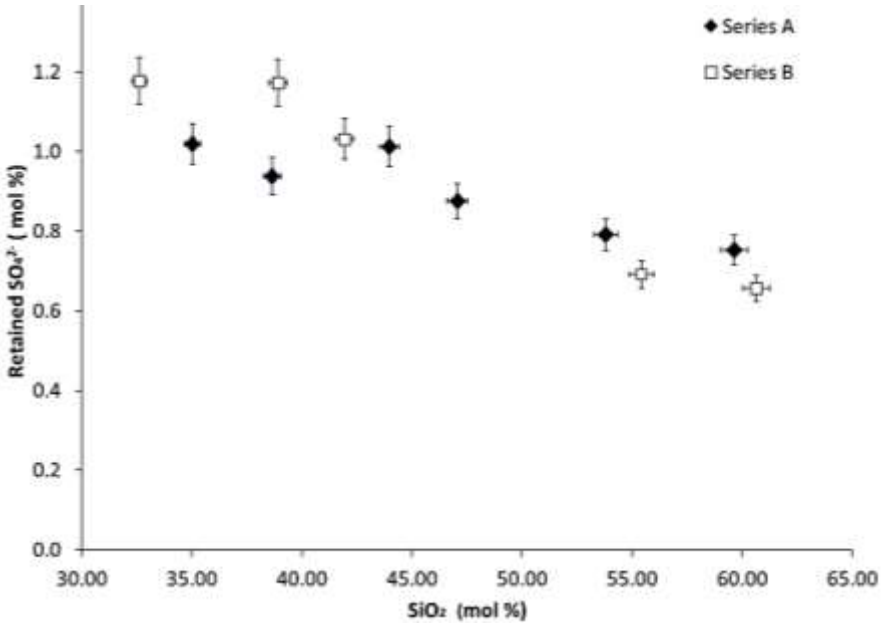

Figure 7.2: Sulphate capacity of the glasses as a function of the SiO_2 content

The sulphate content retained within the glass gradually decreases from A6 to A1 and B6 to B1 glass. For Series A, this behaviour is directly attributable to increase in the SiO_2/ MOx ratio which leads to increase in the degree of polymerisation. Similar results

were obtained by (Baker & Moretti 2011; Nagashima & Katsura 1973; Backnaes & Deubener 2011) for their sulphur solubility studies in sodium silicate glasses. For Series B, the increase in sulphate capacity can be attributable to increase in the concentration of oxides including CaO and Na_2O for which, structural investigation is necessary.

Mol%	B6	B5	B4	B2	B1	A6	A5	A4	A3B3	A2	A1
Al_2O_3	4.04	3.89	4.15	4.02	3.98	5.01	4.96	4.11	3.93	3.76	3.55
B_2O_3	7.87	6.34	7.62	7.24	7.42	7.71	7.94	6.91	7.30	7.34	4.66
Fe_2O_3	4.57	4.57	4.85	4.64	4.48	6.41	5.77	6.13	6.49	5.86	5.47
Li_2O	10.27	`0.43	10.53	10.15	9.89	13.81	12.79	11.85	10.89	8.85	7.79
Na_2O	23.66	20.68	17.26	9.70	6.09	17.85	16.41	15.28	13.95	11.86	10.9
K_2O	0.18	0.20	0.12	0.12	0.12	0.15	0.17	0.13	0.06	0.06	0.17
MgO	0.90	0.91	0.93	0.85	0.81	1.06	1.13	0.59	0.16	0.16	0.16
CaO	14.02	12.20	10.84	6.47	5.22	11.14	10.48	9.25	8.58	6.90	6.29
MnO	0.04	0.04	0.04	0.03	0.03	0.04	0.04	0.05	0.05	0.05	0.05
P_2O_5	0.03	0.03	0.03	0.03	0.03	0.04	0.04	0.03	0.03	0.03	0.03
SiO_2	32.61	38.91	41.93	55.42	60.6	35.02	38.65	43.98	47.06	53.800	59.63
TiO_2	0.02	0.02	0.02	0.02	0.02	0.02	0.02	0.02	0.01	0.01	0.02
ZrO_2	0.62	0.62	0.64	0.62	0.60	0.71	0.66	0.68	0.63	0.53	0.53
SO_4^{2-}	1.18	1.17	1.03	0.69	0.66	1.02	0.94	1.01	0.88	0.79	0.75
Sum	100	100	100	100	100	100	100	100	100	100	100

Table 7.2: Analysed compositions of the studied simulant HLW glasses using ICP and XRF

7.1.3 XRD analysis

The glasses were examined with XRD to check if those were X-Ray amorphous. For all the glasses an amorphous hump is observed between diffraction angles $2\theta = 27.5^{o} – 37.5^{o}$. Tiny crystalline peaks observed for A1 and B1 corresponds to SiO_2 in the silica rich glasses and this is attributable to tiny amounts of undissolved SiO_2 which were observed at the crucible after melting. The XRD patterns for the glasses are shown in Figure 7.3. No further conclusions were made from the XRD spectra.

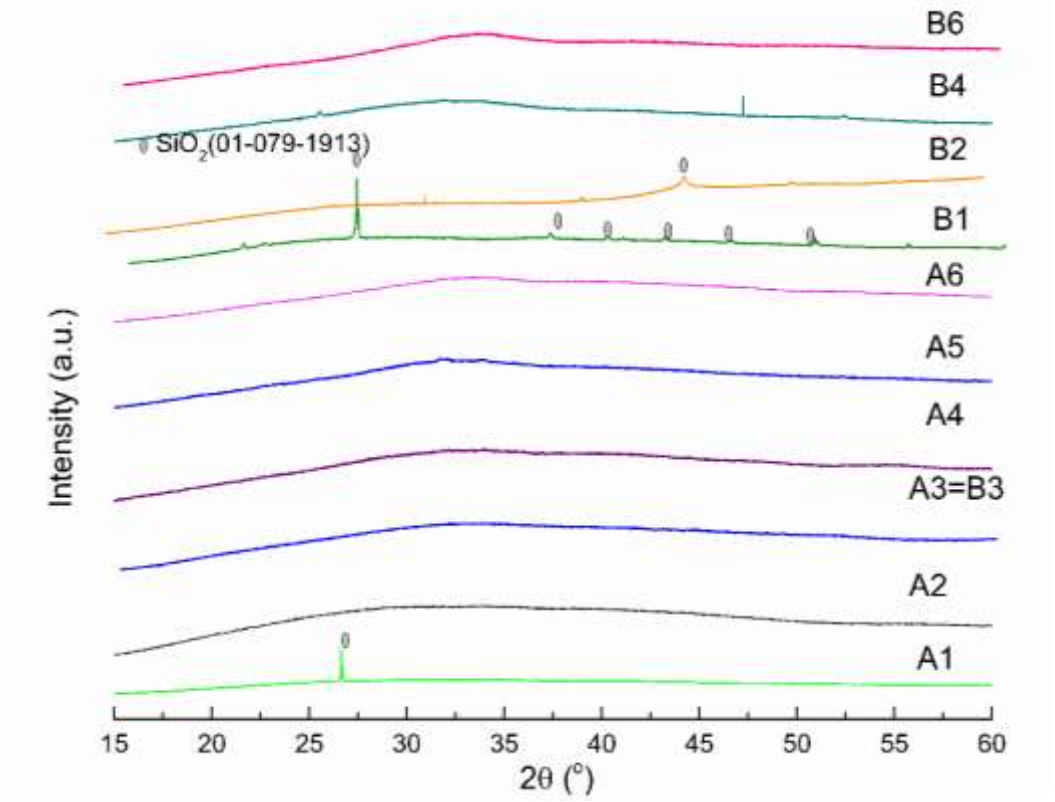

Figure 7.3: XRD patterns obtained for the simulated HLW glass compositions.

7.1.4 Raman spectroscopy

Raman spectra obtained for the glasses are highly convoluted due to overlapping contributions from multiple Raman active constituents present in the glasses. It is not feasible to deconvolute the high frequency region as the technique fails to distinguish

Q^n species related to Si or Al. Figure 7.4 shows many spectral differences through series A1 to A6 and B1 to B6 in the low (400- 800 cm^{-1}), high (850-1200 cm^{-1}) and very high (1300-1500 cm^{-1}) frequency range. However, the centroid of the band at ~990 cm^{-1} corresponding to the υ_1 S-O stretching mode does not shift with change in composition. Only the intensity of this band changes.

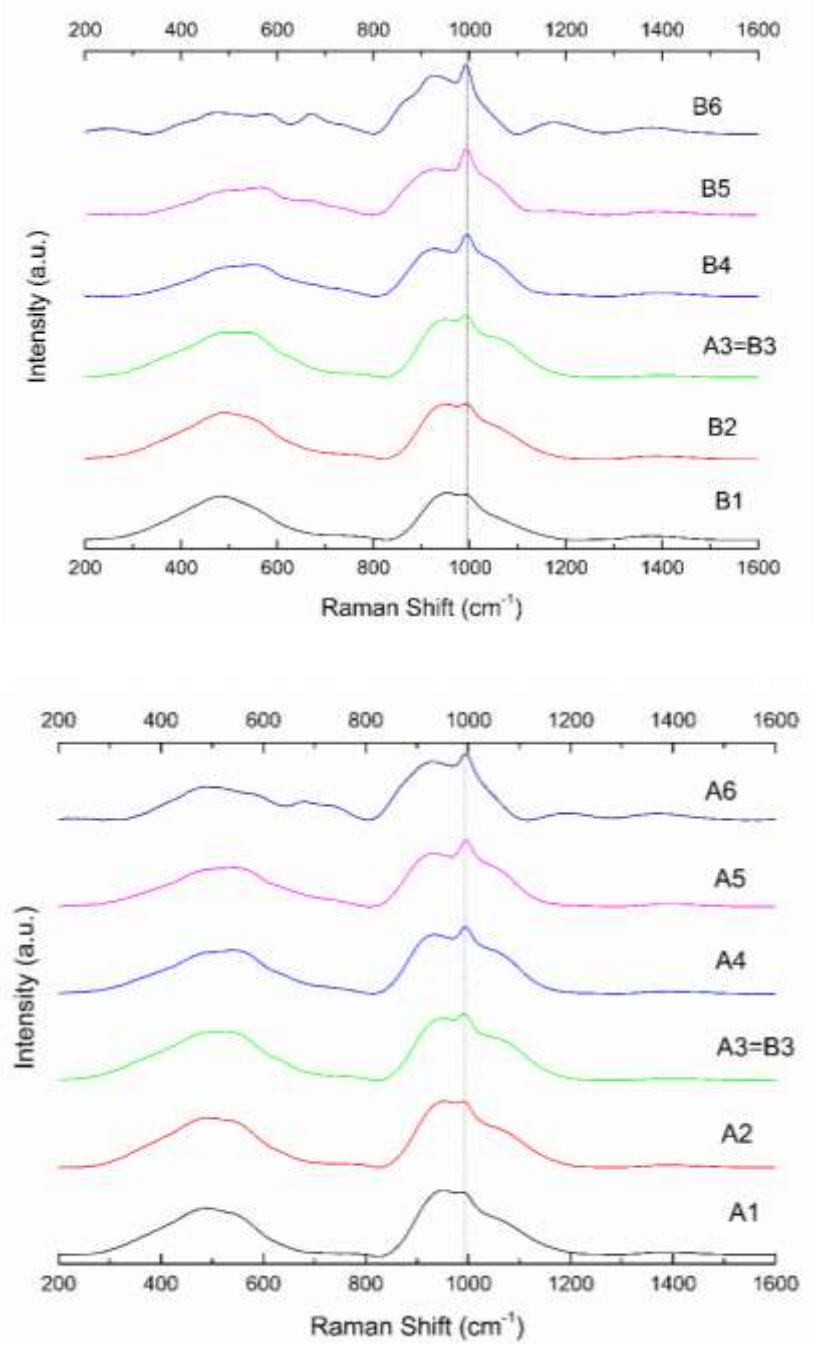

Figure7.4: Raman spectra obtained for Series A and Series B HLW simulant glasses doped with sulphate

In Chapter 5 and 6, through the de-convolution studies of the Raman spectra for SO_3 doped silicate and borosilicate glasses, a qualitative linear relationship was established between the relative intensity of the Raman υ_1 S-O stretching mode and the concentration of SO_3 retained within the glass. The increase in the intensity of the S-O Raman band at ~990 cm^{-1} from A1 to A6 and B1 to B6 indicates increase in sulphate retention. The results qualitatively agree with the the compositional analysis of the sulphate content within these glasses. The position of this band does not change which suggests that the local cation environment around the SO_4^{2-} ions remains same despite change in the overall glass composition. The S-O peak position in the spectra validates that sulphur is present only as S^{6+} in these glasses. The possible presence of S^{2+} or S^{4+} is ruled out as no corresponding bands are seen in the low frequency region (Evans & Bernstein 1954; Mernagh & Trudu 1993).

The low frequency region between 300-550 cm^{-1} does not show significant change within the series. The weak band at around 630 cm^{-1} corresponding to breathing modes of danburite like borosilicate ring units (see section 6.3.1) disappears from A1 to A6 due to decrease in SiO_2 content. The band at 680 cm^{-1} corresponding to the presence of BO_4 units (Manara et al. 2009; Parkinson et al. 2008; Osipov & Osipova 2013) becomes prominent for low silica compositions (A4-A6 and B4-B6). Gradual shift of the bands in the high frequency region at around ~1050 cm^{-1} to lower wavenumbers from A1 to A6 and B1 to B6, suggests a decrease in the concentration of highly polymerised Q^3 units and increase in Q^2 units. The emerging band at ~870 cm^{-1} in samples B6 and A6 indicates formation of highly depolymerised Q^1 units. The very high frequency bands at ~1450-1500 cm^{-1} are attributed to presence of BO_3 units. However, the peak is prominent only in glasses with B_2O_3 concentration > 15 mol%. In these glasses with low B_2O_3 content, the band is not identifiable. The band at ~1380 cm^{-1} has been assigned

by to the BO_3 units linked to BO_4. The emergence of the band is accompanied by bands at 680cm^{-1}, 750 cm^{-1} and 1200cm^{-1}. Further investigation is required to deduce the origin of these spectral changes.

7.1.5 Mössbauer spectroscopy

Room temperature ^{57}Fe Mössbauer spectra were collected for end-member of series A and B, i.e. A1, A6, B1 and B6 over a velocity range of ± 6 mm/s using a constant acceleration spectrometer equipped with a 25 mCi source of ^{57}Co in Rh. Two broadened Lorentzian paramagnetic doublets were fitted to the A1 and A6 spectra while three were fitted to B1 and B6: two strong doublets consistent with Fe^{3+} and the weak doublet consistent with Fe^{2+}, using the Recoil analysis software package. The presence of Fe^{2+} is negligible in B1 and B6 and accounts for only ±1-2% of the total iron content. The high oxidation state of iron is sensible as SO_4^{2-} acts as an oxidising agent in the glasses and leads to high oxygen activities.

The samples presented in the Table 7.4 show that iron predominantly exists as Fe^{3+} (Darby Dyar 1985; Nishida 1994; Dyar et al. 2006). There is little difference between the *s*-electron density around the Fe nuclei in these samples, as indicated by the CS values. Each sample appears to have two sites with different electric field gradients; two bonding systems, as indicated by the two sites with distinctly different QS values.

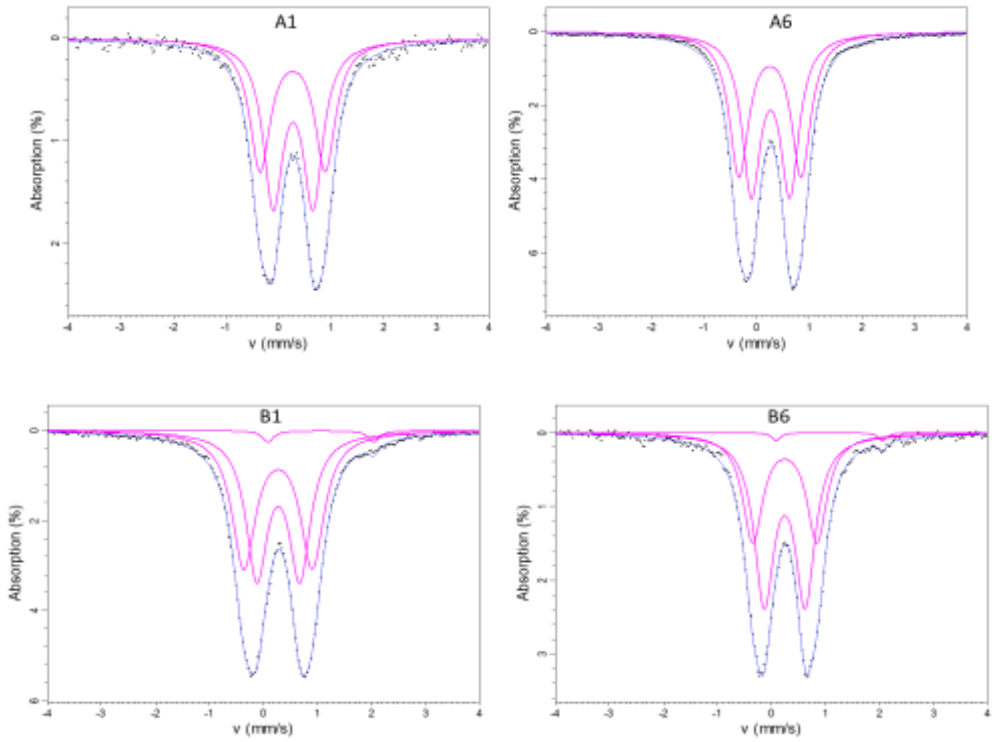

Figure 7.5: Fitted ^{57}Fe Mössbauer spectra for end-members of the simulant HLW glasses: A1, A6, B1 and B6, shows two strong Lorentzian doublets attributed to 4-coordinated Fe^{3+} and one very weak Lorentzian doublet in B1 and B6 corresponding to 6 coordinated Fe^{2+}.

Sample ID	CS (mm s^{-1})	QS (mm s^{-1})	HWHM (mm s^{-1})	Relative Area (%)
A3=B3	0.27	1.25	0.22	35
	0.28	0.78	0.23	65
A1	0.27	1.24	0.24	46
	0.28	0.76	0.23	54
A6	0.26	1.18	0.22	49
	0.26	0.73	0.21	51
B1	0.27	1.27	0.26	49.8
	0.28	0.80	0.24	48.1
	1.07	1.96	0.13	2.1
B6	0.25	1.19	0.23	59
	0.25	0.76	0.22	39
	1.07	1.97	0.10	1.28

Table 7.3 : Fitting parameters for the ^{57}Fe Mössbauer spectra for end-members of the simulant HLW glasses: A1, A6, B1, B6 and A3=B3

This suggests that while all of the iron observed is present in Fe^{3+} state in these samples, there are two ways that the iron may be bound to other atoms- either octahedral or tetrahedral (Cochain et al. 2012; Roca et al. 2007; McCloy et al. 2015) As the data in all these samples has presented with doublets (two absorption lines) it can be said that there are no observable net internal magnetic moments, as this would result in sextets (six absorption lines). The results are in agreement with the work of (Cochain et al. 2012; Cassingham et al. 2008; McCloy et al. 2015; Moretti & Ottonello 2005) on laboratory melted radioactive waste type alkali borosilicate glasses which were prepared under oxidising condition. From the measurements, CS and QS value, therefore, one can assume iron to be present only as Fe^{3+} while calculating the cation field strength index of the glass.

7.1.6 Sulphate capacity against $CFSI_{total}$

For the simple binary and ternary silicate and borosilicate glass compositions, an inverse relationship between the CFSI of the glass and its sulphate capacity was observed in Chapter 5 and 6, where the total CFSI was calculated using the empirical model proposed by (Bingham et al. 2017). In this section, we apply the same model to investigate its application and relevance to complex HLW borosilicate glasses.

However, to obtain the correct total CFSI, it is crucial to know the correct coordination number and bond distances of the cations participating in glass formation. From Mössbauer spectra, the presence of iron as paramagnetic Fe^{3+} with CN of 4 is evident. Si and Li are sensibly assumed to be 4 coordinated while Na coordinates with 6 atoms in its first coordination shell. The assumption is in accordance with the neutron diffraction analysis of the silicate and borosilicate glass compositions. Similarly, the

CN of Oxygen is chosen to be 4 based on the work of (Mountjoy 2007; Hawthorne 1994; Hoppe et al. 2007) and the results obtained by empirical O-O model fit in the neutron diffraction spectra of silicate glasses. Boron is both 3 and 4-fold coordinated in the glasses. Raman spectroscopy confirms the presence of the boron units as mostly BO_3 in the glass. For the current series of glasses, we assumed 2/3 of the total boron content exists as 3-fold coordinated B-O and the rest 1/3 in the form of B (4). Therefore, the average CN chose for B_2O_3 is 3.33. The possible variation in the average CN of boron units has been considered while estimating uncertainties associated with the CFSI model. Table 7.5 summarises the average CN, valence, radius and cation field strength of the modifiers chosen to calculate $CFSI_{total}$. Using the CFS values from Table 7.4 and the analysed concentrations of modifier oxides, $CFSI_{total}$ (excluding the concentration of sulphate in the calculations) was calculated and plotted as a function of sulphate capacity (Figure 7.6). An inverse linear correlation is obtained between the two parameters, with a fit of R^2 = 9.509. This suggests that the $CFSI_{total}$ model not only explains the sulphate capacity in simple binary and ternary glasses but is also consistent for the more complex borosilicate glasses.

	Al_2O_3	B_2O_3	Fe_2O_3	Li_2O	Na_2O	K_2O	MgO	CaO	MnO	P_2O_5	SiO_2	TiO_2	ZrO_2
CN	3	3	3	1	1	1	2	2	2	5	4	4	4
Valence	4	3.33	4	4	6	8	4	6	5	4	4	5	6
A (pm)	1.77	1.42	1.87	1.97	2.4	2.89	1.95	2.38	2.13	1.55	1.64	1.89	2.1
z/a^2	0.96	1.5	0.86	0.26	0.17	0.12	0.53	0.35	0.45	2.08	1.49	1.13	0.91

Table 7.4: Valence, average CN, ionic radii, cation field strength and optical basicity of the modifier oxides present in the HLW simulant glasses.

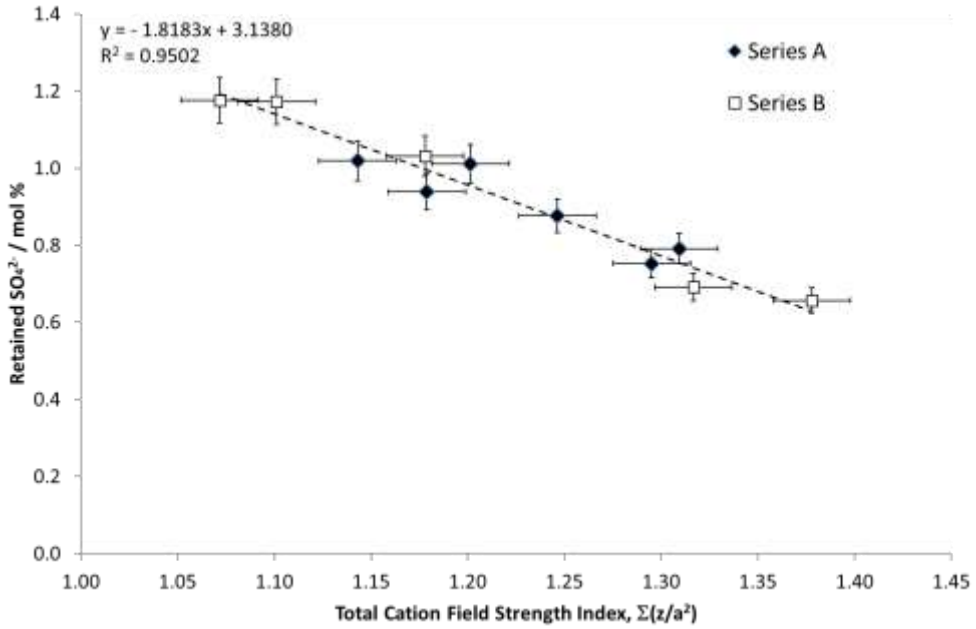

Figure 7.6: SO_3 capacity as function of $CFSI_{total}$ (excluding sulphate) of simulated waste glasses

7.2 Composition change by partial/full replacement of modifier oxide

The agenda behind these studies emerged from the promising sulphate capacity shown by LiSiS and NaBaSiS (Chapter 5). In the binary and ternary silicate glasses, modifier oxides such as Li_2O and BaO demonstrated enhanced sulphate capacities. The rationale presented for such behaviour was that Li_2O containing binary silicates have higher free volumes to accommodate the sulphate anions. In NaBaSi. the negative charge on the anions was compensated either partially or entirely by the larger Ba^{2+}ions while Na^+ modified the silicate network. Twelve glasses simulating effects of DWPF HLW glass are formulated. HLW0 is the un-doped base glass equivalent of HLW1 which is excessively doped with sulphate (~ 2 mol% SO_4^{2-}). Between HLW 2 to HLW 11, compositional variation is introduced in 5 ways:

- Partial and full replacement of Na_2O by Li_2O (HLW 1, 2, 3)

- Partial replacement of Li_2O by Na_2O (HLW 1, 4, 5)
- Partial and full replacement of CaO by BaO (HLW 1, 6, 7)
- Partial and full replacement of CaO by ZnO (HLW 1, 8, 9)
- Partial and full replacement of CaO by MgO (HLW 1, 10, 11)

Batches were prepared for 200g of glass on an electronic scale of precision ~0.001g. After thorough mixing, the batch was transferred to high alumina (~99.6 % high purity Al_2O_3) crucibles with a loose-fitting alumina lid. The melts were achieved at 1150^oC within 1.5 hours per sample and poured on stainless-steel mould to cool at room temperature. The cooled glass exhibited a rather 'yellowish' sulphate salt layer on its surface. The distinct yellow colour is imparted due to the presence of chromium ions in the salt (Figure 7.7). Prior to analysis, the salt layer was washed off under hot water (5-6 minutes) and dried at room temperature.

Figure 7.7: DWPF simulated HLW glasses with varying amount of sulphate deposited on the surface.

7.2.1 Composition analysis

The composition of the glasses was determined using ICP-OES. The analysed values are reported in Table 7.6. The errors associated with the analysis is ±2 % of the

measurements. Following observations were made Partial and complete replacement of Na_2O with Li_2O enhances the sulphate capacity drastically from 1.04 to 1.29 1.67 mol% (HLW 1, 2, and 3). The most interesting and rather unusual behaviour in seen in glasses HLW 1, 6 and 7 where the CaO content was partially and fully replaced by BaO. In HLW6, partial replacement with BaO does not show any significant change in the amount of sulphate retained within the glass. In HLW7, where the entire CaO is replaced by BaO, shows a peculiar behaviour and the sulphate solubility drops. This contradicts the earlier suggestions made through studies of sulphate doped BaO containing silicate and borosilicate glasses. Since the ionic field strength of Ba^{2+} ions are lower than Ca^{2+} ions, the sulphate capacity is expected to increase as per the cation field strength approach. The contradictory behaviour suggests significant structural changes must occur in these glasses which play a role in the poor sulphate capacity. Partial and full replacement of CaO with ZnO in HLW1, 8 and 9 shows reduced sulphate solubility which is sensible as the ionic field strength of Zn^{+} is much higher than Ca^{2+}. No strong conclusions are put forward in HLW1, 10 and 11 where CaO is partially and fully replaced by MgO as the analysed concentration of MgO is significantly higher than the targeted values. However, the slight decrease in the concentration of sulphate retained, is again in agreement with the cation field strength theory as the field strength of Mg^{2+} ions is higher than that of Ca^{2+}.

Glass ID	HLW0	HLW1	HLW2	HLW3	HLW4	HLW5	HLW6	HLW7	HLW8	HLW9	HLW10	HLW11
Al_2O_3	6.000	6.220	5.976	5.744	6.309	4.943	5.460	5.933	5.029	6.019	4.619	6.241
B_2O_3	4.311	4.022	3.775	3.956	3.897	4.238	3.845	3.528	3.836	3.777	4.017	3.676
BaO	0.047	0.047	0.045	0.042	0.048	0.048	3.090	6.052	0.047	0.049	0.046	0.047
CaO	5.796	6.008	5.460	5.625	5.794	5.647	2.947	0.174	2.929	0.166	2.927	0.207
Cr_2O_3	0.211	0.120	0.145	0.104	0.119	0.108	0.128	0.119	0.132	0.137	0.126	0.121
Fe_2O_3	3.999	3.848	3.920	3.922	3.996	3.929	4.031	3.950	4.049	3.964	3.954	3.796
Li_2O	10.687	10.379	17.489	26.008	5.055	5.014	10.460	10.182	10.433	10.360	10.334	10.090
MgO	0.294	0.263	0.255	0.239	0.269	0.271	0.276	0.287	0.266	0.274	4.714	8.417
MnO	1.714	1.604	1.538	1.570	1.613	1.612	1.623	1.613	1.604	1.605	1.736	1.519
Na_2O	15.693	14.751	7.390	0.216	20.252	23.853	14.791	15.311	15.025	15.035	14.873	14.489
P_2O_5	0.427	0.419	0.430	0.441	0.405	0.387	0.434	0.406	0.416	0.415	0.420	0.437
SO_4^{2-}	0.245	1.038	1.285	1.666	0.898	0.862	1.028	0.546	0.888	0.722	0.860	0.688
SiO_2	50.480	51.182	52.198	50.378	51.247	48.990	51.787	51.792	52.952	53.175	51.278	50.174
ZnO	0.098	0.097	0.094	0.088	0.100	0.100	0.102	0.106	2.392	4.303	0.096	0.098

Table 7.5: Analysed molar concentrations of the HLW simulant glasses (normalised to 100%)

7.2.2 XRD Analysis

The XRD patterns for the HLW glass series show clear amorphous humps and no sharp peaks attributing to occurrence of any crystalline phase (Figure 7.8). Shift in position of amorphous peak is due to the change in the average d-spacing with composition of glasses studied.

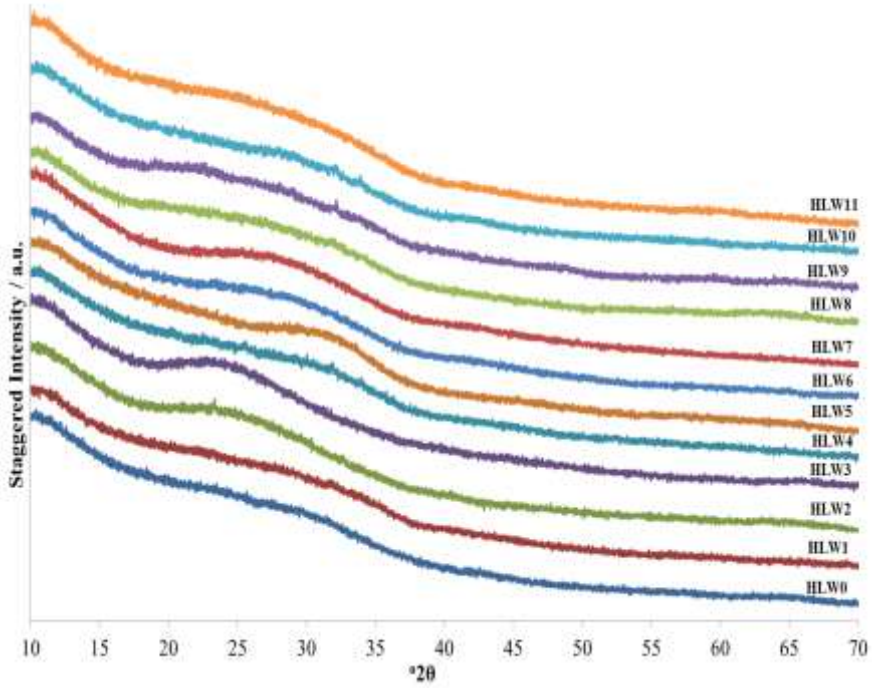

Figure 7.8: XRD patterns obtained for the HLW simulant borosilicate glasses

7.2.1 Raman Spectroscopy Results

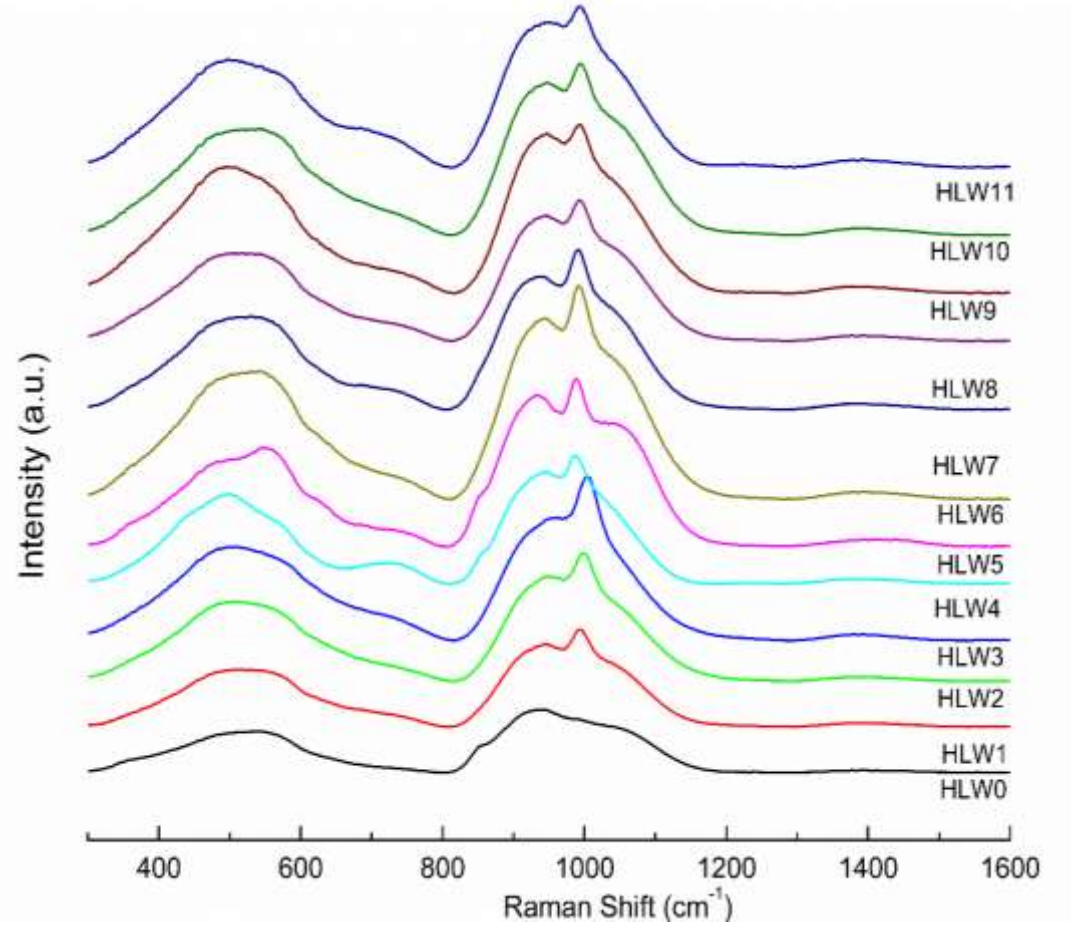

Figure 7.9: Raman spectra obtained for the HLW simulant waste glasses

Figure 7.9 shows the Raman spectra obtained for the HLW simulant waste glasses. The S-O stretching mode for glass HLW1 appears at ~990-1016 cm^{-1} in all glasses. The position shifts to higher frequencies ~ 999cm^{-1} (HLW2) and 1005 cm^{-1} (HLW3) indicating partial and complete stabilisation of the sulphate units with partial and full replacement of Na_2O with Li_2O, respectively. It has already been shown in Chapter 5, that the Raman band assigned to the main S-O stretching mode for crystalline Li_2SO_4 lies at ~1008 cm^{-1}. The position of the S-O stretching mode in the Raman spectra of the glasses shifts position depending on the type of modifier cation the sulphate units are interacting with.

The position shifts to lower frequency ~988 cm^{-1} (HLW4) with partial replacement of Li_2O with Na_2O and remains unchanged for HLW5. Partial and full replacement of CaO with BaO shows no effect on the position of the S-O band which remains unchanged at ~991 cm^{-1}. It suggests that in the complex HLW simulant glasses, unlike as observed for sulphate doped simpler ternary silicate and borosilicate compositions, the sulphate units are mainly stabilised by the alkali (Na_2O) ions and the replacement of the participating alkaline modifier shows its effect only on the sulphate capacity. Similarly, the position of the peak does not change either upon replacement of CaO with ZnO or CaO with MgO. The overall picture suggests that the sulphate units in the complex borosilicate glasses are majorly stabilised by the highly mobile Na^{2+} ions present in the glass. It is also observed that with increasing the concentration of Li_2O to Na_2O in the glass, the role of charge compensation of the anions is distributed between the two alkali oxides.

7.3 Effect of V_2O_5 addition

The addition of V_2O_5 has long been believed to enhance SO_4^{2-} capacity of radioactive waste borosilicate glasses (J.D. Vienna et al. 2014; Manara et al. 2007). The idea first came to light when the Radon Russian research team found that the presence of V_2O_5 in the glass matrix enhanced the liquid state miscibility of sulphates in the melt (Stefanovskii et al. 1989). According to the author, the sulphate capacity of a vitreous matrix is dependent on the chemical compatibility between the cations present in the melt and the sulphate ions. The compatibility decisive chemical parameters are: ionic field strength; ion-oxygen binding energy; coordination environment of the cation; the size and degree of polarisation of the polyhedrons; etc. As per the rationale, the

compatibility of sulphate ions is better with phosphate tetrahedra than silicate tetrahedra. For this key reason, phosphate based glasses are employed in Russia to vitrify sulphate rich radioactive waste (Stefanovskii 1993). The analogous structures of V^{5+} and P^{5+}, set the mark for development of borosilico-vanadate glasses for immobilisation of sulphate rich radioactive waste. However, the very high sulphate solubility (6 wt %) achieved in vanadium containing borosilicate glasses developed by the Radon group has not yet been reproduced, as stated by (McKeown et al. 2002). McKeown et al. (2002) also conducted EXAFS and XANES studies on vanadium valence in waste glasses and predicted non-existence of any V-S-O bonds. V^{5+} was found to be present in the glass as VO_4 tetrahedra. In this study four multiple oxide borosilicate glasses doped with ~2 mol% SO_4^{2-}(nominal) were prepared with stepwise additions of V_2O_5 up to 3.5 mol%. To the author's knowledge, this is the first study that has considered stepwise additions of V_2O_5 to a high level and its influence on sulphate capacity. The XRF-ICP results clearly demonstrate the strong enhancement of SO_4^{2-} retention with increasing V_2O_5 additions (Table 7.6). An almost linear relationship is established between sulphate capacity and concentration of V_2O_5 up to addition of 2.5 mol % (Figure 7.10). Beyond this point, SV4 with 3.5 mol% V_2O_5 shows a very high sulphate capacity ~ 2 mol%

Sample ID	Al_2O_3	B_2O_3	CaO	Fe_2O_3	Li_2O	Na_2O	SO_4^{2-}	SiO_2	ZrO_2	V_2O_5
SV 1	4.209	4.640	7.890	6.231	10.080	12.951	1.243	51.449	0.448	0.857
SV 2	3.808	4.546	6.829	5.745	9.947	12.550	1.395	53.111	0.454	1.616
SV 3	3.904	4.206	7.038	5.371	9.397	12.325	1.498	53.529	0.398	2.336
SV 4	3.932	4.187	7.573	5.957	10.143	12.279	1.893	50.099	0.452	3.486

Table 7.6: XRF-ICP analysis (mol%) of V_2O_5 doped borosilicate glasses

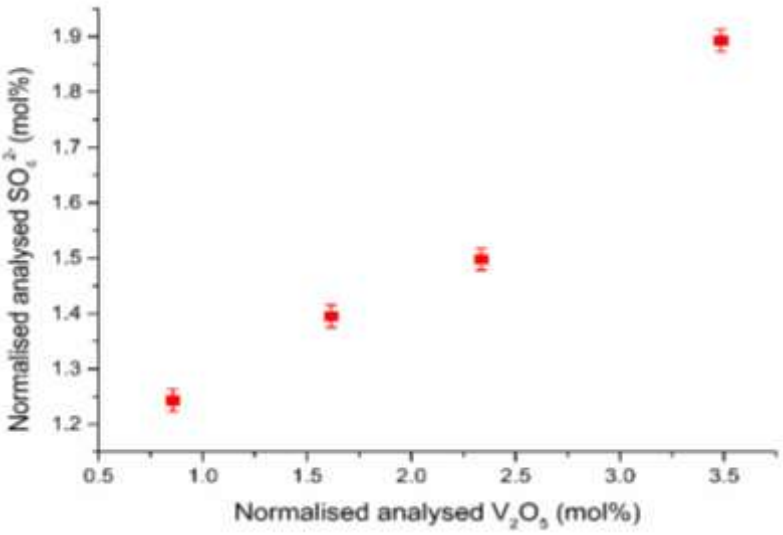

Figure 7.10: Sulphate capacity of vanadium doped borosilicate glasses plotted as a function of the V_2O_5 content present in the glass

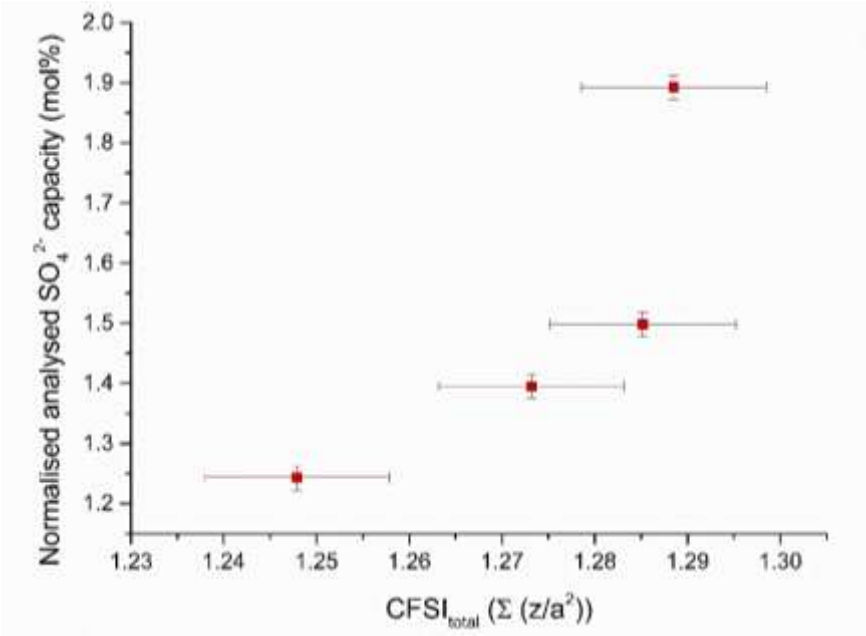

Figure 7.11: Sulphate capacity of vanadium doped borosilicate glasses plotted as a function of total cation field strength index

The total cation field strength index is calculated for the samples and plotted against the sulphate capacity. Contrary to the predicted behaviour where with increase in the concentration of modifier cations with high cation field strength index, a decrease in sulphate capacity was observed for silicate and borosilicate glasses studied by the

author, a positive correlation is observed between the two parameters (Figure 7.11). V^{5+} has a very high CFS due to its pentavalent charge and ionic radius.

The observed increase in SO_4^{2-} solubility confirms the deviation from the behaviour predicted by the $\Sigma(z/a^2)$ model (Bingham et al. 2017; J.D. Vienna et al. 2014). It is suggested to investigate the structural / chemical origins of this behaviour, which indicates SO_4^{2-}—V^{5+} interactions in the glass matrix (contrary to the predictions of (McKeown et al. 2002)). The Raman spectra of the glasses presented in Figure 7.12 confirm the prediction, as a S-O stretching band at ~1000cm^{-1} is visible in the four glasses which identifies with the S-O stretching mode in a corresponding crystalline $VOSO_4$. x H_2O compound.

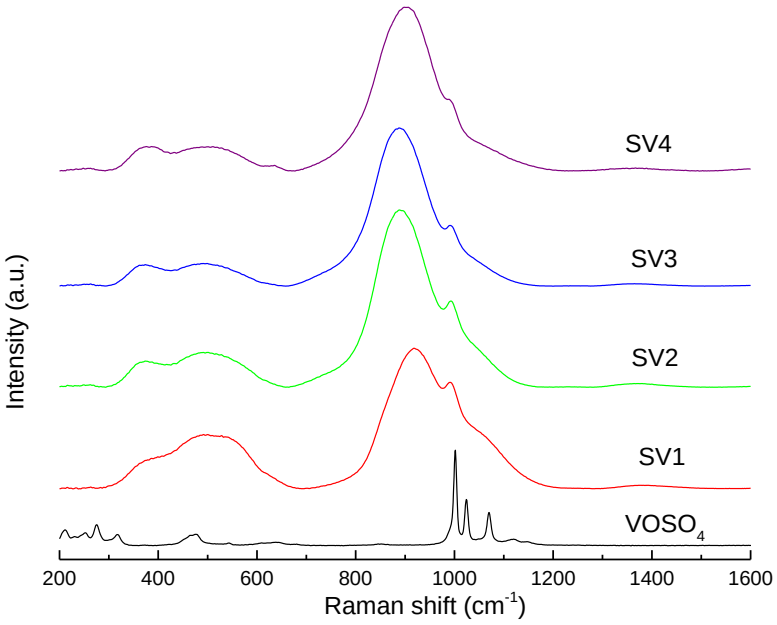

Figure 7.12: Raman spectra of the vanadium and sulphate doped borosilicate glasses and a corresponding crystalline $VOSO_4$

The sample SV4 with highest concentration of V_2O_5 ~ 3.5 mol%, contains a higher SO_4^{2-} content than suggested by the approximately linear patterns produced by the other samples, and may suggest that some form of structural change or possibly phase

separation may have taken place. The XRD patterns, however show clear amorphous humps for SV1, SV2 and SV4 except for SV3 where tiny peaks corresponding to undissolved Fe_2O_3 are present. (Figure 7.13).

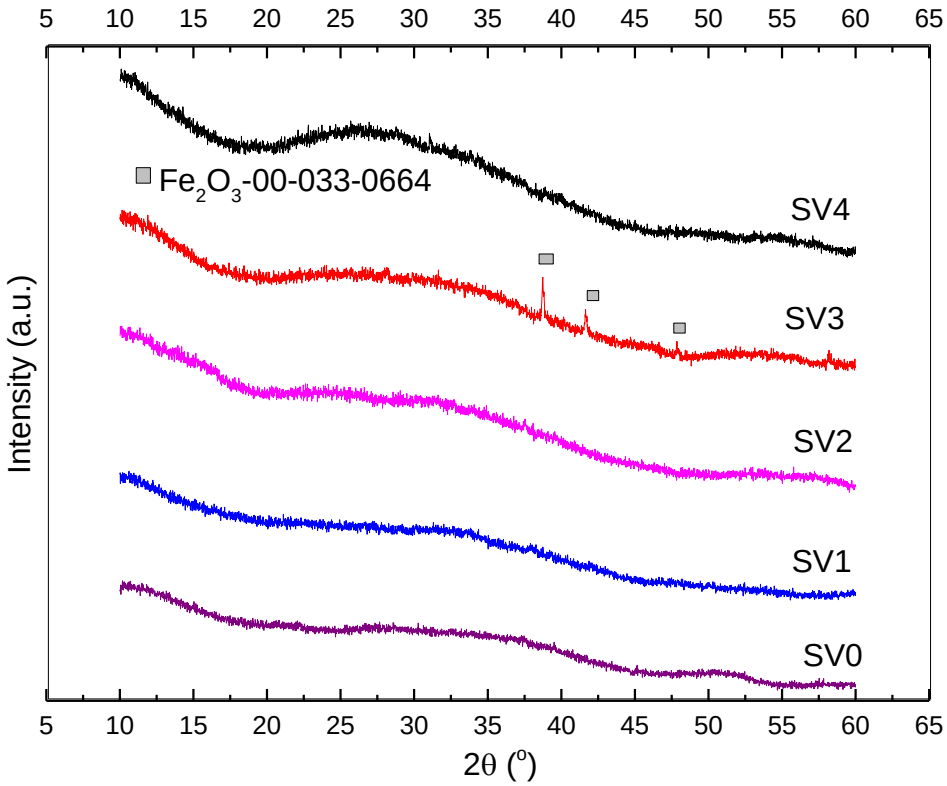

Figure 7.13: XRD patterns obtained for V_2O_5 containing sulphate doped simulated LAW waste glasses

XRD of the salt layer of the base glass, A3B3+S (0 mol% V_2O_5), and SV1 (0.86 mol % V_2O_5 analysed) produces diffraction patterns which are closely similar, indicating that no significant vanadium migration into the salt layer took place. The presence of $LiNaSO_4$ and $(Na_{0.8}Ca_{0.1})_2SO_4$ is confirmed with phase identification, indicating that the makeup of the salt layer is not simply based on raw materials used to supply the sulphate (Na_2SO_4 in all these cases), but that it contains other constituents such as Li and small amounts of Ca. Further work on characterisation of the salt layer composition and phases may shed additional light on the mechanism of solubilisation of sulphate.

CHAPTER 8

CHLORIDE DOPED SILICATE GLASSES

Chloride was the other process additive studied besides sulphate during this project. Similarly to sulphate, chloride has limited solubility and retention within borosilicate waste glass matrices (McKeown et al. 2011; Ilyukhina et al. 2010; Metcalfe & Donald 2004; Marra et al. 1994). In this chapter, the compositional and structural changes on moving from a chloride free silicate glass to the chloride containing equivalent, were analysed using density measurements; XRF; XRD; Raman Spectroscopy; ^{29}Si,^{23}Na, MAS NMR. Neutron diffraction measurements were also carried out but have not been reported in the thesis (the measurements are due for analysis).

The barium containing alkali borosilicate glasses which showed significant sulphate retention, were also compositionally and structurally analysed to investigate their chloride retainability potential. The focus was to look at the structural changes if occur, with addition of chlorine. The effect of addition of the halide on properties such as T_g and viscosity have not been covered in our work.

8.1 Silicate Glasses Doped with Chloride

8.2.1 Glass Preparation

Five sets of glasses were prepared for the silicate glass series. Each set contained one Cl-free 'undoped' base glass and a corresponding Cl 'doped' equivalent. The targeted doping was ~2-5 mol % Cl. The base glasses comprised two binary systems: R_2O –SiO_2 (R = K, Na, Cs) and two ternary systems: Na_2O – MO – SiO_2 (M = Ca, Ba). Analytical grade carbonates Na_2CO_3, K_2CO_3, $BaCO_3$, $CaCO_3$ ~ purity > 99.9% and high purity sand (99.99% purity) were used for glass batch preparation. Chlorine was introduced in the batch as NaCl in Na-based systems KCl in the K_2O-SiO_2 glass and CsCl in Cs_2O-SiO_2. Batch compositions were prepared for 100 g of glass on a calibrated balance with a precision of ± 0.001 g; mixed thoroughly, and melted in a reinforced high alumina crucible partially covered with an alumina lid in order to minimize volatilisation losses of Na and Cl. The crucibles filled with glass batch were ramped in an electric furnace under oxidising atmosphere, to the target temperature of 1330^{o}C at a rate of 3 ^{o}C / min and dwelled for 3 hours before the melt was poured on a stainless-steel plate in a stainless-steel mould. During pouring of NaSi-15Cl, white fumes were seen issuing from the crucible with an odour of bleach-like smell. A thin layer of salt deposited on the surface of NaSi-15Cl upon cooling. The cooled glasses were immediately transferred to a vacuum desiccator to avoid hydration of the glass. Despite providing a vacuumed environment in order to abstain any contact of the final glasses with atmosphere, the high alkali R_2O –SiO_2 (R = K, Cs) hydrated vigorously at the time of density measurements and spectroscopic analysis. Therefore, these two glass sets were not analysed any further and have not been reported in the thesis. Simultaneously, data from only Na based systems has been presented in Table 8.1.

8.2.2. XRF -ICP Analysis

Table 8.1. An "Oxide" program was used to detect the modifiers and silicate as oxides under XRF analysis. The chloride content was not analysed using XRF as Cl atom emits only a 2.7 keV X-ray. This low an energy X-ray is not able to escape the sample unless very near to the surface and Cl is present in considerable amounts. Samples were measured using acid titration ICP to determine the chloride content.

Sample	SiO_2 (mol%)	Na_2O (mol%)	CaO (mol%)	BaO (mol%)	Al_2O_3 (mol%)	2(NaCl) (mol%)	Melt Temp (^oC)
NaSi	54.00 (54.31)	46.00 (45.69)	0	0	0 (0)	0	1330
NaSi-10Cl	54.00 (56.01)	36.00 (40.94)	0	0	0 (1.08)	10.00 Cl^- (1.97)	1350
NaSi-15Cl	54.00 (50.16)	31.00 (41.68)	0	0	0 (1.20)	15.00 Cl^- (6.95)	1350
NaCaSi	57.50 (57.92)	21.25 (20.77)	21.25 (21.31)	0	0 (0)	0	1330
NaCaSiCl	57.50 (55.73)	17.35 (19.21)	21.25 (21.30)	0	0 (1.73)	4.00 Cl^-(2.04)	1330
NaBaSi	57.50 (59.62)	21.25 (23.40)	0	21.25 (16.98)	0 (0)	0	1330
NaBaSiCl	57.50 (59.05)	14.25 (17.76)	0	21.25 (18.86)	0 (1.04)	7.00 Cl^- (3.30)	1330

Table 8.1 : Nominal and analysed (in brackets) compositions from XRF-ICP analysis of the binary and ternary silicate glasses and their chloride doped equivalents.

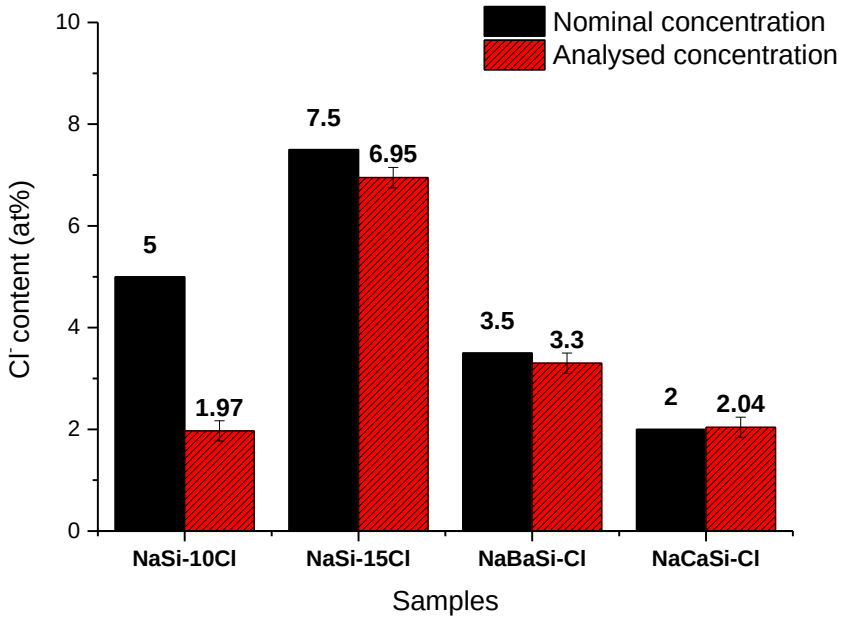

Figure 8.1: XRF-ICP compositional analysis of the chloride doped silicate glasses.

Figure 8.1 shows the analysed Cl content (at%) for the four chloride doped glasses. The analysed values for the chloride doped glasses shows the presence of 1-2 mol% of Al_2O_3 in the final melt. The presence of the Al_2O_3 is due to slight dissolution of Al_2O_3 from the high alumina crucibles that were used for the doped glass preparation. Of the four compositions studied, the ternary compositions NaCaSi-15Cl and NaBaSi-Cl glasses retained >99% chloride added to the glass batch originally. Of the binary sodium silicate glasses, NaSi-15Cl glass incurred a chloride loss of <10% of the initial amount of NaCl added to the batch. In the case of the binary NaSi-10Cl sodium silicate glass, > 55% of chloride was lost during melting of sample. No clear interpretation or trend could be observed from the compositional analysis results. The uncertainty and errors associated with analysis of Cl content using ICP and rest elemental analysis using XRF may be one contributing factor, however, they are unlikely to fully explain this unusual behaviour and further work is needed to more fully elucidate this behaviour.

The XRF analyses indicate that the sodium barium silicate and sodium calcium silicate glasses act as good hosts to retain the chloride added. NaSi-15Cl dissolved a large amount of chloride, however, the poor chemical durability of sodium silicate glasses strongly limits the practical applicability of these glasses. There is a possibility that replacement of Na_2O by BaO/CaO is the reason behind greater chlorine retention as it was suggested by (Webster & De Vivo 2002) that the presence of divalent alkaline earth cations such as Mg^{2+} and Ca^{2+} in the glass network improve chloride solubility. Those authors could not investigate the effect of larger alkaline earth ions such as Ba^{2+} or Sr^{2+} due to limited composition range of the natural aluminosilicate glasses which were being studied. The enhancement of solubility of chloride with CaO addition has been investigated by several researchers (Sandland et al. 2004; Siwadamrongpong et al. 2004; Schofield 2011; Chen et al. 2017; Forto Chungong et al. 2017) and in most of those studies 70-90% of the chloride added to the batch was retained in the final glass samples. However, it is suggested that several more sodium calcium silicate compositions should be prepared with varying Na_2O/CaO and Cl/CaO ratios and compositionally analysed in order to confirm this suggestion.

8.2.2 Density Measurements

The density measurements reported for the chloride doped glasses are the average of five measurements taken per sample. One of the limitations of the density measurements was that these were calculated using the Archimedes principle using distilled water as measuring medium. Since the high alkali sodium silicate glasses hydrate immediately after coming into contact with water in the atmosphere, this led to larger error bars for the density values obtained for these glasses.

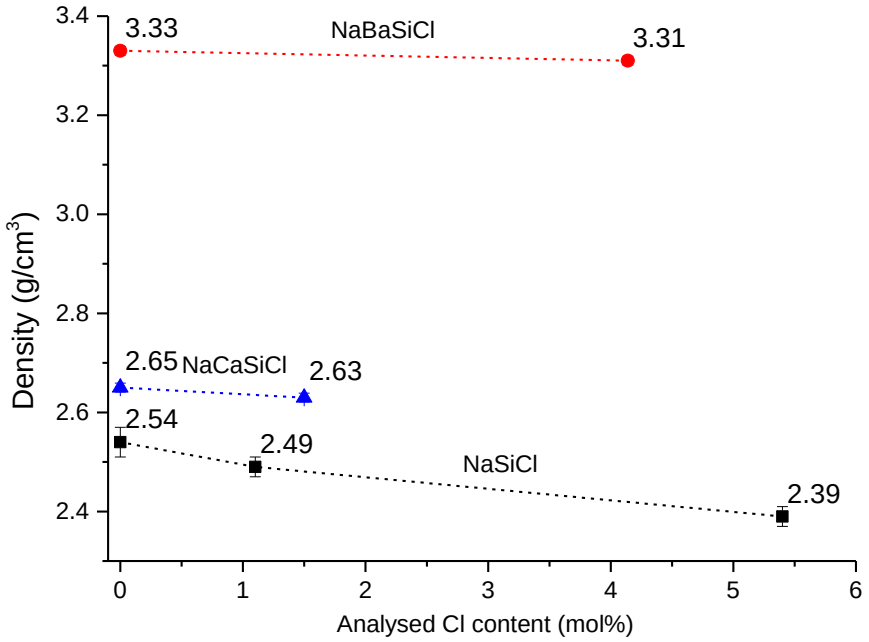

Figure 8.2: Density values of the undoped and chloride doped binary and ternary silicate glasses.

Figure 8.2 clearly shows a systematic decrease in density of the glasses with increasing chloride content. Similar trends of reduced density with chloride content have been reported by (Schofield 2011; Chen et al. 2017; Forto Chungong et al. 2017) for calcium aluminosilicate and calcium silicate glasses. This behaviour is likely due to the incorporation of larger chloride ions which result in an expansion of the glass volume, thus, decreasing the density.

8.2.3 XRD Results and Discussion

Figure 8.3 presents the XRD patterns and identified crystalline phases, of the seven undoped and chloride doped glasses studied.

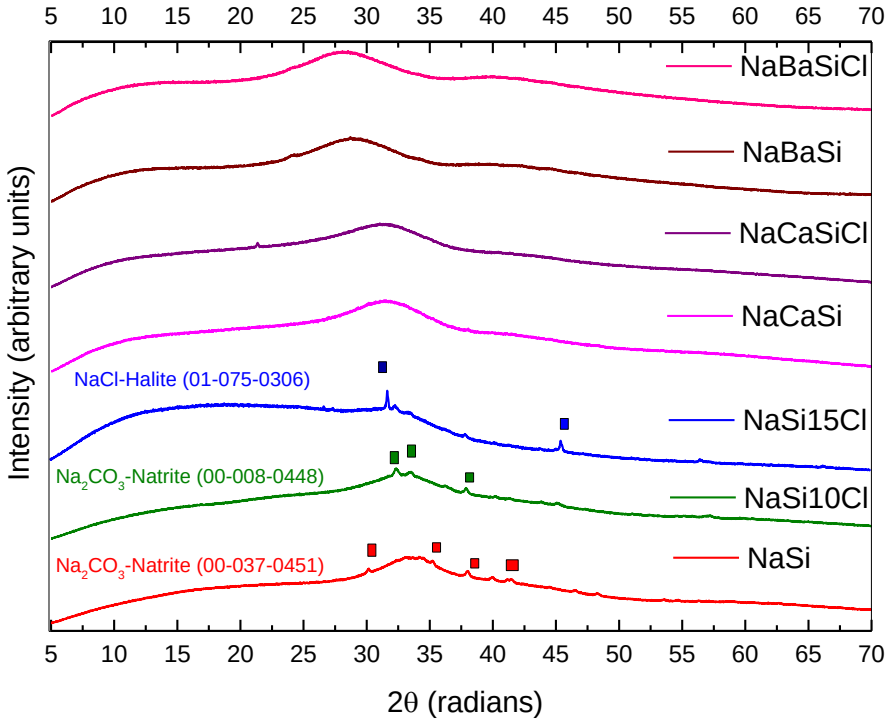

Figure 8.3: XRD patterns for the undoped and chloride doped alkali / alkali-alkaline earth silicate glasses.

As expected, on the basis of the corresponding sulphate-doped sodium silicate glasses (Section 5.2.5), due to the limited chemical durability of sodium silicate glasses, small peaks are visible in the diffraction patterns for NaSi-0Cl, NaSi-10Cl and NaSi-15Cl glasses, which correspond to Na_2CO_3 that formed on the surface of the glasses upon contact with atmospheric CO_2. For the NaSi-15Cl glass, besides Na_2CO_3, diffraction peaks occur which correspond to undissolved chloride in the form of NaCl (halite; ref no.: 01-075-0306), indicating that the solubility limit of Cl in the glass was exceeded under the preparation conditions studied. XRD of the remaining four ternary glasses show a clear broad amorphous hump confirming the glassy nature of the samples

prepared. A clear shift in the hump peak position towards lower 2θ values can be seen as we move from a NaSi to NaCaSi to NaBaSi systems. This shift can be attributed to increasing average d-spacing between atoms due to the introduction of larger Ca^{2+} and Ba^{2+} cations, which results in overall volume expansion.

8.2.4 Raman Spectroscopy

Before analysing the Raman spectra of the glasses made for the chloride doping studies, it was important to investigate the Raman spectra of the corresponding crystalline chloride compounds. Raman spectroscopy was carried out on a range of alkali and alkaline earth chloride compounds and the spectra are presented in Figure 8.4.

Unlike the corresponding crystalline sulphates, for which very strong, sharp bands appeared at Raman shifts in the range 400-1100cm^{-1} (details available in section 5.3.1) representing the bending and stretching modes of O-S-O bonds, multiple broad and less intense peaks are visible in the chloride spectra, mostly occurring between 300-600 cm^{-1}. Due to limited literature being available concerning Raman studies of chloride compounds (Raptis 1986; Nyquist & Kagel 2012), it is difficult to unambiguously assign these broad peaks to a specific breathing / bending or stretching mode, or to specific bonds. The low frequency region of Raman spectra of oxide glasses is complex due to contributions from various O-Si-O breathing and bending modes. Therefore, it was not considered feasible to deconvolute the low frequency region of the Raman spectra for the chloride doped glasses to separate peaks due to chlorine addition from those due to Si-O network.

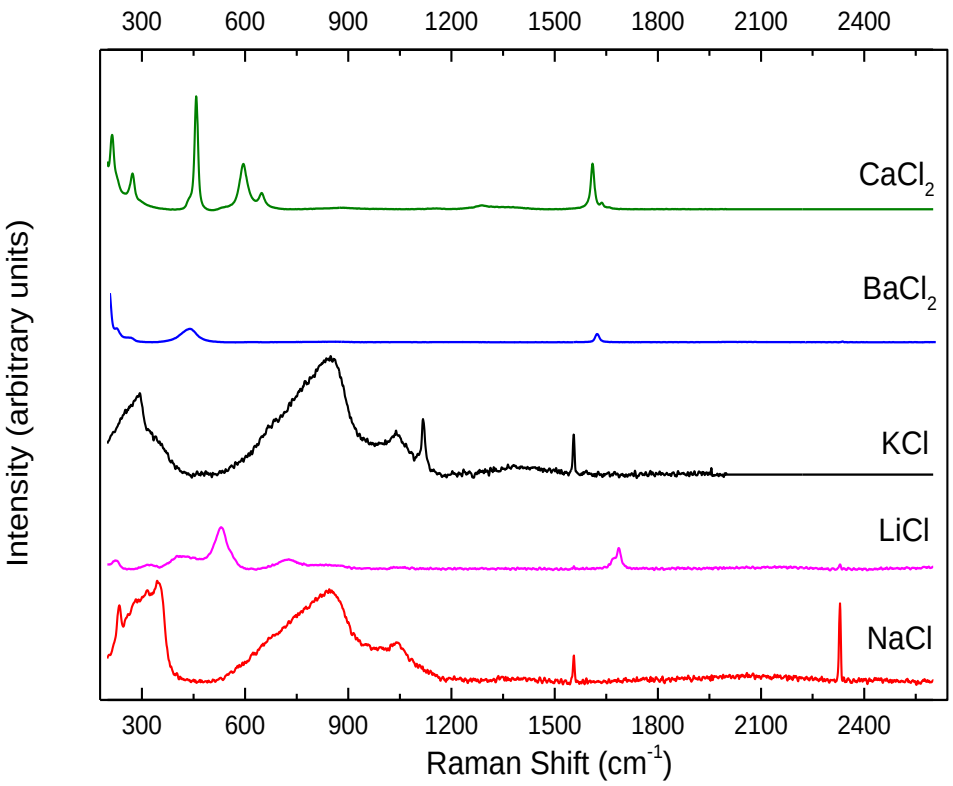

Figure 8.4: Raman spectra of alkali-alkaline earth chloride crystalline salts.

Figures 8.5, 8.6 and 8.7 present the Raman spectra of the undoped and chloride doped glasses. No significant differences are visible in the low frequency region (300-600 cm^{-1}). The intensity of the band corresponding to Q^2 silicate units between 900- 980 cm^{-1}, decreases and that corresponding to Q^3 silicate units between 1000-1100 cm^{-1} increases with chloride addition. The assignments of the bands to Q^2 and Q^3 units have been made in accordance with the literature available for Raman spectroscopy studies of binary and ternary silicate glasses (Steven A Brawer & White 1975; McMillan 1984; Mysen & Frantz 1994; Fukumi et al. 1990).

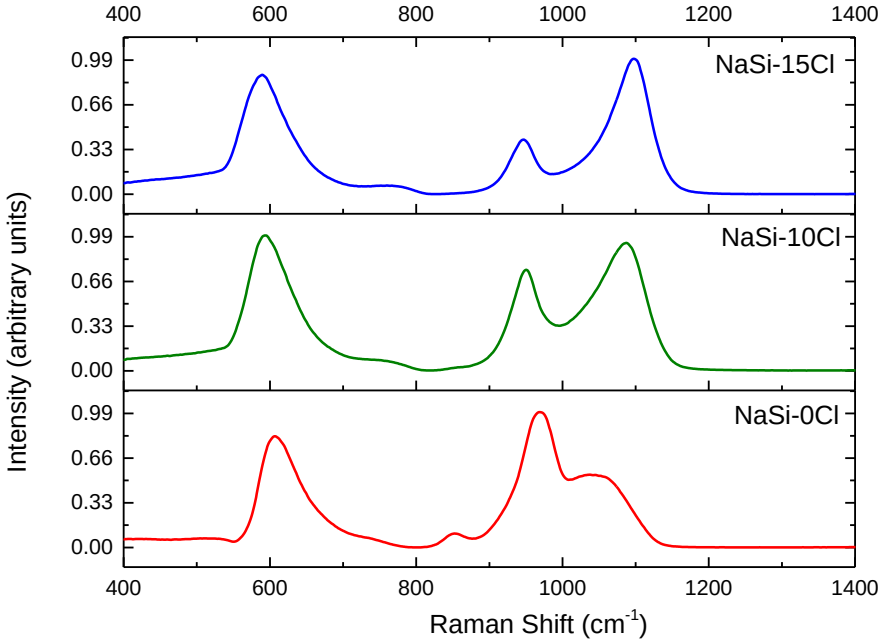

Figure 8.5: Raman spectra of undoped and chloride doped Na_2O-SiO_2 glasses

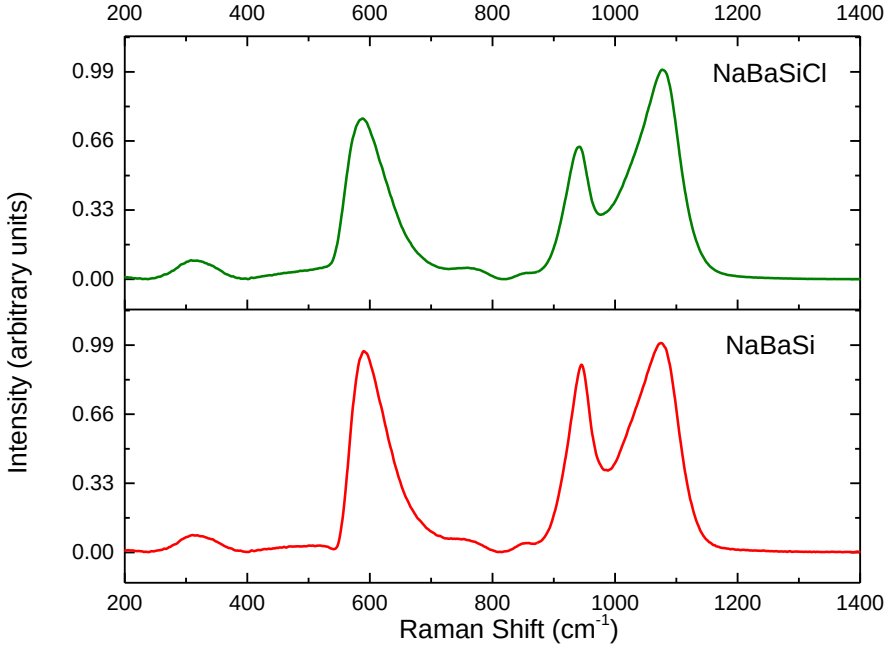

Figure 8.6: Raman Spectrum of undoped and chloride doped Na_2O-BaO-SiO_2 glass

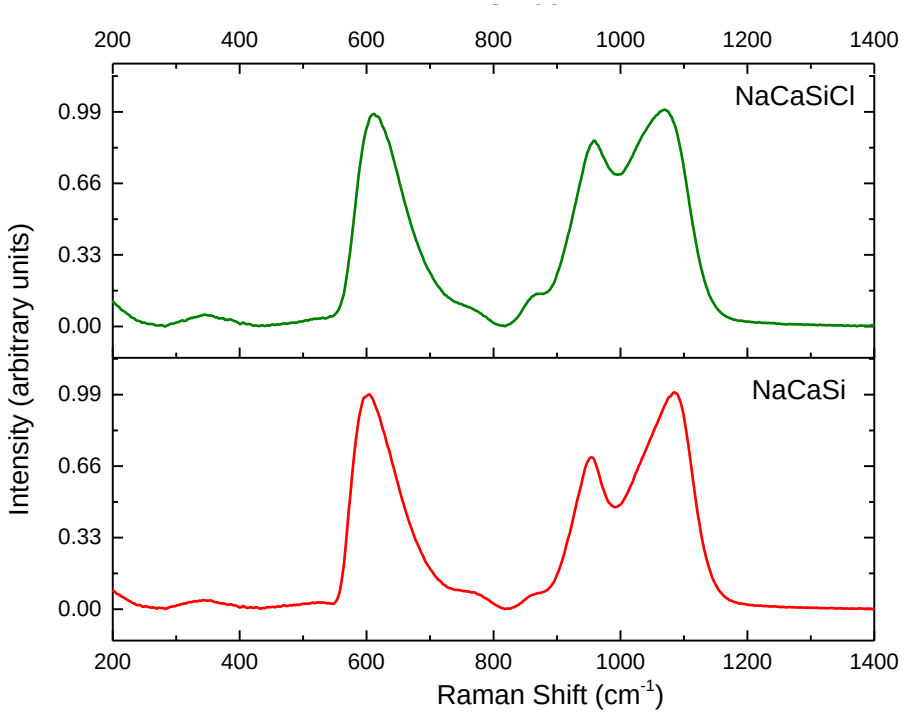

Figure 8.7: Raman Spectrum of undoped and chloride doped Na_2O-CaO-SiO_2 glass

These results indicate that, similarly to the sulphate-doped glasses studied here (Section 5.3.1), the incorporation of chloride has a polymerising effect on the silicate network. In the case of the Na_2O-SiO_2 glasses studied, it may be surmised that Cl^- anions bond with the Na^+ ions and hence, fewer Na^+ ions are available in the chloride-doped glasses to provide NBO's by breaking up the Si-O network to form Q^2 units. Again, this behaviour is consistent with that observed earlier for the incorporation of sulphate in sodium silicate glasses.

The ^{29}Si MAS-NMR measurements carried out for the chloride-doped glasses (Figure 8.8) are consistent with the observations from the Raman studies and show the same structural trends upon incorporation of chloride. In the 500-600 cm^{-1} low frequency range of the Raman spectra, no prominent changes are visible between the base glasses and those doped with chloride. As suggested by Chmel and Svetlov (1996), a prominent Raman band corresponding to the Si-Cl stretching mode should emerge at ~540 cm^{-1} in

silicate glasses if direct bonding interactions occur between the halide ion with the network forming cation. This band is absent from our spectra, therefore our results suggest the absence of any Si-Cl bonds, and this conclusion is in agreement with a number of previous studies (Sandaland et al. 2002; McKeown et al. 2011, Evans et. al 2008, Chungdong et. al 2017) which report that Cl most likely associates itself with the NWM in the glasses. However, it is difficult to predict the preferred bonding sequence for the chloride ions in the ternary silicate glasses where both Na^{+} and Ca^{2+}/ Ba^{2+} are present simultaneously and further work is required in this regard.

8.2.5 NMR Results and Discussion

The observed ^{29}Si spectra were acquired at a frequency of 79.438 MHz, spectral width of 40322.6 Hz, acquisition time of 12.7 ms, and repetitions in the range 56-800 with a recycling time of 120 s at ambient temperature. Direct excitation had a pulse duration of 4.6 ns with a two-pulse phase modulated decoupling spin rate of 6000 Hz with reference to tetra-methylsilane (0 ppm).

Figure 8.8 presents the ^{29}Si MAS-NMR spectra of the undoped and chloride – doped silicate glasses. It is interesting to note a change in the intensities of the broad Q^2 peak at ~ 80 ppm and of Q^3 peak at ~ -90 ppm. The increase in the intensity of the Q^3 peak with simultaneous decrease of Q^2 peak suggests polymerisation of silicate network with chloride doping. A particularly interesting aspect of the behaviour to be noted in the NMR spectra is the shift in the centre position of the broad Q^2 and Q^3 peaks towards more negative chemical shifts with increased chloride doping. These results differ from the ^{29}Si NMR patterns obtained by (Chungong et al. 2017) for their calcium silicate glasses, where they observed no significant differences in chemical shifts for Q^2 and Q^3

units between samples with increasing chloride content. Those authors suggested that this behaviour indicated independence of the Si units from any direct interaction with the Cl incorporated in the glass. However, in this study a clear shift is observed between undoped and chloride-doped glasses, suggesting the possibility of different structural origins or competition for bonding. It is not possible to further elucidate the origins of this behaviour without further detailed study therefore, it is suggested to carry out XANES and EXAFS to obtain deeper understanding of this behaviour.

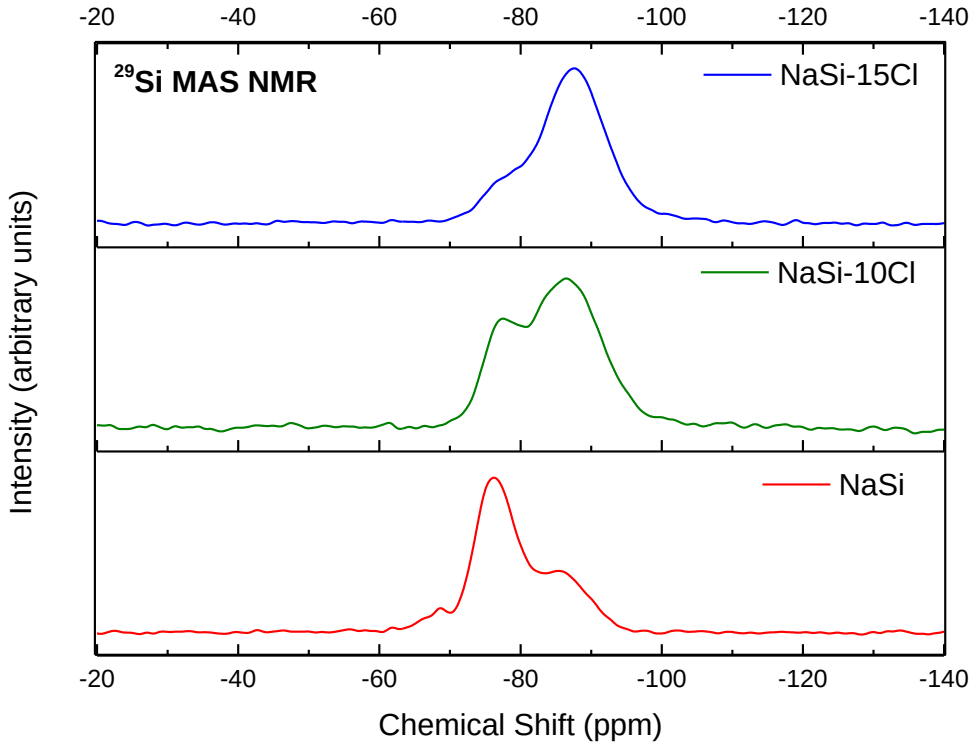

Figure 8.8: ^{29}Si MAS NMR spectra of undoped and chloride doped Na_2O-SiO_2 glasses

8.3 Chloride Doped Borosilicate Glasses

The three borosilicate glasses analysed with various spectroscopic techniques in Chapter 6: Na_2O-B_2O_3-SiO_2; Na_2O-BaO-B_2O_3-SiO_2; BaO-B_2O_3-SiO_2 to investigate the effect of addition of BaO on sulphate solubility in borosilicate glasses were also studied,

in order to understand their chloride retention capacities. The addition of BaO to a borosilicate glass, as already discussed in Chapter 3, was inspired by the work of the Waste Management Research Division, BARC, India where high sulphate solubilities ~ 3 mol% of SO_4^{2-} were achieved without any detectable phase separation. For the experiments conducted here, significant Cl^- retention (~ 4.3 at %) in Na_2O-BaO-SiO_2 glasses made it even more important to determine whether the addition of chloride to a BaO containing borosilicate glass would enable similarly high chloride solubilities.

8.3.1 Glass Preparation

Three sets of glasses were prepared for the borosilicate glass series. Each set contained one Cl-free 'undoped' base glass and a corresponding Cl 'doped' equivalent. The targeted doping was ~5 mol% of Cl, which was added in the form of NaCl. The base glasses comprised three glasses: Na_2O-B_2O_3-SiO_2; Na_2O-BaO-B_2O_3-SiO_2; BaO-B_2O_3-SiO_2. Analytical grade carbonates Na_2CO_3, $BaCO_3$ ~ purity > 99.9% and high purity sand (99.99% purity) were used for glass batch preparation. B_2O_3 used for the glass preparations was isotopically enriched (^{11}B: 99.67%). Chlorine was introduced in the Na_2O-B_2O_3-SiO_2 and Na_2O-BaO-B_2O_3-SiO_2 as NaCl; and as NH_4Cl in the batch for the BaO-B_2O_3-SiO_2 glass. NH_4Cl was chosen due to unavailability of $BaCl_2$ at the time of the experiment. The batches were prepared for 35 g of glass in a similar way as for chloride doped silicate glasses. Reinforced alumina crucibles with an alumina lid were used to melt the glass. These were placed in an electric furnace and heated at 3^{o}C / min to a temperature of 1150^{o}C and held for 2 hours. The melts were poured onto a stainless-steel plate in a stainless-steel mould, cooled, sealed in a polythene sample bag and

immediately transferred to a vacuum desiccator. The nominal and analysed compositions of the chloride doped borosilicate glasses are mentioned in Table 8.2.

8.3.2 XRF-ICP Analyses

The cooled glass melts were ground in the vibration mill to form powders and mixed with LiBr and heated until molten to form fused beads in an electric furnace operating at 1100^{o}C. The Boron and Chloride content were estimated using the ICP technique. The XRF analysis was carried out to measure the remaining elements as oxides. All three glasses showed excellent chloride retention. The maximum chloride loss of the three chloride doped glasses was incurred by sample NaBSiCl which was < 20% of the as-batched chloride content. The presence of Al_2O_3 was detected in the elemental analysis due to slight dissolution of the alumina from the reinforced alumina crucibles being used for glass preparation.

Sample	SiO_2 (mol%)	Na_2O (mol%)	B_2O_3 (mol%)	BaO (mol%)	Al_2O_3 (mol%)	(NaCl) (mol%)	Melt Temp (^{o}C)
NaBSiCl	38.00	38.00	19.00	0	0	5.00	1150
	(36.09)	(40.78)	(16.19)		(2.70)	Cl (4.23)	
NaBaBSiCl	38.00	19.00	19.00	19.00	0	5.00	1150
	(36.95)	(21.76)	(16.90)	(16.86)	(2.64)	Cl (4.89)	
BaBSiCl	38.00	0	19.00	38.00	0	5.00	1150
	(36.69	(0)	(16.95)	(36.74)	(4.35)	Cl (5.27)	

Table 8.2: Nominal and analysed (in brackets) compositions from XRF-ICP analysis of the three chloride doped borosilicate glasses.

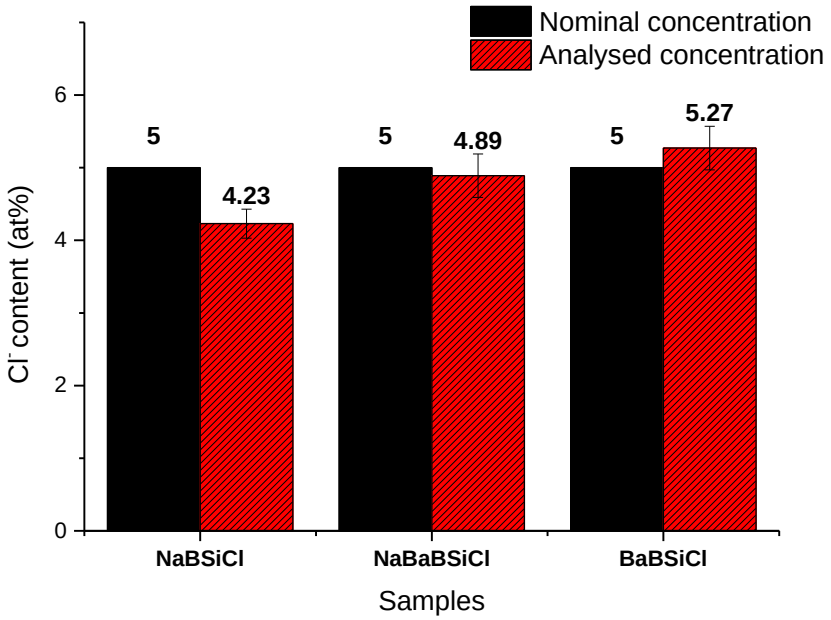

Figure 8.9: XRF analysis of the Cl^- retained by BaO containing borosilicate glasses.

As discussed in section 8.2.2., use of two different techniques to analyse the chloride boron and other oxide content has some limitations and inaccuracies. The uncertainty related to the technique in terms of accuracy and calibration gives rise to the errors shown. It is interesting to note that glass $BaO\text{-}B_2O_3\text{-}SiO_2$ showed excellent chloride retention. A trend is visible wherein the halide retention increases with increases in the content of BaO in the glass. (Siwadamrongpong et al. 2004) had suggested through their studies on CaO aluminosilicate glasses that with increases in CaO content, the glass becomes more depolymerised (which is intuitive and is consistent with the results of this study and established knowledge on glass structure). With increases in depolymerisation, more NBOs are created and lead to higher chloride retention. Although there is no evidence of similar behaviour shown by the glasses if BaO was present instead of CaO, it is hypothesised that the Ba^{2+} ions, which are larger than Ca^{2+}

ions, may cause a higher degree of depolymerisation in the glass network, which should, as per Siwadamrongpong and colleagues suggestion, show higher chloride retention.

The most interesting conclusion from the XRF analysis is that, to this date, and to the best of the author's knowledge, Cl^- solubility in borosilicate glasses has been reported to be < 1wt% (Donald et al. 2007; Metcalfe & Donald 2004; McKeown et al. 2011; Ilyukhina et al. 2010; Marra et al. 1994). Most of these researchers have not touched the issue of poor solubility of Cl^- in borosilicate glasses in detail and neither provided the composition of the glasses which were studied in order to reach this conclusion. The borosilicate waste glasses which were investigated for their Cl^- solubility by McKeown et al. (2011) using XANES, consisted mainly of CaO and Na_2O besides chlorine, B_2O_3 and SiO_2; Cl was introduced as $CaCl_2$ in those glasses. Therefore, whilst taking the errors arising due to the XRF analyses used here into account, the results still indicate that the chloride-retaining capacity of radioactive waste-type borosilicate glasses can be increased by introducing BaO into the glass.

8.3.3 Density measurements

The densities of the base glasses and chloride doped glasses were measured five times per sample and averaged. The error recorded was ±0.03 g/cm^3 for each glass. As expected, the densities of the doped glasses systematically decreased with chloride addition due to expansion in glass volume to accommodate larger Cl^- ions.

Sample	Density (g/cm^3)	Sample	Density (g/cm^3)
NaBSi	2.51	**NaBSiCl**	2.42
NaBaBSi	3.25	**NaBaBSiCl**	3.01
BaBSi	3.89	**BaBSiCl**	3.70

Table 8.3: Densities of the chloride free and chloride doped borosilicate glasses.

8.3.4 Raman Results and Discussion

Figures 8.10. 8.11 and 8.12 show the Raman spectra of the undoped and chloride doped borosilicate glass samples. Since all spectra exhibit contributions from vibrational modes of several bonds including B-O-B, Si-O-Si, B-O-Si, O-Si-O, O-B-O, these overlap strongly and create highly convoluted spectra. Therefore, deconvolution of the data is highly problematic, and it was decided not to pursue this as it would provide no useful additional information.

As shown in Figures 8.10 – 8.12, no significant changes are observed, upon chloride addition, in the high frequency range between 900-1600 cm^{-1}. Only the intensity of the Raman bands in the range 900-980 cm^{-1} and 1000-1100 cm^{-1}, attributed to Q^2 and Q^3 units, change as also observed for borosilicate glasses doped with sulphate (section 6.3.1). Where the addition of Cl^- to the glass has a polymerising effect on the NaBSi and NaBaBSi glasses, the network slightly depolymerises in the BaBSi glass, as demonstrated by the increase in intensity observed for the Q^2 band with a simultaneous decrease observed for Q^3 band. This behaviour demonstrates that both anions studied in this thesis (sulphate and chloride) have broadly similar effects on the structure of silicate and borosilicate glass networks.

The low Raman frequency range between 200-600cm^{-1} shows some differences upon addition of Cl, but these could not readily be investigated in detail due to mixed, overlapping contributions from breathing and bending modes of boron-oxygen and silicon-oxygen units (Manara et al. 2009; Yadav & Singh 2015; Konijnendijk & Stevels 1976). It is hard to elucidate from the Raman spectra of the chloride doped glasses if any Si-Cl bond formations are occurring as the 540 cm^{-1} position assigned to Si-Cl stretching mode, if present, has largely overlapping contributions from B-O-Si and Si-

O-Si breathing modes. No changes are observed in the Raman band corresponding to components arising from BO_3 units interacting with BO_4 units at ~1410 cm^{-1} and BO_3 units interacting with other BO_3 units at ~1480 cm^{-1} (Meera et al. 1990; Maniu et al. 1995; Manara et al. 2009) upon addition of chloride to the glass. Only the intensity of this band decreases upon moving from a $BaO\text{-}B_2O_3\text{-}SiO_2$ glass to its chloride doped equivalent suggesting decrease in the concentration of BO_3 units in the BaBSiCl glass. No literature, to the author's knowledge is present for Raman spectroscopy on any chloride doped borosilicate or a borate glass to study any B-Cl interactions. However, Raman studies done on crystalline boron trichloride suggested a B-Cl stretching band to appear at around 830 cm^{-1} (Clark & Mitchell 1972). The absence of a new band at this position in either of the three chloride doped glasses suggested absence of any direct B-Cl interactions.

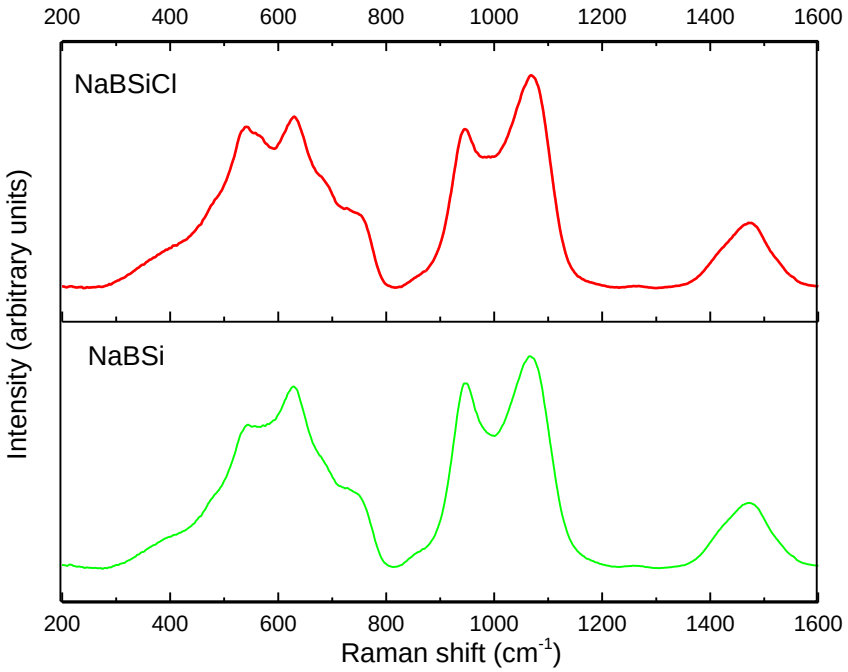

Figure 8.10: Raman spectra of the undoped and chloride doped $Na_2O\text{-}B_2O_3\text{-}SiO_2$

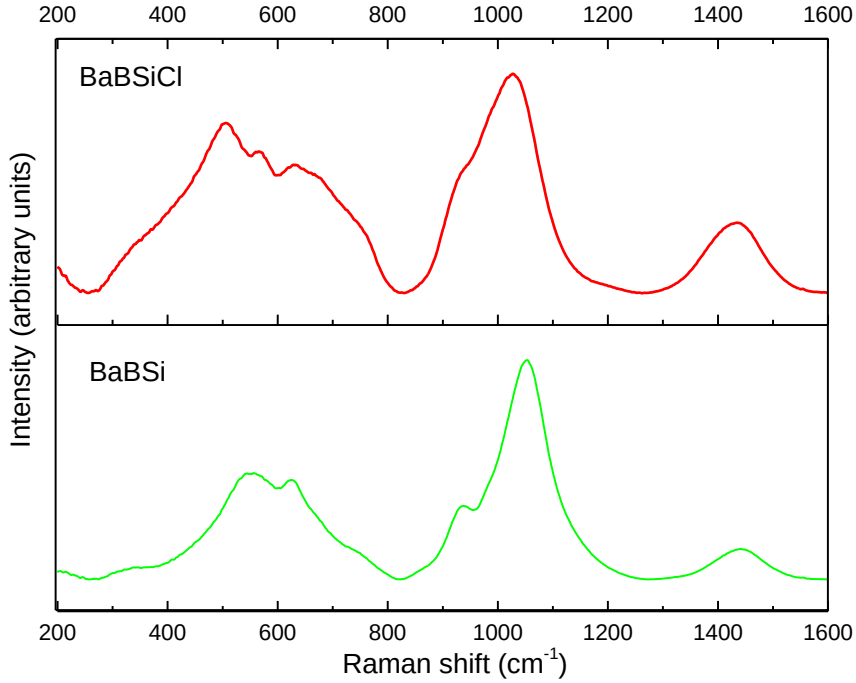

Figure 8.11: Raman spectra of the undoped and chloride doped $BaO-B_2O_3-SiO_2$

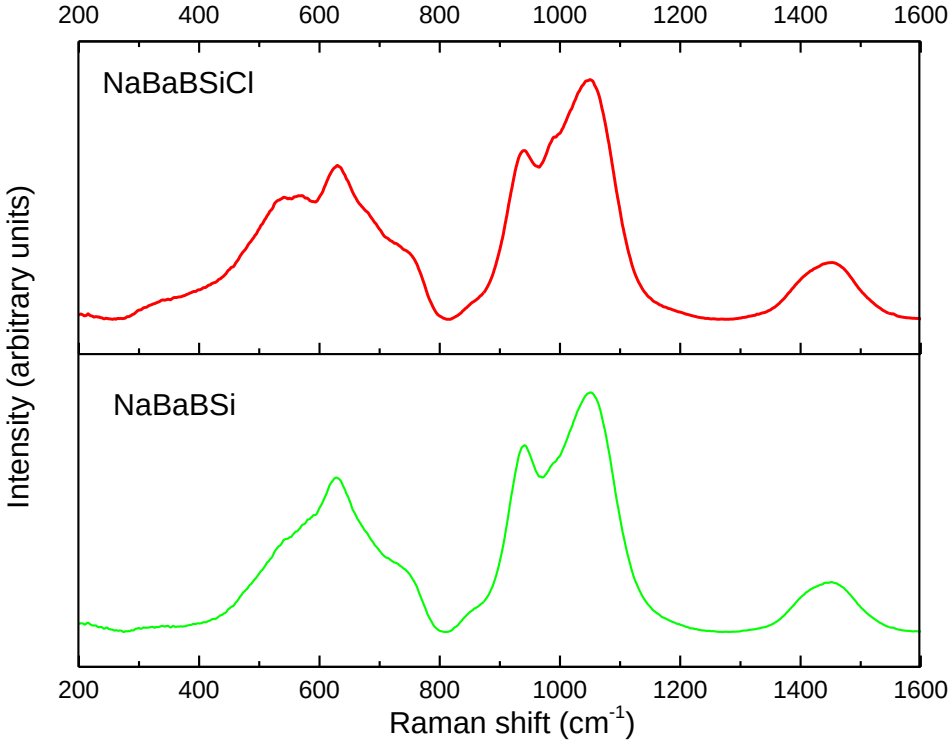

Figure 8.12: Raman spectra of the undoped and chloride doped $Na_2O-BaO-B_2O_3-SiO_2$

8.3.5 NMR Results and Discussion

^{29}Si MAS NMR spectra were obtained at 79.435 MHz and pulse duration of 4.5 µs. The acquisition time per scan was 20 ms and 500-600 scans were acquired for each sample. At spinning speed of 6 kHz, the sidebands were removed if the intensity was only up to 4-5%. The chemical shift for the silicate network lies in the range of -70--- 100 ppm with two major contributions due to Q^2 units (-70 to -80 ppm) and Q^3 units (-80 to -90 ppm).

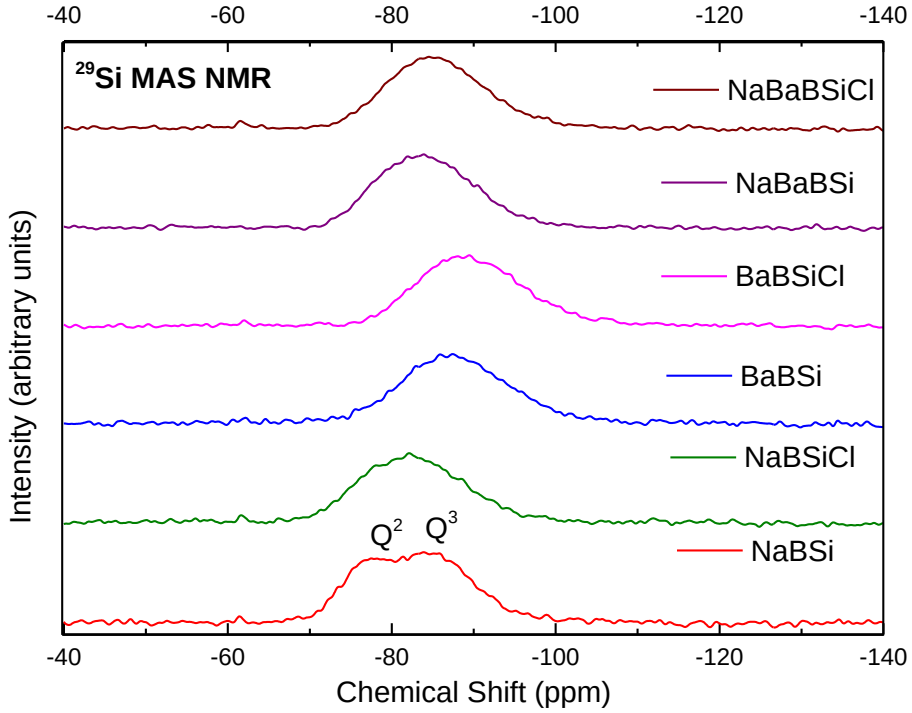

Figure 8.13: ^{29}Si NMR spectra for the undoped and chloride doped borosilicate glasses.

As shown in Figure 8.13, the chemical shift centroid position for the Q^n units (n= 2, 3) decreases with composition (NaBSi > NaBaBSi > BaBSi) suggesting changes in the average Si-O bond lengths. Along with the change in chemical shift centroid position with composition, the addition of Cl to the glass moves the chemical shift centroid position for the Q^n units towards more negative values. Similar behaviour was observed

for the silicate glasses doped with chloride (refer section 8.2.5). However, the NMR peaks for the glasses NaBaBSi and BaBSi between -80 and -100 ppm are so broad that resolving them into two components, corresponding to Q^2 and Q^3 units, is challenging. (Holland et al. 2007; Parkinson et al. 2008) analysed radioactive waste-type borosilicate glasses using ^{29}Si NMR data, and they predicted that the broad features occur due to mixed contributions from Q^3(Si); Q^3(B) and Q^3(Me) units where 'Me' corresponds to the modifier metal oxide present in the glass.

The ^{23}Na-MAS NMR spectra presented in Figure 8.14 were acquired using a single pulse sequence at a Larmor frequency of 105.78MHz (9.4 T) and pulse duration of 1.0 µs. The acquisition time per scan was around 10.0 ms and repetitions close to 600 per sample. As was observed for ^{23}Na-MAS NMR of Na_2O containing binary and ternary silicate and borosilicate glasses (see Sections 5.3.2 and 6.3.2), the NMR peak is broad and asymmetric, tailing towards more negative chemical shifts due to quadrupolar interactions. A small perturbation is visible at around 1-2 ppm for the ^{23}Na spectra of all four glasses but the reason behind its occurrence is not yet clear and further work is needed. The peak maximum for the NaBaBSi glass spectrum is higher than for the NaBSi spectrum, indicating an increase in the number of Na-NBO to Na-BO (Xue & Stebbins 1993). This could perhaps be explained by the large Ba^{2+} ions present in the NaBaBSi glass depolymerising the borosilicate network to a higher degree than Na^+ and thus create more NBO's than are present in the NaBSi glass. Based upon this data, it is difficult to assign the role of Na^+ as a modifier or charge compensator because in a borosilicate glass, Na^+ ions may either act as a charge compensator for the borate units or modify the silicate network or perform both roles simultaneously.

In the chemical shift range of -8 to +1.2 ppm, the peak maximum position of the symmetric part of the ^{23}Na MAS-NMR peak decreases by almost 4ppm in the

NaBaBSiCl sample spectrum; and changes very little (possible small increase of 0.5ppm) in the NaBSiCl sample spectrum, compared with their respective Cl-free base glasses. This suggests differences in Na-O bonding environments in both glasses (Charpentier et al. 2004; Angeli et al. 2011; Angeli et al. 2007; Lee & Stebbins 2003; Angeli et al. 2000; Gambuzzi et al. 2014; Gaudio et al. 2015; Maekawa et al. 1997) associated decreases in chemical shift of the ^{23}Na NMR symmetric peak with formation of longer Na-O bonds. If their suggestion is applied in the case of the results of this study, then it is shown that in the NaBaBSiCl glass, addition of chloride affects the bonding environment around Na^+ ions and may lead to formation of longer bonds, whereas in the NaBSiCl glass, the addition of chloride did not have significant effect on the sodium environment or bonding.

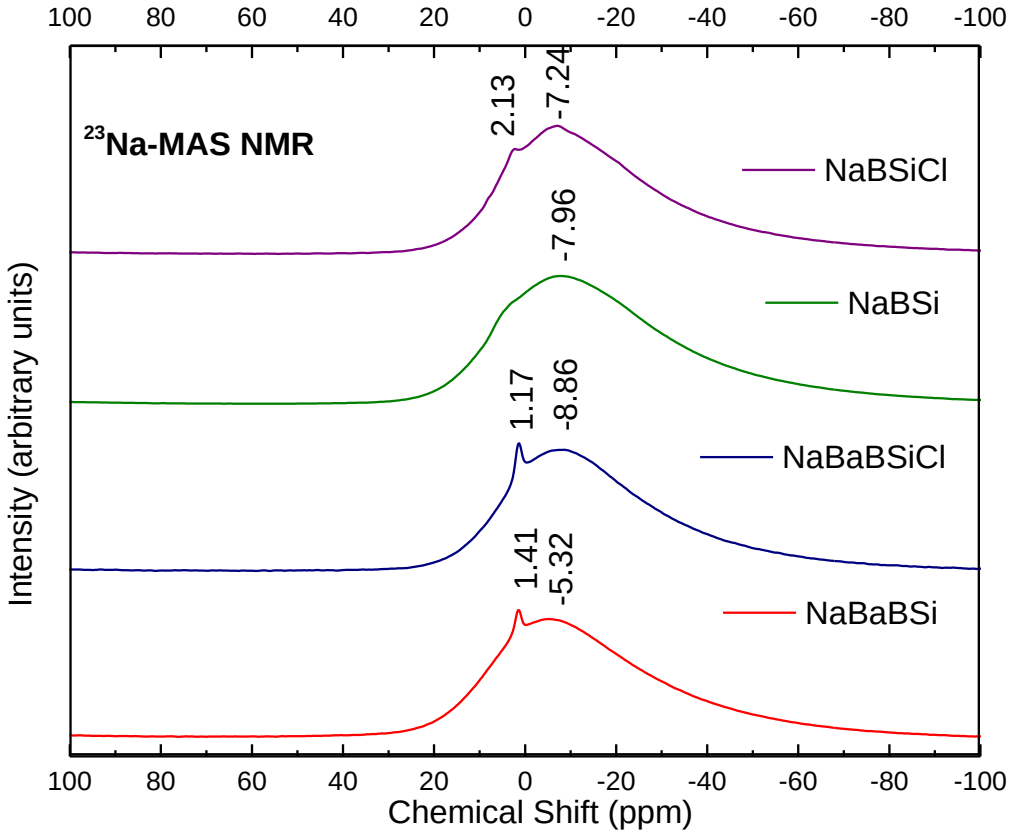

Figure 8.14: ^{23}Na NMR spectra for the undoped and chloride doped borosilicate glasses.

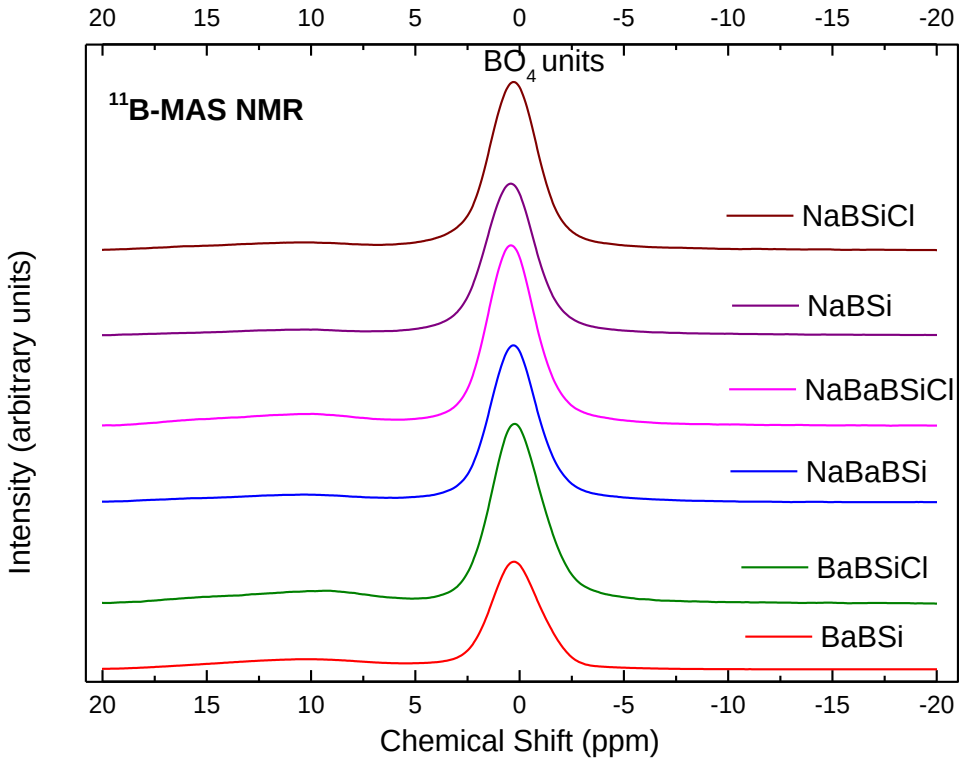

Figure 8.15: ^{11}B MAS NMR of the undoped and chloride doped borosilicate glasses.

The ^{11}B MAS NMR results obtained at a Larmor frequency of 192.4 MHz (14.1 T) are shown in Figure 8.15. A single hard 0.3 µs long pulse of RF frequency 200kHz was used to obtain each spectrum. Due to the high magnetic field, signals arising due to 3-fold coordinated BO_3 and 4-fold coordinated BO_4 are well resolved and are separated at 10 ppm and 0 ppm, respectively. The peaks corresponding to 3-fold coordinated BO_3 are weak due to their low concentration relative to BO_4 units. The relative percentages of BO_3 and BO_4 units extracted from the NMR data are presented in Table 8.3.

Sample	δ(B(IV) / ppm	% R.I. (B(IV))	% R.I. B(III)
NaBSi	0.38	98.1	1.9
NaBSiCl	0.24	95.7	4.3
NaBaBSi	0.28	94.5	5.5
NaBaBSiCl	0.38	91.9	8.1
BaBSi	0.20	84	16
BaBSiCl	0.21	90.7	9.3

Table 8.4: Relative intensities of BO_3 and BO_4 units and the centre peak position of chemical shift for 4-fold coordinated BO_4 of the chloride free and chloride doped borosilicate glasses.

As shown in Table 8.4, over 90% of all boron species present in these glasses exist as BO_4 units, with an exception of sample BaBSi, for which the BO_4 fraction is slightly lower, at 84%. It is also interesting to note that the relative intensity of BO_3 units increases by almost 3 % for samples NaBSiCl and NaBaBSiCl decreases by 6% for sample BaBSiCl, compared with their Cl-free base glasses. Two potential explanations are hypothesised:

1) With addition of chloride, and due to the formation of Na-Cl bonds, fewer Na^+ ions are available to charge-compensate 3-coordinated boron to form BO_4 units and therefore an increase in the fraction of BO_3 units occurs.
2) The large chloride ions incorporated in the glass network break B-O-B bonds and generate NBO's, resulting in more BO_3 units. However, it is difficult to analyse this behaviour using Raman spectroscopy as B-Cl bonds, if they exist, could not be resolved from the spectra.

Neutron diffraction provided no further insight into this issue, as B-Cl bonds are expected at ~1.7 Å in the T(*r*) spectrum of a chloride doped glass sample, based on

Shannon ionic radii. In cases such as the glasses studied here, containing low concentrations of Cl^- relative to their SiO_2 contents, any B-Cl correlations would overlap the much stronger correlations due to Si-O bonds at ~1.62 Å. In the case of sample BaBSiCl, it is possible that the large Ba^{2+} ions are compensating the charge for tetrahedral boron while at the same time stabilising Cl^- ions in the glass. To further investigate this situation, Ba XAS studies are required for these glasses.

8.4 Conclusions

This study was conducted in order to investigate the dependence of chlorine on glass composition and to investigate the structural changes which occur in the network of the amorphous matrix with introduction of chloride. Limited prior research work has concluded that borosilicate glasses are not suitable for incorporation of chloride containing wastes, but no through investigations have been conducted on radioactive waste-type borosilicate glasses in order to understand this behaviour more fully. There are various discrepancies in the published research available concerning the structural environment around chloride ions that are incorporated in oxide glass matrices. Where researchers (Chmel & Svetlov 1996; Kiprianov et al. 2004) have suggested that Cl^- ions interact directly with the network formers, the work of others (Sandland et al. 2004; Webster & De Vivo 2002; Chen et al. 2017; Forto Chungong et al. 2017; McKeown et al. 2011a) has predicted the presence of multiple Cl^- sites which are surrounded closely by NWM's present in the glass, and no direct associations of the chloride ion with network forming cations were recorded.

The chloride doped silicate glasses studied here demonstrated that whilst the NaSi-15Cl sample retained the maximum amount of chloride, the chloride solubility limit was

achieved which was visibly evidenced by the presence of a thin layer of molten salt (NaCl) on the surface of the molten glass. Additionally, for practical purposes, the binary alkali silicate glasses exhibit poor chemical durability.

On the other hand, the ternary glasses studied here, NaCaSiCl and NaBaSiCl, retained ~70% to ~100% of the chlorine initially added to the glass batch. It is believed that the presence of alkaline earth cations such as Ca^{2+} and Ba^{2+} have a positive influence on Cl^- retention. The retention capacity improves with introduction of larger ion such as Ba^{2+}, which depolymerises the network and may create larger voids more capable of incorporating large Cl^- ions. Though studies by Webster & De Vivo (2002); Chen et al. (2017); Forto Chungong et al. (2017); and McKeown et al. (2011) have shown that addition of Ca to a silicate/aluminosilicate glass improve chloride solubility, no literature was identified concerning the effects of BaO addition on chloride retention. The Raman and NMR studies on these glasses indicate the polymerising effect of chloride on the silicate glass network, similarly to the effects of sulphate doping in Chapter 5. This behaviour is again suggestive of NWM-Cl bond formations which lead to decreased availability of NWM ions to depolymerise the network.

Given the high chloride solubility shown by the NaBaSi glass, the author investigated the effect of BaO on chloride retention in borosilicate glasses, which are generally believed to have < 1 wt% chloride solubility. BaO containing borosilicate glasses have already shown their excellent ability to incorporate large amounts of SO_4^{2-} as shown by the work of Mishra et al. (2008) and in Chapter 6 of this thesis.

The XRF-ICP analysis shows that indeed BaO has an excellent effect on Cl^- retention and almost 100% of the chloride added to the glass batch was retained by the barium-containing glasses. It was shown that the Cl^- capacity improved with increasing

concentration of BaO in the glass. Almost 5 mole % of Cl^- was easily retained within the glass without any clear evidence of phase separation. This study has therefore demonstrated, for the first time, the high chloride capacities of barium-rich borosilicate glasses.

CHAPTER 9

KEY CONCLUSIONS AND FUTURE WORK

9.1 Sulphate studies

The overall aim of this study was to understand the factors behind sulphate solubility in the simple silicate glasses and more complex industrial HLW borosilicate waste glasses, the latter of which was difficult due to the complexity of the waste glass composition. In order to achieve the aim the authors developed sets of un-doped and sulphate doped simple binary, ternary and quaternary silicate and borosilicate glasses. The sulphate retained by the glasses was then analysed as a function of composition to evaluate the calibre of a particular alkali / alkaline earth oxide to enhance the sulphate solubility. The structural differences between the un-doped and sulphate doped samples were investigated in order to elucidate the effect of sulphate incorporation on the glass network in terms of degree of polymerisation, NBO/ BO ratios and change in the coordination environment of the cations in the glass. Structural studies also aided to find the local environment around the sulphate ions in the glasses.

Structural techniques such as MAS-NMR, Raman spectroscopy and Neutron diffraction aided the calculation of NBO/ BO ratio, first coordination shell bond distance between cations and neighbouring anions (O) and the coordination number. The information is

required to calculate cation field strength index of the glass and in measuring the degree of polymerisation of the melt. Sulphate solubility was plotted as a function of these two parameters which was useful in deducing the robustness and versatility of the empirical models suggested by Papadopoulos (1973) and Bingham & Hand (2008) to determine sulphate capacity of a glass melt.

The results obtained for binary and ternary sulphate doped silicate glasses were further useful in developing modified simulant HLW/ LAW U.S. glass compositions. The effect of the modified compositions on sulphate solubility was then investigated using composition analysis techniques such as XRF and ICP-OES.

The key conclusions from this study are as follows:

Among the binary and ternary silicate glasses, the author noted that Na_2O-SiO_2 retained the maximum amount of sulphate (~6.25 mol %) which reaffirmed the fact that Na_2O is a positive modifier to enhance the sulphate capacity of a melt. The next glass to have shown a considerable sulphate capacity (~4.5 mol%) was the Na_2O-BaO-SiO_2 glass where half of the molar content of Na_2O was replaced by BaO. This is suggestive of BaO being a positive modifier oxide to enhance sulphate capacity and can be justified as the large BaO ions affects the degree of silicate network depolymerisation significantly which possibly creates interstitial spaces to incorporate large sulphate anions . A binary Li_2O-SiO_2 glass developed in this series also showed considerable sulphate capacity (~4.25 mol %) which suggested that addition of Li_2O positively affects the sulphate retention within the glass. Amongst the four simple silicate glasses, the glass Na_2O-CaO-SiO_2 showed the minimum sulphate capacity of 2 mol % beyond which the glass reached its sulphate saturation limit.

Another interesting conclusion was made by comparing the Raman shift position of the υ_1 S-O stretching mode for the SO_3 doped glasses with that of corresponding crystalline alkali and alkaline earth sulphate compounds & fitting the S-O correlation in the ND spectra for sulphate doped glasses. Sulphur existed only as S^{6+} in these glasses in the form of SO_4^{2-} anions with an average S-O CN close to 4. The sulphate anion sites are closely associated with the modifier cations present in its first coordination shell. No evidence of direct S-Si bond formations was observed in the Raman and neutron diffraction spectra of SO_3 doped glass. Electrostatic Bond Strength (EBS) of a S-O bond is 6/4= 1.5. Likewise, the EBS in a SiO_4 tetreahedron is 4/4=1.0. The EBS sum for the bonds to an O atom should be 2. If an oxygen were bonded to both Si and S in a Si-O-S bridge, the EBS sum would be 2.5 and not 2. Thus, we can say that an oxygen atom cannot bond to both Si and S together.

The comparison of the υ_1 S-O stretching modes for the SO_3 doped ternary silicate glasses Na_2O-CaO-SiO_2-SO_3 and Na_2O-BaO-SiO_2-SO_3 and crystalline Na_2SO_4, $BaSO_4$ and $CaSO_4$ shows that the sulphate ions are stabilised either entirely or partially by the Ba^{2+} ions in glass Na_2O-BaO-SiO_2-SO_3 whereas in Na_2O-CaO-SiO_2-SO_3. mostly Na^+ ions act as charge compensators for the anions. The influence of the alkaline earth modifier cation on sulphate solubility, however, has not been fully understood. Figure 9.1 shows the sketch of possible sulphate bonding environment within the glass where the sulphate units are surrounded by NaO_5 units forming S-O-Na-O-Si linkages.

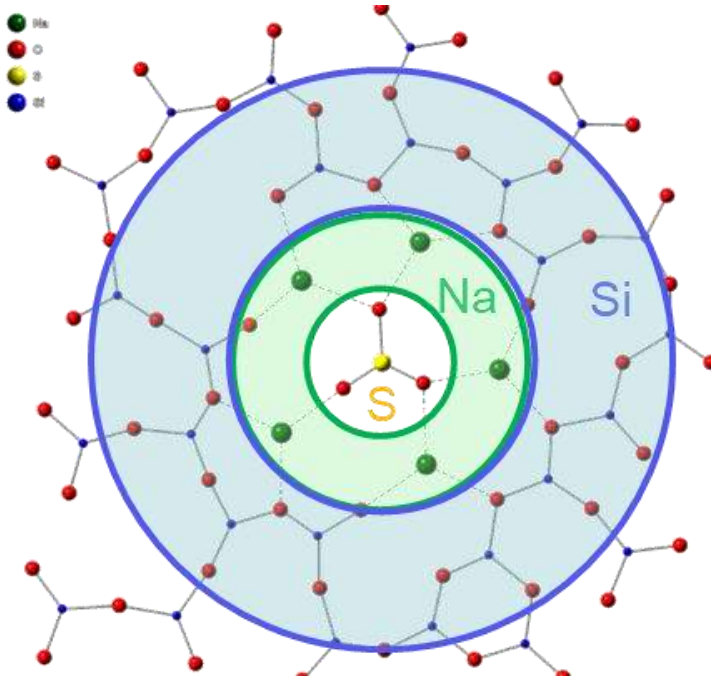

Figure 9.1: A sketch of possible bonding environment surrounding the sulphate anion in a sodium silicate glass.

Effect of BaO and Li_2O on sulphate retention: As seen for the silicate glasses, addition of BaO positively enhanced the sulphate capacity. In the borosilicate glass series however, the sulphate capacity was remarkable ~ 5mol% only for Na_2O- B_2O_3-SiO_2 and Na_2O-BaO-B_2O_3- SiO_2 . In the glass containing only BaO as a modifier, i.e. BaO-B_2O_3-SiO_2, sulphate capacity dropped to < 3 mol%. This suggested that BaO effectively enhanced sulphate solubility only in the presence of an alkali modifier oxide such as Na_2O. On its own, BaO does not effectively increase sulphate solubility.

For the simulated HLW glass compositions, it was observed that substitution of half molar content of the Na_2O with Li_2O positively impacts the sulphate solubility (~1.86 wt%). However, a reverse effect is seen on substitution of half molar concentration of CaO with BaO. These results suggest that where BaO shows a tremendous effect on increasing sulphate capacity in simple ternary silicate and quarternary borosilicate

glasses by sharing the role as charge compensators for SO_4^{2-} anions with Na^+ modifying cations, a similar behaviour does not occur upon increasing the BaO content in simulant waste glasses. The authors observed that addition of V_2O_5 to the waste glass could enhance the sulphate solubility up to ~ 2 wt%

These studies suggest that the industrially used HLW glass compositions by the U.S. to incorporate HLW with high sulphate content, can be modified with incorporating higher concentration of Li_2O and V_2O_5 in the glass frit used for vitrification to enhance the waste glass's sulphate capacities. However, this study could not be undertaken during the course of the PhD work.

9.2 Chlorine Studies

The studies related to incorporation of chloride ions in silicate and borosilicate glasses suggests that chloride ions behave similarly as sulphate ions in these glasses. As observed for sulphate doped glasses, addition of chloride also leads to polymerisation of the silicate and borosilicate networks.

It was also interesting to note that BaO containing sodium borosilicate glasses which could retain upto ~3 mol% of SO_4^{2-} retained more than 90% of chloride added to the batch. No borosilicate glass, to the author's best knowledge, has shown such high chloride capacities. Therefore, this work suggests that with addition of BaO to the industrial HLW glass composition, it might be possible to increase waste loading of chloride rich radioactive waste.

9.3 Future Work and Recommendations

In this section scope of the future work is discussed based on the knowledge earned during the course of research.

a) In silicate glasses, it was observed that addition of Li^+ had a positive effect on sulphate solubility. This was also proven upon replacement of half molar content of Na_2O with Li_2O in HLW waste simulant glass. However, only a binary silicate glass : Li_2O- SiO_2 was studied in order to investigate the effect of lithium ions on sulphate retention. It is suggested to investigate a series of Li_2O including ternary silicate glasses to study the effect of Li^+ in presence of a dissimilar cation upon sulphate retention. Since both Li_2O and BaO improved the sulphate capacity in silicate and borosilicate glasses, characterisation of structure of Li_2O-BaO-SiO_2 glasses with sulphate doping will make an interesting case of study.

b) The authors also suggest S-K edge XANES and EXAFS studies on the sulphate doped silicate and borosilicate glasses, to investigate the local sulphate environment Data for this study has already been collected at the ESRF synchrotron facility, Grenoble, France.

c) ^{23}Na 3Q MAS NMR and ^{17}O MAS NMR are recommended to study the sodium and oxygen environment in the undoped and sulphate doped glasses This will give a clearer insight of structural changes that occur with addition of the sulphate anions as the quadrupolar interactions are averaged out using the triple quantum MAS NMR technique.

d) Neutron diffraction of the chloride doped glasses are suggested to investigate the coordination environment around the chloride ions. Neutron diffraction data has been collected for the chloride doped glasses and awaited to be analysed,

e) It is also suggested to develop simulant HLW waste glass compositions for vitrification of chloride rich HLW. The studies in this thesis have shown that the chloride capacity can be enhanced with substitution of a fraction of Na_2O with BaO. It will be interesting to see if the chloride capacity enhances within simulated borosilicate glasses with high BaO content.

REFERENCES

- Abdelouas, A. (2006). Uranium Mill Tailings: Geochemistry, Mineralogy, and Environmental Impact. Elements, 2(6), 335–341.
- Ackerman, J. P. (1991). Chemical basis for pyrochemical reprocessing of nuclear fuel. Industrial & Engineering Chemistry Research, 30(1), 141–145.
- Ackerman, J. P., Johnson, T. R., & Laidler, J. J. (1994). Waste Removal in Pyrochemical Fuel Processing for IFR.
- Advocat, T., Dussossoy, J. L., & Petitjean, V. (2008). Radioactive wastes vitrification. Techniques de l'Ingenieur. Genie Nucleaire, (BN194), BN36641--BN366424.
- Affatigato, M. (2015). Modern Glass Characterization. (M. Affatigato, Ed.). Wiley and sons.
- Aloy, A., Soshnikov, R., Trofimenko, A. V, Vienna, J. D., Elliott, M. L., Northwest, P., River, S. (2006). Improved Loading of Sulfate-Limited Waste in Glass. In WM'06 conference.
- Ando, Y., Nishihara, K., & Takano, H. (2000). Estimation of spent fuel compositions from light water reactors. Journal of Nuclear Science and Technology (Vol. 37).
- Andrews, A. (2006). Nuclear Fuel Reprocessing: U.S. Policy Development.
- Andrews, A. (2006). Radioactive Waste Streams: Waste Classification for Disposal.
- Angeli, F., Charpentier, T., Molières, E., Soleilhavoup, A., Jollivet, P., & Gin, S. (2013). Influence of lanthanum on borosilicate glass structure: A multinuclear MAS and MQMAS NMR investigation. Journal of Non-Crystalline Solids, 376, 189–198.
- Angeli, F., Delaye, J. M., Charpentier, T., Petit, J. C., Ghaleb, D., & Faucon, P. (2000). Influence of glass chemical composition on the Na-O bond distance: A23Na 3Q-MAS NMR and molecular dynamics study. Journal of Non-Crystalline Solids, 276(1), 132–144.
- Angeli, F., Gaillard, M., Jollivet, P., & Charpentier, T. (2007). Contribution of ^{43}Ca MAS NMR for probing the structural configuration of calcium in glass. Chemical Physics Letters, 440(4–6), 324–328.
- Angeli, F., Villain, O., Schuller, S., Ispas, S., & Charpentier, T. (2011). Insight into sodium silicate glass structural organization by multinuclear NMR combined with first-principles calculations. Geochimica et Cosmochimica Acta, 75(9), 2453–2469.
- Arkosiová, M., Kloužek, J., Němec, L., Krečmer, N., Liška, M., Chocholoušek, J., others. (2008). the role of sulfur in glass melting processes. Ceramics- Silikáty, 52(3), 155–159.
- Avramov, I., Rüssel, C., & Keding, R. (2003). Effect of chemical composition on viscosity of oxide glasses. Journal of Non-Crystalline Solids, 324(1–2), 29–35.
- Avramov, I., Vassilev, T., & Penkov, I. (2005). The glass transition temperature of silicate and borate glasses. Journal of Non-Crystalline Solids, 351(6–7), 472–476.
- Azevedo, C. R. F. (2011). Selection of fuel cladding material for nuclear fission reactors. Engineering Failure Analysis, 18(8), 1943–1962.

- Backnaes, L., & Deubener, J. (2011). Experimental Studies on Sulfur Solubility in Silicate Melts at Near-Atmospheric Pressure. Reviews in Mineralogy and Geochemistry, 73(1), 143–165.
- Bacon, G. E., & Bacon, G. E. (1966). Chapter VII– The Diffraction of Neutrons. X-Ray and Neutron Diffraction, 64–74.
- Baehr, W. (1989). Industrial vitrification processes for high-level liquid waste solutions. International Atomic Energy Agency Bulletin, 31(4), 43–46.
- Baker, D. R., & Moretti, R. (2011). Modelling the Solubility of Sulfur in Magmas: A 50-Year Old Geochemical Challenge. Reviews in Mineralogy and Geochemistry, 73(1), 167–213.
- Bancroft, A. R. (1960). The incorporation of fission products into glass for disposal. The Canadian Journal of Chemical Engineering, 38(1), 19–24.
- Barnes, R. M., & Boumans, P. W. J. M. (1978). Recent Advances in Emission Spectroscopy: Inductively Coupled Plasma Discharges for Spectrochemical Analysis. C R C Critical Reviews in Analytical Chemistry, 7(3), 203–296.
- Barrere, M. (1978). Nuclear waste vitrification. Recherche (Paris), 9(91), 698–702.
- Bauer, N., Brecha, R. J., & Luderer, G. (2012). Economics of nuclear power and climate change mitigation policies. PNAS, 109(42), 16805–16810.
- Beerkens, R. G. C., & Kahl, K. (2002). Chemistry of sulphur in soda--lime--silica glass melts. Physics and Chemistry of Glasses, 43(4), 189–198.
- Betzen, A. R., Kudlacek, B. L., Kapoor, S., Berryman, J. R., Lower, N. P., Feller, H. A., … Feller, S. A. (2003). Physical properties of barium borosilicate glasses related to atomic structure. Physics and Chemistry of Glasses, 44(3), 207–211.
- Bickford, D. F., Applewhite-Ramsey, A., Jantzen, C. M., & Brown, K. G. (1990). Control of radioactive waste glass melters: I, Preliminary general limits at Savannah River. Journal of the American Ceramic Society, 73(10), 2896–2902.
- Billings, A. L., & Fox, K. M. (2010). Retention of Sulfate in Savannah River Site High-Level Radioactive Waste Glass. International Journal of Applied Glass Science, 1(4), 388–400.
- Bingham, P. A., & Hand, R. J. (2008). Sulphate incorporation and glass formation in phosphate systems for nuclear and toxic waste immobilization. Materials Research Bulletin, 43(7), 1679–1693.
- Bingham, P. A., & Jackson, C. M. (2008). Roman blue-green bottle glass: chemical-optical analysis and high temperature viscosity modelling. Journal of Archaeological Science, 35(2), 302–309.
- Bingham, P. A., Connelly, A. J., Hand, R. J., Hyatt, N. C., Northrup, P. A., Alonso Mori, R., … Edge, R. (2010). A multi-spectroscopic investigation of sulphur speciation in silicate glasses and slags. Glass Technology: European Journal of Glass Science and Technology Part A, 51(2), 63–80.
- Bingham, P. A., Parker, J. M., Searle, T., Williams, J. M., & Fyles, K. (1999). Redox and clustering of iron in silicate glasses. Journal of Non-Crystalline Solids, 253(1–3), 203–209.
- Bingham, P. A., Vaishnav, S., Forder, S. D., Scrimshire, A., Jaganathan, B., Rohini, J., Vienna, J. D. (2017). Modelling the sulfate capacity of simulated radioactive waste borosilicate glasses. Journal of Alloys and Compounds, 695, 656–667.

- Bingham, P., C Hyatt, N., Hand, R., & R Wilding, C. (2009). Glass Development for Vitrification of Wet Intermediate Level Waste (WILW) from Decommissioning of the Hinkley Point "A" Site. Materials Research Society Symposia Proceedings. Materials Research Society, 1124, 161–166.
- Bingham, P., Connelly, a J., Hyatt, N. C., & Hand, R. J. (2011). Corrosion of glass contact refractories for the vitrification of radioactive wastes: a review. International Materials Reviews, 56(4), 226–242.
- Bouty, O., Delaye, J. M., Beuneu, B., & Charpentier, T. (2014). Modelling borosilicate glasses of nuclear interest with the help of RMC, WAXS, neutron diffraction and ^{11}B NMR. Journal of Non-Crystalline Solids, 401, 27–31.
- Bradley, D. J., & Schneider, K. J. (1990). Radioactive Waste Management in the USSR: A Review of Unclassified Sources, 1963-1990 Pacific Northwest Laboratory, 1963–1990.
- Brawer, S. A., & White, W. B. (1975). Raman spectroscopic investigation of the structure of silicate glasses. I. The binary alkali silicates. The Journal of Chemical Physics, 63(6), 2421–2432.
- Brawer, S. A., & White, W. B. (1977). Raman Spectroscopic Investigation of The Structure of Silicate Glasses (II). Soda-Alkaline Earth-Alumina Ternary and Quaternary Glasses. Journal of Non-Crystalline Solids, 23, 261–278.
- Brendebach, B., Denecke, M. A., Roth, G., & Weisenburger, S. (2009). Sulfur incorporation in high level nuclear waste glass: A S K-edge XAFS investigation. Journal of Physics: Conference Series, 190.
- Brese, N. E., & O'Keeffe, M. (1991). Bond-valence parameters for solids. Acta Crystallographica Section B, 47(2), 192–197.
- Briner, W. H. (1985). Low-level rad waste compacts: An update. Diagnostic Nuclear Medicine, 2(18).
- Brouwer, P. (2010). Theory of XRF. Almelo: PANalytical BV Manual.
- Bruno, J., & Ewing, R. C. (2006). Spent Nuclear Fuel. Elements, 2(6), 343–349.
- Bunker, B. C. (1994). Molecular mechanisms for corrosion of silica and silicate glasses. Journal of Non-Crystalline Solids, 179(C), 300–308.
- Bunn, M., Holdren, J. P., Fetter, S., & Van Der Zwaan, B. (2005). The economics of reprocessing versus direct disposal of spent nuclear fuel. Nuclear Technology, 150(3), 209–230.
- Cabral, A. A., Cardoso, A. A. D., & Zanotto, E. D. (2003). Glass-forming ability versus stability of silicate glasses. I. Experimental test. Journal of Non-Crystalline Solids, 320(1–3), 1–8.
- Cabral, a. a., Fredericci, C., & Zanotto, E. D. (1997). A test of the Hrubÿ parameter to estimate glass-forming ability. Journal of Non-Crystalline Solids, 219, 182–186.
- Calestani, G., Montenero, A., Ferraguti, E., Ingletto, G., & Bettinelli, M. (1986). Influence of some oxides on the durability of a borosilicate glass. Journal of Non-Crystalline Solids, 84, 452–462.
- Carlsson, T., & Viitanen, P. (1997). Low and intermediate level radioactive waste : waste characterization and activity measurements.
- Carroll, M. R., & Webster, J. D. (1994). Solubilities of sulfur, noble gases, nitrogen, chlorine, and fluorine in magmas. Reviews in Mineralogy and Geochemistry, 30(1), 231–279.

- Cassingham, N. J., Bingham, P., Hand, R. J., & Forder, S. (2008). Property modification of a high level nuclear waste borosilicate glass through the addition of Fe_2O_3. Glass Technology.: European Journal of Glass Science Tecnhology-. A, February 2008, 49 (1), 21–26.
- Caurant, D., Loiseau, P., Bardez, I., & Quintas, A. (2009). Glasses, Glass-ceramics and Ceramics for Immobilization of Highly Radioactive Nuclear Wastes.
- Chapman, C. C., & Buelt, J. J. (1978). Nuclear waste vitrification.
- Charpentier, T. (2012). NMR of Amorphous Materials. EPJ Web of Conferences, 30, 4004.
- Charpentier, T., Ispas, S., Profeta, M., Mauri, F., & Pickard, C. J. (2004). First-Principles Calculation of ^{17} O, ^{29} Si, and ^{23} Na NMR Spectra of Sodium Silicate Crystals and Glasses. The Journal of Physical Chemistry B, 108(13), 4147–4161.
- Charpentier, T., Menziani, M. C., & Pedone, A. (2013). Computational simulations of solid state NMR spectra: a new era in structure determination of oxide glasses. RSC Advances, 3(27), 10550.
- Chauhan, A., & Chauhan, P. (2014). Powder XRD Technique and its Applications in Science and Technology. Journal of Analytical & Bioanalytical Techniques, 5(6), 1–5.
- Chen, X., Karpukhina, N., Brauer, D. S., & Hill, R. G. (2017). High chloride content calcium silicate glasses. Phys. Chem. Chem. Phys., 19(10), 7078–7085.
- Chick, L. A., Piepel, G. F., Mellinger, G. B., May, R. P., Gray, W. J., & Buckwalter, C. Q. (1981). Effects of composition on properties in an 11-component nuclear waste glass system.
- Chmel, A., & Svetlov, V. N. (1996). Si- Cl groups in chlorine-impregnated silica. Journal of Non-Crystalline Solids, 195(1–2), 176–179.
- Cicero, C. A., Pierce, R. A., & Bickford, D. F. (1995). Savannah River Site Reactor Basin Ion Exchange Resin Bench Scale Studies.
- Clark, R. J. H., & Mitchell, P. D. (1972). Raman Spectra and Factor Group Analyses of Crystalline Boron Trihalides. The Journal of Chemical Physics, 56 (5), 2225-2232.
- Cochain, B., Neuville, D. R., Henderson, G. S., McCammon, C. A., Pinet, O., & Richet, P. (2012). Effects of the Iron Content and Redox State on the Structure of Sodium Borosilicate Glasses: A Raman, Mössbauer and Boron K-Edge XANES Spectroscopy Study. Journal of the American Ceramic Society, 95(3), 962–971.
- Cochran, R. G., Lewis, E. E., Tsoulfanidis, N., & Miller, W. F. (1990). The nuclear fuel cycle: analysis and management. American Nuclear Society.
- Colthup, N. B., Daly, L. H., & Wiberley, S. E. (1990). Chapter1 : Vibrational and Rotational Spectra. In N. B. Colthup, L. H. Daly, & S. E. Wiberley (Eds.), Introduction to Infrared and Raman Spectroscopy (Third Edition) (Third Edit, pp. 171–213). San Diego: Academic Press.
- Connelly, A. J., Hand, R. J., Bingham, P. A., & Hyatt, N. C. (2011). Mechanical properties of nuclear waste glasses. Journal of Nuclear Materials, 408(2), 188–193.
- Coops, M. S., Knighton, J. B., & Mullins, L. J. (1983). Pyrochemical Processing of Plutonium. In Plutonium Chemistry (pp. 381–408).
- Cormier, L., & Neuville, D. R. (2004). Ca and Na environments in Na_2O-CaO-Al_2O_3-SiO_2 glasses: Influence of cation mixing and cation-network interactions. Chemical Geology, 213(1–3), 103–113.

- Cox, B. (1990). Pellet-clad interaction (PCI) failures of zirconium alloy fuel cladding—a review. Journal of Nuclear Materials, 172(3), 249–292.
- Crawford, G., Martin, R., & Pearson, S. (2011). Portable and Modular Cementation Systems for Stabilization of Nuclear Wastes – 11367. In WM2011.
- Cunnane, J. C. (1994). High-Level Waste Borosilicate Glass A Compendium of Corrosion Charecteristics - Volume 1 (DOE-EM-0177). U.S. Department of Energy Office of Waste Management.
- Darab, J. G., Graham, D. D., Macissac, B. D., Smith, H. D., & Vienna, J. D. (2001). Sulfur Partitioning During Vitrification of INEEL Sodium Bearing Waste: Status Report (PNNL-13588).
- Darby Dyar, M. (1985). A review of Mossbauer data on inorganic glasses: the effects of Composition on Iron Valency and Coordination, 304–316.
- Day, D. E. (1976). Mixed alkali glasses—their properties and uses. Journal of Non-Crystalline Solids, 21(3), 343–372.
- Day, D. E., Chandra, C. S., Kim, C.-W., Huang, W., Leerssen, R. D., Reis, S. T., & Zhu, D. (2002). Iron phosphate glasses: an alternative for vitrifying certain nuclear wastes (Vol. 45618).
- Degen, I. A., & Newman, G. A. (1993). Raman spectra of inorganic ions. Spectrochimica Acta Part A: Molecular Spectroscopy, 49(5), 859–887.
- Deissmann, G., Brenk, F., Gmbh, S., & Wiegers, R. (2016). Dissolution behaviour of HLW glasses under Dissolution behaviour of HLW glasses under OPERA repository conditions OPERA-PU-IBR511A. Opera-Pu-Ibr511a, (October).
- Dell, W. J., Bray, P. J., & Xiao, S. Z. (1983). ^{11}B NMR studies and structural modelling of Na_2O-B_2O_3-SiO_2 glasses of high soda content. Journal of Non-Crystalline Solids, 58(1), 1–16.
- Devine, J. D., Sigurdsson, H., Davis, A. N., & Self, S. (1984). Estimates of sulfur and chlorine yield to the atmosphere from volcanic eruptions and potential climatic effects. Journal of Geophysical Research: Solid Earth, 89(B7), 6309–6325.
- Dey, P. K. (2003). Spent fuel reprocessing: an overview.
- Dey, P. K., & Bansal, N. K. (2006). Spent fuel reprocessing: A vital link in Indian nuclear power program. Nuclear Engineering and Design, 236(7–8), 723–729.
- DiBello, P. M. (1989). Controlling the oxidation state of a glass as a means of optimising sulphate usage in melting and refining. Glass Technology, 30(5), 160–165.
- Dietzel, A. (1942). Die Kationenfeldstärken und ihre Beziehungen zu Entglasungsvorgängen, zur Verbindungsbildung und zu den Schmelzpunkten von Silicaten. Zeitschrift Für Elektrochemie Und Angewandte Physikalische Chemie, 48(1), 9–23.
- Do Remus, R. H., Mehrotra, Y., Lanford, W. A., & Burman, C. (1983). Reaction of water with glass: influence of a transformed surface layer. Journal of Materials Science, 18(2), 612–622.
- Donald, I. W. (2010). Waste immobilization in glass and ceramic based hosts: radioactive, toxic and hazardous wastes. John Wiley & Sons.
- Donald, I. W., Metcalfe, B. L., & Fong, S. K. (2007). Development of a glass-encapsulated calcium phosphate wasteform for the immobilization of actinide and halide containing radioactive wastes

from the pyrochemical reprocessing of plutonium metal. Journal of Nuclear Materials, 361(SPEC. ISS.), 78–93.

- Donald, I., Metcalfe, B. L., & Taylor, R. N. J. (1997). The immobilization of high level radioactive wastes using ceramics and glasses. Journal of Materials Science, 32(22), 5851–5887.
- Doremus, R. H. (1975). Interdiffusion of hydrogen and alkali ions in a glass surface. Journal of Non-Crystalline Solids, 19(C), 137–144.
- Douglas, R. W., & El-shamy, T. M. M. (1967). Reactions of Glasses with Aqueous Solutions. Journal of the American Ceramic Society, 50(1), 1–8.
- Doweidar, H. (1990). Consideration of the boron oxide anomaly. Journal of Materials Science, 25(1), 253–258.
- Doweidar, H. (1998). Density and molar volume of Li_2O SiO_2 glasses in relation to their microstructure. Physics and Chemistry of Glasses, 39(5), 286–289.
- Doweidar, H. (1999). Density-structure correlations in silicate glasses. Journal of Non-Crystalline Solids, 249(2–3), 194–200.
- Doweidar, H.., Feller, S.., Affatigato, M.., Tischendorf, B.., Ma, C.., & Hammarsten, E. (1999). Density and molar volume of extremely modified alkali silicate glasses. Physics and Chemistry of Glasses, 40(6), 339–344.
- Du, J., & Cormack, A. N. (2004). The medium range structure of sodium silicate glasses: A molecular dynamics simulation. Journal of Non-Crystalline Solids, 349(1–3), 66–79.
- Du, J., & Corrales, L. R. (2006). Compositional dependence of the first sharp diffraction peaks in alkali silicate glasses: A molecular dynamics study. Journal of Non-Crystalline Solids, 352(30–31), 3255–3269.
- Du, L. S., & Stebbins, J. F. (2003). Site preference and Si/B mixing in mixed-alkali borosilicate glasses: A high-resolution ^{11}B and ^{17}O NMR study. Chemistry of Materials, 15(20), 3913–3921.
- Du, L. S., & Stebbins, J. F. (2003). Solid-state NMR study of metastable immiscibility in alkali borosilicate glasses. Journal of Non-Crystalline Solids, 315(3), 239–255.
- Du, L., & Stebbins, J. F. (2003). Nature of Silicon-Boron Mixing in Sodium Borosilicate Glasses: A High-Resolution ^{11}B and ^{17}O NMR Study. Journal of Physical Chemistry- B, 107, 10063–10076.
- Dupree, R., Holland, D., & Williams, D. S. (1986). The structure of binary alkali silicate glasses. Journal of Non-Crystalline Solids, 81(1–2), 185–200.
- Dupree, R., Holland, D., McMillan, P. W., & Pettifer, R. F. (1984). The structure of soda-silica glasses: A MAS NMR study. Journal of Non-Crystalline Solids, 68(2–3), 399–410.
- Dwivedi, B. P., & Khanna, B. N. (1995). Cation dependence of Raman scattering in alkali borate glasses. Journal of Physics and Chemistry of Solids, 56(1), 39–49.
- Dyar, M. D., Agresti, D. G., Schaefer, M. W., Grant, C. A., & Sklute, E. C. (2006). Mössbauer Spectroscopy of Earth and Planetary Materials. Annual Review of Earth and Planetary Sciences, 34(1), 83–125.
- Eckert, H. (1992). Structural Characterization of Noncrystalline Solids and Glasses Using Solid-State Nmr. Progress in Nuclear Magnetic Resonance Spectroscopy, 24, 159–293.

- Evans, J. C., & Bernstein, H. J. (1954). The vibrational spectrum of the sulphite ion in sodium sulphite. Canadian Journal of Chemistry, 33(3619), 1270–1273.
- Evans, K. A., Mavrogenes, J. A., O'Neill, H. S., Keller, N. S., & Jang, L. Y. (2008). A preliminary investigation of chlorine XANES in silicate glasses. Geochemistry, Geophysics, Geosystems, 9(10).
- Ewing, R. C. (2006). The Nuclear Fuel Cycle: A Role for Mineralogy and Geochemistry. Elements, 2(6), 331–334.
- Ewing, R. C., & Wang, L. (2002). Phosphates as Nuclear Waste Forms. Reviews in Mineralogy and Geochemistry, 48(1), 673.
- Ewing, R. C., Weber, W. J., & Clinard, F. W. (1995). Radiation effects in nuclear waste forms for high-level radioactive waste. Progress in Nuclear Energy, 29(2), 63–127.
- Ewing, R. C., Whittleston, R. A., & Yardley, B. W. D. (2016). Geological Disposal of Nuclear Waste: a Primer. Elements, 12(4), 233–237.
- Fábián, M., Sváb, E., Proffen, T., & Veress, E. (2008). Structure study of multi-component borosilicate glasses from high-Q neutron diffraction measurement and RMC modelling. Journal of Non-Crystalline Solids, 354(28), 3299–3307.
- Feller, S. (2008). Density, volume and Packing: Part 3, Lecture Series
- Feller, S. A., Mullenbach, T., Franke, M., Bista, S., O'Donovan-Zavada, A., Hopkins, K., Wren, J. (2012). Structure and properties of barium and calcium borosilicate glasses. Physics and Chemistry of Glasses: European Journal of Glass Science and Technology Part B, 53(5), 210–218.
- Figueroa, R. (2003). Selective excitation and integral counting of x-ray fluorescence (SEICXRF). X-Ray Spectrometry, 32(4), 299–306.
- Fincham, C. J. B., & Richardson, F. D. (1954). The Behaviour of Sulphur in Silicate and Aluminate Melts. Proceedings of the Royal Society A: Mathematical, Physical and Engineering Sciences, 223(1152), 40–62.
- Forto Chungong, L., Swansbury, L. A., Mountjoy, G., Hannon, A. C., Lee, A. F., & Martin, R. A. (2017). Atomic structure of chlorine containing calcium silicate glasses by neutron diffraction and ^{29} Si solid-state NMR. International Journal of Applied Glass Science, 8(4), 383–390.
- Fox, J., & Koetting, J. (1974). Purification process for recovering uranium from an acidic aqueous solution by ph control. Google Patents.
- Fox, K. M., Edwards, T. B., & Peeler, D. K. (2006). Sulfate retention in high level waste (HLW) Sludge batch 4 (SB4) glasses: A preliminary assessment (Vol. 4).
- Frantz, J. D., & Mysen, B. O. (1995). Raman spectra and structure of $BaO-SiO_2$, $SrO-SiO_2$ and $CaO-SiO_2$ melts to 1600°C. Chemical Geology, 121, 155–176.
- Freiesleben, H. (2013). Final disposal of radioactive waste. In EPJ Web of Conferences (Vol. 54, p. 1006).
- Frizon, F., & Cau-dit-Coumes, C. (2006). Cementation of ILW ion exchange resins: Impact of sulfate ions released by radiolysis on hydrated matrix. Journal of Nuclear Materials, 359(3), 162–173.
- Frugier, P., Martin, C., Ribet, I., Advocat, T., & Gin, S. (2005). The effect of composition on the leaching of three nuclear waste glasses: R7T7, AVM and VRZ. Journal of Nuclear Materials, 346(2–3), 194–207.

- Fukumi, K., Hayakawa, J., & Komiyama, T. (1990). Intensity of Raman band in silicate glasses. Journal of Non-Crystalline Solids, 119(3), 297–302.
- Furukawa, T., Fox, K. E., & White, W. B. (1981). Raman spectroscopic investigation of the structure of silicate glasses. III. Raman intensities and structural units in sodium silicate glasses. The Journal of Chemical Physics, 75(7), 3226–3237.
- Gaines, P. R. (2011). ICP Operations Guide a Guide for using ICP-OES and ICP-MS.
- Gambuzzi, E., Charpentier, T., Menziani, M. C., & Pedone, A. (2014). Computational interpretation of ^{23}Na MQMAS NMR spectra: A comprehensive investigation of the Na environment in silicate glasses. Chemical Physics Letters, 612, 56–61.
- Gaudio, S. J., Edwards, T. G., & Sen, S. (2015). An in situ high-pressure NMR study of sodium coordination environment compressibility in albite glass. American Mineralogist, 100(1), 326–329.
- Gehlhoff, G., & Thomas, M. (1926). Die physikalischen Eigenschaften der Gläser in Abhängigkeit von der Zusammensetzung. Z. Techn. Physik, 6.
- Gershey, E. L., Klein, R. C., Party, E., & Wilkerson, A. (1990). Low-level radioactive waste.
- Gin, S., Abdelouas, A., Criscenti, L. J., Ebert, W. L., Ferrand, K., Geisler, T., Vienna, J. D. (2013). An international initiative on long-term behaviour of high-level nuclear waste glass. Materials Today, 16(6), 243–248.
- Gin, S., Beaudoux, X., Angéli, F., Jégou, C., & Godon, N. (2012). Effect of composition on the short-term and long-term dissolution rates of ten borosilicate glasses of increasing complexity from 3 to 30 oxides. Journal of Non-Crystalline Solids, 358(18–19), 2559–2570.
- Giri, S., Gaebler, C., Helmus, J., Affatigato, M., Feller, S., & Kodama, M. (2004). A general study of packing in oxide glass systems containing alkali. Journal of Non-Crystalline Solids, 347(1–3), 87–92.
- Glasser, F. P., & Atkins, M. (1994). Cements in radioactive waste disposal. MRS Bulletin, 19(12), 33–38.
- Goel, A., McCloy, J. S., Fox, K. M., Leslie, C. J., Riley, B. J., Rodriguez, C. P., & Schweiger, M. J. (2012). Structural analysis of some sodium and alumina rich high-level nuclear waste glasses. Journal of Non-Crystalline Solids, 358(3), 674–679.
- Goel, A., McCloy, J. S., Windisch, C. F., Riley, B. J., Schweiger, M. J., Rodriguez, C. P., & Ferreira, J. M. F. (2013). Structure of Rhenium-Containing Sodium Borosilicate Glass. International Journal of Applied Glass Science, 4(1), 42–52.
- González, A. J., Akashi, M., Jr, J. D. B., Chino, M., Homma, T., Ishigure, N., Yonekura, Y. (2013). Radiological protection issues arising during and after the Fukushima nuclear reactor accident. Journal of Radiological Protection, 33(3), 497.
- Gopalakrishnan, V., Dhami, P., Ramanujam, A., Krishna, M., Murali, M., Mathur, J., Banerji, A. (1995). Extraction and extraction chromatographic separation of minor actinides from sulphate bearing high level waste solutions using CMPO. Journal of Radio analytical and Nuclear Chemistry, 191(2), 279–289.
- Grambow, B. (2006). Nuclear waste glasses - How durable? Elements, 2(6), 357–364.

- Gras, J.-M., Do Quang, R., Masson, H., Lieven, T., Ferry, C., Poinssot, C., Delbecq, J.-M. (2007). Perspectives on the closed fuel cycle--Implications for high-level waste matrices. Journal of Nuclear Materials, 362(2), 383–394.
- Gray, L. W., Holliday, K. S., Murray, A., Thompson, M., Thorp, D. T., Yarbro, S., & Venetz, T. J. (2015). Separation of Plutonium from Irradiated Fuels and Targets.
- Greaves, G. N., Fontaine, A., Lagarde, P., Raoux, D., & Gurman, S. J. (1981). Local structure of silicate glasses. Nature, 293(5834), 611–616.
- Greaves, G. N., Smith, W., Giulotto, E., & Pantos, E. (1997). Local structure, microstructure and glass properties. Journal of Non-Crystalline Solids, 222, 13–24.
- Grofmeier, M., Natrup, F. V., & Bracht, H. (2007). Barium diffusion in mixed cation glasses. Physical Chemistry Chemical Physics, 9(43), 5822.
- Groska, J., Vajda, N., Molnár, Z., Bokori, E., Szeredy, P., & Zagyvai, M. (2016). Determination of actinides in radioactive waste after separation on a single DGA resin column. Journal of Radioanalytical and Nuclear Chemistry, 309(3), 1145–1158.
- Guzella, M. F. R., & Da Silva, T. V. (2001). Evaluation of bitumens for radioactive waste immobilization. In WM'01 Conference.
- Hamodi, N. H., & Iqbal, Y. (2009). Glass Melting Techniques Used in Radioactive Waste Immobilization. Journal of Pakistani Material Sciety, 3(2), 47–57.
- Hamodi, N., & Iqbal, Y. (2009). Immobilization of Spent Ion Exchange Resin Arising from Nuclear Power Plants An Introduction. Journal of Pakistani Material Society, 3(1), 7–18.
- Han, K. W., Heinonen, J., & Bonne, A. (1997). Radioactive waste disposal: Global experience and challenges. IAEA Bulletin.
- Hannon, A. (2006). Neutron Diffraction as a Probe of Local Structure. In 8th ESG Conference, Sunderland.
- Hannon, A. C. (2005). Results on disordered materials from the GEneral Materials diffractometer, GEM, at ISIS. Nuclear Instruments and Methods in Physics Research, Section A: Accelerators, Spectrometers, Detectors and Associated Equipment, 551(1), 88–107.
- Hapanowicz, R. P., & Condrate, Sr, R. a. (1996). Raman Spectral Investigation of Sulfate Inclusions in Sodium Calcium Silicate Glasses. Journal of Solid State Chemistry, 123(123), 183–185.
- Harding, F. L. (1972). Dependence of Melt Oxygen Activity and Water Retention on Composition of Amber Glass. Journal of the American Ceramic Society, 55(7), 368–372.
- Harrison, M. T. (2014). Vitrification of High Level Waste in the UK. Procedia Materials Science, 7, 10–15.
- Harvey, K. B., & Litke, C. D. (1984). Model for Leaching Behavior of Aluminosilicate Glasses Developed as Matrices for Immobilizing High-Level Wastes. Journal of the American Ceramic Society, 67(8), 553–556.
- Hawthorne, F. C. (1994). Structural aspects of oxide and oxysalt crystals. Acta Crystallographica Section B, 50(5), 481–510.
- Hayward, P.J.; Cecchetto, E. V. (1982). Development of sphene-based glass ceramics tailored for Canadian waste disposal conditions. Elsevier Science Publishing Company, Inc.

- Heimberg, J. (2016). Low-level radioactive waste management and disposition: background information discussion paper for the low-level radioactive waste management and disposition: background information. In USNRC proceedings.
- Hohlein, G., Tittmann, E., Weisenburger, S., & Wiese, H. (1986). Vitrification of High Level Radioactive Waste - Operating Experience with the PAMELA plant. Wmsjournal, 2(71), 413–420.
- Holland, D., Parkinson, B. G., Islam, M. M., Duddridge, A., Roderick, J. M., Howes, A. P., & Scales, C. R. (2007). NMR insights into wasteforms for the vitrification of high-level nuclear waste. Applied Magnetic Resonance, 32(4), 483–497.
- Holmquist, S. B. (1966). Ionic Formulation of Redox Equilibria in Glass Melts. Journal of the American Ceramic Society, 49(4), 228–229.
- Hoppe, U., Stachel, D., & Beyer, D. (2007). The oxygen coordination of metal ions in phosphate and silicate glasses studied by a combination of x-ray and neutron diffraction. Physica Scripta, T57, 122–126.
- Hou, X., & Jones, B. T. (2000). Inductively Coupled Plasma Optical Emission Spectrometry. Encyclopedia of Analytical Chemistry, 9468–9485.
- Hrma, P., Piepel, G., Schweiger, M., Smith, D., Kim, D., Redgate, P., Peeler, D. (1994). Property/composition relationships for Hanford high-level waste glasses melting at 1150 C (Vol. 1).
- Hrma, P., Vienna, J. D., & Ricklefs, J. S. (2002). Mechanism of Sulfate Segregation during Glass Melting. In MRS Proceedings (Vol. 757). Cambridge University Press.
- Hrubý, A. (1972). Evaluation of glass-forming tendency by means of DTA. Czechoslovak Journal of Physics B, 22(11), 1187–1193.
- Huang, C., & Cormack, A. N. (1990). The structure of sodium silicate glass. The Journal of Chemical Physics, 93(11), 8180–8186.
- Hubert, M., & Faber, A. J. (2014). On the structural role of boron in borosilicate glasses. Physics and Chemistry of Glasses-European Journal of Glass Science and Technology Part B, 55(3), 136–158.
- Hujova, M., & Vernerova, M. (2017). Influence of fining agents on glass melting: A review Part 1. Ceramics--Silikáty, 61(2), 119–126.
- IAEA. (1970). Bituminization of Radioactive Wastes.
- IAEA. (1978). Treatment of Low and Intermediate Level Liquid Radioactive Wastes. Technical Report Series n°236.
- IAEA. (1985). Chemical Durability and Related Properties of Solidified High-Level Waste Forms. Vienna: International Atomic Energy Agency.
- IAEA. (1988). Design and operation of off-gas cleaning systems Technical Reports at high level liquid waste conditioning facilities. Technical Reports Series No. 291.
- IAEA. (1988). Nuclear, power performance and safety. In IAEA.
- IAEA. (1992). Design and Operation of High Level Waste Vitrification and Storage Facilities. Technical Report Series No. 339.
- IAEA. (1993). Bituminization Processes to Condition Radioactive Wastes (Technical Reports Series). Vienna: International Atomic Energy Agency.

- IAEA. (1997). Technologies for in situ immobilization and isolation of radioactive wastes at disposal and contaminated sites.
- IAEA. (1998). Interim Storage of Radioactive Waste Packages.
- IAEA. (1999). Inventory of radioactive waste disposals at sea. Encyclopedia of Atmospheric Sciences, 4(August), 1549–1555.
- IAEA. (2003). Innovative Technologies for Nuclear Fuel Cycles and Nuclear Power. In IAEA proceedings (pp. 23–26).
- IAEA. (2004). Disposal of Low Activity Radioactive Waste. Proceedings of an International Symposium, Córdoba, Spain, 13–17 December 2004, (December), 13–17.
- IAEA. (2005). Fissile Material Management Strategies for Sustainable Nuclear Energy. In Proceedings of Technical Meeting, Vienna.
- IAEA. (2007). Spent Fuel and High-Level Waste: Chemical Durability and Performance under Simulated Repository Conditions. October.
- IAEA. (2008). Spent Fuel Reprocessing Options. Nuclear Fuel Cycle and Materials Section, (August), 151.
- IAEA. (2011). Focus on Low and Intermediate Level Waste. Iaea.
- IAEA. (2013). Management of Discharge of Low Level Liquid Radioactive Waste Generated in Medical, Educational, Research and Industrial Facilities.
- IAEA. (2017). International Status and Prospects for Nuclear Power 2017, GOV/INF/2017/12-GC (61)/INF/8.
- Ilyukhina, N. S., Ponomaryova, I. Y., Laschchenova, T. N., & Stefanovsky, S. V. (2010). Solubility of Sulfate and Chloride Ions in Borosilicate Melts at Vitrification of Intermediate-Level Radioactive Wastes - 10348 Natalia. In WM2010Conference (Vol. 3, pp. 3–10).
- Inglis, K. K., Corley, J. P., Florian, P., Cabana, J., Bayliss, R. D., & Blanc, F. (2016). Structure and Sodium Ion Dynamics in Sodium Strontium Silicate Investigated by Multinuclear Solid-State NMR. Chemistry of Materials, 28(11), 3850–3861.
- Isard, J. O. (1969). The mixed alkali effect in glass. Journal of Non-Crystalline Solids, 1(3), 235–261.
- Islam, M., & Holland, D. (2010). The effect of divalent additions on the structure of a mixed alkali borosilicate glass for high level waste immobilisation. Physics and Chemistry of Glasses: European Journal of Glass Science and Technology Part B, 51(3), 137–145.
- Jacobsen, S. D., Smyth, J. R., Swope, R. J., & Downs, R. T. (1998). Rigid-body character of the SO~ 4 groups in celestine, anglesite and barite. Canadian mineralogist, 36, 1053-1060.
- Jahagirdar, P. B., & Wattal, P. K. (1998). Vitrification of sulphate bearing high level wastes in borosilicate matrix. Waste Management, 18(4), 265–273.
- Janssens, K., De Nolf, W., Van Der Snickt, G., Vincze, L., Vekemans, B., Terzano, R., & Brenker, F. E. (2010). Recent trends in quantitative aspects of microscopic X-ray fluorescence analysis. TrAC - Trends in Analytical Chemistry, 29(6), 464–478.
- Jantzen, C. M. (1986). Systems approach to nuclear waste glass development. Journal of Non-Crystalline Solids, 84(1–3), 215–225.

- Jantzen, C. M. (1991). First principles process-product models for vitrification of nuclear waste: Relationship of glass composition to glass viscosity, resistivity, liquidus temperature, and durability.
- Jantzen, C. M., & Plodinec, M. J. (1984). Thermodynamic model of natural, medieval and nuclear waste glass durability. Journal of Non-Crystalline Solids, 67(1–3), 207–223.
- Jantzen, C. M., Smith, M. E., & Peeler, D. K. (2005). Dependency of sulfate solubility on melt composition and melt polymerization. Ceramic Transactions, 168(865), 141–152.
- Jayasuriya, K. D., O'Neill, H. S. C., Berry, A. J., & Campbell, S. J. (2004). A Mössbauer study of the oxidation state of Fe in silicate melts. American Mineralogist, 89(11–12), 1597–1609.
- Jen, J. S., & Kalinowski, M. R. (1980). An ESCA study of the bridging to non-bridging oxygen ratio in sodium silicate glass and the correlations to glass density and refractive index. Journal of Non-Crystalline Solids, 38, 21–26.
- Jena, H., Maji, B. K., AsuvathRaman, R., & Kutty, K. V. G. (2015). Effect of pyrochemical chloride waste loading on thermo-physical properties of borosilicate glass bonded Sr-chloroapatite composites. Materials Chemistry and Physics, 162, 188–196.
- Johnson, L. H. (1988). Spent fuel. In Radioactive waste forms for the future.
- Joseph, I., Bowan II, B. W., Kruger, A. A., Gan, H., Kot, W. K., Matlack, K. S., & Pegg, I. L. (2009). High Aluminum HLW Glasses for Hanford â€^{TM} s WTP.
- Kaewjaeng, S., Kaewkhao, J., Limsuwan, P., & Maghanemi, U. (2012). Effect of BaO on optical, physical and radiation shielding properties of SiO_2-B_2O_3-Al_2O_3-CaO- Na_2O glasses system. Procedia Engineering, 32, 1080–1086.
- Kamitsos, E. I., Karakassides, M. A., & Chryssikos, G. D. (1986). A Vibrational Study of Lithium Sulfate Based Fast Ionic Conducting Borate Glasses. Journal of Physical Chemistry, 90(19), 4528–4533.
- Kamizono, H. (1985). Leaching behavior of simulated high-level waste glass in groundwater. Journal of Nuclear Materials, 127(2–3), 242–246.
- Kamizono, H. (1990). Effects of carbonate and sulphate ions in synthetic groundwater on high-level waste glass leaching. Journal of Materials Science Letters, 9(7), 841–844.
- Kamizono, H., & Nakamura, H. (1988). Simulated high-level nuclear waste glass leached in one type of Japanese groundwater. Journal of Nuclear Materials, 152(2–3), 339–342.
- Kanehashi, K. (2017). Structural roles of calcium in alkaline and alkaline-earth aluminosilicate. Solid State Nuclear Magnetic Resonance, 84(January), 158–163.
- Kaneko, S., Tokuda, Y., Takahashi, Y., Masai, H., & Ueda, Y. (2017). Structural analysis of mixed alkali borosilicate glasses containing Cs + and Na + using strong magnetic field magic angle spinning nuclear magnetic resonance. Journal of Asian Ceramic Societies, 5(1), 7–12.
- Kapoor, S., Bola George, H., Betzen, A., Affatigato, M., & Feller, S. (2000). Physical properties of barium borate glasses determined over a wide range of compositions. Journal of Non-Crystalline Solids, 270(1–3), 215–222.
- Karlsson, C., Zanghellini, E., Swenson, J., Roling, B., Bowron, D. T., & Borjesson, L. (2005). Structure of mixed alkali/alkaline earth silicate glasses from neutron diffraction and vibrational spectroscopy. Physical Review B, 72(1), 2–7.

- Karpius, P. J. (2017). Uranium Mining and Milling.
- Katsura, T., & Nagashima, S. (1974). Solubility of sulfur in some magmas at 1 atmosphere. Geochimica et Cosmochimica Acta, 38(4), 517–531.
- Kaur, R., Singh, S., & Pandey, O. P. (2013). Gamma ray irradiation effects on the optical properties of BaO-Na_2O-B_2O_3-SiO_2 glasses. Journal of Molecular Structure, 1048, 78–82.
- Kaushik, C. P. (2014). Indian Program for Vitrification of High Level Radioactive Liquid Waste. 2nd International Summer School on Nuclear Glass Wasteform: Structure, Properties and Long-Term Behavior, SumGLASS 2013, 7, 16–22.
- Kaushik, C. P., Mishra, R. K., Kumar, A., Raj, K., Division, W. M., Atomic, B., Atomic, B. (2007). Studies of Material Issues, Science and Technology for Immobilization of Sulphate-Bearing High-Level Radioactive Liquid Waste, (285), 73–77.
- Kaushik, C. P., Mishra, R. K., Sengupta, P., Kumar, A., Das, D., Kale, G. B., & Raj, K. (2006). Barium borosilicate glass - a potential matrix for immobilization of sulfate bearing high-level radioactive liquid waste. Journal of Nuclear Materials, 358(2–3), 129–138.
- Kaushik, C. P., Mishra, R. K., Thorat, V., Ramchandran, M., Kumar, A., Raj, K., & Das, D. (2004). Development of a Glass matrix for vitrification of sulphate bearing high level radioactive liquid waste -BARC/2004/E/018.
- Kelly, J. E., Cordaro, J. F., & Tomozawa, M. (1980). Correlation effects on alkali ion diffusion in binary alkali oxide glasses. Journal of Non-Crystalline Solids, 41(1), 47–55.
- Kersting, A. B., Efurd, D. W., Finnegan, D. L., Rokop, D. J., Smith, D. K., & Thompson, J. L. (1999). Migration of plutonium in ground water at the Nevada Test Site. Nature, 397(6714), 56–59.
- Khan, S., Syed, A. T., Ahmad, R., Rather, T. A., Ajaz, M., & Jan, F. A. (2010, January). Radioactive Waste Management in a Hospital. International Journal of Health Sciences.
- Kim, C. W., & Day, D. E. (2003). Immobilization of Hanford LAW in iron phosphate glasses. Journal of Non-Crystalline Solids, 331(1–3), 20–31.
- Kim, D., Buchmiller, W., Schweiger, M. J., Vienna, J. D., Day, D. E., Kim, C. W., … Workman, R. J. (2003). Iron Phosphate Glass as an Alternative Waste-Form for Hanford LAW. PNNL-14251, Pacific …, (February 2003).
- Kim, D.-S., & Hrma, P. (1991). Foaming in Glass Melts Produced by Sodium Sulfate Decomposition under Isothermal Conditions. Journal of the American Ceramic Society, 74(3), 551–555.
- Kim, J.-S., Kwon, S.-K., Sanchez, M., & Cho, G.-C. (2011). Geological storage of high level nuclear waste. KSCE Journal of Civil Engineering, 15(4), 721–737.
- Kiprianov, A. A., & Karpukhina, N. G. (2006). Oxyhalide silicate glasses. Glass Physics and Chemistry, 32(1), 1–27.
- Kiprianov, A. A., Karpukhina, N. G., & Molodozhen, V. A. (1998). Investigation into the Influence of Fluorine on the Bulk and Electrode Properties of Lithium Silicate Glasses. Vestn. St. Petersburg Gos. Univ. Ser. 4: Fiz. Khim, (3), 53–58.
- Kiprianov, A. A., Karpukhina, N. G., & Molodozhen, V. A. (2004). Investigation into the influence of chloride additives on the properties of alkali silicate glasses. Glass Physics and Chemistry, 30(4), 325–332.

- Kirchheim, R. (2003). On the mobility of alkaline earth ions in mixed alkali alkaline earth silicate glasses. Journal of Non-Crystalline Solids, 328(1–3), 157–163.
- Kitamura, N., Fukumi, K., Mizoguchi, H., Makihara, M., Higuchi, A., & Ohno, N. (1998). Structure of Densified Lithium Silicate Glasses.
- Konijnendijk, W. L., & Buster, J. H. J. M. (1977). Raman-scattering measurements of silicate glasses containing sulphate. Journal of Non-Crystalline Solids, 23(3), 401–418.
- Konijnendijk, W. L., & Stevels, J. M. (1975). The structure of borate glasses studied by Raman scattering. Journal of Non-Crystalline Solids, 18(3), 307–331.
- Konijnendijk, W. L., & Stevels, J. M. (1976). The structure of borosilicate glasses studied by Raman scattering. Journal of Non-Crystalline Solids, 20(2), 193–224.
- Konijnendijk, W. L., & Stevels, J. M. (1978). Structure of Borate and Borosilicate Glasses by Raman Spectroscopy. Borate Glasses: Structure, Properties, Applications (pp. 259–279). Boston, MA: Springer US.
- Kosson, D. S., Gallay, D. R., Pegg, I. L., Wymer, R. G., & Krahn, S. (2008). External Technical Review of System Planning for Low-Activity Waste Treatment at Hanford.
- Kruger, A. A. (2013). Advances in Glass Formulations for Hanford High-Aluminum, High-Iron and Enhanced Sulphate Management in HLW Streams – 13000. In WM2013 Conference (pp. 1–16).
- Kruger, A. A., Pegg, I. A., Kot, W. K., Gan, H., & Matlack, K. S. (2012). Enhanced Sulfate Management in HLW Glass Formulations, VSL 12R2540-1, Rev. 0 A.
- Kupfer, M. J., Boldt, A. L., Hodgson, K. N., Shelton, L. W., Simpson, B. C., Watrous, R. A., & Leclair, M. D. (1998). Standard Inventories of Chemicals and Radionuclides in Hanford Site Tank Wastes, 73, 109.
- Langowski, M. H. (1996). The Incorporation of P, S, Cr, F, CI, I, Mi Ti, U, and Bi into Simulated Nuclear Waste Glasses: Literature Study.
- Larson, C., Doerr, J., Affatigato, M., Feller, S., Holland, D., & Smith, M. E. (2006). A 29 Si MAS NMR study of silicate glasses with a high lithium content. Journal of Physics: Condensed Matter, 18(49), 11323.
- Laurent, O., Mantisi, B., & Micoulaut, M. (2014). Structure and topology of soda-lime silicate glasses: Implications for window glass. Journal of Physical Chemistry B, 118(44), 12750–12762.
- Lee, S. K. (2011). Simplicity in melt densification in multicomponent magmatic reservoirs in Earth's interior revealed by multinuclear magnetic resonance. Proceedings of the National Academy of Sciences, 108(17), 6847–6852.
- Lee, S. K., & Stebbins, J. F. (2003). The distribution of sodium ions in aluminosilicate glasses: A high-field Na-23 MAS and 3Q MAS NMR study. Geochimica et Cosmochimica Acta, 67(9), 1699–1709.
- Lee, S., Mysen, B., & Cody, G. (2003). Chemical order in mixed-cation silicate glasses and melts. Physical Review B, 68(21), 1–7.
- Lee, W. E., Ojovan, M. I., Stennett, M. C., & Hyatt, N. C. (2006). Immobilisation of radioactive waste in glasses, glass composite materials and ceramics. Advances in Applied Ceramics, 105(1), 3–12.

- Lenoir, M., Grandjean, A., Dussossoy, J., Neuville, D. R., Chimie, I. De, Marcoule, S. De, & Nanomatériaux, L. (2008). Sulphate Incorporation in Borosilicate Glasses and Melts : a Kinetic Approach, (September), 20–26.
- Lenoir, M., Grandjean, A., Linard, Y., Cochain, B., & Neuville, D. R. (2008). The influence of Si, B substitution and of the nature of network-modifying cations on the properties and structure of borosilicate glasses and melts. Chemical Geology, 256(3–4), 315–324.
- Lenoir, M., Grandjean, A., Poissonnet, S., & Neuville, D. R. (2009). Quantitation of sulfate solubility in borosilicate glasses using Raman spectroscopy. Journal of Non-Crystalline Solids, 355(28–30), 1468–1473.
- Lenoir, M., Neuville, D. R., Malki, M., & Grandjean, A. (2010). Volatilization kinetics of sulphur from borosilicate melts: A correlation between sulphur diffusion and melt viscosity. Journal of Non-Crystalline Solids, 356(50–51), 2722–2727.
- Li, H., Hrma, P. R., & Vienna, J. D. (2000). Sulfate retention and segregation in simulated radioactive waste borosilicate glasses.
- Li, H., Hrma, P., Vienna, J. D., Qian, M., Su, Y., & Smith, D. E. (2003). Effects of Al_2O_3, B_2O_3, Na_2O, and SiO_2 on nepheline formation in borosilicate glasses: Chemical and physical correlations. Journal of Non-Crystalline Solids, 331(1–3), 202–216.
- Li, H., Vienna, J. D., & Hrma, P. (1996). Borosilicate based glasses for immobilization of plutonium-bearing materials.
- Liberge, R., Desvaux, J. L., Pageron, D., & Saliceti, C. (1998). Industrial Experience of HLW Vitrification at La Hague and Marcoule. Waste Management, 98, 5–14.
- Lifanov, F. A., Sobolev, I. A., Dimitriev, S. A., & Stefanovsky, S. V. (2004). vitrification of low and intermediate level waste: Technology and Glass Performance. In WM'04 Conference (pp. 9–11).
- Li-Jun, L., Jin-Ying, L., & Dong-Sheng, Q. (2009). Dependence of Sulfate solubility on waste glass composition during vitrification of high level wastes. Journal of Nuclear and Radiochemistry, 31(2), 11.
- Lin, C. C., Chen, S. F., Liu, L. gun, & Li, C. C. (2007). Anionic structure and elasticity of Na_2O-MgO-SiO_2 glasses. Journal of Non-Crystalline Solids, 353(4), 413–425.
- Liu, H., Smedskjaer, M. M., Tao, H., Jensen, L. R., Zhao, X., Yue, Y. Z., Yue, Y. (2016). A medium range order structural connection to the configurational heat capacity of borate-silicate mixed glasses. Phys. Chem. Chem. Phys. Phys. Chem. Chem. Phys, 0, 1–3.
- Liu, Y., Samaha, N. T., & Baker, D. R. (2007). Sulfur concentration at sulfide saturation (SCSS) in magmatic silicate melts. Geochimica et Cosmochimica Acta, 71(7), 1783–1799.
- Lobsinger, R. J. (1974). Fast breeder reactor fuel cladding.
- Long, D. A. (2002). The Raman Effect: a unified treatment of the theory of Raman scattering by molecules. West Sussex, England: John Wiley & Sons Ltd (Vol. 8).
- López, A., Frost, R. L., Xi, Y., & Scholz, R. (2013). A vibrational spectroscopic study of the sulphate mineral glauberite. Spectroscopy Letters, 47(10), 740–745.
- Lorier, T. H., Reamer, I. a., & Workman, R. J. (2005). Initial sulfate solubility study for sludge batch 4 (SB4).

- Loubser, M., Strydom, C., & Potgieter, H. (2004). A thermogravimetric analysis study of volatilization of flux mixtures used in XRF sample preparation. X-Ray Spectrometry, 33(3), 212–215.
- Lovera, P., Le Bescop, P., Adenot, F., Li, G., Tanaka, Y., & Owaki, E. (1997). Physico-chemical transformations of sulphated compounds during the leaching of highly sulphated cemented wastes. Cement and Concrete Research, 27(10), 1523–1532.
- Luckscheiter, B., & Nesovic, M. (1996). Development of glasses for the vitrification of High Level Liquid Waste (HLLW) in a joule heated ceramic melter. Waste Management, 16(7), 571–578.
- Lutze, W. (1988). Silicate glasses. In Radioactive waste forms for the future.
- Lyle, A. K., Horak, W., & Sharp, D. E. (1936). The Effect of Alumina upon the Chemical Durability of Sand-Soda-Lime Glasses. Journal of the American Ceramic Society, 19(1–12), 142–147.
- Maekawa, H., Maekawa, T., Kawamura, K., & Yokokawa, T. (1991). The structural groups of alkali silicate glasses determined from 29Si MAS-NMR. Journal of Non-Crystalline Solids, 127(1), 53–64.
- Maekawa, H., Nakao, T., Shimokawa, S., & Yokokawa, T. (1997). Coordination of sodium ions in NaAlO 2 -SiO 2 melts: a high temperature 23 Na NMR study. Physics and Chemistry of Minerals, 24(1), 53–65.
- Manaktala, H. K. (1992). An Assessment of Borosilicate Glass as a High-Level Waste Form. Center for Nuclear Waste Regulatory Analyses San Antonio, Texas.
- Manara, D., Grandjean, A., & Neuville, D. R. (2009). Advances in understanding the structure of borosilicate glasses: A Raman spectroscopy study. American Mineralogist, 94(5–6), 777–784.
- Manara, D., Grandjean, A., Pinet, O., Dussossoy, J. L., & Neuville, D. R. (2007). Sulfur behavior in silicate glasses and melts: Implications for sulfate incorporation in nuclear waste glasses as a function of alkali cation and V2O5 content. Journal of Non-Crystalline Solids, 353(1), 12–23.
- Maniu, D., Ardelean, I., & Iliescu, T. (1995). Raman spectroscopic investigations of the structure of $xV_2O_5 \cdot (1 - x)$ [3 $B_2O_3 \cdot K_2O$] glasses. Materials Letters, 25(3–4), 147–149.
- Maniua, D., Iliescu, T., Ardelean, I., Cinta-Pinzaru, S., Tarcea, N., & Kiefer, W. (2003). Raman study on B_2O_3-CaO glasses. Journal of Molecular Structure, 651–653(March 2014), 485–488.
- Mannan, S. L., Chetal, S. C., Raj, B., & Bhoje, S. B. (2003). Selection of materials for prototype fast breeder reactor. Transactions-Indian Institute of Metals, 56(2), 155–178.
- Marion, L., Agnès, G., Jean-luc, D., Aurélien, L., Dit, C. A. U., Céline, C., & Marcoule, C. De. (2009). Sulphate in liquid nuclear wastes: from production to containment, (January).
- Marivoet, J., Volckaert, G., Labat, S., De Canniere, P., Dierckx, A., Kursten, B., others. (1999). Geological disposal of conditioned high-level and long-lived radioactive waste. Values for the near Field and Clay Parameters Used in the Perfomance Assessment of the Geological Disposal of Radioactive Waste in the Boom Clay Formation at the Mol Site, Vols, 1.
- Marples, J. A. C. (1988). The preparation, properties, and disposal of vitrified high-level waste from nuclear fuel reprocessing. Glass Technology, 29(6), 230–247.
- Marra, J. C., & Fox, K. M. (2014). Chemical Analysis of Simulated High-Level Waste Glasses to Support Sulfate Solubility Modeling.

- Marra, J. C., Andrews, M. K., & Schumacher, R. F. (1994). Vitrification in the presence of molten salts.
- Martel, L., Massiot, D., & Deschamps, M. (2014). Phase separation in sodium silicates observed by solid-state MAS-NMR. Journal of Non-Crystalline Solids, 390, 37–44.
- Mason, J. (2012). Multinuclear NMR. Springer Science & Business Media.
- Matson, D. W., Sharma, S. K., & Philpotts, J. A. (1983). The structure of high-silica alkali-silicate glasses. A Raman spectroscopic investigation. Journal of Non-Crystalline Solids, 58(2–3), 323–352.
- Matsuda, M., Nishi, T., & Kikuchi, M. (1992). Solidification of Spent Ion Exchange Resin Using New Cementitious Material, (II). Journal of Nuclear Science and Technology, 29(11), 1093–1099.
- McCloy, J., Washton, N., Gassman, P., Marcial, J., Weaver, J., & Kukkadapu, R. (2015). Nepheline crystallization in boron-rich alumino-silicate glasses as investigated by multi-nuclear NMR, Raman, & Mössbauer spectroscopies. Journal of Non-Crystalline Solids, 409, 149–165.
- McGann, O. J., Bingham, P. A., Hand, R. J., Gandy, A. S., Kavčič, M., Žitnik, M., … Hyatt, N. C. (2012). The effects of γ-radiation on model vitreous wasteforms intended for the disposal of intermediate and high level radioactive wastes in the United Kingdom. Journal of Nuclear Materials, 429(1), 353–367.
- McGrail, B. P., Icenhower, J. P., Shuh, D. K., Liu, P., Darab, J. G., Baer, D. R., … Nachimuthu, P. (2001). The structure of Na_2O-Al_2O_3-SiO_2 glass: Impact on sodium ion exchange in H2O and D2O. Journal of Non-Crystalline Solids, 296(1–2), 10–26.
- McGrail, B. P., Kumar, A., & Day, D. E. (1984). Sodium diffusion and leaching of simulated nuclear waste glass. Journal of the American Ceramic Society, 67(7), 463–467.
- Mckay, H. A. C. (1990). The PUREX process. In Science and technology of tribuytl phosphate.
- McKeown, D. A., Gan, H., Pegg, I. L., Stolte, W. C., & Demchenko, I. N. (2011). X-ray absorption studies of chlorine valence and local environments in borosilicate waste glasses. Journal of Nuclear Materials, 408(3), 236–245.
- McKeown, D. A., Muller, I. S., Gan, H., Pegg, I. L., & Kendziora, C. A. (2001). Raman studies of sulfur in borosilicate waste glasses: Sulfate environments. Journal of Non-Crystalline Solids, 288(1–3), 191–199.
- McKeown, D. A., Muller, I. S., Gan, H., Pegg, I. L., & Stolte, W. C. (2004). Determination of sulfur environments in borosilicate waste glasses using X-ray absorption near-edge spectroscopy. Journal of Non-Crystalline Solids, 333(1), 74–84.
- McKeown, D. A., Muller, I. S., MAtlack, K. S., & Pegg, I. L. (2002). X-ray absorption studies of vanadium valence and local environment in borosilicate waste glasses using vanadium sulfide, silicate, and oxide standards. Journal of Non-Crystalline Solids, 298, 160–175.
- Mckibben, J. M., Chostener, D. F., & Orebaugh, E. G. (1983). Plutonium-uranium separation in the purex process using mixtures of hydroxylamine nitrate and ferrous sulfamate by this report was prepared as an account of work sponsored by an agency of the United States Government. Neither the United States Government.

- McLain, S. E., Bowron, D. T., Hannon, A. C., & Soper, A. K. (2006). GUDRUN, a computer program developed for analysis of neutron diffraction data. ISIS Facility, Rutherford Appleton Laboratory, Chilton, UK.
- McMillan, P. F. (1984). Structural Studies of Silicate Glasses and Melts-Applications and Limitations of Raman Spectroscopy. American Mineralogist, 69, 622–644.
- McMillan, P., & Piriou, B. (1983). Raman spectroscopic studies of silicate and related glass structure - a review. Bull. Mineral.
- Meera, B. N., & Ramakrishna, J. (1993). Raman spectral studies of borate glasses. Journal of Non-Crystalline Solids, 159(1–2), 1–21.
- Meera, B. N., Sood, a. K., Chandrabhas, N., & Ramakrishna, J. (1990). Raman study of lead borate glasses. Journal of Non-Crystalline Solids, 126, 224–230.
- Megahed, A. A. (1999). Density of mixed alkali silicate glasses. Physics and Chemistry of Glasses, 40(3), 130–134.
- Melnyk, F. W., Walton, F. B., & Johnson, L. H. (1984). High-level waste glass field burial test: leaching and migration of fission products. Nuclear and Chemical Waste Management, 5(1), 49–62.
- Mernagh, T. P., & Trudu, A. G. (1993). A laser Raman microprobe study of some geologically important sulphide minerals. Chemical Geology, 103(1), 113–127.
- Merrill, R. A., Whittington, K. F., & Peters, R. D. (1994). Vitrification of high sulfate wastes (PNL-SA-24672).
- Merritt, R. C. (1971). Extractive metallurgy of uranium.
- Metcalfe, B., & Donald, I. W. (2004). Candidate wasteforms for the immobilization of chloride-containing radioactive waste. Journal of Non-Crystalline Solids, 348, 225–229.
- Mishra, R. K., Kumar, S., Tomar, B. S., Tyagi, A. K., Kaushik, C. P., Raj, K., & Manchanda, V. K. (2008). Effect of barium on diffusion of sodium in borosilicate glass. Journal of Hazardous Materials, 156(1–3), 129–134.
- Mishra, R. K., Sudarsan, K. V., Sengupta, P., Vatsa, R. K., Tyagi, A. K., Kaushik, C. P., … Raj, K. (2008). Role of sulfate in structural modifications of sodium barium borosilicate glasses developed for nuclear waste immobilization. Journal of the American Ceramic Society, 91(12), 3903–3907.
- Mitchell, T. N., & Costisella, B. (2004). NMR-From Spectra to Structures, an Experimental Approach (Second Edi).
- Miyake, M., Minato, I., Morikawa, H., & Iwai, S. (1978). Crystal structures and sulphate force constants of barite, celestite, and anglesite. American Mineralogist, 63(5-6), 506-510.
- Möncke, D., Tricot, G., Winterstein-Beckmann, A., Wondraczek, L., & Kamitsos, E. I. (2015). On the connectivity of borate tetrahedra in borate and borosilicate glasses. Physics and Chemistry of Glasses: European Journal of Glass Science and Technology Part B, 56(5), 203–211.
- Moretti, R. (2005). Polymerisation, basicity, oxidation state and their role in ionic modelling of silicate melts. Annals of Geophysics, 48(4–5), 583–608.
- Moretti, R., & Ottonello, G. (2005). Solubility and speciation of sulfur in silicate melts: The Conjugated Toop-Samis-Flood-Grjotheim (CTSFG) model. Geochimica et Cosmochimica Acta, 69(4), 801–823.

- Morizet, Y., Gennaro, E., Jego, S., Zajacz, Z., Iacono-Marziano, G., Pichavant, M., Lesne, P. (2017). A Raman calibration for the quantification of SO_4^{2-} groups dissolved in silicate glasses: Application to natural melt inclusions. American Mineralogist, 102(10), 2065–2076.
- Motz, J. W., & Missoni, G. (1961). Compton Scattering by K-Shell Electrons. Phys. Rev., 124(5), 1458–1468.
- Mountjoy, G. (2007). The local atomic environment of oxygen in silicate glasses from molecular dynamics. Journal of Non-Crystalline Solids, 353(18–21), 1849–1853.
- Moyer, B. A., Custelcean, R., Hay, B. P., Sessler, J. L., Bowman-James, K., Day, V. W., & Kang, S. O. (2013). A case for molecular recognition in nuclear separations: Sulfate separation from nuclear wastes. Inorganic Chemistry, 52(7), 3473–3490.
- Mudd, G. M. (2014). The future of Yellowcake: A global assessment of uranium resources and mining. Science of the Total Environment, 472, 590–607.
- Mudd, G. M., & Diesendorf, M. (2008). Sustainability of uranium mining and milling: toward quantifying resources and eco-efficiency. Environmental Science & Technology, 42(7), 2624–2630.
- Muller-Warmuth, W., & Eckert, H. (1982). Nuclear Magnetic Resonance and Mossbauer Spectroscopy of Glasses.
- Murdoch, J. B., & Stebbins, J. F. (1985). High-resolution 29Si NMR study of silicate and aluminosilicate glasses: the effect of network-modifying cations. American Mineralogist, 70, 332–343.
- Murray, R. L. (1981). Understanding radioactive waste.
- Mysen, B. O., & Frantz, J. D. (1992). Raman spectroscopy of silicate melts at magmatic temperatures: Na_2O-SiO_2, K_2O- SiO_2 and Li_2O- SiO_2 binary compositions in the temperature range 25–1475°C. Chemical Geology, 96(3), 321–332.
- Mysen, B. O., Finger, L. W., Virgo, D., & Seifert, F. A. (1982). Curve-fitting of Raman spectra of silicate glasses. American Mineralogist, 67(7–8), 686–695.
- Mysen, B. O., Virgo, D., & Scarfe, C. M. (1980). Relations between anionic structure and viscosity of silicate melts - A Raman spectroscopic study. American Mineralogist, 65, 690–710.
- Mysen, B. O., Virgo, D., & Seifert, F. A. (1982). The structure of silicate melts: Implications for chemical and physical properties of natural magma. Reviews of Geophysics, 20(3), 353–383.
- Nagashima, S., & Katsura, T. (1973). The Solubility of Sulfur in Na_2O--SiO_2 Melts under Various Oxygen Partial Pressures at 1100° C, 1250° C, and 1300° C. Bulletin of the Chemical Society of Japan, 46(10), 3099–3103.
- Namikawa, H. (1974). Multichannel conduction in alkali silicate glasses. Journal of Non-Crystalline Solids, 14(1), 88–100.
- Natarajan, R. (2017). Reprocessing of spent nuclear fuel in India: Present challenges and future programme. Progress in Nuclear Energy, 101, 118–132.
- NEA, N. S. C. (1997). Actinide Separation Chemistry in Nuclear Waste Streams and Materials.
- NEA. (2000). Pyrochemical Separations. Pyrochemical Separations : Workshop Proceedings.
- NEA. (2012). Spent nuclear fuel reprocessing flowsheet.

- Neuville, D. R. (2006). Viscosity, structure and mixing in (Ca, Na) silicate melts. Chemical Geology, 229(1–3), 28–41.
- Newbury, D. E., & Ritchie, N. W. M. (2013). Is scanning electron microscopy/energy dispersive X-ray spectrometry (SEM/EDS) quantitative? Scanning, 35(3), 141–168.
- Nikiforov, A. S., Zakharova, K. P., & Polyakov, A. S. (1986). Physicochemical foundations of bituminization of liquid radioactive wastes from a nuclear power plant with RBMK reactor and the properties of the compounds formed. Atomic Energy, 61(3), 664–669.
- Nishida, T. (1994). 57-Fe and 119Sn Mossbauer effect of oxide glasses. Journal of Radioanalytical and Nuclear Chemistry, 182(2), 451–476.
- NRC. (1957). the Disposal of Radioactive Waste on Land. Washington, DC: The National Academies Press.
- NRC. (2003). Improving the Regulation and Management of Low-Activity Radioactive Wastes: Interim report on current regulations, inventories and practices.
- Nyquist, R. A., & Kagel, R. O. (2012). Handbook of infrared and Raman spectra of inorganic compounds and organic salts: infrared spectra of inorganic compounds (Vol. 4). Academic press.
- Occhipinti, J. E., Carter, J. T., Edwards, R. E., Beck, R. S., & Iverson, D. C. (1998). Defense Waste Processing Facility Radioactive Operations-Year Two.
- OECD. (2002). Engineered Barrier Systems (EBS) in the Safety Case. In NEA workshop proceedings (pp. 3–116).
- OECD. (2006). Physics and Safety of Transmutation Systems: A status report. NEA (Vol. 6090).
- OECD. (2010). Radioactive Waste in Perspective (NEA No. 6350). Nuclear Energy Agency.
- Ohigashi, T., Watanabe, N., Aota, T., Takano, H., Takeuchi, A., & Aoki, S. (2002). Elemental analysis with a full field X-ray Fluorescence microscope and a CCD photon-counting system. Journal of Synchrotron Radiation, 9, 128–131.
- Ojovan, M. I., & Batyukhnova, O. G. (2007). Glasses for Nuclear Waste Immobilization. In WM ’07 Conference (p. 15).
- Ojovan, M. I., & Lee, W. E. (2005). An Introduction to Nuclear Waste Immobilisation (Oxford: Elsevier).
- Ojovan, M. I., & Lee, W. E. (2011). Glassy wasteforms for nuclear waste immobilization. Metallurgical and Materials Transactions A: Physical Metallurgy and Materials Science, 42(4), 837–851.
- Okoshi, M., & Nakayama, S. (2015). Generation and Characteristics of Radioactive Wastes. In Radioactive Waste Engineering and Management (pp. 17–46).
- Ooura, M., & Hanada, T. (1998). Compositional Dependence of Solubility of Sulfate in Silicate Glasses. Glass Technol., 39(2), 68–73.
- Orlhac, X., Fillet, C., & Phalippou, J. (1999). Study of crystallization mechanisms in the French nuclear waste glass. MRS Online Proceedings Library Archive, 556.
- Osipov, A. A., & Osipova, L. M. (2009). Structure of glasses and melts in the Na_2O-B_2O_3 system from high-temperature Raman spectroscopic data: II. Superstructural units in melts. Glass Physics and Chemistry, 35(2), 132–140.

- Osipov, A. A., & Osipova, L. M. (2013). Raman scattering study of barium borate glasses and melts. Journal of Physics and Chemistry of Solids, 74(7), 971–978.
- Osipov, A. A., Osipova, L. M., & Eremyashev, V. E. (2013). Structure of alkali borosilicate glasses and melts according to Raman spectroscopy data. Glass Physics and Chemistry, 39(2), 105–112.
- Osmanlioglu, A. E. (2002). Immobilization of radioactive waste by cementation with purified kaolin clay. Waste Management, 22(5), 481–483.
- Pacary, V., Barré, Y., & Plasari, E. (2010). Method for the prediction of nuclear waste solution decontamination by coprecipitation of strontium ions with barium sulphate using the experimental data obtained in non-radioactive environment. Chemical Engineering Research and Design, 88(9), 1142–1147.
- Pant, A. K. (1968). A reconsideration of the crystal structure of {$β$}-Na${\sb 2}$Si${\sb 2}$O${\sb 5}$. Acta Crystallographica Section B, 24(8), 1077–1083.
- Pant, A. K., & Cruickshank, D. W. J. (1968). The crystal structure of {$α$}-Na${\sb 2}$Si${\sb 2}$O${\sb 5}$. Acta Crystallographica Section B, 24(1), 13–19.
- Papadopoulos, K. (1973). Solubility of SO3 in soda -lime-silicate- melts. Physics and Chemistry of Glasses, 14(3), 60–65.
- Park, S. Y., & Lee, S. K. (2016). Effects of Difference in Ionic Radii on Chemical Ordering in Mixed-Cation Silicate Glasses: Insights from Solid-State 17O and 7Li NMR of Li???Ba Silicate Glasses. Journal of the American Ceramic Society, 99(12), 3948–3956.
- Parkinson, B. G., Holland, D., Smith, M. E., Larson, C., Doerr, J., Affatigato, M., Scales, C. R. (2008). Quantitative measurement of Q^3 species in silicate and borosilicate glasses using Raman spectroscopy. Journal of Non-Crystalline Solids, 354(17), 1936–1942.
- Paul, A. (1977). Chemical durability of glasses; a thermodynamic approach. Journal of Materials Science, 12(11), 2246–2268.
- Peeler, D., Kim, D.-S., Vienna, J., Scheiger, M., & Piepel, G. (2015). Office of River Protection Advanced Low-Activity Waste Glass Research and Development Plan.
- Persson, H. R. (1962). Improvement of the chemical durability of soda-lime-silica glass bottles by treating with various agents. Glass Technology, 3(1), 17–35.
- Pichestapong, P., Sriwiang, W., & Injarean, U. (2016). Separation of Yttrium-90 from Strontium-90 by Extraction Chromatography Using Combined Sr Resin and RE Resin. Energy Procedia, 89, 366–372.
- Plecas, I. B., Peric, A. D., Drljaca, J. D., Kostadinovic, A. M., & Glodic, S. D. (1992). Immobilization of radioactive waste water residues in a cement matrix. Cement and Concrete Research, 22(4), 571–576.
- Plodinec, M. J. (2000). Borosilicate glasses for nuclear waste immobilisation. Glass Technology, 41(6), 186–192.
- Plodinec, M. J., & Wiley, J. R. (1979). Evaluation of glass as a matrix for solidifying Savannah River Plant Waste: Properties of Glasses containing Li_2O.
- Potts, P. J. (1987). Inductively coupled plasma-atomic emission spectrometry. In A Handbook of Silicate Rock Analysis (pp. 153–197). Dordrecht: Springer Netherlands.

- Potts, P. J., & Webb, P. C. (1992). X-ray fluorescence spectrometry. Journal of Geochemical Exploration, 44(1), 251–296.
- Pyare, R., & Nath, P. (1991). Free oxygen ion activity in binary alkali silicate glasses. Journal of Non-Crystalline Solids, 128(2), 154–161.
- Qvist, S. A., & Brook, B. W. (2015). Potential for Worldwide Displacement of Fossil-Fuel Electricity by Nuclear Energy in Three Decades Based on Extrapolation of Regional Deployment Data. PLOS ONE, 1–10.
- Rabinovich, E. M. (1967). On the behavior of fluorine in silicate glasses. Izv. Akad. Nauk SSSR, Neorg. Mater, 3(5), 855–859.
- Rai, M., & Mountjoy, G. (2014). Molecular dynamics modelling of the structure of barium silicate glasses $BaO\text{-}SiO_2$. Journal of Non-Crystalline Solids, 401, 159–163.
- Raj, K., Prasad, K. K., & Bansal, N. K. (2006). Radioactive waste management practices in India. Nuclear Engineering and Design, 236(7–8), 914–930.
- Ramkumar, J., Chandramouleeswaran, S., Sudarsan, V., Mishra, R. K., Kaushik, C. P., Raj, K., & Tyagi, A. K. (2009). Barium borosilicate glass as a matrix for the uptake of dyes. Journal of Hazardous Materials, 172(1), 457–464.
- Ramsey, W. G. (1995). Compositions and durabilities of glasses for immobilization of Plutonium and Uranium
- Range, C., & Charpentier, T. (2017). Mixed network formers and modifiers, borosilicate and boroaluminosilicate glasses : a NMR point of view.
- Raptis, C. (1986). Evidence of temperature-defect-induced first-order Raman scattering in pure NaCl crystals. Physical Review B, 33(2), 1350–1352.
- Rechard, R. P. (1995). Performance assessment of the direct disposal in unsaturated tuff of spent nuclear fuel and high-level waste owned by US Department of Energy.
- Riley, A., Walker, S., & Gribble, N. R. (2009). Composition Changes and Future Challenges for the Sellafield Waste Vitrification Plant. MRS Proceedings, 1193.
- Ringwood, 1 A E, Kesson, S. E., Ware, N. G., Hibberson, W., & Major, A. (1979). Immobilisation of high level nuclear reactor wastes in SYNROC. Nature, 278(5701), 219.
- Ringwood, A. E., Kesson, S. E., Reeve, K. D., Levins, D. M., & Ramm, E. J. (1988). Synroc. In Radioactive waste forms for the future.
- Roca, A. G., Marco, J. F., Morales, M. del P., & Serna, C. J. (2007). Effect of nature and particle size on properties of uniform magnetite and maghemite nanoparticles. The Journal of Physical Chemistry C, 111(50), 18577–18584.
- Roderick, J. M., Holland, D., & Scales, C. R. (2000). Characterisation and radiation resistance of a mixed alkali borosilicate glass for high level waste vitrification. Physics and Chemistry of Glasses, 41(6), 392–395.
- Roderick, J. M., Holland, D., Howes, A. P., & Scales, C. R. (2001). Density-structure relations in mixed-alkali borosilicate glasses by 29Si and 11B MAS-NMR. Journal of Non-Crystalline Solids, 293–295(1), 746–751.

- Roth, G., & Weisenburger, S. (2000). Vitrification of high-level liquid waste: Glass chemistry, process chemistry and process technology. Nuclear Engineering and Design, 202(2–3), 197–207.
- Ru, E. C. Le, & Etchegoin, P. G. (2009). Principles of Surface-Enhanced Raman Spectroscopy.
- Samskog, L.-E., Van Santen, A., & Tornblom, L. (1971). Fuel assembly for nuclear reactors. Google Patents.
- Sandland, T. O., Du, L. S., Stebbins, J. F., & Webster, J. D. (2004). Structure of Cl-containing silicate and aluminosilicate glasses: A35Cl MAS-NMR study. Geochimica et Cosmochimica Acta, 68(24), 5059–5069.
- Saw, C. K., Lian, T., Day, S. D., & Farmer, J. C. (2006). X-ray Diffraction Techniques for Structural Determination of Amorphous Materials.
- Schaeffer, H. A., Mecha, J., & Steinmann, J. (1979). Mobility of Sodium Ions in Silica Glass of Different OH Content. Journal of the American Ceramic Society, 62(7–8), 343–346.
- Schlenz, H., Kirfel, A., Schulmeister, K., Wartner, N., Mader, W., Raberg, W., Neuefeind, J. (2002). Structure analyses of Ba-silicate glasses. Journal of Non-Crystalline Solids, 297(1), 37–54.
- Schofield, J. M. (2011). Vitrification of a chloride containing actinide waste surrogate.
- Schofield, J. M., Bingham, P. A., & Hand, R. J. (2009). The immobilisation of a chloride containing actinide waste surrogate in calcium aluminosilicate glasses. Ceramic Transactions, 207, 69–80.
- Schreiber, H. D., & Hockman, A. L. (1987). Redox chemistry in candidate glasses for nuclear waste immobilization. Journal of the American Ceramic Society, 70(8), 591–594.
- Schreiber, H. D., & Stokes, M. E. (2002). Ehnacing the sulfate capacity of glasses for nuclear waste immobilization. Journal of Undergraduate Chemistry Research, 2, 53–58.
- Schreiber, H. D., Kozak, S. J., Leonhard, P. G., & McManus, K. K. (1987). Sulfur chemistry in a borosilicate melt Pt 1. Glastechnische Berichte, 60(13), 589–598.
- Sengupta, P. (2012). A review on immobilization of phosphate containing high level nuclear wastes within glass matrix--Present status and future challenges. Journal of Hazardous Materials, 235, 17–28.
- Sengupta, P., Dey, K. K., Halder, R., Ajithkumar, T. G., Abraham, G., Mishra, R. K., Dey, G. K. (2015). Vanadium in borosilicate glass. Journal of the American Ceramic Society, 98(1), 88–96.
- Sengupta, P., Kaushik, C. P., & Dey, G. K. (2013). Immobilization of High Level Nuclear Wastes: The Indian Scenario. In on a Sustainable Future of the Earth's Natural Resources (pp. 25–51).
- Seong-won, P., Pomper, M. A., & Scheinman, L. (2010). The domestic and international politics of spent nuclear fuel in South Korea: are we approaching meltdown? Korea Economic Institute Academic Paper Series, 5(3).
- Seuthe, T., Grehn, M., Mermillod-Blondin, A., Bonse, J., & Eberstein, M. (2013). Compositional dependent response of silica-based glasses to femtosecond laser pulse irradiation. Proc. of SPIE, 8885(March 2014), 88850M.
- Shannon, R. D. (1976). Revised effective ionic radii and systematic studies of interatomic distances in halides and chalcogenides. Acta Crystallographica Section A, 32(5), 751–767.
- Shartsis, L., Spinner, S., & Capps, W. (1952). Density, Expansivity, and Viscosity of Molten Alkali Silicates. Journal of the American Ceramic Society, 35(6), 155–160.

- Shelby, J. E. (2005). Introduction to Glass Science and Technology. The Royal Society of Chemistry.
- Sheng, J. (2004). Vitrification of a spent ion exchanged resin from a nuclear power plant. Glass Technology, 45(3), 153–6.
- Sheng, J., Choi, K., Yang, K.-H., Lee, M.-C., & Song, M.-J. (2000). Vitrification of polyvinyl chloride waste from Korean nuclear power plants. Nuclear Technology, 129(2), 246–256.
- Shermer, H. F. (1956). Thermal expansion of binary alkali silicate glasses. Journal of Research of the National Bureau of Standards, 57(2), 97.
- Sherry, A. (2014). Development of Advanced Reprocessing Technologies - Position Paper. National Nuclear Laboratory, 1–11.
- Signorelli, S., & Carroll, M. R. (2000). Solubility and fluid-melt partitioning of Cl in hydrous phonolitic melts. Geochimica et Cosmochimica Acta, 64(16), 2851–2862.
- Silver, A. H., & Bray, P. J. (1958). Nuclear magnetic resonance absorption in glass. I. Nuclear quadrupole effects in boron oxide, soda-boric oxide, and borosilicate glasses. The Journal of Chemical Physics, 29(5), 984–990.
- Singh, M. P., Sandhu, B. S., & Singh, B. (2007). Measurement of the effective atomic number of composite materials using Rayleigh to Compton scattering of 279 keV gamma rays. Physica Scripta, 76, 281–286.
- Siwadamrongpong, S., Koide, M., & Matusita, K. (2004). Prediction of chloride solubility in CaO-Al_2O_3-SiO_2 glass systems. Journal of Non-Crystalline Solids, 347(1–3), 114–120.
- Skoog, D. A., Holler, F. J., & Crouch, S. R. (2007). Principles of Instrumental Analysis. Thomson Brooks/Cole.
- Smets, B. M. J., Tholen, M. G. W., & Lommen, T. P. A. (1984). The effect of divalent cations on the leaching kinetics of glass. Journal of Non-Crystalline Solids, 65(2–3), 319–332.
- Smith, W. E., & Dent, G. (2005). Chapter 1 Introduction, Basic Theory and Principles. In Modern Raman spectroscopy - A practical approach (Vol. 5, pp. 1–21).
- Sobolev, A. I., Brykin, S. N., & Gorbunova, O. A. (2013). 10 - Russia: experience of radioactive waste (RAW) management and contaminated site clean-up BT - Radioactive Waste Management and Contaminated Site Clean-Up. Woodhead Publishing Series in Energy.
- Sobolev, I. A., Dmitriev, S. A., Lifanov, F. A., Kobelev, A. P., Stefanovsky, S. V., & Ojovan, M. I. (2005). Vitrification processes for low, intermediate radioactive and mixed wastes. Glass Technology, 46(1), 28–35.
- Soper, A. K. (2012). GudrunN and GudrunX : Programs for correcting raw neutron and x-ray total scattering data to differential cross section. ISIS Facility, Rutherford Appleton Laboratory, Chilton, UK.
- Spalding, B. P. (1994). Volatilization of cesium-137 from soil with chloride amendments during heating and vitrification. Environmental Science & Technology, 28(6), 1116–1123.
- Stebbins, J. F., & Du, L. S. (2002). Chloride ion sites in silicate and aluminosilicate glasses: A preliminary study by ^{35}Cl solid-state NMR. American Mineralogist, 87(2–3), 359–363.
- Stebbins, J. F., & Xu, Z. (1997). NMR evidence for excess non-bridging oxygen in an aluminosilicate glass. Nature, 390(6655), 60–62.

- Stefanovskii, S. V, Minaev, A. A., & Lifanov, F. A. (1989). Lead-silicate glasses with sodium sulfate. Glass and Ceramics, 46(4), 142–145.
- Stefanovskii, S. V. (1993). Immobilising sulphate bearing radioactive waste in glass. Phys. Chem. Mater. Treat. 27(2), 157–167.
- Stefanovsky, S. V, Yudintsev, S. V, Gieré, R., & Lumpkin, G. R. (2004). Nuclear waste forms. Geological Society, London, Special Publications, 236(1), 37 LP-63.
- Stefanovsky, S. V., Ivanov, I. A., & Gulin, A. N. (1995). Aluminophosphate glasses with high sulfate content. Materials Research Society Symposium - Proceedings, 353(1).
- Stolenberg, J., VanDyck, R., & Pengra, D. (2006). X-ray Fluorescence and Moseley's Law.
- Sullivan, G. K., Langowski, M. H., & Hrma, P. R. (1995). Sulfate segregation in vitrification of simulated Hanford nuclear waste. Ceramic Transactions, 61, 187–193.
- Tait, J. C., & Jensen, C. D. (1982). The effect of zn(ll) ion adsorption on the durability of sodium borosilicate glasses *. Journal of Non-Crystalline Solids, 49, 363–377.
- Tait, J. C., & Mandolesi, D. L. (1983). The chemical durability of alkali aluminosilicate glasses.
- Takeda, D., Matusita, K., & Koide, M. (2003). Thermal Properties of CaO-Al 2 O 3-SiO 2 glass containing chlorine. Journal of Ceramic Society of Japan, 111(5), 339–342.
- Tanaka, S. (2012, November). Accident at the Fukushima Dai-ichi Nuclear Power Stations of TEPCO —Outline & lessons learned—. (T. YAMAZAKI, Ed.), Proceedings of the Japan Academy. Series B, Physical and Biological Sciences. Tokyo, Japan.
- Terrani, K. A., Snead, L. L., & Gehin, J. C. (2012). Microencapsulated fuel technology for commercial light water and advanced reactor application. Journal of Nuclear Materials, 427(1), 209–224.
- Tison, E., & Bretault, P. (2006). COGEMA Experience in Uranous Nitrate Preparation. In WM'06 conference.
- Todd, M., & Janelle, E. (2012). HR-MAS NMR Spectroscopy in Material Science. Advanced Aspects of Spectroscopy, 279–306.
- Tokuda, Y., Takahashi, Y., Masai, H., Kaneko, S., Ueda, Y., Fujimura, S., & Yoko, T. (2015). Local structure of alkalis in mixed-alkali borate glass to elucidate the origin of mixed-alkali effect. Journal of Asian Ceramic Societies, 3(4), 412–416.
- Tsujimura, T., Xue, X., Kanzaki, M., & Walter, M. J. (2004). Sulfur speciation and network structural changes in sodium silicate glasses: Constraints from NMR and Raman spectroscopy. Geochimica et Cosmochimica Acta, 68(24), 5081–5101.
- Tsunawaki, Y., Iwamoto, N., Hattori, T., & Mitsuishi, A. (1981). Analysis of CaO- SiO_2 and CaO-SiO_2-CaF_2 glasses by Raman spectroscopy. Journal of Non-Crystalline Solids, 44(2–3), 369–378.
- Uhlig, H., Hoffmann, M. J., Lamparter, H.-P., Aldinger, F., Bellissent, R., & Steeb, S. (1996). Short-Range and Medium-Range Order in Lithium Silicate Glasses, Part I: Diffraction Experiments and Results. Journal of the American Ceramic Society, 79(11), 2833–2838.
- Vance, E. R., Davis, J., Olufson, K., Chironi, I., Karatchevtseva, I., & Farnan, I. (2012). Candidate waste forms for immobilisation of waste chloride salt from pyroprocessing of spent nuclear fuel. Journal of Nuclear Materials, 420(1–3), 396–404.

- Varshneya, A. K. (1994). Fundamentals of Inorganic Glasses. (A. K. Varshneya, Ed.), Fundamentals of Inorganic Glasses. San Diego: Academic Press.
- Vashman, A. A., & Polyakov, A. S. (1997). Phosphate glasses with radioactive waste. Tsniiatominform, Moscow, 172.
- Vassilev, T., Penkov, I., Tzvetkova, C., & Pascova, R. (2016). Glass transition temperatures and structures of multicomponent borate glasses: Influence of modifier cation field strengths. Journal of Non-Crystalline Solids, 438, 1–6.
- Verma, H. R. (2007). X-ray Fluorescence (XRF) and Particle-Induced X-ray Emission (PIXE). In Atomic and Nuclear Analytical Methods (pp. 1–90).
- Vessal, B., Wright, A. C., & Hannon, A. C. (1996). Alkali silicate glasses: Interpreting neutron diffraction results using the molecular dynamics simulation technique. Journal of Non-Crystalline Solids, 196, 233–238.
- Vienna, J. D. (2010). Nuclear Waste Vitrification in the United States: Recent Developments and Future Options. International Journal of Applied Glass Science, 1(3), 309–321.
- Vienna, J. D., Hrma, P. R., Buchmiller, W. C., & Ricklefs, J. S. (2004). Preliminary Investigation of Sulfur Loading in Hanford LAW Glass.
- Vienna, J. D., Kim, D.-S., Muller, I. S., Piepel, G. F., & Kruger, A. A. (2014). Toward Understanding the Effect of Low-Activity Waste Glass Composition on Sulfur Solubility. Journal of the American Ceramic Society, 97(10), 3135–3142.
- Villani, S. (1979). Uranium enrichment.
- Volf, M. B. (1984). Chemical approach to glass. Glass Science and Technology, 7, 465–469.
- Wassick, T. H., Doremus, R. H., Lanford, W. A., & Burman, C. (1983). Hydration of soda lime silicate glass, effect of alumina. Journal of Non-Crystalline Solids, 54, 139–151.
- Watanabe, M. (2015). Sample preparation for X-ray fluorescence analysis IV . Fusion bead method part 1 basic principles. The Rigaku Journal, 31(2), 12–17.
- Wattal, P. K. (2013). Indian programme on radioactive waste management. Sadhana - Academy Proceedings in Engineering Sciences (Vol. 38).
- Webb, G. A. (1995). Annual reports on NMR spectroscopy (Vol. 30). Academic Press.
- Webster, J. D. (1997). Chloride solubility in felsic melts and the role of chloride in magmatic degassing. Journal of Petrology, 38(12), 1793–1807.
- Webster, J. D., & De Vivo, B. (2002). Experimental and modelled solubilities of chlorine in aluminosilicate melts, consequences of magma evolution, and implications for exsolution of hydrous chloride melt at Mt. Somma-Vesuvius. American Mineralogist, 87(8–9), 1046–1061.
- Wei, Y., Liu, R., Wu, Y., Zu, J., Wang, X., & Chen, Z. (2013). Chromatographic separation of actinides and fission products. Energy Procedia, 39, 110–119.
- Weiss, W. (2016). Radiological Protection Issues Arising During and After the Fukushima Nuclear Reactor Accident—Memorandum of TG 84 of ICRP. Radiation Protection Dosimetry, 171(1), 20–22.
- White, M. J., Hicks, T. W., Mackenzie, J., McKinley, I., & Wilson, J. (2013). Geological Disposal Concept Options for Spent Fuel (Vol. 44).

- Wilke, M., Klimm, K., & Kohn, S. C. (2011). Spectroscopic Studies on Sulfur Speciation in Synthetic and Natural Glasses. Reviews in Mineralogy and Geochemistry, 73(1), 41–78.
- Williams, K. F. E., Johnson, C. E., & Thomas, M. F. (1998). Mössbauer spectroscopy measurement of iron oxidation states in float composition silica glasses. Journal of Non-Crystalline Solids, 226, 19–23.
- Wilson, P. D. (1996). The nuclear fuel cycle from ore to wastes.
- Winterstein-Beckmann, A., Möncke, D., Palles, D., Kamitsos, E. I., & Wondraczek, L. (2014). A Raman-spectroscopic study of indentation-induced structural changes in technical alkali-borosilicate glasses with varying silicate network connectivity. Journal of Non-Crystalline Solids, 405, 196–206.
- Wojcik, J., & Kamienska-Trela, K. (2013). Nuclear Magnetic Resonance (Vol. 42). Royal Society of Chemistry.
- Wojdyr, M. (2010). Fityk: A general-purpose peak fitting program. Journal of Applied Crystallography, 43(5 PART 1), 1126–1128.
- World Nuclear Association. (2011). uranium from mine to mill.
- World Nuclear Association. (2017). World Nuclear Performance Report 2017.
- World-nuclear.org. (2017). Radioactive Waste Management- www.world-nuclear.org.
- Wright, A. C. (1988). Neutron and X-ray amorphography. Journal of Non-Crystalline Solids, 106(1–3), 1–16.
- Wright, A. C. (1994). Neutron scattering from vitreous silica. V. The structure of vitreous silica: What have we learned from 60 years of diffraction studies? Journal of Non-Crystalline Solids, 179(C), 84–115.
- Wu, J., & Stebbins, J. F. (2009). Effects of cation field strength on the structure of aluminoborosilicate glasses: High-resolution 11B, 27Al and 23Na MAS NMR. Journal of Non-Crystalline Solids, 355(9), 556–562.
- Wymer, R. G. (n.d.). Spent Nuclear Reactor Fuel Reprocessing : Past, Present, and Future Why Should We Care About Reprocessing ?
- Xianyu Xue, Stebbins, J. F., & Kanzaki, M. (1994). Correlations between 17O NMR parameters and local structure around oxygen in high-pressure silicates: implications for the structure of silicate melts at high pressure. American Mineralogist, 79(1–2), 31–42.
- Xue, X., & Stebbins, J. F. (1993). 23Na NMR chemical shifts and local Na coordination environments in silicate crystals, melts and glasses. Physics and Chemistry of Minerals, 20(5), 297–307.
- Xuequan, W., Sheng, Y., Xiaodong, S., Mingshu, T., & Liji, Y. (1991). Alkali-activated slag cement based radioactive waste forms. Cement and Concrete Research, 21(1), 16–20.
- Yadav, A. K., & Singh, P. (2015). A review of the structures of oxide glasses by Raman spectroscopy. RSC Adv., 5(83), 67583–67609.
- Yamada, Y. (2010). X-ray fluorescence analysis by fusion bead method for. The Rigaku Journal, 26(2), 15–23.
- Young, A. L. (2012). XRD-Powder X-ray Diffraction and its Application to Biotherapeutic Formulation Development. American Pharmaceutical Review, 15(1), 74.

- Yun, Y. H., & Bray, P. J. (1978). Nuclear magnetic resonance studies of the glasses in the system Na_2O B_2O_3 SiO_2. Journal of Non-Crystalline Solids, 27(3), 363–380.
- Zachariasen, W. H. (1932). The atomic arrangement in glass. Journal of the American Chemical Society, 54(10), 3841–3851.
- Zhang, H., Corkhill, C. L., Heath, P. G., Hand, R. J., Stennett, M. C., & Hyatt, N. C. (2015). Effect of Zn- and Ca-oxides on the structure and chemical durability of simulant alkali borosilicate glasses for immobilisation of UK high level wastes. Journal of Nuclear Materials, 462, 321–328.
- Zhao, P., Kroeker, S., & Stebbins, J. F. (2000). Non-bridging oxygen sites in barium borosilicate glasses: Results from 11B and 17O NMR. Journal of Non-Crystalline Solids, 276(1), 122–131.
- Zheng, M., Wang, H., Haizheng, T., Yourong, H., & Hong, J. (2014). The effect of tin on sulfur K-edge X-ray absorption near edge structure spectra of soda-lime-silicate glass: An experimental and comparative study. Journal of Non-Crystalline Solids, 383, 714.

APPENDIX A

Chemical Formula	Purity	Delivered by:
Na_2CO_3	> 99%	Better Equipped/ ACROS organics
Li_2CO_3	>99%	Better Equipped
K_2CO_3	>99%	Better Equipped
Cs_2CO_3	>99%	Sigma Aldrich
$CaCO_3$ (precipitated)	>99%	Better Equipped
$MgCO_3$	99%	Better Equipped
$BaCO_3$	99%	Alfa Aesar
H_3BO_3	99%	Better Equipped/ ACROS organics
H_3BO_3 (Isotopically enriched)	^{11}B: 99.27%	Eagle Picher
B_2O_3 (Isotopically enriched)	^{11}B: 99.62%	Sigma Aldrich
Fe_2O_3	98% metals basis	Alfa Aesar
Na_2SO_4 (anhydrous)	>99%	Sigma Aldrich
Li_2SO_4	99%	Sigma Aldrich
$BaSO_4$	>99%	Better Equipped
$V_2(SO_4)_3$	99.9% metals basis	Alfa Aesar
V_2O_5	99.6%	Alfa Aesar
$Al(OH)_3$	99%	Better Equipped
Al_2O_3	>99%	Better Equipped
NaCl	>99%	Better Equipped
NH_4Cl	99.5%	Sigma Aldrich
LiCl(anhydrous)	>98%	Prime chemicals
$CaCl_2$	>97%	Better Equipped
KCl	>99%	Sigma Aldrich
$BaCl_2$	>99%	Better Equipped
ZrO_2	99% metals basis	Sigma Aldrich
ZnO_2	>99%	Sigma Aldrich
SiO_2 (white sand)	White quartz, 99%	Better Equipped

List of chemicals used for glass preparation

APPENDIX B (HLW composition)

Elemental Classification of HLW (Sengupta *et. al.*., 2013)